



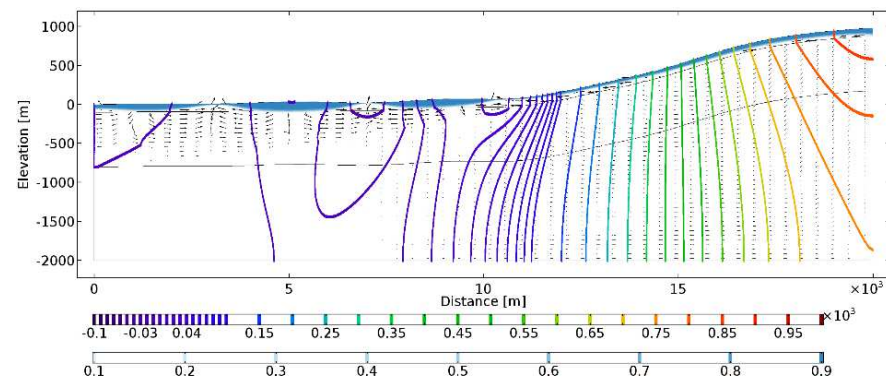
**British
Geological Survey**

NATURAL ENVIRONMENT RESEARCH COUNCIL

Coupled modelling of permafrost and groundwater. A case study approach

Environmental Modelling Programme

Commissioned Report CR/16/053



BRITISH GEOLOGICAL SURVEY

ENVIRONMENTAL MODELLING PROGRAMME

COMMISSIONED REPORT CR/16/053

Coupled modelling of permafrost and groundwater. A case study approach

J. Scheidegger

Contributors

J.P. Busby, C.R. Jackson, F.M. McEvoy, R.P. Shaw

The National Grid and other Ordnance Survey data © Crown Copyright and database rights 2017. Ordnance Survey Licence No. 100021290 EUL.

Keywords

Permafrost; numerical modelling, heat flow and phase change, glaciation, last one million years.

Front cover

Permafrost and hydraulic head distribution for Case 1.

Bibliographical reference

SCHEIDEGGER, J, BUSBY, JP, JACKSON, CR, MCEVOY, FM., SHAW, R.P. 2017. Coupled modelling of permafrost and groundwater. A case study approach. *British Geological Survey Commissioned Report*, CR/16/053. 157pp.

Copyright in materials derived from the British Geological Survey's work is owned by the Natural Environment Research Council (NERC) and/or the authority that commissioned the work. You may not copy or adapt this publication without first obtaining permission. Contact the BGS Intellectual Property Rights Section, British Geological Survey, Keyworth, e-mail ipr@bgs.ac.uk. You may quote extracts of a reasonable length without prior permission, provided a full acknowledgement is given of the source of the extract.

Maps and diagrams in this book use topography based on Ordnance Survey mapping.

Keyworth, Nottingham British Geological Survey 2017

BRITISH GEOLOGICAL SURVEY

The full range of our publications is available from BGS shops at Nottingham, Edinburgh, London and Cardiff (Welsh publications only) see contact details below or shop online at www.geologyshop.com

The London Information Office also maintains a reference collection of BGS publications, including maps, for consultation.

We publish an annual catalogue of our maps and other publications; this catalogue is available online or from any of the BGS shops.

The British Geological Survey carries out the geological survey of Great Britain and Northern Ireland (the latter as an agency service for the government of Northern Ireland), and of the surrounding continental shelf, as well as basic research projects. It also undertakes programmes of technical aid in geology in developing countries.

The British Geological Survey is a component body of the Natural Environment Research Council.

British Geological Survey offices

BGS Central Enquiries Desk

Tel 0115 936 3143 Fax 0115 936 3276
email enquiries@bgs.ac.uk

Environmental Science Centre, Keyworth, Nottingham NG12 5GG

Tel 0115 936 3241 Fax 0115 936 3488
email sales@bgs.ac.uk

The Lyell Centre, Research Avenue South, Edinburgh EH14 4AP

Tel 0131 667 1000 Fax 0131 668 2683
email scotsales@bgs.ac.uk

Natural History Museum, Cromwell Road, London SW7 5BD

Tel 020 7589 4090 Fax 020 7584 8270
Tel 020 7942 5344/45 email bgs_london@bgs.ac.uk

Columbus House, Greenmeadow Springs, Tongwynlais, Cardiff CF15 7NE

Tel 029 2052 1962 Fax 029 2052 1963

Maclean Building, Crowmarsh Gifford, Wallingford OX10 8BB

Tel 01491 838800 Fax 01491 692345

Geological Survey of Northern Ireland, Department of Enterprise, Trade & Investment, Dundonald House, Upper Newtownards Road, Ballymiscaw, Belfast, BT4 3SB

Tel 028 9038 8462 Fax 028 9038 8461

www.bgs.ac.uk/gsni/

Parent Body

Natural Environment Research Council, Polaris House, North Star Avenue, Swindon SN2 1EU

Tel 01793 411500 Fax 01793 411501
www.nerc.ac.uk

Website www.bgs.ac.uk

Shop online at www.geologyshop.com

Conditions of Publication

This report is made available under the Radioactive Waste Management (RWM) Transparency Policy. In line with this policy, RWM is seeking to make information on its activities readily available, and to enable interested parties to have access to and influence on its future programmes. The report may be freely used for non-commercial purposes. RWM is a wholly owned subsidiary of the Nuclear Decommissioning Authority (NDA), accordingly all commercial uses, including copying and re publication, require permission from the NDA. All copyright, database rights and other intellectual property rights reside with the NDA.

Applications for permission to use the report commercially should be made to the NDA Information Manager.

Although great care has been taken to ensure the accuracy and completeness of the information contained in this publication, the NDA cannot assume any responsibility for consequences that may arise from its use by other parties.

© Nuclear Decommissioning Authority 2017. All rights reserved.
ISBN

Other Publications

If you would like to see other reports available from RWM and the NDA, a complete listing can be viewed at our website www.nda.gov.uk, or please write to us at the address below.

Feedback

Readers are invited to provide feedback on this report and on the means of improving the range of reports published. Feedback should be addressed to:

RWM Feedback
Radioactive Waste Management Limited
Building 587
Curie Avenue
Harwell
Oxford
Didcot
OX11 0RH

email rwmfeedback@nda.gov.uk

Foreword

This report is the result of a commissioned study funded by Radioactive Waste Management Ltd. It is Phase II of an investigation into the potential impact of permafrost in a future climate on a UK geological disposal facility. This Phase II study uses coupled flow and heat transport numerical modelling, incorporating water-ice phase changes, to further investigate future permafrost development, how deep it might penetrate, and how it might vary across the land mass of Great Britain. We investigate the sensitivity of simulated permafrost thickness, and dynamics, to a variety of climatic, geological and hydrogeological conditions.

Contents

| | |
|--|------------|
| Foreword | ii |
| Contents | iii |
| Executive Summary | 1 |
| Summary | 3 |
| 1 Introduction | 7 |
| 1.1 Background..... | 7 |
| 1.2 Effects of permafrost on a repository | 7 |
| 1.3 Previous permafrost modelling for proposed repository sites for radioactive waste | 8 |
| 1.4 Previous modelling of the potential for permafrost in Great Britain..... | 9 |
| 1.5 Aims and Objectives..... | 9 |
| 1.6 Report overview | 11 |
| 2 Permafrost Hydrogeology | 12 |
| 2.1 Definition of permafrost | 12 |
| 2.2 Groundwater flow in permafrost | 13 |
| 2.3 Influence of glaciations on groundwater flow systems | 14 |
| 3 Case studies and model definition | 17 |
| 3.1 Numerical model | 17 |
| 3.2 Modelled localities and model conceptualisation..... | 17 |
| 4 Factors and processes influencing the thickness and extent of permafrost in a geological environment | 22 |
| 4.1 Temperature..... | 22 |
| 4.2 Geological Variability | 25 |
| 4.3 Influence of advective heat flow on the thickness and distribution of permafrost..... | 25 |
| 4.4 Comparison of maximum permafrost thickness and frozen DEPTH for the coupled models depth for case 1 and Case 2 | 28 |
| 4.5 Surface water bodies..... | 29 |
| 5 Influences of periglacial and glacial conditions on the groundwater flow system | 30 |
| 5.1 Periglacial influence on the groundwater flow system..... | 30 |
| 5.2 Glacial influence on the groundwater flow system | 34 |
| 6 Summary of results, conclusions and recommendations for further work | 40 |
| 6.2 Conclusions | 45 |
| 6.3 Recommendations and potential for further work..... | 47 |
| Appendix 1 Theoretical background to numerical modelling of groundwater in permafrost | 50 |
| Heat transport | 50 |

| | |
|--|------------|
| Fluid transport | 53 |
| Groundwater flow including the effects of glacial loading..... | 56 |
| Appendix 2 Boundary conditions and model conceptualisation..... | 57 |
| Modelled localities | 57 |
| Model set-up..... | 57 |
| Boundary conditions and model conceptualisation..... | 61 |
| Modelling methodology | 69 |
| Appendix 3 Factors and processes influencing the thickness and extent of permafrost in a geological environment | 73 |
| Temperature | 73 |
| Geological Variability | 81 |
| Influence of advective heat flow on the thickness and distribution of permafrost | 88 |
| Influence of taliks on the thickness and distribution of permafrost | 98 |
| Thermal pecllet number | 100 |
| Appendix 4 Influences of periglacial and glacial conditions on the groundwater flow system | 104 |
| Periglacial influence on the groundwater flow system | 104 |
| Glacial influence on the groundwater flow system..... | 114 |
| Appendix 5 COMSOL Multiphysics benchmarking with InterFrost test cases..... | 129 |
| Comparison to analytical solutions | 129 |
| References | 142 |

FIGURES

- Figure 1. Definition of permafrost and associated features based on the intersection between the 0°C line and annual maximum and minimum ground temperature profiles. Frozen ground is defined on the basis of the intersection of the annual maximum temperature profile with the temperature of ice nucleation, which is usually <0°C and varies with soil type. After (*Woo, 2012*).
- Figure 2. Taliks found under lakes, springs and drained lake basins, from *Scheidegger (2013)* and modified after *Sloan and Van Everdingen (1988)*.
- Figure 3. Cross-section along an ice flow line showing hydraulic conditions during a glacial cycle. The ice sheet is polythermal, with the marginal ice below melting temperature whereas the remaining glacier bed is at melting temperature. After *Lemieux et al. (2008c)*.
- Figure 4. Model set-up and boundary conditions for Case 1. The boundary conditions in blue correspond to hydraulic head and those in red to temperature. At the surface, hydraulic head is set to the topography, and the temperature to a temperature time series. The right hand side of the model is closed to heat and fluid flow. At the left hand side of the model, as specified hydraulic head is applied and is open to heat flow. The base of the model is closed to fluid flow, and a constant heat flow is applied. The scale of the vertical axis is exaggerated by a factor of 2.

- Figure 5. Model set-up and boundary conditions for Case 2. The boundary conditions in blue correspond to hydraulic head and those in red to temperature. The scale of the vertical axis is exaggerated by a factor of 100. 21
- Figure 6. Permafrost thickness for Case 1 (lower plot) using temperature time series (upper plot) that are scaled between 10 and 25 °C below the present day temperature. 23
- Figure 7. Permafrost thickness for different glaciation scenarios. “max” refers to a maximum glaciation scenario and “med” refers to the medium glaciation scenario after *Boulton and Broadgate* (1993). The base case is for an unglaciated scenario. 24
- Figure 8. Permafrost thickness time series for the T-25 temperature scenario for Case 1 using a heat conduction (C) only and conduction-advection (CA) models using a minimum ($\Omega=6$), medium ($\Omega=3$), and maximum ($\Omega=1$) permafrost permeability scenario. The left hand plots show permafrost depth and those on the right hand the difference between the two types of models (C-CA). Location 7 km and 9 km refer to the distance of Figure 4. 26
- Figure 9. Comparison of permafrost distribution at 74.75 ka BP for the T-25_Max models using $\Omega=6$ (above) and $\Omega=1$ (below). Hydraulic head (spectrum contours), ice saturation (blue fill) and groundwater flow vectors are presented. For the model using $\Omega=6$ (above), the low permeability at the surface results in a reduction in recharge, and hydraulic heads underneath the permafrost drop as a consequence. For the model using $\Omega=1$ (below), the permeability only decreases by one order of magnitude and recharge decreases less than for the $\Omega=6$ case, maintaining an active groundwater flow system underneath the permafrost and discharging at topographic lows, where taliks form as a result. 27
- Figure 10. Lines of equal ice saturation for Case 1 at 5 km from the left hand boundary for a) the T-14_max and b) T-25_max temperature scenario. 28
- Figure 11. Permafrost and hydraulic head distribution at 21.75 ka for a scenario with lakes at topographic low places. Hydraulic head (spectrum contours), ice saturation (blue fill) and flow vectors are presented. 29
- Figure 12. Surface fluxes for Case 1 for the T-25 scenario. a) non-permafrost (0 ka BP), b) thin permafrost (74.75 ka BP) and c) continuous permafrost (58.25 ka BP). Two permafrost permeability scenarios are considered; firstly, permafrost that is more permeable and decreases in permeability by one order of magnitude ($\Omega=1$), and secondly permafrost that is less permeable and decreases in permeability by six orders of magnitude ($\Omega=6$). For a) both scenarios are identical. When there is thin permafrost taliks develop in the higher permeability permafrost, resulting in higher discharge than under ambient conditions. In contrast the lower permeable permafrost model shows recharge and discharge reduced by six orders of magnitude. c) Fluxes are reduced compared to the ambient scenario to as many orders of magnitude as characterised by the factor Ω . A similar graph (not using a log scale) is presented in Figure 50. 31
- Figure 13. Ice saturation and groundwater flow velocities at 300 m depth for Case 2 and model run T-25 at 80 km from the left hand boundary. The grey shading indicates the times when the surface is frozen. 32
- Figure 14. Virtual tracer (in kg/m^3) from a point source release to the surface under ambient conditions and permafrost (blue) conditions for Case 1, model T_14_tracer. 33
- Figure 15. Hydraulic head and permafrost distribution in front of an advancing ice sheet at 460.75 ka BP for Case 2 with one layer. 34
- Figure 16. Hydraulic head during the Anglian glaciation at different depths of profile 2 (80 km from the left hand side of the model domain). 36

| | |
|--|----|
| Figure 17. Top to bottom, time series of hydraulic head, temperature, velocity magnitude and Darcy flow in x and y at the location 80 km from the left hand boundary over the duration of the Anglian glaciation. The grey shaded times are when the surface is frozen and the light blue covered by an ice sheet. | 39 |
| Figure 18. a) Unfrozen water content and b) hydraulic conductivity for subzero temperatures for clay, silt and illite, after <i>Burt and Williams</i> (1976). | 51 |
| Figure 19. Comparison of freezing curves. | 52 |
| Figure 20. Comparison of relative permeability curves over 1°C decreasing by six orders of magnitude. Shown with a linear and a log scale. | 55 |
| Figure 21. Layers for 1D model for Case 1. | 58 |
| Figure 22. Model set-up and boundary conditions for Case 1 including glaciation. The boundary conditions in blue correspond to hydraulic head and those in red to temperature. The scale of the vertical axis is exaggerated 50 times | 60 |
| Figure 23. Global $\delta^{18}\text{O}$ time series after <i>Lisiecki and Raymo</i> (2005). | 62 |
| Figure 24. Scaled temperature time series after <i>Lisiecki and Raymo</i> (2005) using ΔT ranging from 10°C to 25 °C. | 62 |
| Figure 25. Comparison of scaled temperature time series with temperature time series used in the Phase I study (<i>Busby et al.</i> , 2014). Tabs -10, Tabs-12 and Tabs-18, are the temperature time series used in <i>Busby et al.</i> (2014) and refers to the temperature difference between the present day and minimum temperature during the last 123 ka of 10°C, 12°C and 18°C. | 63 |
| Figure 26. Temperature time series with modelled (a) maximum and (b) median ice coverages after <i>Boulton and Broadgate</i> (1993) for Case 1, and (c) ice coverage for Case 2. The blue lines indicate glaciated times. | 65 |
| Figure 27. Position of the ice margin in the model domain for the Devensian (a) and Anglian glaciation (b). The distance is relative to the left hand boundary of the model domain. | 68 |
| Figure 28. (a) Global relative sea-level curve after <i>Bintanja et al.</i> (2005), and (b) global relative sea-level curve translated to shore position. | 68 |
| Figure 29. Thermal conductivity and heat flow density of Great Britain (Rollin, 2002; Busby et al., 2011). Heat flow density estimation combines bottom hole temperature observation with a mean thermal resistance at each depth, derived from the borehole geology and a databank of mean thermal conductivity (Rollin, 2002; Busby et al., 2011) | 75 |
| Figure 30. Steady state permafrost simulation for $T_s = -5^\circ\text{C}$, using the thermal properties from Figure 29. | 76 |
| Figure 31. Permafrost thickness over time at the nine locations from Figure 30. | 77 |
| Figure 32. Permafrost thickness for Case 1 using temperature time series that are scaled between 10 and 25 °C below the present day temperature. | 79 |
| Figure 33. Permafrost thickness for different glaciation scenarios. “max” refers to a maximum glaciation scenario and “med” refers to the medium glaciation scenario after <i>Boulton and Broadgate</i> (1993) presented Figure 26 a and b. | 81 |
| Figure 34. Sensitivity of heat flow using a combination of three different thermal conductivities (λ) and porosity (ϵ). | 82 |
| Figure 35. Permafrost thickness for Case 1 using a heat flow density of 50, 70, and 100 mW/m ² | 83 |
| Figure 36. Sensitivity of thermal conductivity (λ) using a combination of three different heat flows (q_{heat}) and porosity (ϵ). | 83 |

| | |
|---|-----|
| Figure 37. Sensitivity of porosity (epsilon) using a combination of three different heat flows (qheat) and thermal conductivity (lambda). | 84 |
| Figure 38. Sensitivity of heat capacity (Cs) and density (rho) using a combination of three different heat flows, thermal conductivity, and porosity. | 85 |
| Figure 39. a) Three different location of the depth profiles: Profile 1 at 20 km, Profile 2 at 80 km and Profile 3 at 160 km with respect to left hand edge of the modelled domain. Profile 1 is through the basement, profile 2 through the Jurassic sequence, and profile 3 through the Cretaceous Chalk overlying the Jurassic sequence. The filled contours in a) represent the location of the different geological layers. These profiles refer to the locations 20 km, 80 km and 160 km of b) and c). Permafrost depth time series for one Million years is presented for the three profiles of Case 2 for the T-14 run (b) and (c) T-25 run. | 87 |
| Figure 40. Permafrost thickness for the T-25 temperature scenario for Case 2 using a heat conduction model and a conduction-advection model. | 88 |
| Figure 41. Permafrost thickness for the T-14 temperature scenario for Case 1 using a heat conduction-only (C) model, and a conduction-advection (CA) model using a minimum, medium and maximum permeability scenario. The left-hand plots show permafrost depth and those on the right the difference between the two types of model (C minus CA). The permeability scenarios used here refer to the minimum, medium, and maximum permeability as listed in Table 3, using $\Omega=6$ | 90 |
| Figure 42. Permafrost thickness for the T-25 temperature scenario for Case 1 using a heat conduction-only (C) model, and a conduction-advection (CA) model using a minimum, medium and maximum permeability scenario. The left-hand plots show permafrost depth and those on the right the difference between the two types of model (C minus CA). The permeability scenarios used here refer to the minimum, medium, and maximum permeability as listed in Table 3, using $\Omega=6$ | 91 |
| Figure 43. Permafrost time series for the T-25 scenario using different Ω from Equation 16. | 92 |
| Figure 44. Temperature and ice saturation for model T-25 using a conduction scenario and a max permeability scenario using $\Omega =6, 3, \text{ and } 1$ | 93 |
| Figure 45. Hydraulic head (spectrum contours), ice saturation (blue fill) and flow vectors for model T-25_Max for different time steps. | 96 |
| Figure 46. Comparison of permafrost distribution for two different time steps for the T-25_Max models using $\Omega =6$ (a, c) and 1 (b, d). Hydraulic head (spectrum contours), ice saturation (blue fill) and flow vectors are presented. | 97 |
| Figure 47. Permafrost and hydraulic head distribution for a scenario with lakes at topographic low places. | 99 |
| Figure 48. Thermal Peclet number for different model runs; Case 1: T-14_Max, T-14_Talik, and T-14 Case 2 T-14, for unfrozen, fully frozen and thawing conditions. | 102 |
| Figure 49. Thermal Peclet number for different T-25_max and T-25_Max_Omega_1 runs, for shallow thawing, freezing and deep thawing. | 103 |
| Figure 50. Recharge (blue) and discharge (red) for the time steps as Figure 45 and Figure 46 for run T-25_Max. | 107 |
| Figure 51. Surface fluxes for the T-14_Max model and the T-14_Max_Talik model for the time steps as in Figure 47. | 107 |
| Figure 52. Ice saturation and velocity at 100 m and 400 m depth for locations of 7 km, 9 km and 13 km for Case 1 for model runs T-25_Max (Omega 6), T-25_Max_Omega3 and T-25_Max_Omega1. The grey shaded times are for when the surface is frozen. | 110 |

| | |
|--|-----|
| Figure 53. Ice saturation and groundwater flow velocities at a) 100m, b) 300m and c) 450 m depth at the location of the repository for Case 2 for model run T-25. The grey shading indicates the times when the surface is frozen. | 112 |
| Figure 54. Tracer from a point source release at 500 m depth and 7 km from the left hand boundary to the surface under a) ambient conditions (100 ka BP), b) forming permafrost (65 ka BP), permafrost (18 ka BP), thawing permafrost (14 ka BP) and post permafrost conditions (0 ka BP) for Case 1 run T_14_tracer. | 113 |
| Figure 55. Integrated surface flux of the tracer over time for the point source release placed at 500 m depth and 7 km from the left hand boundary for Case 1 run T_14_tracer. | 114 |
| Figure 56. Hydraulic head, permafrost distribution and flow vectors for different glaciation scenarios during ice advance (left) at 539.25 ka, fully glaciated at 542.75 ka (middle), and ice retreat (right) at 553.5 ka | 117 |
| Figure 57. Time series for hydraulic head, temperature, velocity magnitude, and Darcy velocity in x and y for the one layer model for Profile 3 at 160 km. Times presented are a) the entire simulation time, b) the Anglian glaciation c) the Devensian glaciation and d) during submerged conditions. The grey shaded times are when the surface is frozen, dark blue submerged and light blue covered by an ice sheet. | 120 |
| Figure 58. Time series of hydraulic head, temperature, velocity magnitude and Darcy flow in x and y at the location of the repository over the duration of the Anglian glaciation. | 122 |
| Figure 59. Model results including a tracer for Case 2 including ice sheet loading for pre-glaciation, during ice advance, during ice retreat, post glaciation and present day. | 128 |
| Figure 60. Three-zone model with an ice, mushy zone and liquid water zone. | 129 |
| Figure 61. Temperatures at t=0 and t=168 h for the one dimensional three phase heat flow model after Lunardini. | 132 |
| Figure 62. Comparison of the modelled temperatures of the analytical Lunardini solution and the numerical solution from Comsol for different time steps. The coloured lines are the numeric solution and the black dotted line the analytical solution. | 133 |
| Figure 63. Temperature difference between numerical and analytical Lunardini solution. | 134 |
| Figure 64. Model set up. After <i>Kurylik et al.</i> (2014). | 135 |
| Figure 65. Freezing function for TH1. From <i>Kurylik et al.</i> (2014). | 136 |
| Figure 66. Comparison of numerical and analytical solutions for $v = 10$ m/a. | 137 |
| Figure 67. Comparison of numerical and analytical solutions for $v = 100$ m/a. | 137 |
| Figure 68. Geometrical setup for TH2 Test Case. | 138 |
| Figure 69. Comparison of conduction only (left) and advection scenario (right) with $dh/dx=0.15$ for test case TH2. Time steps presented are 0, 90, 420, 525, 675, 2040 min. | 140 |
| Figure 70. Minimum temperature over time for different dH scenarios. | 141 |
| Figure 71. Comparison of COMSOL to other TH codes (<i>Grenier et al.</i> , 2016). | 141 |

TABLES

| | |
|--|-----|
| Table 1. Maximum depths of >0, 50 and 95% ice saturation for Case 1 at 5 km from the left hand boundary and Case 2 at 80 km from the left hand boundary..... | 28 |
| Table 2. Thermal properties for 1D model for Case 1. | 58 |
| Table 3. Thermal and hydraulic properties for Case 1. The different Kx values refer to the minimum, medium and maximum permeability scenario. | 61 |
| Table 4. Thermal and hydraulic properties for Case 2. | 61 |
| Table 5. 1D model runs for Case 1..... | 70 |
| Table 6. Coupled model runs for Case 1. | 71 |
| Table 7. Model runs for Case 2. | 71 |
| Table 8. Model runs including glaciation..... | 72 |
| Table 9. Thermal properties, steady state permafrost thickness and maximum permafrost thickness for a transient simulation using a Tmin of -5.5C (T-14 scenario). | 77 |
| Table 10. Maximum permafrost thickness for Case 1 using temperature time series that are scaled between 10 and 25 °C below the present day temperature. | 80 |
| Table 11. Maximum permafrost thickness for temperature time series corrected for the insulating effect of an ice coverage. Max, and Med denote the glaciation scenario from Figure 26 a and b and the value the subglacial temperature is set to. | 80 |
| Table 12. Parameters for sensitivity study: thermal conductivity, λ , porosity, ϵ , heat capacity, C_s , heat flow density, q_{heat} , and density, ρ | 81 |
| Table 13. Influence of geological parameters on the range of permafrost thickness..... | 85 |
| Table 14: Parameter values used for the Lunardini analytical solution, after McKenzie et al. 2007 and INTERFROST. | 131 |
| Table 15. Parameters for TH1 | 136 |
| Table 16. Model parameters for TH2..... | 139 |

Executive Summary

This report investigates the sensitivity of simulated permafrost thickness and dynamics to a variety of climatic, geological and hydrogeological conditions for two geological environments, basement under sedimentary cover and a low permeability succession of Mesozoic shales and siltstones (Case 1 and Case 2 respectively). A combination of one dimensional heat conduction modelling, including the effects of freeze-thaw, and two dimensional heat conduction-advection modelling, including freeze thaw, has been undertaken to simulate permafrost development in these two contrasting geological environments. This enables an assessment of the sensitivities to a range of possible geological parameters, advective heat flow, and the effect of glaciation with and without the influence of glacial loading.

In this report, permafrost is defined as the sub-surface in which ice is present even in very small amounts, i.e. ice content is greater than 0%, and in the model, this is at the zero degree isotherm. The maximum permafrost thickness is strongly dependent on the mean annual surface temperature, the presence of ice that will insulate the system and the duration of the cold phase. By scaling the minimum temperature of 57 Pliocene-Pleistocene globally distributed benthic $\delta^{18}\text{O}$ records to temperatures of 14°C, 18°C and 25 °C below the present day mean annual temperature, the maximum permafrost thickness for Case 1 is simulated to reach 171 m, 248 m, and 475 m, and for Case 2 80 m, 138 m, and 238 m respectively. The difference in permafrost thickness between the two Cases is attributed to the variation in subsurface rock properties. Deeper permafrost depths than for Case 1 and 2 can be expected where the thermal conductivity is higher than for Case 1 and 2.

A sensitivity study of the geological parameters has shown that there is a strong, non-linear, relationship between thermal conductivity, latent heat and geothermal heat flow for a series of temperatures representative of the glacial cycles of the past one million years. This is in contrast to a steady state temperature profile, where permafrost thickness relates linearly to thermal conductivity, heat flow and ground surface temperature. Thickest permafrost under unchanged climatic conditions is to be expected where there is a low heat flow, a high thermal conductivity and a low porosity, such as for example in the north of Scotland.

The results of the modelling show that when the temperature regime is dominated by heat conduction, such as for the low permeability Case 2, a heat conduction only model is sufficient to estimate the thickness and distribution of permafrost. However, when heat advection is likely to be important, such as in Case 1, the coupling of permafrost and groundwater flow is necessary to simulate the permafrost distribution during freeze and thaw, or during shallow permafrost events. This particularly holds true when permafrost is modelled to be relatively permeable, where modelling suggests that heat advection of cold water at recharge points (interfluves) results in cooling and thicker permafrost compared to discharge points where discharge of warmer water results in thinner permafrost. However, these variabilities in local permafrost thickness are of minor importance for the question of freezing of the repository. However, when assessing the broader influences of permafrost on a geological environment, local variations in permafrost extent of thickness can have consequences on the biosphere.

Glaciation influences the thermal regime of the ground surface. If the glacier bed is undergoing pressure melting, as found in the ablation zone, a reduction in permafrost depth can be expected. If the glacier bed is cold based, as often found in the accumulation zone or at ice divides where strong vertical advection of cold ice has a cooling effect, then the maximum permafrost thickness can be expected to be similar to the scenario without glaciation. It may even increase if the temperatures at the glacier bed are colder than the ground surface temperatures, which may occur

when the temperature in the area where the ice is forming is colder than that prevailing downstream.

Recharge and discharge decrease considerably during periods when permafrost is present. In the case of a model with an open model boundary to one side, representing the coast for example, and a high topographic gradient (Case 1), a large drop in hydraulic heads is observed beneath the permafrost. This results in lower groundwater flows at depth compared to unfrozen conditions. Where a modelled area is closed on all sides (Case 2), a decrease in flow at depth is also observed, however the hydraulic heads do not decrease to the same extent as the hydraulic gradient is less than for Case 1. During permafrost thaw, hydraulic heads rise, resulting in an uptake of groundwater into elastic storage from recharge over the top boundary of the model domain.

When taliks underneath surface water bodies develop, the groundwater flow system remains more active than during continuous permafrost. Recharge and discharge are focused on the lakes and a regional groundwater flow system connecting the lakes can develop. Heat advection remains more important during thick permafrost when through taliks remain open.

In the model, during periods of glaciation, hydraulic heads increase by ~1500 m at depth for Case 1 and Case 2 when ice loading is applied. When ice-sheet loading is not accounted for, the hydraulic head signal in low permeability layers is dampened. During glacial advance, groundwater recharge increases by up to two orders of magnitude, and during glacial retreat discharge increases. During ice advance, groundwater flow is in a downward direction but during ice retreat it is in an upward direction. Depending on the flow direction of the glacier, groundwater flow directions can be reversed during a glaciation. Modelling the Anglian Glaciation (middle Pleistocene glaciation, equivalent to the Elsterian or Mindel glaciation in Europe and the Alps, most extensive glaciation in the British Isles, MIS 12), the hydraulic head and groundwater flow magnitude are affected by the glaciation for tens of thousands of years, whereas after the Devensian glaciation (late Pleistocene glaciation, equivalent to the Weichselian/Vistulian or Würm glaciation in Europe and the Alps, MIS 5d to 2), the signal remains for thousands of years.

High hydraulic heads that may be present during glaciation are likely to modify the groundwater flow around a GDF. The modelling presented here based on two settings and typical thermal and hydraulic properties for the rocks present, demonstrates that the depth of permafrost could extend up to a depth of 300m below the surface and, depending on specific characteristics (large thermal conductivity and low porosity) and an exceptionally long cold period, could extend to greater depths. Permafrost to these depths may affect the engineering properties of some rock types and could lead to the development of new fracture pathways in more brittle formations. Permafrost could also affect some of the engineered components of a GDF in similar ways, such as the properties of clay materials.

Summary

Radioactive Waste Management (RWM) commissioned the British Geological Survey (BGS) to undertake a Phase 1 study to investigate the potential for permafrost development across Great Britain under possible future periglacial climates. The Phase 1 study by *Busby et al.* (2014) applied one-dimensional heat conduction models at ten locations across Great Britain. Suggestions for further work included a full sensitivity analysis of parameters influencing permafrost thickness in the UK rather than using a best estimate. Recommendations regarding model development included work to add the effects of latent heat produced during freeze/thaw, which results in thinner permafrost compared to a heat conduction model without freeze/thaw effects, and the inclusion of advective heat flow arising from groundwater flow.

Following on from the work from the Phase 1 study, this Phase 2 study aims to estimate the impact of future climate and glaciation on a coupled system of permafrost dynamics and groundwater flow of two environments of the UK, in contrasting geological settings and with differing positions with respect to future ice-sheet development. We used coupled groundwater flow and heat transport modelling, incorporating water-ice phase changes, to investigate the sensitivity of permafrost thickness and dynamics to a variety of climatic (temperature time series and glaciation scenarios), geological (thermal conductivity, density, heat capacity) and hydrogeological (hydraulic conductivity) conditions for two contrasting geological environments (Case 1 and Case 2).

Case studies and model definition

The two contrasting geological environments, Case 1 and Case 2, are informed by Environment 2 and Environment 5 described in *Towler et al.* (2008b) and do not represent any specific site. Case 1 is characterised by a basement under sedimentary cover (BUSC) located on the margin of a Permo-Triassic sedimentary basin, and Case 2 by a sequence of Lower Jurassic shales and mudstones and Triassic mudstones and siltstones.

The first set of simulations was performed using a 1D heat conduction only model including phase change; a sensitivity study of different model input parameters was undertaken. For the 1D model, two different sets of parameters were used. The first set uses the geology for Case 1 and tests the influence of different temperature time series, glaciation scenarios and geothermal heat flows on the permafrost depth. The second set of 1D models consist of a one layer model and is used to test the influence of different model input parameters (thermal conductivity, heat capacity, geothermal heat flow, and porosity) on the maximum permafrost depth.

Subsequent to 1D modelling, we undertook detailed 2D (vertical slice) modelling of permafrost dynamics in two example settings: Case 1 and Case 2. For Case 1, the right hand boundary is closed to heat flow and fluid flow, as this represents a topographic high, and the left hand boundary is set to a specified head and a flux boundary for heat. At the top boundary, variable temperature, hydrological and glaciological conditions are applied to the land-surface. The base of the model is closed to fluid flow and a constant geothermal heat flow is specified. The model boundaries for Case 2 are the same as for Case 1, except that both sides are set to zero flux boundaries for heat and fluid flow.

In addition to modelling a periglacial system, the influence of glaciation on the permafrost distribution and groundwater flow system is studied. For the model including glaciation, the model set-up of Case 2 is used, applying three different geological scenarios: a one-layer model representing the geology of a basement, the geology of Case 1 and the geology of Case 2. For the one layer model and Case 2, the model is run with and without the influence of glacial loading, whereas for Case 1, only the model including loading is presented.

Results from this report include the following key processes and findings: evaluation of the equilibrium state of permafrost in Great Britain, the influence on the permafrost thickness of the temperature scaling of the time series, the temperature correction for ice cover, the geological variability, heat advection by groundwater flow and the existence of surface water bodies. Furthermore, the effects of permafrost, glaciation and sea-level changes on the groundwater flow system are studied.

Transient permafrost thickness

Comparison of the results from 1D models, applied at nine locations with contrasting thermal properties and heat flows, showed that the decision of whether to use a steady-state or a transient model can have a significant impact on the simulated maximum permafrost depth. Modelling indicates that when using a steady model, permafrost thickness extended to greater depths than when using a transient model, as much as 167 m deeper for a scenario with a minimum temperature of -5.5°C . Therefore, assuming the temperatures oscillations experienced over the past one million years, there was insufficient time for the permafrost thickness to reach steady state condition in Great Britain.

Surface temperature time series

The scaling of the global surface temperatures, to generate appropriate local temperatures, has a large influence on modelled permafrost thickness. The temperature is set to different minimum temperatures; the T-10 scenario is set to be 10°C below the present day temperature, the T-14 scenario 14°C and the T-25 scenario 25°C below the present day temperature. For the first conceptualised locality, Case 1, the simulated permafrost thickness ranges between 49 m and 475 m for a ΔT of 10°C (T-10 scenario) to ΔT of 25°C (T-25), respectively. For Case 2, the maximum simulated permafrost thickness ranges between 80 m and 238 m for a ΔT of 14°C (T-14) and ΔT of 25°C .

Temperature correction for ice cover

The timing of a glaciation and the associated temperature correction for ice cover have a large influence on the permafrost thickness. The maximum modelled thickness of permafrost ranges between 100 m and 177 m, depending on the glaciation scenario for the T-14 temperature scenario for Case 1. However, the insulation of a glacier can result in no ground freezing, whereas under non-glaciated conditions permafrost thickness would be several hundred metres.

Geological variability

The influence of thermal and geological properties based on ranges of UK geologies (see Figure 29) on the permafrost thickness is non-linear and the relative importance of different parameters is related to the magnitude of other parameters. The variation in permafrost because of differences in thermal conductivity and geothermal heat flux can range between tens of metres to approximately 400 m, whereas the variation as a result of porosity variability, is between zero to 300 m. Mass heat capacity and density have been found to be of minor importance in influencing the maximum permafrost thickness, with maximum ranges of 30-40 m. The largest variability in permafrost thickness with respect to porosity is when it is associated with low heat flow and high thermal conductivity. The largest variability in permafrost thickness with respect to heat flow arises with high thermal conductivity and low porosity. The largest variability in permafrost with respect to thermal conductivity is associated with low porosity and low heat flow.

Heat advection

The influence of heat advection on permafrost thickness for the base case model, as described in Section 4.3, reduces as permafrost develops. This relationship is not well known and a number of

different functions can be used to describe it. When the permafrost permeability reduction function is changed, the difference in permafrost thickness at a point in time can be as much as 100 m. Generally, the influence of heat advection is largest when permafrost is shallow, and less when permafrost is deeper, as with deeper permafrost the regime changes from advection dominated to conduction dominated. Heat advection can result in an uneven permafrost distribution, with thicker permafrost where there is advective cooling and thinner or no permafrost where there is advective warming.

Surface water bodies

Surface water bodies insulate the ground from lower air temperatures and can result in taliks or unfrozen zones that perforate the permafrost. The presence of taliks alters the permafrost distribution from continuous to discontinuous, allowing a groundwater-surface water connection through otherwise thick permafrost (Section 4.4).

Groundwater flow in and below permafrost

When the model domain is unfrozen, recharge and discharge are topographically driven. When ice starts to form at the surface, recharge and discharge decrease by up to several orders of magnitude, as determined by the permafrost permeability function. For Case 1, reduced recharge and discharge at the surface result in a drop in hydraulic heads beneath the permafrost, as groundwater drains out the side of the model, representing an open boundary (e.g. sea), resulting in lower groundwater velocity magnitudes at depth. A decrease in velocity magnitudes at depth can also be observed for Case 2, but hydraulic heads do not decrease to the same extent as for Case 1 because the boundary to the side is closed, representing for example groundwater flow divides or impermeable fault zones, and the hydraulic gradient is smaller. During permafrost thaw, hydraulic heads rise, resulting in an uptake of groundwater into elastic storage.

For the scenario in which permafrost is set to be more permeable, with a decrease in permeability of one order of magnitude ($\Omega = 1$), recharge and discharge both decrease when permafrost starts to form, but discharge focusses on topographic lows, resulting in taliks. Flow into the taliks is focused, resulting in higher velocity magnitudes than under unfrozen conditions.

Observing the plume of a tracer released at depth showed that under ambient conditions the plume spreads towards the surface, affecting a small area. The existence of permafrost can fundamentally alter the area which is affected. During a permafrost event, discharge to the surface ceases, and the flow direction changes, spreading the tracer laterally. The tracer concentrates below the permafrost and is then released after the permafrost has disappeared (Section 5.1).

Glaciations

Glaciations influence the thickness and distribution of permafrost as they isolate the ground from the air temperatures. When ice is at pressure melting and liquid water is present, temperatures at the base of the ice are close to, or below 0°C. In the numerical model, we ignore the pressure effects on temperature and the subglacial temperature at pressure melting is set to 0°C, as previously done in *Bense and Person (2008)* and *Scheidegger and Bense (2014)*. When the base of an ice sheet is cold-based, temperatures are lower than 0°C and permafrost either forms or persists beneath the ice.

For Case 1, correcting the temperature time series for ice coverage where the subglacial temperature is set to 0°C, -1°C and -5°C for a temperature scenario of T-14 has a significant impact on the simulated maximum permafrost thickness over the past one million years. For the maximum glaciation scenario with subglacial temperatures at pressure melting, the maximum permafrost thickness was calculated to be 100 m compared to 171 m without glaciation. When the subglacial temperature is set to -5°C, the modelled maximum permafrost thickness was

177 m. Whether the maximum or the medium glaciation scenario is selected does not have a large influence on the maximum permafrost thickness overall, because the medium glaciation scenario is glaciated when temperatures are coldest.

High hydraulic gradients beneath an ice sheet considerably alter the groundwater flow system compared to ambient conditions. When the gradient of the ice sheet is against the topographic gradient, groundwater flow is reversed by the presence of a glacier.

When an ice sheet is present, hydraulic heads underneath the ice sheet and at depth increase to the ice overburden (1500-2000 m) for the one layer model representing basement, and Case 1. However, for Case 2 the signal of high hydraulic heads is dampened and penetrates slowly in the low permeable units. During ice advance and ice retreat the hydraulic gradient is largest, resulting in the highest groundwater velocity magnitudes, which are one to two orders of magnitude higher than under ambient conditions for all geological scenarios. During ice advance and ice sheet build up, flows are in a downward direction, resulting in uptake of groundwater into elastic storage. During ice retreat, flows are in an upward direction, releasing groundwater mainly underneath the ice sheet that has been taken into storage during ice advance. The lateral flow directions are reversed during the glaciation and its magnitude is highest during advance and retreat.

For the modelled groundwater velocity magnitudes and direction at depth to return to their initial states after the Anglian glaciation took tens of thousands of years, and after the Devensian glaciation it took several thousands of years. This difference is because of the length of time the region has been glaciated, set at 20 ka for the Anglian and 2 ka for the Devensian for this study.

The loading efficiency of the rock matrix determines how the ice load is apportioned between the rock and pore fluid and depends on the relative compressibility of the porous medium to the pore fluid and the porosity. For the one layer model and Case 1, the influence of ice sheet loading is minimal. However, for Case 2, the effect of ice sheet loading is large in the low permeability layers, since the ice sheet loading may result in an expulsion of water as a result of a consolidation of the bedrock matrix. For the model excluding loading, the high hydraulic heads propagate slowly in the low permeability layers, resulting in high gradients around the low permeability layer. In contrast, when the effects of ice loading are included, the high hydraulic heads still propagate to the low permeability layers at a slower rate than in the aquifer above, however, at a faster rate than when loading is not considered. Therefore, the effects of loading are largest for Case 2 in the low permeability layers, whereas for Case 1 and the one layer model the impacts of loading are small.

Implications for a GDF in the UK

The depth to which permafrost penetrates is dependent on a number of variables that include surface temperature, geothermal heat flux, thermal conductivity, groundwater flux and ice cover. Many of these properties are site specific and cannot be determined accurately for a 'generic' site so will require a site specific assessment once a site is being evaluated.

This study does show, depending on the specifics of the scenarios under consideration, that when modelled on past glaciations, permafrost in the UK can readily extend to depths of up to 300m below the surface and, depending on specific characteristics (large thermal conductivity and low porosity) and a long cold period, can extend to greater depths. While the former is an important consideration for a GDF at shallow depth the latter is an important consideration for a deep GDF. However, these depths will only be reached by permafrost where and when conditions and rock characteristics are particularly favourable for its development and there are no other factors, such as the presence of taliks, which may reduce the depth to which permafrost develops. Such features may also influence groundwater flow regimes. Sub-permafrost changes to groundwater flow-paths and hydrochemistry may also affect a GDF beneath permafrost.

1 Introduction

1.1 BACKGROUND

As outlined by *Shaw et al.* (2013) and subsequently by *McEvoy et al.* (2016), there are a number of processes that may have an effect over the next one million years on a UK geological disposal facility (GDF) emplaced at a depth of between 200 m and 1000 m below surface:

- Erosion (in the order 10s of metres and occasionally up to 200 m)
- Permafrost
- Changes in groundwater flow patterns

Most climate models suggest that the northern hemisphere will continue to undergo cycles of glacial advance and retreat over the next million years, even with consideration of anthropogenic climate change. Therefore, the site of the GDF is likely to be glaciated and/or permafrost covered several times (*McEvoy et al.*, 2016) over the next one million years and hence, predictions of the duration, thickness and extent of future ice cover and permafrost thickness are important for assessing the post-closure safety of a UK GDF.

Glacial-interglacial cyclicity results in different climate domains, including temperate climate glaciated conditions and permafrost covered landscape, and this will profoundly impact the hydrology, hydrogeology and geomorphology of any affected UK site. The depth of groundwater flow will increase under temperate or wet-based glaciers, as the pressure underneath wet-based ice increases up to the ice overburden pressure. Ice sheet loading and subsequent land-surface uplift will influence the near-surface stress field within the shallow geosphere, control regional relative sea-level, and indirectly change groundwater regimes. Furthermore, eustatic sea-level fluctuations influence groundwater in terms of, for example, composition, flow pathways and flow rates (*McEvoy et al.*, 2016).

Under periglacial conditions, the extent and depth of permafrost will alter the geomechanical properties of the land-surface, reduce the recharge of aquifers resulting from precipitation and alter the positions of recharge and discharge locations relative to those of the present day temperate conditions (*McEvoy et al.*, 2016).

How future glaciation and permafrost coverage will affect the groundwater system of a potential, as yet unknown GDF site in the UK is largely unknown, however forcing a coupled permafrost-groundwater model with a range of boundary conditions and model parameterisations will provide us with an array of groundwater-permafrost interactions. These models require predictions from future climate models, which themselves use understanding of recent and past climate, including the extent, duration and interval of glacial periods. Further, the modelling needs to take account of the geological characteristics of the host rock and surrounding formations, and how they are likely to respond to the aforementioned natural changes. Specifically, there is a need to better understand how groundwater recharge, flow and discharge will be affected, and how groundwater composition will change in response to freeze-thaw mechanisms or fresh glacially recharged groundwater.

1.2 EFFECTS OF PERMAFROST ON A REPOSITORY

Possible impacts of permafrost on a geological disposal facility include an influence on groundwater flow direction and magnitude, reduction of recharge and discharge, and focussing of groundwater flow through taliks underneath surface water bodies and around any high permeability fracture zones (*Ruskeemiemi et al.*, 2002). In addition, changes in the chemical composition of groundwater, salinity increase due to freeze out of solutes and the formation of

cryopegs (which are defined as unfrozen zones that are perennially cryotic) can occur (*Hartikainen et al.*, 2010). Furthermore, mechanical effects of freezing and thawing on rock and soil stability are of importance as they could reduce the performance of the engineered components of a GDF, such as clay (*McEwen and de Marsily*, 1991). In addition, aggregation of methane hydrates within cavities in the GDF, or underneath, the permafrost is possible, giving rise to releases of gas during warmer periods. Rapid releases of gas in sufficient quantities (overpressure) could give rise to the formation of cracks and potentially increase groundwater flow in the host rock above the GDF.

1.3 PREVIOUS PERMAFROST MODELLING FOR PROPOSED REPOSITORY SITES FOR RADIOACTIVE WASTE

Permafrost modelling coupled with groundwater modelling has been undertaken to inform the long-term safety cases for a number of proposed sites for deep geological repositories for radioactive waste, for example in Sweden (SKB), Finland (POSIVA), France (Andra), Canada (NWMO), Belgium (SCK CEN) and Switzerland (NAGRA).

Andra has developed a fully coupled 3D groundwater and heat transport model that includes permafrost formation, and this has been applied to the entire Paris basin on the Meuse/Haute-Marne Sector area (*Holmén et al.*, 2011). The maximum permafrost depth simulated for the past 130 ka is ~110 m. Groundwater flow has been found to decrease by 10-25% when there is a large extent of permafrost and with extensive permafrost the hydraulic conductivity and recharge will be reduced to zero. The hydraulic head values below the permafrost may also fall as much as 50 m, resulting in a reduction of groundwater flow close to the outcrops (*Holmén et al.*, 2011).

Extensive permafrost simulations including the effects of groundwater, pressure, salinity and glaciation have been undertaken for Forsmark by SKB (*Hartikainen et al.*, 2010; *Vidstrand et al.*, 2010; *Vidstrand et al.*, 2014). The emphasis of the permafrost simulation study is on modelling surface conditions depending on climate and landscape, and transient processes of snow, vegetation and water bodies are included in this work. An extensive sensitivity analysis of the variation of air temperature, geothermal heat flow, thermal conductivity, thermal diffusivity, heat from a repository and convective heat transfer is undertaken. The report presents two different temperature scenarios; the repetition of the last glacial cycle, which includes the effects of an ice sheet and a severe permafrost case, which does not include the effects of an ice sheet. Modelled permafrost depths for Forsmark are 310-460 m for the severe permafrost case and 160-290 m for the repetition of the last glacial cycle (*Hartikainen et al.*, 2010). Groundwater flow modelling of periods with periglacial and proglacial conditions comprises a coupled thermal-hydraulic-chemical analysis for a temperate case, a glacial case without permafrost and a glacial case with permafrost (*Vidstrand et al.*, 2010). Overall, their modelling work concludes that an ice sheet covering the Fennoscandian Shield during the Weichselian impacted the deep groundwater system. Their modelling shows that during glacial periods the primary driving force for groundwater below and in front of an ice sheet is driven by the hydraulic pressure difference, which is assigned as boundary conditions. In addition, their result shows that local hydrogeological characteristics, such as deformation zones and variation in hydrogeological properties, have the strongest impact on the model results (*Vidstrand et al.*, 2013).

At Bruce nuclear site, the impact of glaciations on groundwater was studied, using the 3D model FRAC3DVS-OPG, which includes hydromechanical coupling and solute transport (*Normani and Sykes*, 2012). The ice loads are assumed to be spatially homogeneous, and therefore lateral strains can be neglected. 1D vertical loading and unloading of glaciation, erosion, or deposition is a common simplification in hydromechanical coupling (*Normani and Sykes*, 2012). Permafrost occurrence and depth is calculated using a glacial systems model and then included into the hydrogeological model. The hydrogeological and the permafrost model are not coupled (*Normani and Sykes*, 2012). Modelled results show that the impact of glaciations and

deglaciation does not lead to a groundwater penetration to the depths of the proposed site. *Normani and Sykes (2012)* find that the most significant consequence of glacial loading is the generation of higher pressures during loading throughout the rock column, with the level dependent on the one-dimensional loading efficiency of the rock mass. In addition, the model used was unable to yield the abnormal pressure patterns observed.

1.4 PREVIOUS MODELLING OF THE POTENTIAL FOR PERMAFROST IN GREAT BRITAIN

Radioactive Waste Management (RWM) commissioned the British Geological Survey (BGS) to undertake a Phase 1 study to investigate the potential for permafrost development across Great Britain under possible future periglacial climates. The Phase 1 study by *Busby et al. (2014)* applied one-dimensional heat conduction models at ten locations across Great Britain, selected to represent a range of geological settings, latitudes and elevations, and found that the occurrence of permafrost will be virtually certain over the next one million years, using past temperature time series as a proxy for future predictions (*Shaw et al., 2013; McEvoy et al., 2016; Busby et al., 2014*).

Model outputs indicated permafrost thicknesses in Great Britain of between several tens to over 100 m depending on various factors, including elevation, glacier ice cover, geothermal heat flow, and air temperature. The thickness of permafrost strongly depends on the surface temperature time series used. In the literature (e.g. *Bintanja et al., 2005; Lisiecki and Raymo, 2005*), there is general agreement on the timing of the past major cold events, but not on the minimum temperatures that will be reached during these periods. In the Phase 1 study by *Busby et al. (2014)*, two temperature scenarios were applied, an average cold estimate and an extreme cold estimate. For the ten locations, permafrost thickness was modelled to be between 30 m and 180 m for the average climate estimate and between 180 m and 245 m for the cold climate estimate (*Busby et al., 2014; Busby et al., 2015a; Busby et al., 2015b*).

The subglacial thermal regime was found to be an important parameter for the development of permafrost. The presence of ice alters the ground surface temperature; underneath the ablation zone, temperate ice will result in higher ground surface temperatures than for non-glaciated terrain, whereas underneath the accumulation zone, cold ice can reduce the ground surface temperature relative to unglaciated terrain.

This first study presented temporal and spatial variation in permafrost thickness across the UK over the past 130 ka. Suggestions for further work included a full sensitivity analysis of parameters influencing permafrost thickness in the UK rather than using a best estimate. Recommendations regarding model development included work to add the effects of latent heat during freeze/thaw, which results in thinner permafrost compared to a heat conduction model without freeze/thaw effects, and the inclusion of advective heat flow by groundwater flow.

1.5 AIMS AND OBJECTIVES

The recommendations by *Busby et al. (2014)* and subsequent discussions with RWM determined the overall aim of this study, which are: to estimate the impact of future climate and glaciation on a coupled system of permafrost dynamics and groundwater flow in two environments of the UK, in contrasting geological settings and with differing positions with respect to future ice-sheet development. As the thickness of permafrost is determined by heat conduction, driven by a temperature gradient in the subsurface, and heat advection by moving groundwater, a coupled model of heat flow including phase changes of freezing and thawing water/ice will be used. This will allow the permafrost dynamics related to predicted climate changes, and dynamics of groundwater flow driven by future glaciations, to be better understood.

The following objectives will be addressed:

Objective 1: Identify the factors affecting permafrost thickness.

Permafrost thickness is influenced by the surface temperature time series, the ground thermal properties and heat flow, latent heat and change in thermal properties associated to phase change and the insulating effect of glaciation. Hence, in order to identify the relative importance of these factors, this objective is divided into the following sub-objectives:

a) Understand the influence of different scaling of the surface temperature time series on the maximum permafrost thickness.

The minimum temperature during the last glacial cycles is unknown and estimates range over several degrees. In addition, the ground surface temperature is strongly influenced by local factors, such as topography, vegetation, cooling by tree shadow and warming by insulating winter snow cover. To take into account different surface temperature scaling and local factors, a sensitivity of surface temperature time series is performed on one geological environment, Case 1.

b) Identify the influence of different geological properties found in the UK on the maximum permafrost thickness.

Two geological environments, Case 1 and Case 2, are used in this report. In addition, a series of one dimensional, homogeneous models with a variety of geological properties present in the UK are compared in order to find their relative importance on permafrost thickness.

c) Understand the influence of advective heat transport by groundwater flow for a periglacial scenario.

Two models, a heat conduction only case and a case including heat conduction and advection, will be compared in order to determine the relative importance of advective heat flow on permafrost development. This will show whether the influence of groundwater flow in a periglacial environment is significant, or whether a permafrost model using heat conduction only is sufficient to estimate permafrost distributions. For both models two climates will be considered: an average climate estimate representative of the conditions during the last glacial cycle; and a cold estimate case that defines the coldest temperatures that might occur in a future glacial cycle in the next million years.

d) Understand the influence of glacial conditions on the permafrost thickness and dynamics at the selected localities.

The existence of an ice sheet influences the subsurface temperature regime as well as the hydrogeological regime through subglacial infiltration, ice sheet loading, eustatic sea-level changes and density dependent groundwater flow. Here, the influence of glaciation on the temperature regime, subglacial infiltration, ice sheet loading and eustatic sea-level changes will be added step-wise into the model. Similarly to Objective 1, a heat conduction only model will be compared to a heat conduction and advection model for each case, in order to investigate the influence of advective heat flow driven by glacially recharged groundwater on the dynamics of permafrost.

Objective 2: Understand the influence of periglacial and glacial conditions on the groundwater flow direction and magnitude at the selected localities.

The change in groundwater flow direction and groundwater magnitude with permafrost dynamics will be assessed. Questions such as whether there are any pressure anomalies in permafrost dynamics, or whether groundwater is taken up and released into elastic storage, and how the model responds to different model parameterisation will be addressed.

In addition, the influence of glaciation and permafrost coverage on the groundwater flow direction and magnitude will be considered.

1.6 REPORT OVERVIEW

The report is divided into the following further sections.

Section 2 introduces the definition of permafrost, permafrost hydrogeology and processes related to glacial recharged groundwater.

Section 3 summarises the case studies and model definition. The full description of the numerical model is given in Appendix 1 and the full description of model conceptualisation and choice of boundary conditions in Appendix 2.

The key results are presented in Sections 4 and 5, whilst the full results are described in Appendix 3 and Appendix 4. Section 4 focuses on the processes that influence the thickness and extent of permafrost, and Section 5 on simulations used to investigate groundwater dynamics. The model results are presented in a process-based approach combined for both geological cases, aiming to present the relative importance of different factors influencing permafrost depth and distribution, rather than describing case one and two separately. The two geological cases represent contrasting geologies; the first represents sandstones overlying a basement and the second describes a low permeability Jurassic sequence.

Section 6 compares the relevant factors and processes, and gives recommendations for further work. Complete model results are compiled in Appendix 6.

2 Permafrost Hydrogeology

2.1 DEFINITION OF PERMAFROST

The definition of *permafrost* is solely based on temperature; permafrost is defined as soil, unconsolidated deposits, and bedrock, in which temperatures below 0°C exist for two years or more (Williams, 1970).

As the definition of permafrost is solely temperature dependent, the occurrence of permafrost does not determine whether liquid water is present. Hence, there are two schemes to define cold ground: based on temperature (Figure 1, left) and the state of liquid water (Figure 1, right). Permafrost, or *perennially cryotic ground*, is defined as ground at, or below, a temperature of 0°C regardless of whether its water is in a liquid or frozen state. In contrast, *perennially frozen ground* refers to ground where most (>50%) of the soil water is frozen (Woo, 2012). Below the perennially frozen ground, there is a cryopeg, which has a temperature below 0°C , but with liquid water present (Woo, 2012).

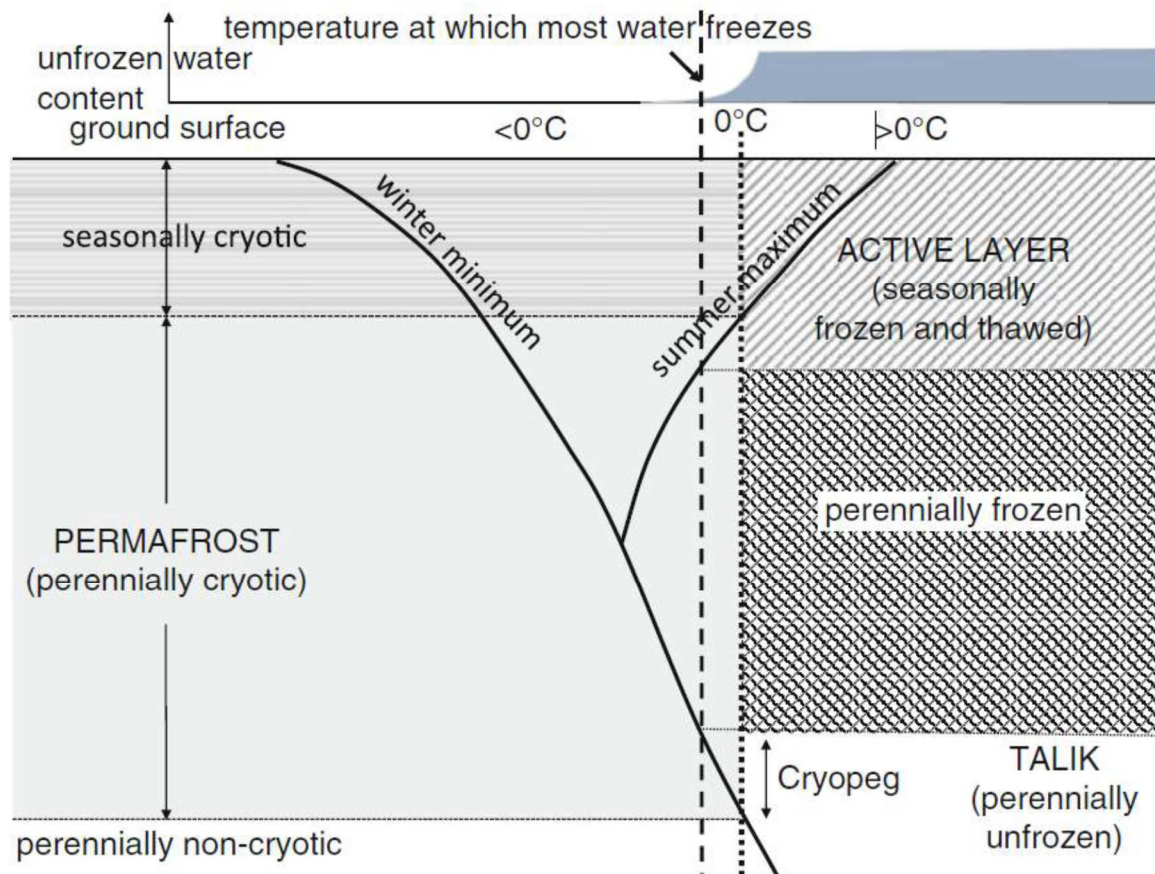


Figure 1. Definition of permafrost and associated features based on the intersection between the 0°C line and annual maximum and minimum ground temperature profiles. Frozen ground is defined on the basis of the intersection of the annual maximum temperature profile with the temperature of ice nucleation, which is usually $<0^{\circ}\text{C}$ and varies with soil type. After (Woo, 2012).

The active layer that overlays perennially frozen ground is subject to seasonal freeze and thaw conditions, and is deeper than the seasonally cryotic zone above the permafrost table, because of

the depression of the freezing point. The depression of the freezing point is a minor effect in the shallow active layer, but more important beneath glaciers and ice sheets. In discontinuous, or relict permafrost areas, the active layer and the perennially frozen layer may be separated by an unfrozen zone; an intra-permafrost talik (*Williams and Smith, 1989; French, 2007; Woo, 2012*).

The lower boundary of permafrost is referred to as the *permafrost base*. The cryopeg is the difference between the depth of the permafrost base and the base of the perennially frozen zone, which has a temperature below 0°C but with water remaining unfrozen (*Williams and Smith, 1989; French, 2007; Woo, 2012*).

The thermal regime of permafrost is different from that of unfrozen ground due to the influence of latent heat and a change of thermal conductivity. When water freezes, latent heat of fusion is released and ground temperatures remain initially around 0°C. This effect is called the "zero curtain" (*Williams and Smith, 1989; French, 2007*). The thermal conductivity of frozen ground is larger than that of unfrozen ground because the thermal conductivity of ice is approximately four times higher than that of water. Therefore, heat penetrates frozen ground faster than unfrozen ground (*Williams and Smith, 1989; French, 2007*). Because of this, this study defined permafrost as the sub-surface in which ice is present even in very small amounts, i.e. an ice content greater than 0%, equating the zero degree isotherm in the model. .

2.2 GROUNDWATER FLOW IN PERMAFROST

Perennially frozen ground acts as a low permeability barrier because the pore spaces are generally filled with ice within the zone of saturation. Ice- and water-saturation in permafrost are important for the groundwater flow because the hydraulic conductivity in frozen media decreases over the freezing interval by several orders of magnitude (*Kleinberg and Griffin, 2005*). However, as the definition of permafrost is only temperature dependent, liquid water content can occur at temperatures <0°C due to depression of the freezing point (*Williams and Smith, 1989*). Unfrozen water can be found below 0°C due to a high solute content shifting the freezing point to sub-zero temperatures, the surface tension effect attracting liquid water to fine particles, and hydrostatic pressure at depth or beneath an ice sheet depressing the freezing point (*Marshall, 2012*). As there is a distribution of pore size, freezing occurs over a temperature range where water and ice coexist. Generally, water in larger pores freezes before water in smaller pores, and smaller pores thaw before ice thaws in larger pores (*Ireson et al., 2013*). The very low permeability of permafrost hinders both recharge and discharge (*Williams, 1970; French, 2007*).

Generally, groundwater movement in permafrost covered regions follows the same physical principles as in permafrost free areas. For fully saturated fluid flow in porous media, groundwater movement is described by Darcy's Law. However, groundwater flow in permafrost covered areas is restricted to unfrozen zones, also called *taliks* (Figure 2). As shown in Figure 2, taliks occur in three different forms as supra-permafrost taliks, intra-permafrost taliks and sub-permafrost taliks (*Sloan and Van Everdingen, 1988; Woo, 2012*).

Bense et al. (2012) suggest that recharge in a thawing permafrost environment is not sufficient for advective heat flow to have a significant impact on permafrost degradation in a nested groundwater flow system. In contrast, advective heat flow can influence transient taliks, where geothermal heat flux anomalies occur, where flow is strongly focused, or where recharge is not limited by effective rainfall, such as glacial recharge. However, other studies have shown that permafrost thaw can be accelerated by advective heat transport. *McKenzie and Voss (2013)* find that during permafrost thaw groundwater first flows laterally above the permafrost, then flows downward below recharge areas, and when taliks fully penetrate the permafrost, groundwater passes from the surface through the permafrost to the sub-permafrost aquifer, transporting heat at a greater rate than by conduction only. The authors state that this thaw-flow feedback accelerates thawing, especially at early stages of permafrost thaw.

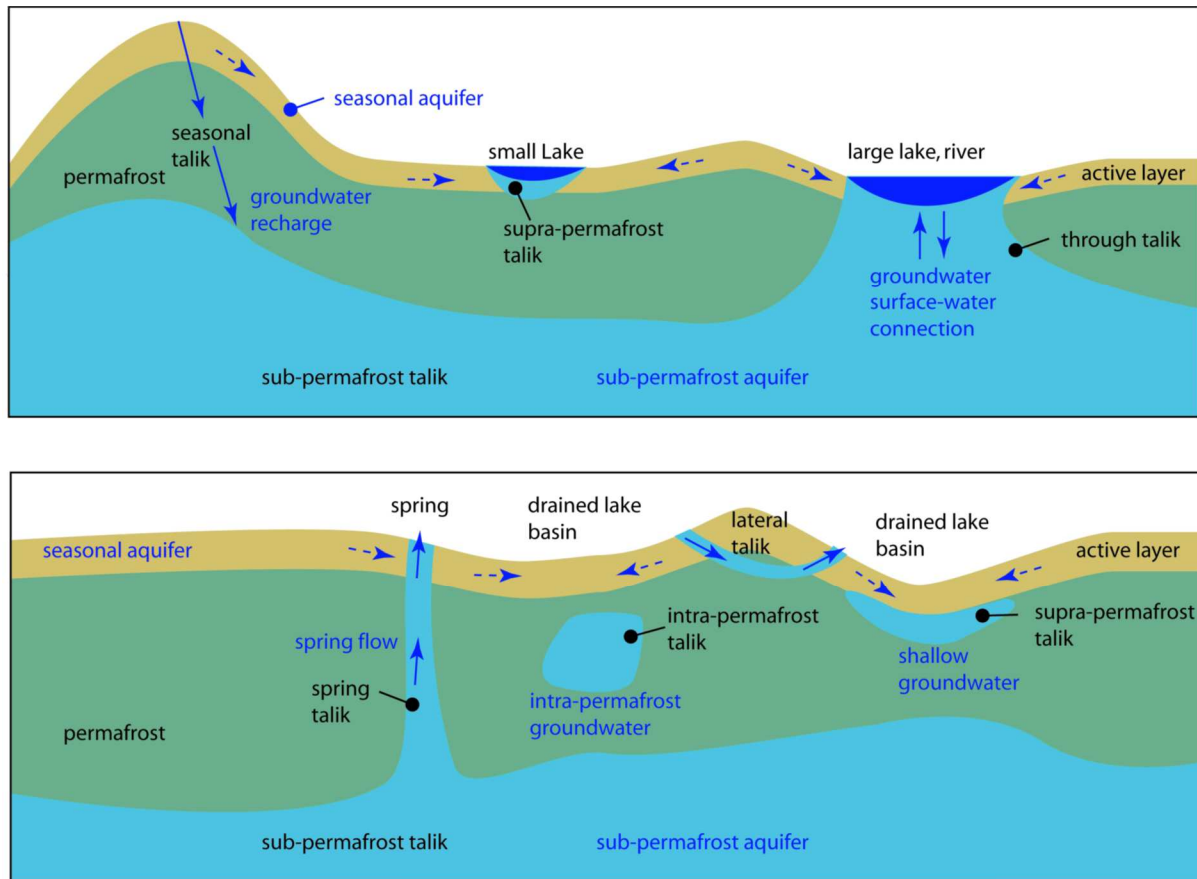


Figure 2. Taliks found under lakes, springs and drained lake basins, from Scheidegger (2013) and modified after Sloan and Van Everdingen (1988).

2.3 INFLUENCE OF GLACIATIONS ON GROUNDWATER FLOW SYSTEMS

Previous studies have suggested a large influence of glaciations on groundwater systems. For example, recharge rates across glaciated basins were as much as two to six times higher than modern rates and glacial meltwater penetrated to depths of hundreds of metres (*Person et al.*, 2012b).

Lemieux et al. (2008c) identify the following key processes for a large-scale (continental scale) groundwater flow system during glaciations, as shown in Figure 3. Subglacial processes are: recharge from a glacial meltwater source, isostatic depression and subglacial recharge. Periglacial processes include permafrost evolution, development of a forebulge, proglacial lake development and eustatic sea-level changes.

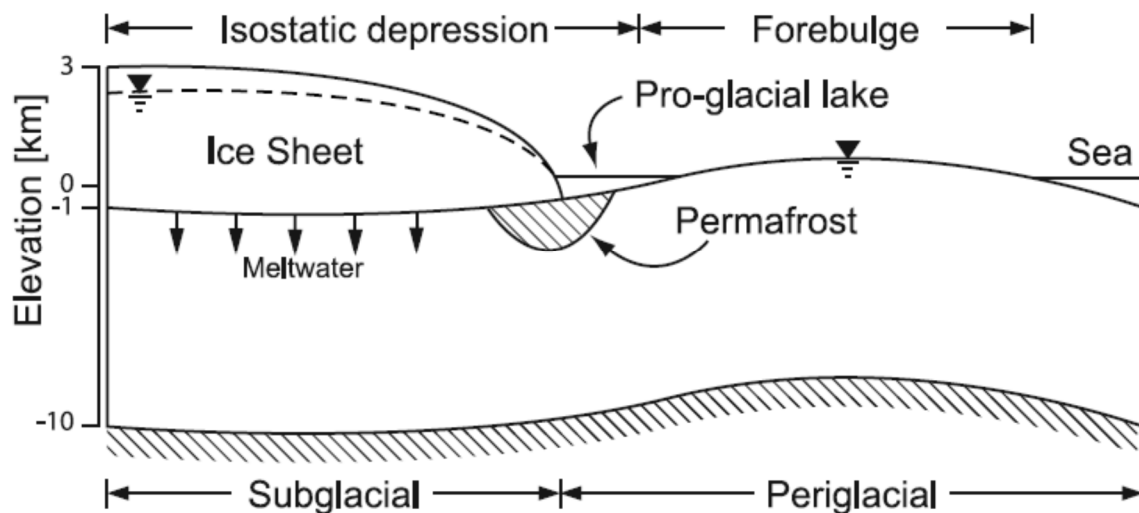


Figure 3. Cross-section along an ice flow line showing hydraulic conditions during a glacial cycle. The ice sheet is polythermal, with the marginal ice below melting temperature whereas the remaining glacier bed is at melting temperature. After Lemieux *et al.* (2008c).

Subglacial meltwater can recharge an aquifer when the glacier bed is wet-based, which means that subglacial water can either originate from in-situ basal melting or from surface melting during the melt season. The latter occurs from drainage from the surface to the ice base, through crevasses, moulins, or englacial drainage structures (Zwally *et al.*, 2002). Subglacial water leaves the glacier system through a combination of Darcian flow through the till, laminar flow through a water film at the ice bed interface (rare, only for unfractured crystalline rock surfaces) and through laminar or turbulent flow through conduits at the ice bed interface. Water discharges at the bed are generally too large to be discharged by groundwater flow only (Iverson and Person, 2012). Hydraulic heads can be near flotation ($\sim 90\%$ of the local ice sheet thickness for warm-based conditions where the ice is effectively floating on a sub-glacial layer of water) where the ice is underlain by a subglacial till with low permeability. High subglacial water pressures and melting result in much higher rates of groundwater recharge under temperate ice than during ice-free conditions (Provost *et al.*, 2012).

If perennially frozen ground underlies the glacial forefield, glacially recharged groundwater is forced under the permafrost (Person *et al.*, 2012a). Groundwater then discharges either near the ice sheet margin by hydrofracturing the sediments (Boulton *et al.*, 1993), into taliks under surface water bodies (Scheidegger and Bense, 2014) or at the sea (Boulton *et al.*, 1993).

In addition to hydraulic heads being near the ice overburden underneath the ice sheet, hydraulic heads are also influenced by the deformation of the Earth's surface. The weight of an ice sheet results in the deformation of the Earth's surface and the surface will be depressed below the ice sheet (isostatic depression) and raised distally, resulting in compressive stresses under the ice sheet and horizontal tensile stresses in the forebulge (Lemieux *et al.*, 2008c). This will affect the large-scale groundwater flow system by lowering the hydraulic potential under the ice sheet and increasing it in the forebulge (Lemieux *et al.*, 2008c). In the margins in the isostatic depression, proglacial lakes form. In addition, compaction of the geologic medium can reduce both the porosity and the hydraulic conductivity, and can increase pore pressure (Lemieux *et al.*, 2008c).

The loading efficiency of the rock matrix determines how the ice load is apportioned between the rock and pore fluid (Neuzil, 1995). Changes in external loads can be accounted for by the addition of a simple source-type term to the fluid mass balance equation. However, it should be

noted that the 1D vertical loading concept is only valid during symmetric conditions, and this assumption is not valid where vertical loads vary significantly, as expected near the margin of an advancing or retreating glacier (*Vidstrand et al.*, 2010). The magnitude of the error caused by using 1D loading efficiency has not been investigated (*Neuzil*, 1995; *Lemieux et al.*, 2008c).

The existence of brines in deeper parts of the aquifer and flushing of cold and fresh, glacially recharged groundwater results in large density differences in the waters. Pressure gradients along an ice sheet profile or transient changes in pressure will drive recharge or discharge into the subglacial aquifer. Therefore, fluid flow is also driven by buoyancy forces caused by solute concentration, temperature and pressure in the bedrock (*Lemieux et al.*, 2008c; *Provost et al.*, 2012).

Person et al. (2012b) point out that the initial salinity conditions used in palaeohydrological models are difficult to constrain accurately and that it is likely that salinity conditions in sedimentary basins are never in equilibrium with present-day climate forcing. However, when simulating impacts like that of a past glaciation the final results should be comparable with the present day salinity distribution, or else the initial conditions or boundary conditions were incorrectly assigned. For Forsmark it has been found that the initial salinity conditions are more or less restored after a complete glacial cycle and that the observed water chemistry can be simulated (*Vidstrand et al.*, 2014).

Eustatic sea-level fluctuations occur due to the increased volume of water stored in the ice sheets and modify the location of the sea shore (*Lemieux et al.*, 2008c). This means that the hydrogeological base level is modified over time.

3 Case studies and model definition

3.1 NUMERICAL MODEL

Coupled permafrost and groundwater models have been developed using the advection diffusion equation including latent heat of fusion to model permafrost and the groundwater flow equation as shown in Appendix 1. Groundwater flow is coupled to the permafrost model by using a hydraulic conductivity that is several orders of magnitude lower in frozen conditions than under unfrozen conditions and through a source term that is related to volume changes between ice and water. Heat flow is coupled to groundwater flow through the advective heat flow term, which is proportional to Darcy flow. The equations are solved within COMSOL Multiphysics mathematical modelling environment (COMSOL, 2016). Details of the numerical model are provided in Appendix 1 and the model is benchmarked against analytical solutions and other TH codes in Appendix 5.

3.2 MODELLED LOCALITIES AND MODEL CONCEPTUALISATION

3.2.1 Model localities

The localities used in this study are conceptual and hypothetical geological environments relevant to the UK, however their parameterisation is based on Environment 2 and Environment 5 described in *Towler et al. (2008b)*. These environments represent possible locations for a GDF on the UK mainland and are generic representations of geology and hydrogeology. It should be noted though that the environments have been modified slightly from *Towler et al. (2008b)*; the model domains for both environments have been extended to include an upstream water divide, any faults have been removed, and the hydrogeology characterised as topographically-driven systems that do not take into account variations in density or viscosity due to temperature or salinity.

Environment 2 in *Towler et al. (2008b)* is referred to here as Case 1, and describes a basement under sedimentary cover (BUSC) located on the margin of a Permo-Triassic sedimentary basin (Figure 4). The hydrogeology is characterised by a very shallow groundwater system within the drift deposits, a shallow fresh system in the uppermost 50-100 m, and a deeper, relatively stagnant system in the basement rocks. The groundwater flow in the basement rocks is influenced by dense brines that are derived from evaporite deposits offshore. In the host rock, fracture flow is dominant and in the sedimentary cover rocks matrix flow is dominant (*Towler et al., 2008b*). During the last ice age, the Case 1 environment was ice-covered (*Chiverrell and Thomas, 2010*).

Environment 5, referred to here as Case 2 (Figure 5), is based on a type of geological setting found in the east of England and consists of Lower Jurassic shales and mudstones and Triassic mudstones and siltstones, dipping uniformly to the east. The environment has a very low topographic relief and is hundreds of kilometres from the nearest areas of significant topography. During the last glacial maximum this locality was at the margin of the ice sheet. There are two aquifers within the sequence that influence the environment, the Mid-Jurassic limestone aquifer and Triassic sandstones. The Cretaceous Chalk aquifer in Case 2 is submerged. The other formations consist of mudstones, and siltstones. The upper part of the sequence has been modelled by *Towler et al. (2008a)*, however, in this study, the model thickness has been extended to a greater depth and captures the full lateral extent of the outcrop of the Permian basin. Because of the low hydraulic gradient, the flow rates in the higher permeable zones are suggested to be low (*Towler et al., 2008b*).

3.2.2 Model set-up

3.2.2.1 CASE 1

The model set-up is shown in Figure 4. The model domain is 20 km long and 2 km deep. The right hand boundary is closed to heat flow (red) and to fluid flow (blue), as this represents a topographic high and potential groundwater divide. The left hand boundary is a specified head to represent the sea and a flux boundary for heat flow. This means that groundwater and heat can enter and leave the system. At the top boundary, the hydraulic head is set to the elevation of the land-surface and the temperature is specified in time. The base of the model is closed to fluid flow and heat flow is specified, allowing heat to enter the model domain by heat conduction. The layers used for Case 1 are a basement, overlain by a lower and upper sandstone, and a weathered layer, - the thermal and hydraulic properties used for the different layers are taken from *Towler et al.* (2008b) and listed in Table 3. The model domain is characterised by a higher ground near the right hand boundary, followed by a steeper slope (10-20 km of the model domain). The left hand side of the model domain (0-10 km) is characterised by lowlands and the topography is characterised by three hills (at 1 km, 5 km and 9 km and of 2 m, 10 m and 18 m height) and topographic depressions (at 3 km, 7 km, 11 km of 6 m, 14 m and 18 m depth). The thermal and hydraulic properties used for the different geological layers are from *Towler et al.* (2008b) and listed in Appendix 2, Table 3.

For the Case 1 model including glaciation, the model domain had to be extended. As a starting point, the model geometry of Case 2 was used (see below), however using the thermal and hydraulic properties of Case 1.

3.2.2.2 CASE 2

The model set-up is presented in Figure 5. The model domain is 300 km long and 1500 m deep. For fluid flow, hydraulic head is assigned at the top boundary and is set to the elevation of the topography. The sides and the base of the model are no-flow for fluid flow. For temperature, the ground surface temperature is assigned at the top boundary, and heat flow is specified at the base. The sides of the model are closed boundaries. The thermal and hydraulic properties used for the different geological layers are from *Towler et al.* (2008b) and are listed in Appendix 2, Table 4.

3.2.3 Model drivers

The model is driven by the surface temperature time series, and the hydraulic head at the ground surface. The temperature and hydraulic head are altered when covered by an ice sheet or submerged.

The surface temperature time series is scaled from a Pliocene-Pleistocene stack of 57 globally distributed benthic $\delta^{18}\text{O}$ records with 1 ka temporal resolution (*Lisiecki and Raymo, 2005*). The model is forced with different scaling of the surface temperature time series, in which the minimum temperature over the last one million years is set between 10°C and 25°C below the present day temperature (set to 8.5°C mean UK temperature from 1910-2009). The temperature difference between present day temperature and the minimum temperature in the temperature time series is set in the model name, e.g. the model T-14 refers to a model in which the minimum temperature is 14°C below the present day temperature. When the surface is covered by an ice sheet, the local temperature is altered to a subglacial temperature. For the coupled models, warm based subglacial temperatures are assigned and for simplicity set to T=0°C. When the land-surface is submerged, then the surface temperature is set to 7°C to prevent freezing.

Hydraulic head is set to be topography driven, where the hydraulic head at the surface set to be at the elevation of the land-surface. When the surface is ice covered, then the local ice overburden

is added to the land-surface elevation. When the land-surface is submerged, the hydraulic head is set to the elevation of the shore position.

More details of model boundary conditions and modelling methodology are found in Appendix 2.

3.2.4 Modelling assumptions and limitations

The modelling presented in this study uses the generic Cases 1 and 2 and boundary conditions as described above with the following assumptions and limitations.

- For the hydrogeology, fully saturated, topography-driven flow was assumed, for which the hydraulic head at the top boundary was set to the land-surface elevation. This is a simplification of the real world hydrogeology; however in a temperate climate the groundwater table is close to the land-surface. To date, the majority of codes use the assumption of fully saturated, topography-driven flow. Codes that include variably saturated fluid flow (e.g. permaFoam (*Orgogozo et al.*, 2014), or PFLOTRAN (*Karra et al.*, 2014)) are massively parallel codes and consider short time and/or small spatial scales. An increase in model complexity with the addition of variably saturated flow adds further uncertainties with the characterisation of freezing curves and relative permeability curves. Therefore, the assumption of fully saturated flow over the time scales of millennia is fully justified here.
- A further limitation to the groundwater flow system is that buoyancy driven flow was not considered. The influence of temperature or salinity on density and viscosity were not considered in this work. However, for further assessment the impact of brines will need to be included into the groundwater model.
- The scaled temperature time series are assigned to the model at the upper boundary. Therefore thermal effects at the ground-atmosphere boundary were not considered, e.g. effects of soil, vegetation, and snow cover. Furthermore, one freezing curve and relative permeability curve are used for all layers.
- The model domains were simplified to 2D cross sections, and the model domain and topography did not change over one million years. No erosion or deposition was included in the model. Also, thermal, hydraulic and geological properties did not change over one million years, e.g. permeability and porosity remain unchanged after a glaciation.
- The ice sheets are treated as a boundary condition and the ice sheet dynamic is not solved for explicitly in the model. Therefore the ice sheets are treated as follows: the pressure underneath the ice sheet is set to the ice overburden and the basal temperatures are assumed to be constant over time. For the 2D coupled models, the basal temperature is assumed to be at pressure melting, here set to 0°C. Further, deformation of the model domain due to isostatic depression and forebulge is not considered.

Theoretical geological environments are used and not actual sites, and thus no glacial models are present.

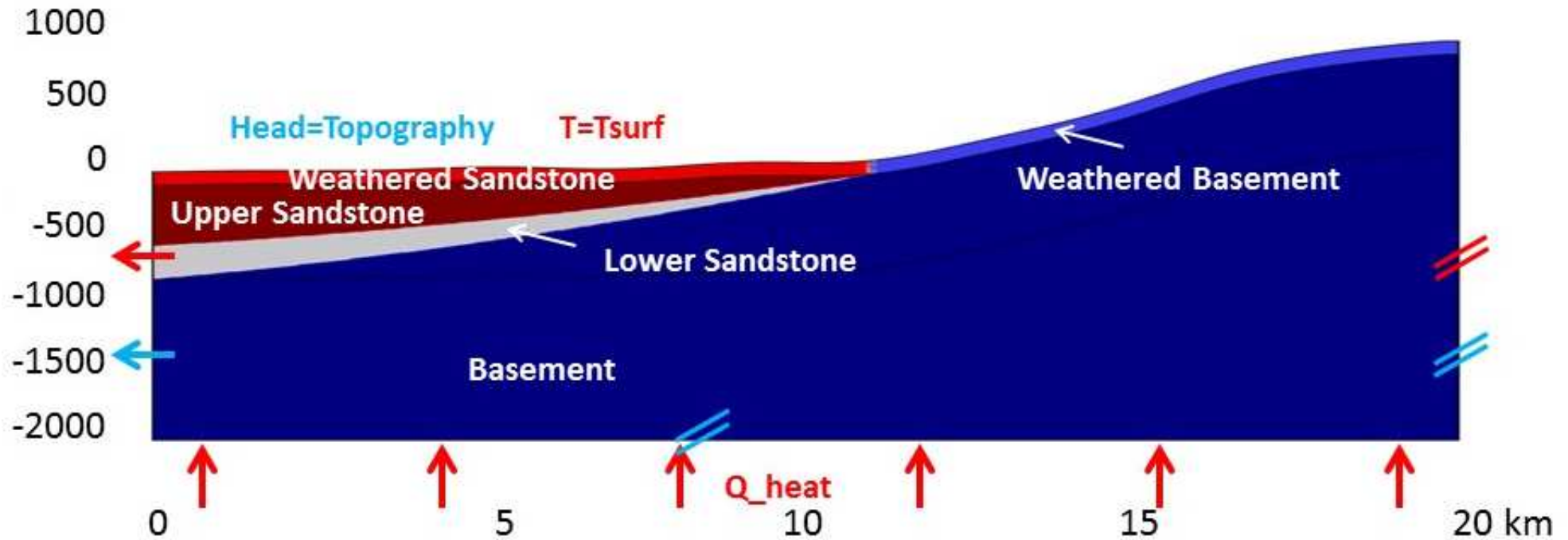


Figure 4. Model set-up and boundary conditions for Case 1. The boundary conditions in blue correspond to hydraulic head and those in red to temperature. At the surface, hydraulic head is set to the topography, and the temperature to a temperature time series. The right hand side of the model is closed to heat and fluid flow. At the left hand side of the model, as specified hydraulic head is applied and is open to heat flow. The base of the model is closed to fluid flow, and a constant heat flow is applied. The scale of the vertical axis is exaggerated by a factor of 2.

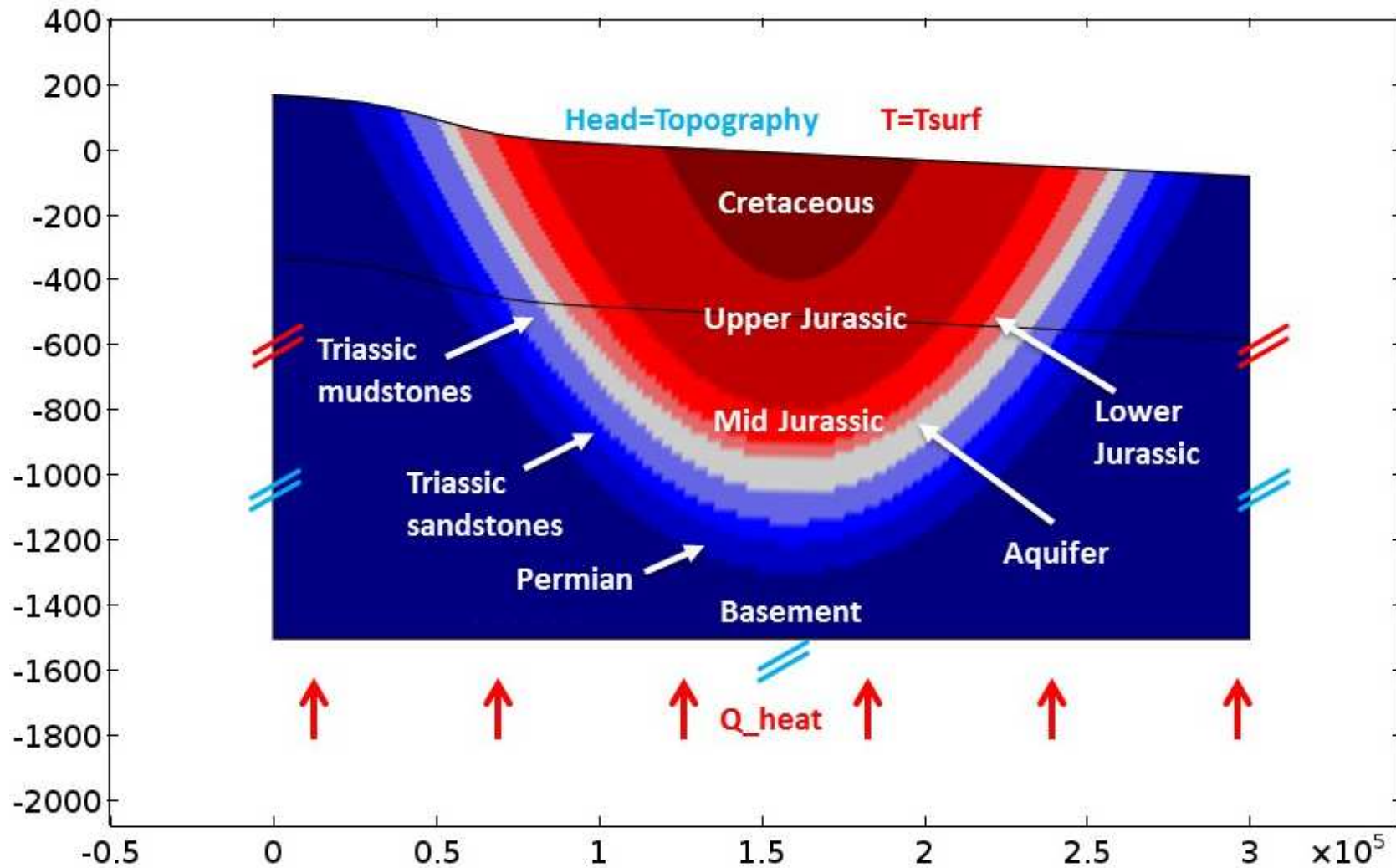


Figure 5. Model set-up and boundary conditions for Case 2. The boundary conditions in blue correspond to hydraulic head and those in red to temperature. The scale of the vertical axis is exaggerated by a factor of 100.

4 Factors and processes influencing the thickness and extent of permafrost in a geological environment

4.1 TEMPERATURE

4.1.1 Steady state vs transient model

If the climatic conditions were unchanging and mean annual ground surface temperatures were below freezing, the permafrost thickness would reach a steady state. This means that the permafrost thickness is in equilibrium with the climate and the maximum permafrost thickness is reached for the climate scenario. Comparison of a 1D transient model with a steady state model at nine locations with contrasting thermal properties and heat flows gives a maximum difference of 165 m for a minimum temperature of -5.5°C (detailed results in Appendix 3). The steady state permafrost thickness is deeper than the maximum permafrost thickness from the transient model runs, ranging from 87 m to 487 m, compared to 77 m to 320 m. Therefore, assuming the temperature oscillations from the past one million years, results from modelling show that a steady state permafrost thickness did not have time to occur in Great Britain.

4.1.2 Sensitivity of the scaling of the temperature time series

The generation of the temperature time series is one of the main uncertainties for estimating the permafrost thickness over the last glaciation, or even over the past one million years. For the last glaciation, *Annan and Hargreaves* (2013) have compiled a dataset based on a combination of numerical models and pollen temperature proxies. For southern England and Wales temperatures are estimated to be $8\text{-}12^{\circ}\text{C}$ below present, and for northern England and Scotland $12\text{-}20^{\circ}\text{C}$ below the present day temperature. In contrast, *Westaway and Younger* (2013) reconstructed a temperature difference to the present day temperature for southern England of 20°C , and for northern England of 18°C .

In order to address uncertainty in the LGM temperature estimation a range of temperature scenarios are used, ranging from a ΔT between present day and minimum temperature of 10°C to a ΔT of 25°C .

The maximum permafrost thickness for the 1D model of Case 1 ranges between 49 m for a ΔT of 10°C and 475 for a ΔT of 25°C , as shown in Figure 6. For Case 2, the maximum permafrost thickness ranges between 80 m and 238 m for a ΔT of 14°C (T-14) and ΔT of 25°C .

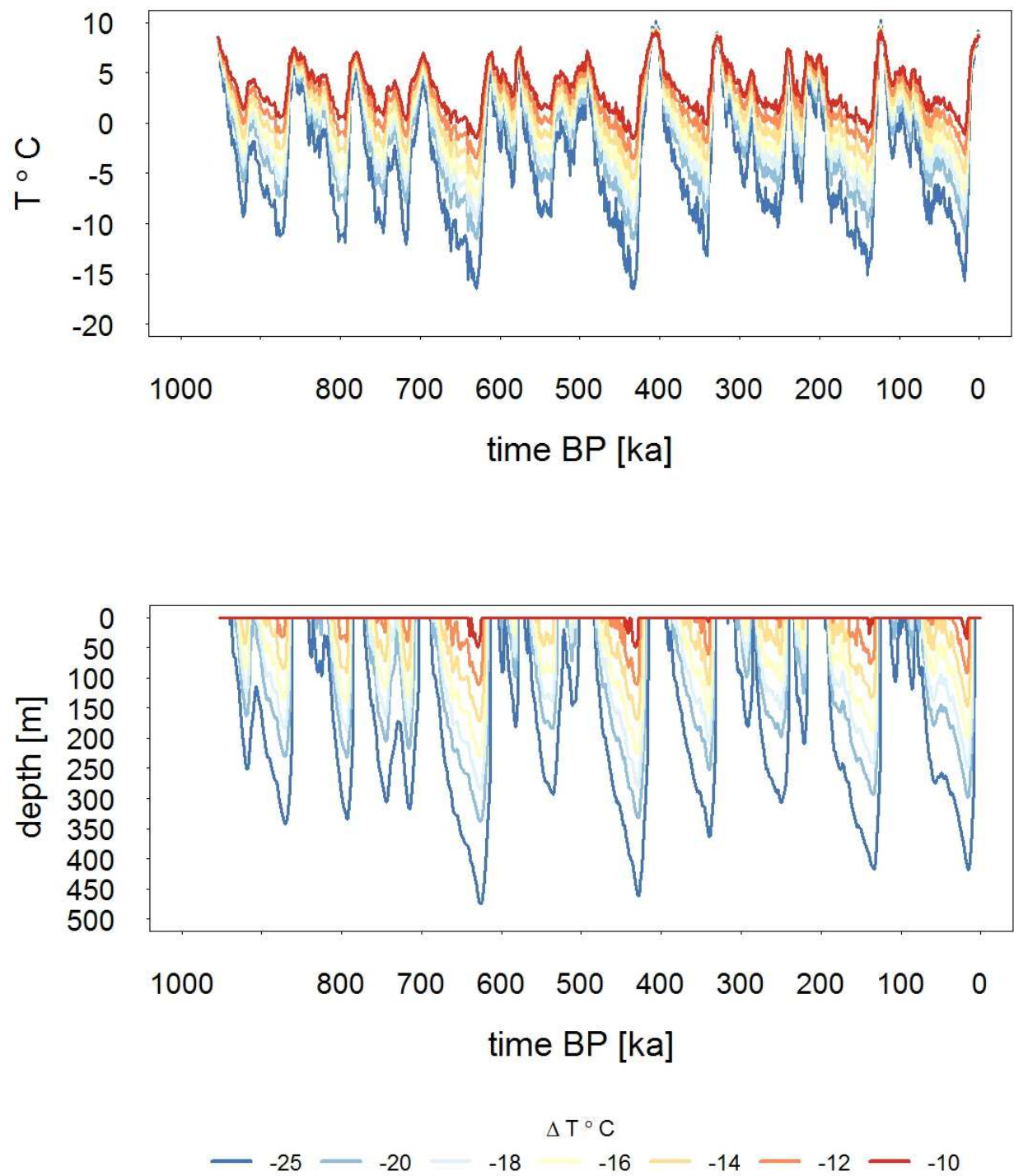


Figure 6. Permafrost thickness for Case 1 (lower plot) using temperature time series (upper plot) that are scaled between 10 and 25 °C below the present day temperature.

4.1.3 Correction of the temperature time series for ice cover and its influence on permafrost thickness

The timing of a glaciation and the associated temperature correction for ice cover has a large influence on the permafrost thickness. Constant subglacial temperatures of 0°C, -1°C and -5°C were assigned for both the maximum ice coverage and medium ice coverage conditions for the temperature scenario of T -14°C for Case 1. The definition of the glaciation scenarios is given in Appendix 2, Figure 26.

The permafrost time series for all scenarios are presented in Figure 7. The maximum thickness of permafrost ranges between 100 m and 177 m, depending on the glaciation scenario for the T-14 temperature scenario for Case 1. However, the insulation of a glacier can result in no permafrost whereas under non-glaciated conditions permafrost thickness would be several hundred metres.

The difference in permafrost thickness caused by the insulating effects of an ice sheet for Case 1, with a temperature scenario of T-14, ranges between -71 m and + 6 m. If a warm-based ice sheet is assumed, the ground surface temperatures are insulated from the air temperatures and there is a reduction in permafrost thickness. However, if cold based ice is assumed, ice coverage might lead to an increase in permafrost thickness compared to the base-case scenario (unglaciated).

It is important to note that basal ice sheet temperatures vary spatially and temporally, so when modelling a specific site, output from an ice sheet model could improve this first estimation of permafrost thickness.

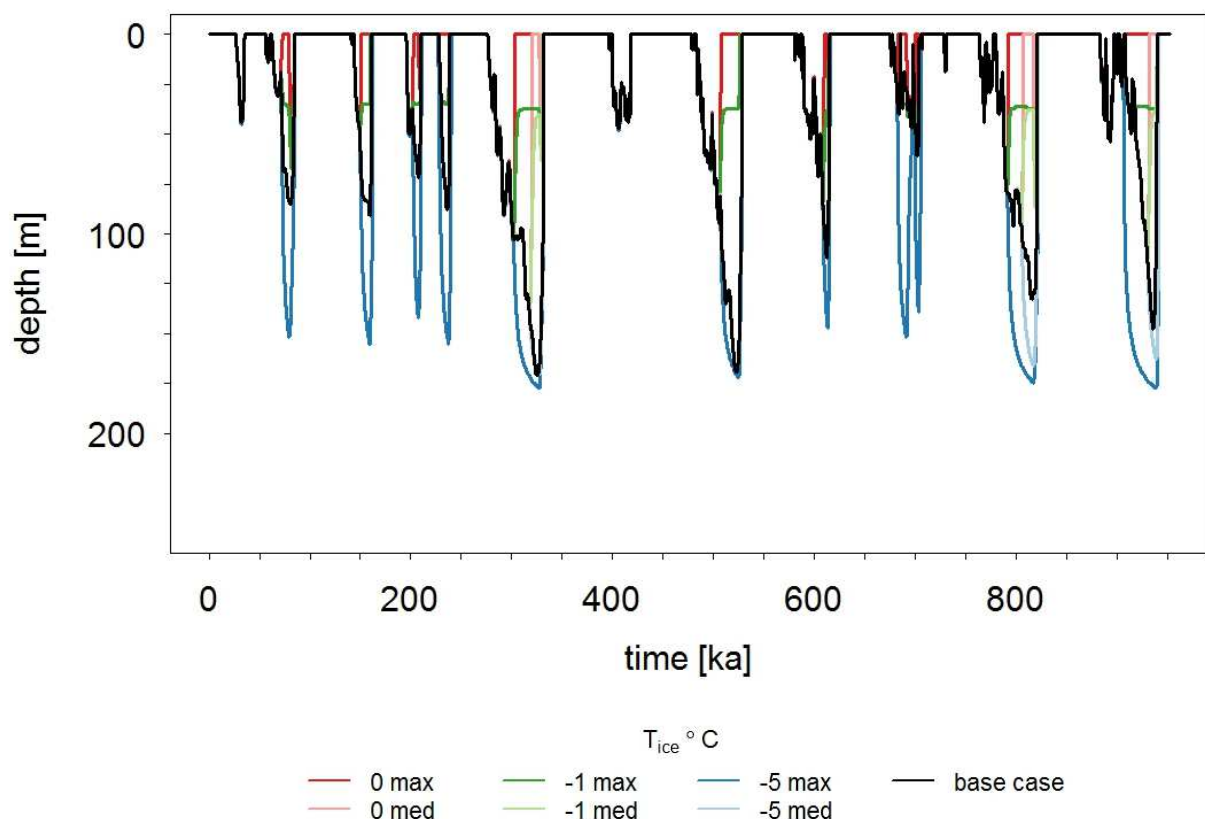


Figure 7. Permafrost thickness for different glaciation scenarios. “max” refers to a maximum glaciation scenario and “med” refers to the medium glaciation scenario after Boulton and Broadgate (1993). The base case is for an unglaciated scenario.

4.2 GEOLOGICAL VARIABILITY

- The thickest permafrost is to be expected where there is a low heat flow, a high thermal conductivity and a low porosity.
- The influence of thermal and geological properties on the permafrost thickness is non-linear and the relative importance of different parameters is related to the magnitude of other parameters.
- The largest ranges in permafrost thickness were simulated when thermal conductivity and heat flow (0 to 400 m) were modified, followed by porosity (0 to 300 m).
- Mass heat capacity and density have been found to be of minor importance in influencing the maximum permafrost thickness, with maximum ranges of 30-40 m.
- The largest variability in permafrost thickness due to porosity is associated with low heat flow and high thermal conductivity.
- The greatest influence on permafrost thickness due to heat flow is high thermal conductivity and low porosity.
- The most significant change in permafrost due to thermal conductivity is associated with low porosity and low heat flow.

A detailed analysis of geological variability is found in Appendix 3.

4.3 INFLUENCE OF ADVECTIVE HEAT FLOW ON THE THICKNESS AND DISTRIBUTION OF PERMAFROST

The influence of heat advection on the modelled permafrost distribution depends on the permeability of the rock, the thickness of the permafrost and the relative permeability function used. The relative permeability of permafrost in the model is $k_{rw}=10^{-S_i*\Omega}$, where S_i is the ice saturation and Ω a fitting parameter, and the function is described in Appendix 1, Equation 16. In Case 2 the permeability of the rock is low and heat advection has a negligible influence on the permafrost thickness. In contrast, for Case 1, in which the geology is more highly permeable in the weathered layers and the sandstone, the influence of heat advection on the permafrost thickness is modelled to be up to several tens of metres when the relative permeability of permafrost is low, or up to 100 m when the relative permeability of permafrost is higher (Figure 8). At interfluves, permafrost thickness, including the effects of heat advection, is simulated to be thicker than under a conduction only scenario (location 9 km). In contrast, at discharge points, permafrost is simulated to be thinner than under a conduction only case (location 7 km). Advective heat flow is simulated to thaw permafrost beneath the topographic lows and to develop permafrost beneath topographic highs. Generally, the influence of heat advection is modelled to be largest when permafrost is shallow and less when permafrost is deeper, as with deeper permafrost the regime changes from advection dominated to conduction dominated.

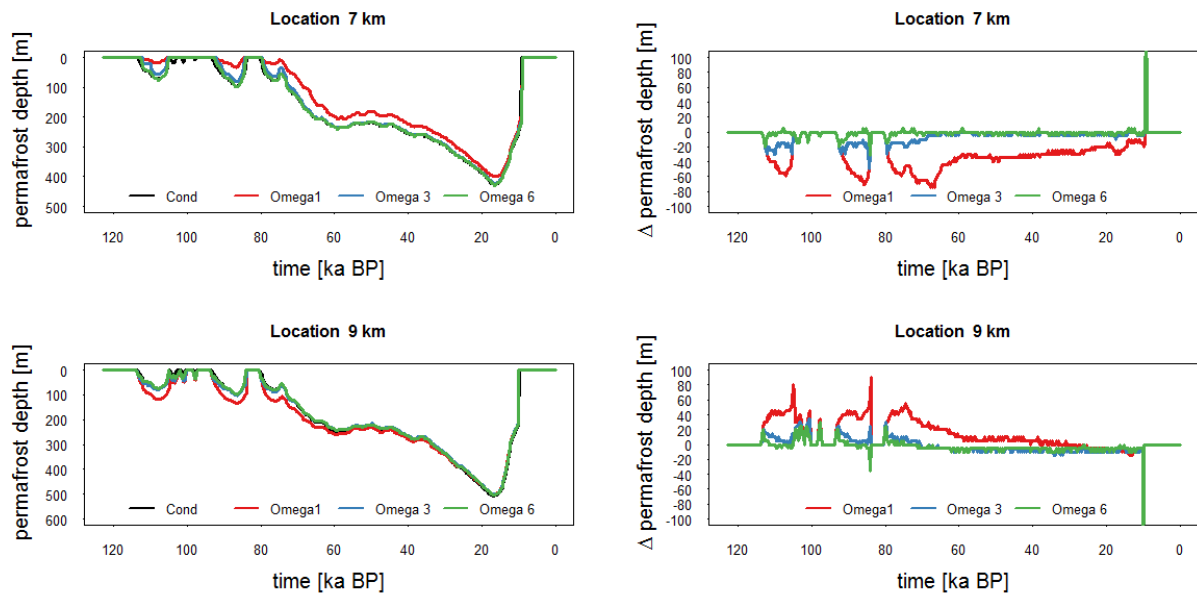


Figure 8. Permafrost thickness time series for the T-25 temperature scenario for Case 1 using a heat conduction (C) only and conduction-advection (CA) models using a minimum ($\Omega=6$), medium ($\Omega=3$), and maximum ($\Omega=1$) permafrost permeability scenario. The left hand plots show permafrost depth and those on the right hand the difference between the two types of models (C-CA). Location 7 km and 9 km refer to the distance of Figure 4.

Comparison of permafrost simulations with different relative permeabilities shows that in permafrost with a higher relative permeabilities, advective heat flow can result in a non-uniform permafrost distribution, with thinner or no permafrost at locations where warm water is discharging, and thicker permafrost where cold water is downwelling (Figure 9). This results in thicker permafrost at interfluves and thinner permafrost at discharge points compared to a conduction only case.

As recharge decreases across the model domain due to the low permeability of the permafrost, and groundwater is allowed to discharge through the left hand boundary, the hydraulic heads underneath the permafrost drop substantially to values around zero, or slightly negative (Figure 9; upper plot). If permafrost is modelled to be more permeable ($\Omega=1$) recharge decreases less, and higher hydraulic heads than for the less permeable permafrost case ($\Omega=6$) can be maintained underneath the permafrost, enabling groundwater to flow underneath the permafrost.

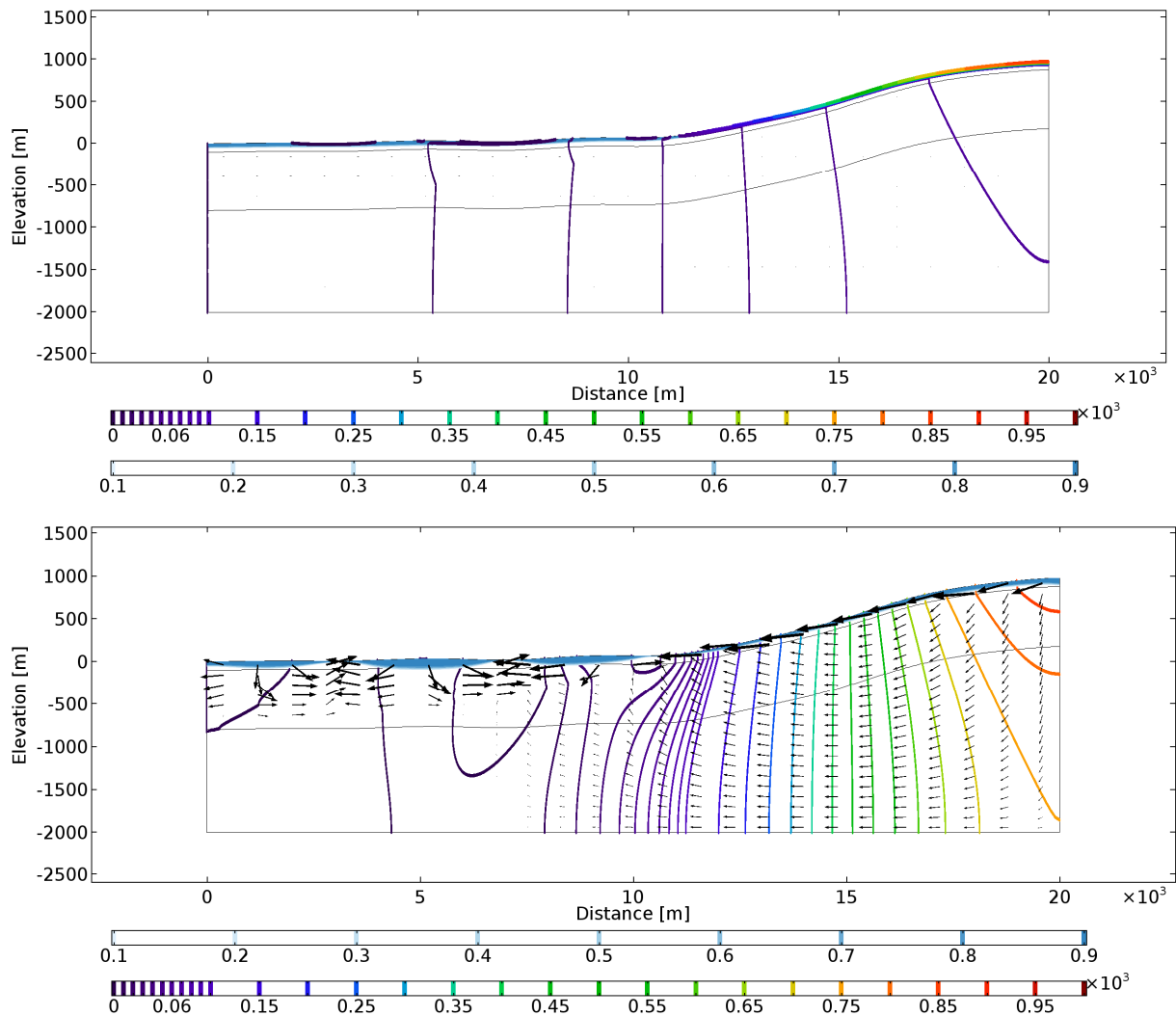


Figure 9. Comparison of permafrost distribution at 74.75 ka BP for the T-25_Max models using $\Omega=6$ (above) and $\Omega=1$ (below). Hydraulic head (spectrum contours), ice saturation (blue fill) and groundwater flow vectors are presented. For the model using $\Omega=6$ (above), the low permeability at the surface results in a reduction in recharge, and hydraulic heads underneath the permafrost drop as a consequence. For the model using $\Omega=1$ (below), the permeability only decreases by one order of magnitude and recharge decreases less than for the $\Omega=6$ case, maintaining an active groundwater flow system underneath the permafrost and discharging at topographic lows, where taliks form as a result.

4.4 COMPARISON OF MAXIMUM PERMAFROST THICKNESS AND FROZEN DEPTH FOR THE COUPLED MODELS DEPTH FOR CASE 1 AND CASE 2

In this report, permafrost has been defined as the sub-surface in which ice is present even in very small amounts, i.e. ice content is greater than 0%, which is at the 0 degree isotherm. As a large proportion of the permafrost can be unfrozen or consisting of a low ice saturation, it is important to differentiate between permafrost depth and the frozen depth. Figure 10 compares the permafrost definition of this report (>0% ice saturation) with the 50% ice saturation and 95% ice saturation (which is the maximum ice saturation in the model). The difference for the maximum permafrost between the three ice saturations is given in Table 1. The difference varies between the Cases; for Case 1 the difference between the permafrost definition of this report and full ice saturation is 30 m and for Case 2 it is 20 m. For the maximum permafrost thickness the temperature scenario does not seem to impact this difference. Temporally, this difference is larger; when thawing occurs after a permafrost event, then a large part of the subsurface in the model is partially frozen.

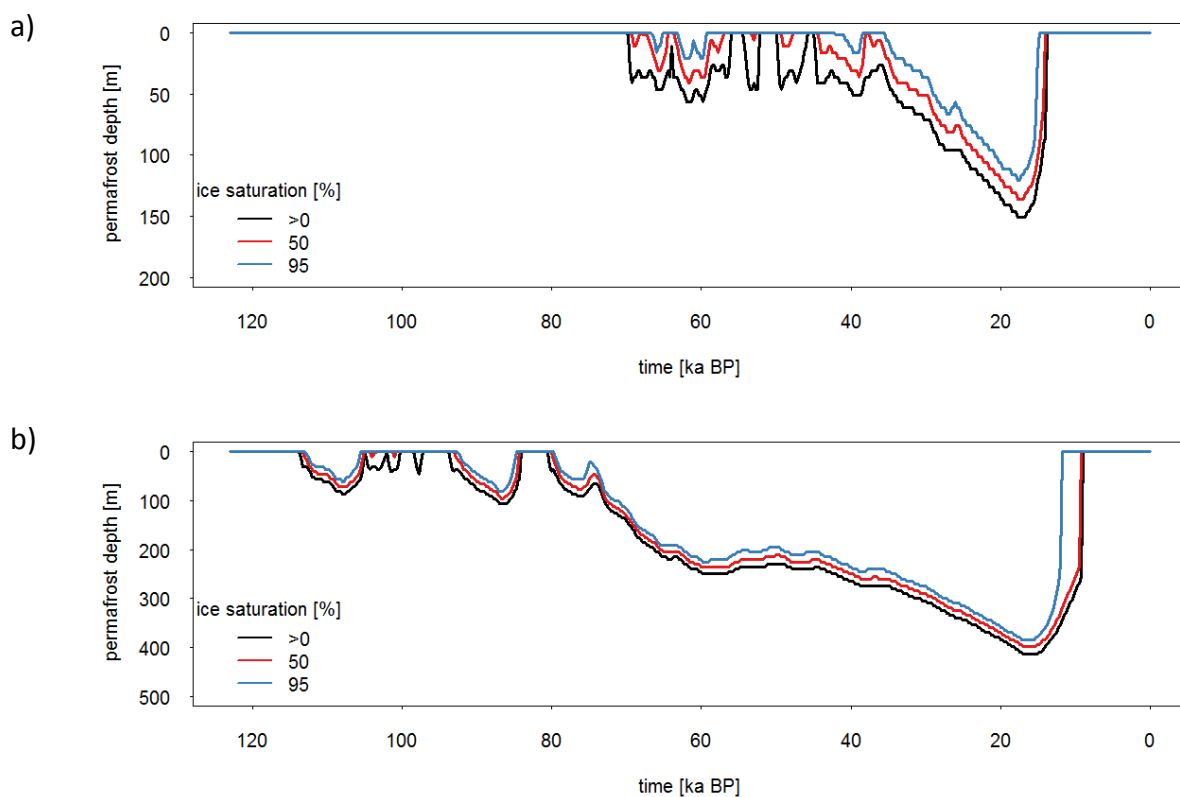


Figure 10. Lines of equal ice saturation for Case 1 at 5 km from the left hand boundary for a) the T-14_max and b) T-25_max temperature scenario.

Table 1. Maximum depths of >0, 50 and 95% ice saturation for Case 1 at 5 km from the left hand boundary and Case 2 at 80 km from the left hand boundary.

| ice saturation/ T scenario | Case 1 | | Case2 | | |
|-------------------------------|--------|------|-------|------|------|
| | T-14 | T-25 | T-14 | T-18 | T-25 |
| >0% | 151 | 414 | 79 | 138 | 237 |
| 50% | 136 | 399 | 69 | 128 | 227 |
| 95% | 121 | 384 | 59 | 118 | 217 |

4.5 SURFACE WATER BODIES

Surface water bodies can insulate the ground locally from the sub-zero air temperature and can prevent the subsurface directly below them from freezing, or they can cause permafrost to thaw locally if they form when permafrost is present. The unfrozen zones, taliks, can penetrate the entire thickness of the permafrost (Figure 11), or an upper part of it. These taliks provide pathways for groundwater flow and can alter the influence of heat advection compared to a case for which there is no thermal disturbance at the surface. During periods of permafrost, advective heat flow can be more important when through-taliks are present than when the entire surface is frozen.

A model was constructed that incorporates taliks based on the set-up for Case 1. Within this model the temperature is set to 4°C in three zones of 200 m width. In the talik model (T_14_Talik), the taliks remain open during the entire simulation. For cases when there is thick permafrost, the modelled surface fluxes remain high in the taliks. At the location of the lake, approximately ~11 km relative to the left-hand boundary, the groundwater flux is higher than under unfrozen conditions, as groundwater is focused from the area of steeper slope (Figure 11).

During thaw the discharge at the valley bottom is larger for the model without surface water bodies. For the T-14_Max model, discharge is focused at only one location at the foot of the steeper slope, whereas for the talik model discharge is distributed at the locations of the three surface water bodies (See Appendix 3 for detailed results).

If a GDF is placed below a surface water body under which a talik remains open over the entire duration of a cold period, the location of the GDF might still be hydrogeologically active, and groundwater flow magnitudes could potentially be higher within the talik than under unfrozen conditions, as observed at the lake at 11 km relative to the left hand boundary (Figure 51). Therefore, recharge and discharge rates will be focused on the locations of the taliks, which can lead to high local groundwater flow rates.

Note, however, that the lifecycle of lakes is likely transient over space and time, and their location and timing and lake bed temperature from a lake model could be used as an input. This would imply that taliks would not form at the same location over several glaciations.

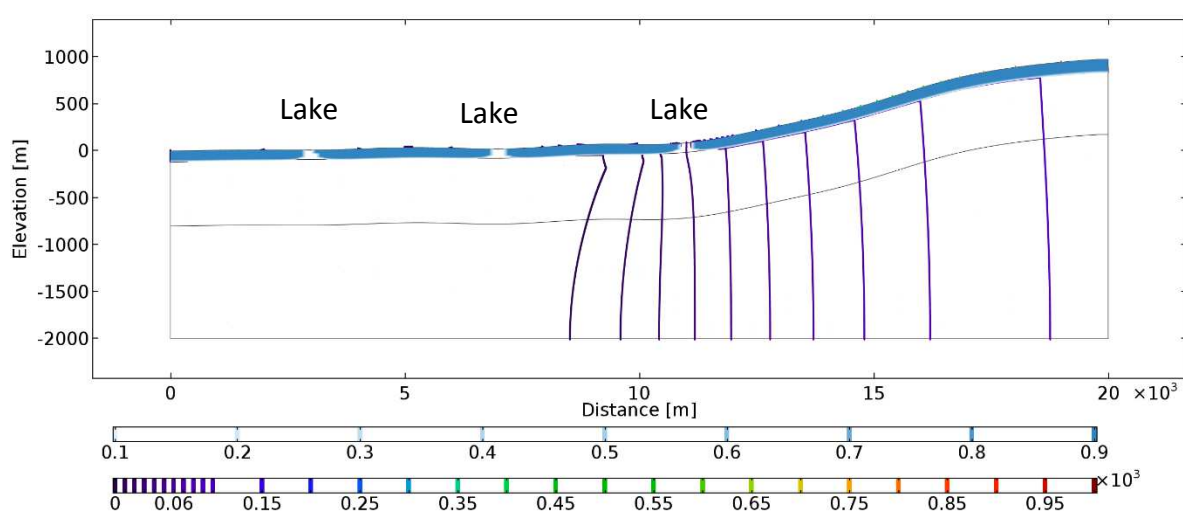


Figure 11. Permafrost and hydraulic head distribution at 21.75 ka for a scenario with lakes at topographic low places. Hydraulic head (spectrum contours), ice saturation (blue fill) and flow vectors are presented.

5 Influences of periglacial and glacial conditions on the groundwater flow system

5.1 PERIGLACIAL INFLUENCE ON THE GROUNDWATER FLOW SYSTEM

When the model domain is unfrozen, groundwater flow in the model is heavily influenced by the topographic gradient and the permeability of the weathered layer. When permafrost forms at the surface, recharge and discharge decrease as a result of the reduction in permeability related to the permafrost permeability function. When permafrost is set to be at a very low permeability, both recharge and discharge decrease to near zero (in this study they decrease by six orders of magnitude, $\Omega=6$). In contrast, when permafrost is set to be more permeable (here: decrease by one order of magnitude, $\Omega=1$), discharge focusses on topographic low places, preventing permafrost from forming there and taliks developing at these location. Under such occasions, discharge at the topographic depressions can be higher than under unfrozen conditions for Case 1 for the T-25 scenario (Figure 12).

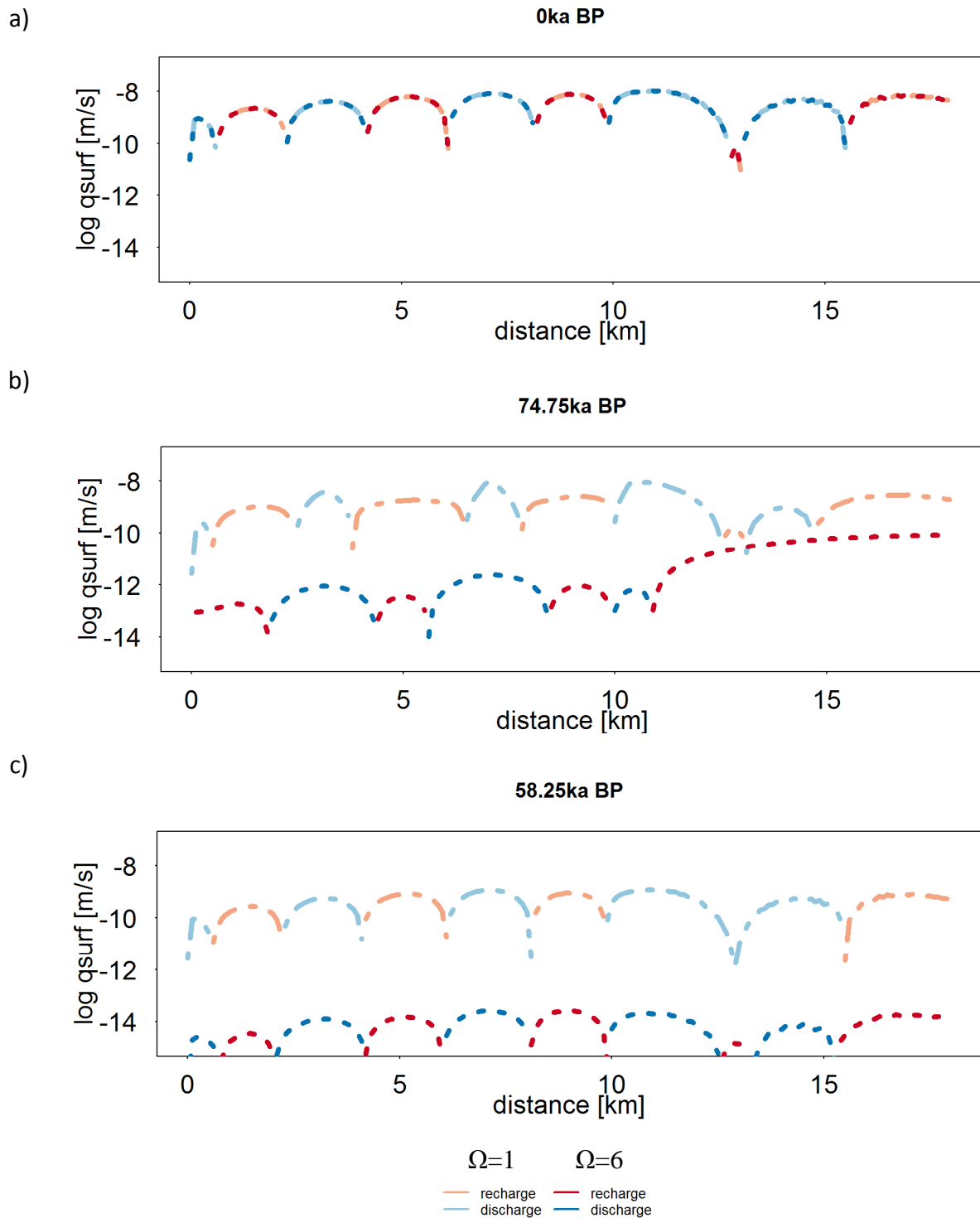


Figure 12. Surface fluxes for Case 1 for the T-25 scenario. a) non-permafrost (0 ka BP), b) thin permafrost (74.75 ka BP) and c) continuous permafrost (58.25 ka BP). Two permafrost permeability scenarios are considered; firstly, permafrost that is more permeable and decreases in permeability by one order of magnitude ($\Omega=1$), and secondly permafrost that is less permeable and decreases in permeability by six orders of magnitude ($\Omega=6$). For a) both scenarios are identical. When there is thin permafrost taliks develop in the higher permeability permafrost, resulting in higher discharge than under ambient conditions. In contrast the lower permeable permafrost model shows recharge and discharge reduced by six orders of magnitude. c) Fluxes are reduced compared to the ambient scenario to as many orders of magnitude as characterised by the factor Ω . A similar graph (not using a log scale) is presented in Figure 50.

The order of magnitude of groundwater flow in the permafrost is highly related to the order of magnitude as specified in the permafrost permeability function. Underneath the permafrost, velocity magnitudes are also modelled to decrease by ~ 2 orders of magnitude at depth when the surface is frozen compared to non-permafrost conditions for Case 2 (Figure 13). In Figure 13, permafrost exceeds a depth of 300 m for one cold event before 600 ka (MIS 16), which corresponds to the Happisburgh Glaciation. This low hydraulic head gradient underneath the permafrost is responsible for lower flow than under ambient conditions.

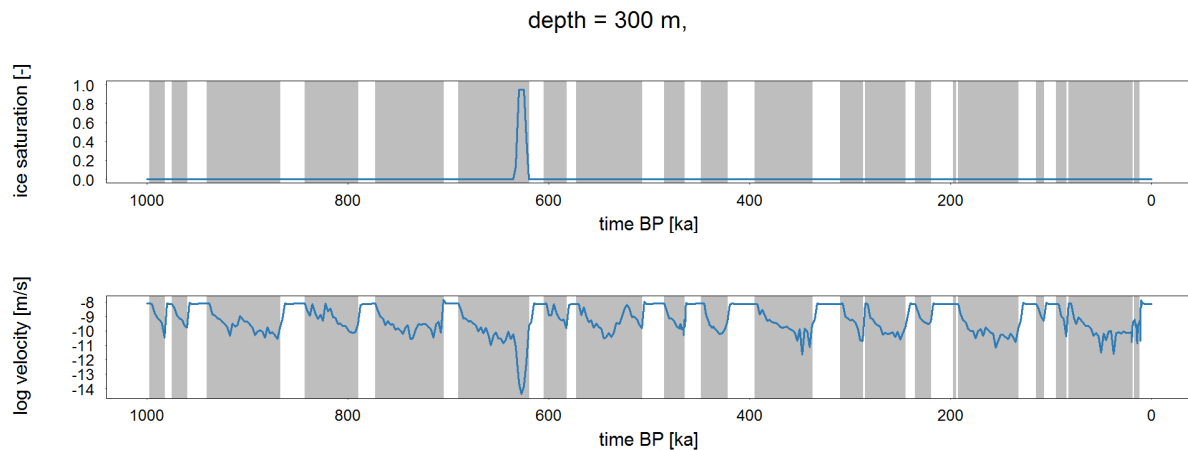
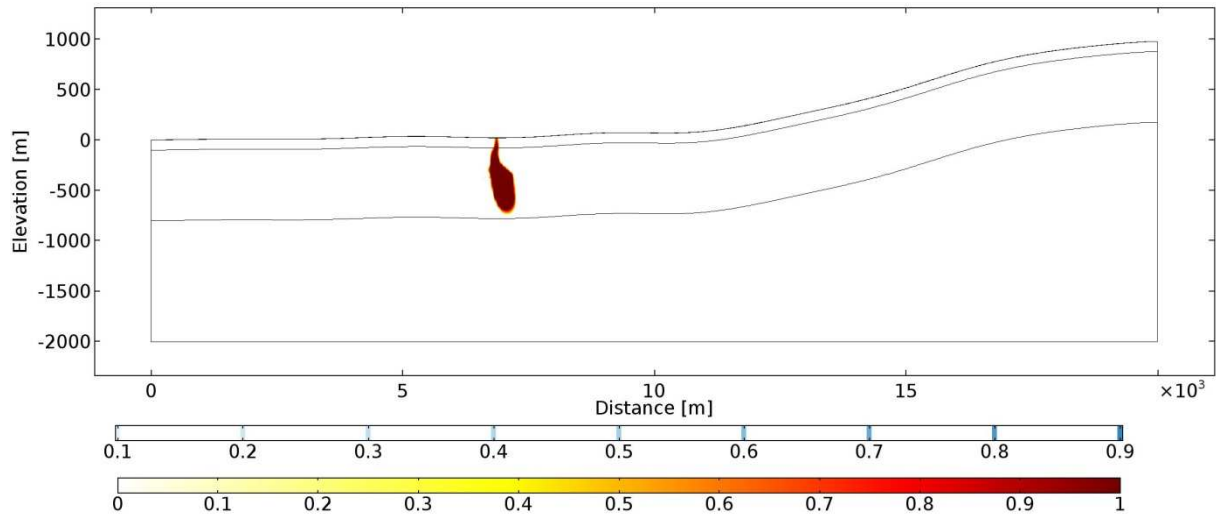


Figure 13. Ice saturation and groundwater flow velocities at 300 m depth for Case 2 and model run T-25 at 80 km from the left hand boundary. The grey shading indicates the times when the surface is frozen.

The groundwater flow directions and magnitudes are influenced by the existence of permafrost. Releasing a constant virtual tracer at a point source of $1 \text{ kg m}^{-3}\text{a}^{-1}$ (Figure 14) demonstrates that the existence of permafrost can fundamentally alter the area which is affected by a tracer and the flux of the tracer to the surface. During a permafrost event, discharge to the surface stops and the tracer spreads laterally, affecting a larger area than under unfrozen conditions. The tracer concentrates below the permafrost and disperses spatially, and is then released after the permafrost has disappeared, resulting in higher surface flux after a permafrost event than under constantly unfrozen conditions.

unfrozen



frozen

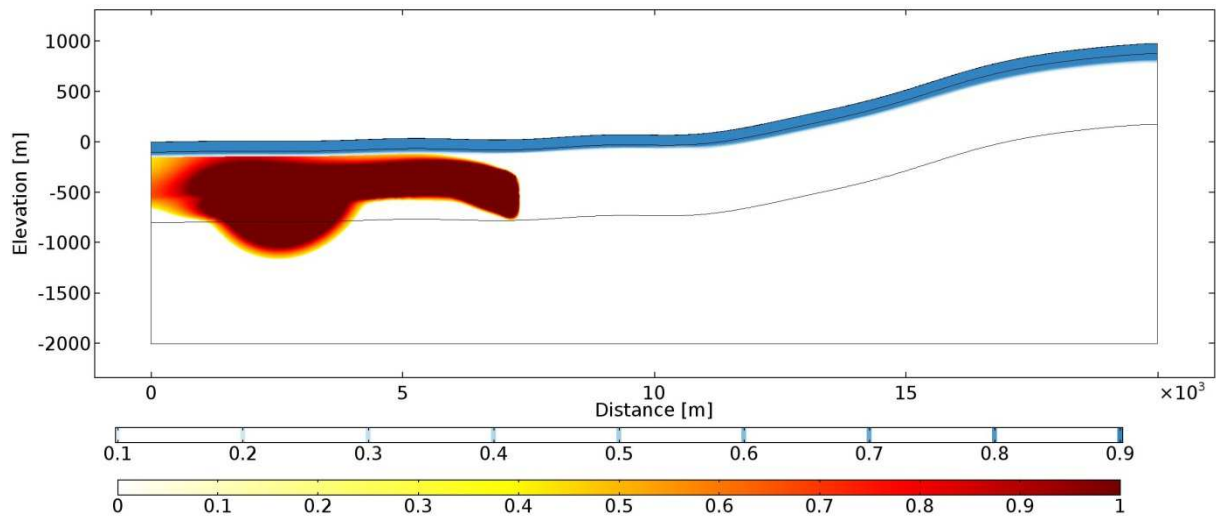


Figure 14. Virtual tracer (in kg/m^3) from a point source release to the surface under ambient conditions and permafrost (blue) conditions for Case 1, model T_14_tracer.

5.2 GLACIAL INFLUENCE ON THE GROUNDWATER FLOW SYSTEM

For the models of Case 1, including glaciation, the model domain is expanded and the same topography as in Case 2 is used (Figure 22). The glacial models for Case 1 use the same boundary conditions as for Case 2, which allows the differences between the model runs to be associated to geological factors only and exclude any differences in topography or ice sheet history or geometry.

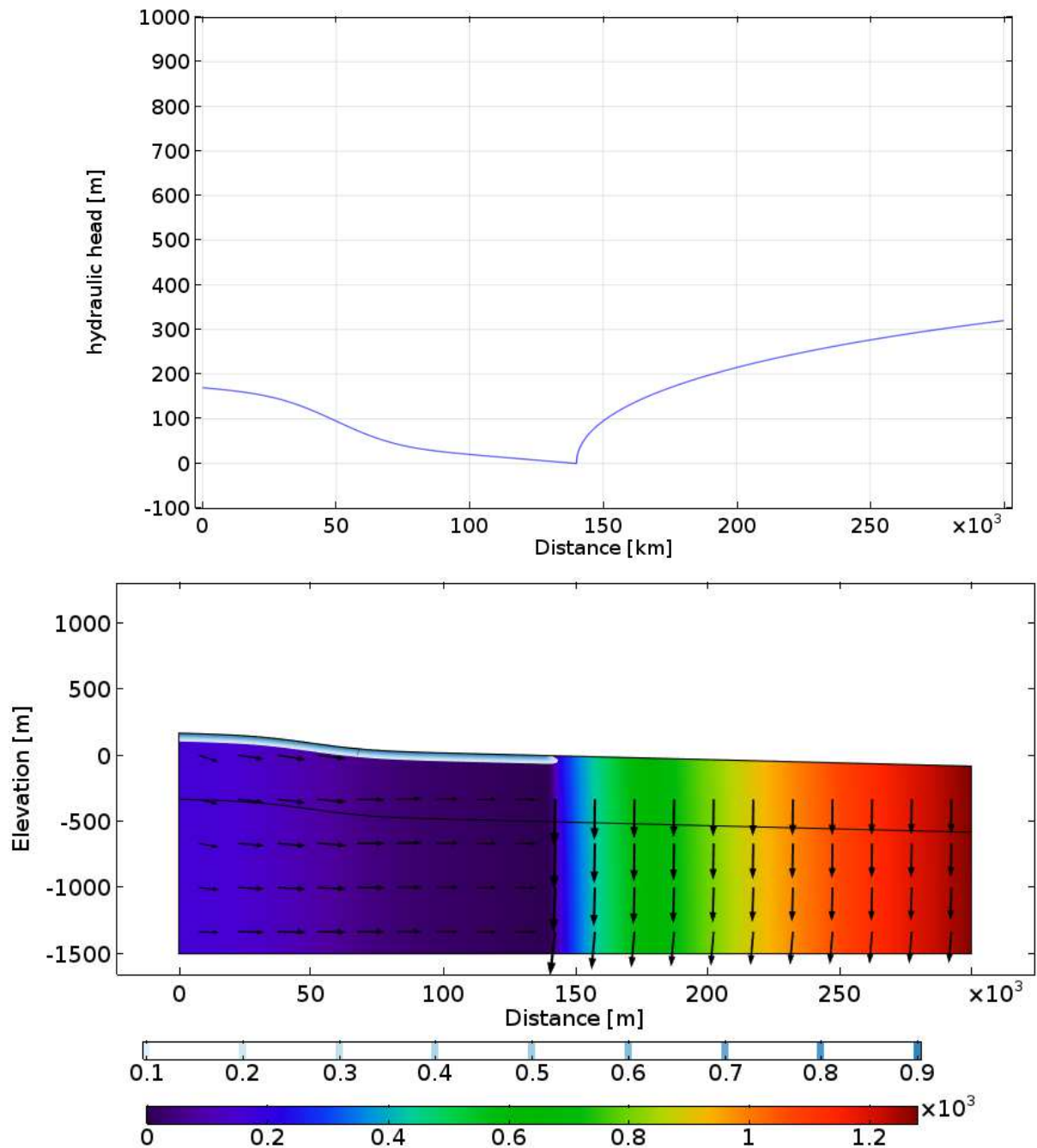


Figure 15. Hydraulic head and permafrost distribution in front of an advancing ice sheet at 460.75 ka BP for Case 2 with one layer.

For Case 1, when the land-surface is covered by a warm-based ice sheet, hydraulic heads underneath the ice and at depth increase to the ice overburden (Figure 15). In contrast, for Case 2 the signal of the high hydraulic heads is dampened at depth, and only slowly penetrates the low

permeability layers. At a depth of 500 m, the maximum hydraulic head occurs after the Anglian glaciation, and the decrease of the magnitude of the hydraulic head takes ~ 200 ka. For Case 2, including 1D vertical loading, the hydraulic heads at depth are similar to those of Case 1 and there is no time lag from the surface to a depth of 500 m, however elevated heads persist during the duration of the permafrost event following the Anglian glaciation for Case 2 including loading, whereas for Case 1 the hydraulic heads are at the original value after the glaciation (Figure 16). For Case 2, as the high hydraulic head decreases more slowly at depth than at the surface, there is upward flow at depth; however in the model this does not reach the surface (Appendix, Section 3.1.4). The velocity magnitudes for both Case 1 and Case 2 (Figure 57) are largest during ice advance and ice retreat as the hydraulic head gradient is largest then, and where the hydraulic heads are one to two orders of magnitude higher than under ambient conditions. During ice advance, groundwater flow is in a downward direction and during ice retreat in an upward direction. In the model here for Case 1 and 2, the lateral flow directions are reversed during the glaciation, as the ice sheet topography and flow direction are against the topographic gradient, and groundwater flow is driven by the ice overburden pressure.

For the flow direction and magnitude to return to their initial states after the Anglian glaciation takes tens of thousands of years in our model, however after the Devensian glaciation it takes only thousands of years. This difference is due to the length of the glaciation, 20 ka for the Anglian and 2 ka for the Devensian glaciation (Figure 17, and in Appendix Figure 56).

The loading efficiency of the rock matrix determines how the ice load is apportioned between the rock and pore fluid and depends on the relative compressibility of the porous media to the pore fluid and the porosity (*Neuzil, 1995; Normani and Sykes, 2012*). The influence of glacial loading is minimal for Case 1, however for Case 2 the effect of ice sheet loading is large in the low permeability layers and ice sheet loading may result in an expulsion of water due to a consolidation of the bedrock matrix. For Case 2, including the effects of mechanical loading, the high hydraulic heads propagate the low permeability layers at a slower rate than in the aquifer above, but at a faster rate than when loading is not considered. For Case 2, without the considerations of loading, the high hydraulic heads from the ice sheet propagate slowly in the low permeability layers, resulting in high gradients around the low permeability layer. Therefore, the effects of mechanical loading are a crucial consideration for low permeability layers. However, only vertical loading has been considered and this assumption is only valid where homogenous and laterally extensive overburden changes occur, but not where vertical loads vary significantly over short distances as found near an ice sheet margin (*Vidstrand et al., 2010*). Furthermore, in the model the compression of the ground is all taken up in the crust and no deformation in the mantle has been considered.

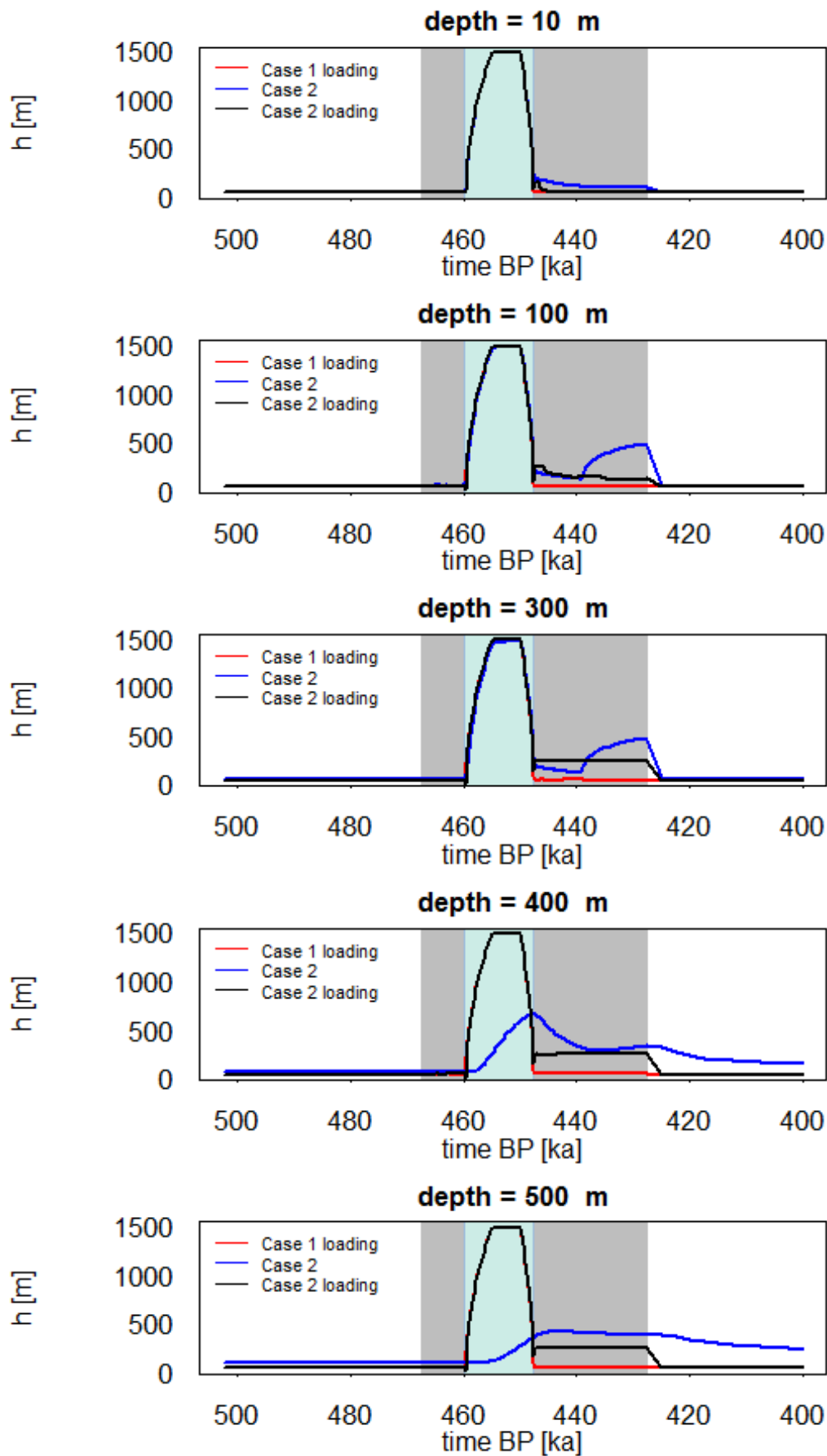
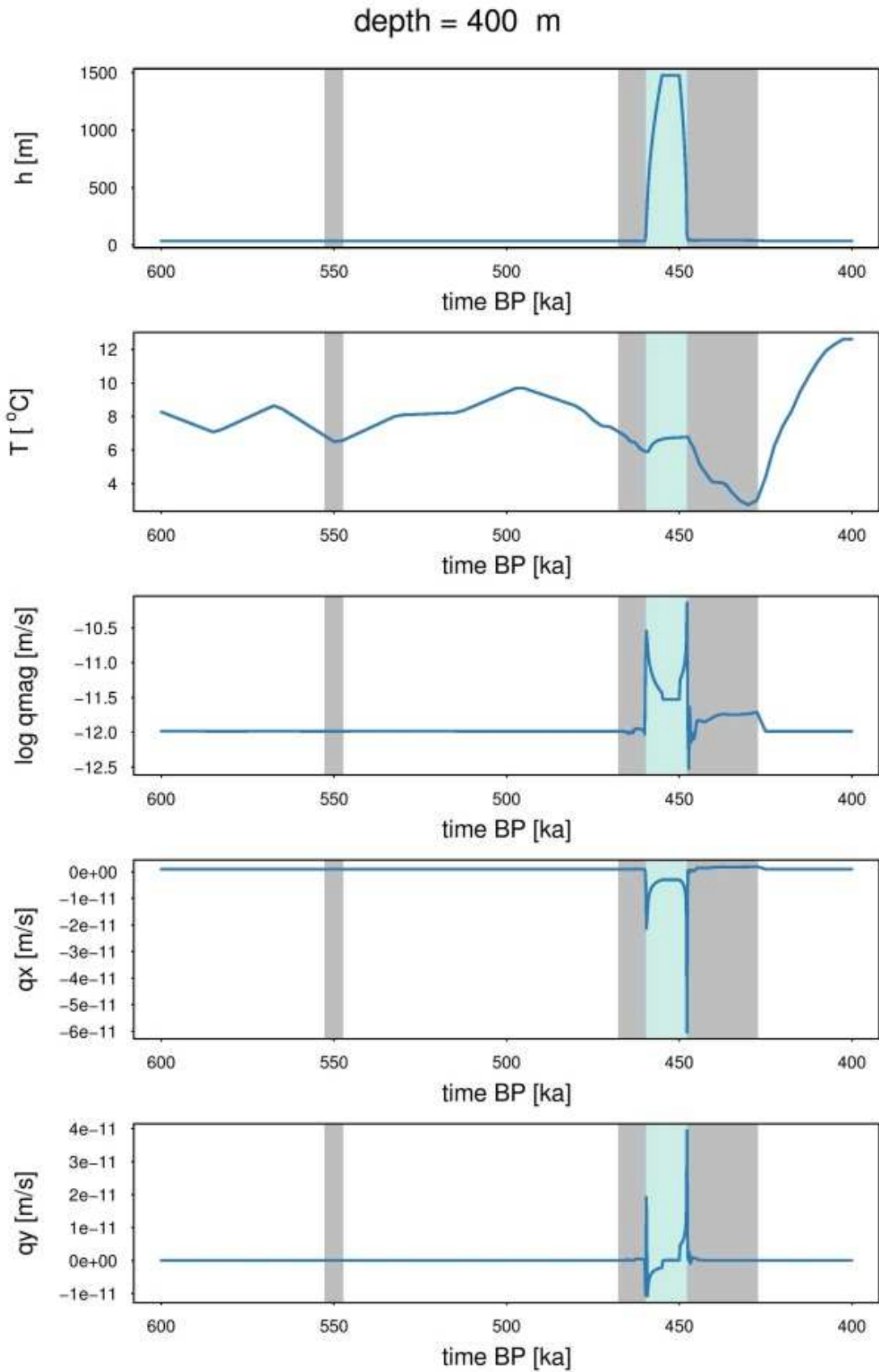
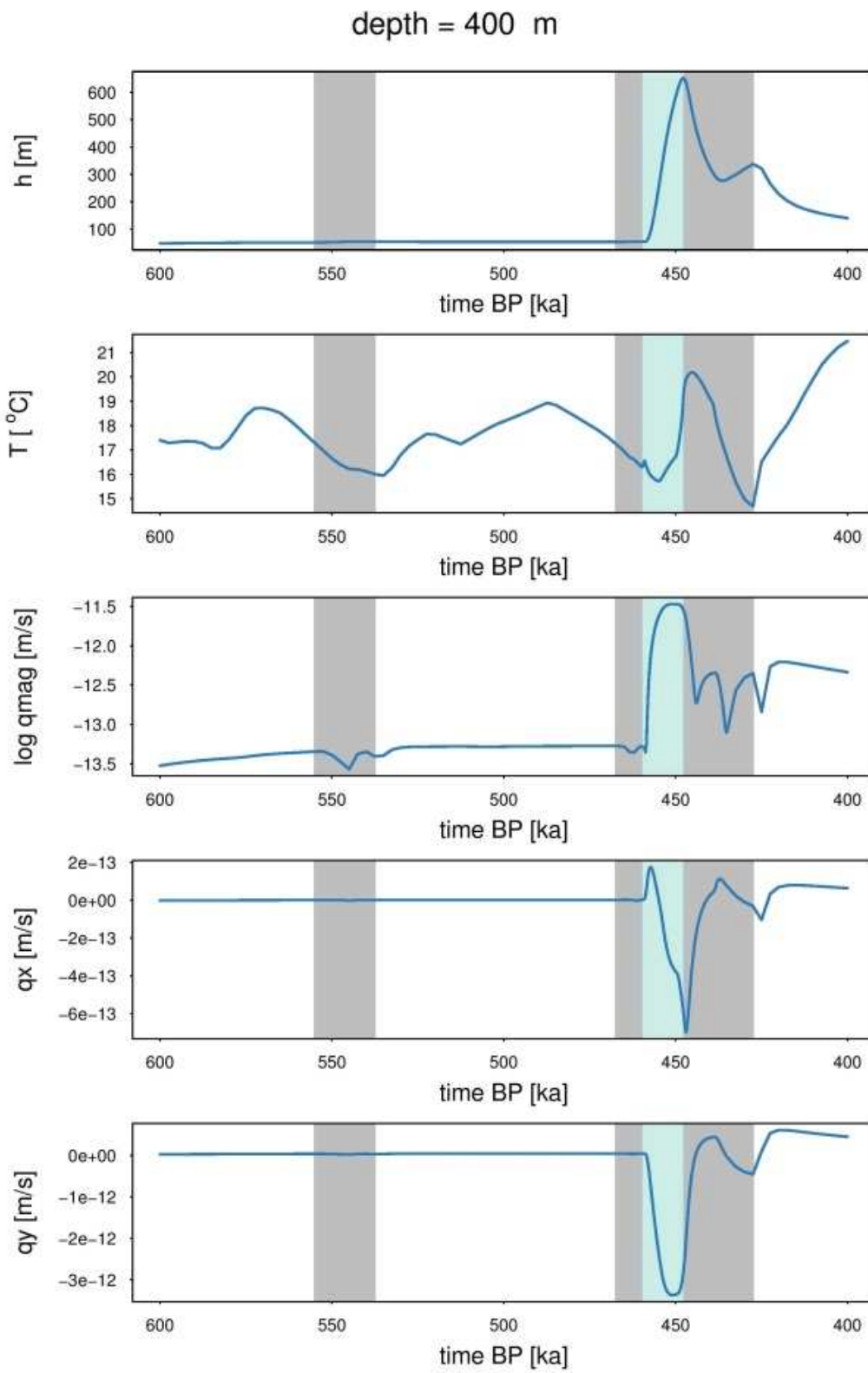


Figure 16. Hydraulic head during the Anglian glaciation at different depths of profile 2 (80 km from the left hand side of the model domain).

Case 1 with mechanical loading



Case 2 without mechanical loading



Case 2 with mechanical loading

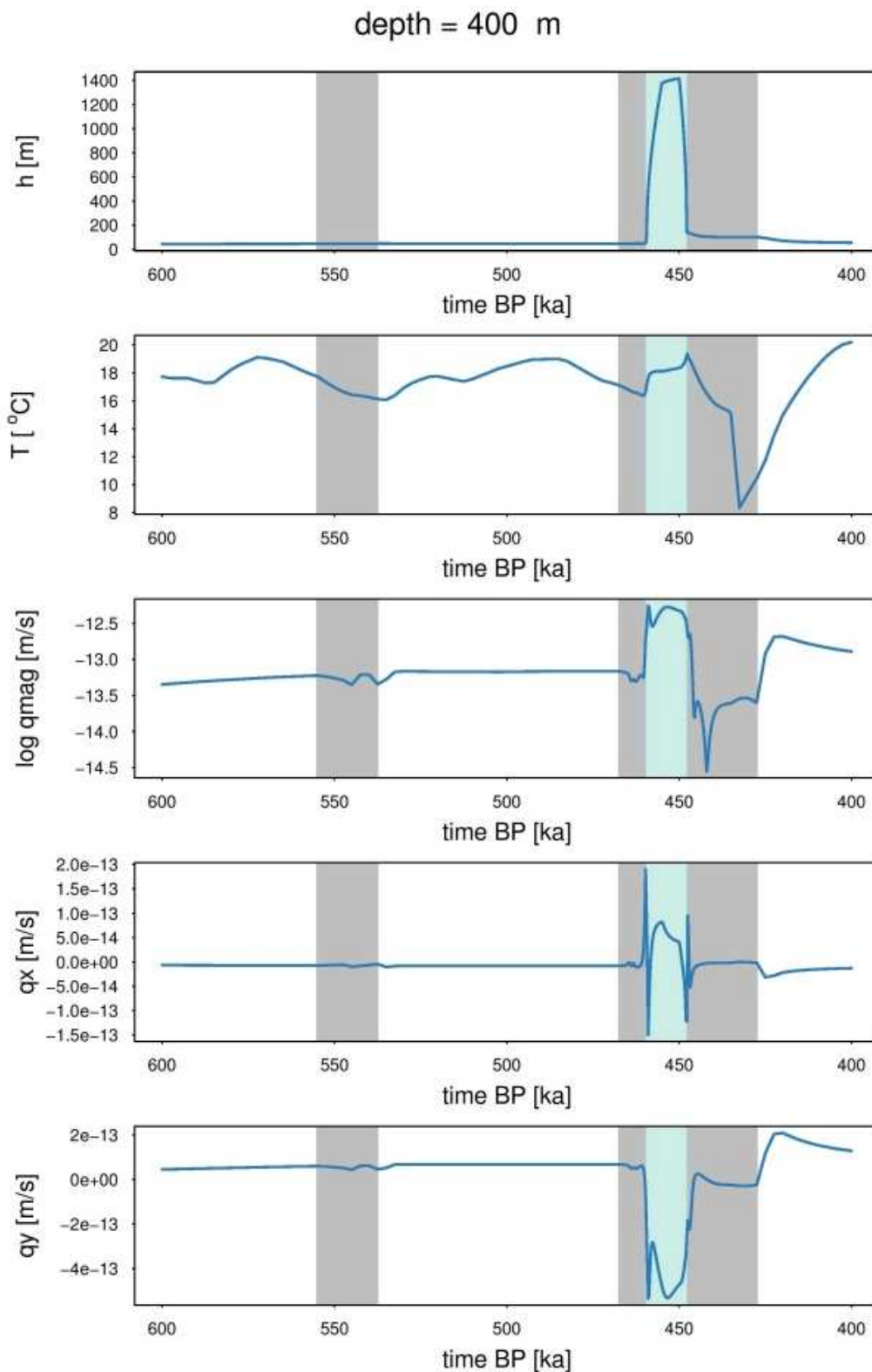


Figure 17. Top to bottom, time series of hydraulic head, temperature, velocity magnitude and Darcy flow in x and y at the location 80 km from the left hand boundary over the duration of the Anglian glaciation. The grey shaded times are when the surface is frozen and the light blue covered by an ice sheet.

6 Summary of results, conclusions and recommendations for further work

6.1.1 Relevant factors and processes for permafrost thickness

6.1.1.1 TEMPERATURE TIME SERIES

Assuming the pattern of fluctuation of past temperatures to be based on regionally adjusted benthic $\delta^{18}\text{O}$ records, permafrost thickness has never reached a steady state in Great Britain over the past one million years. Therefore, the temperature history must to be taken into account when estimating the maximum permafrost thickness.

The variation of the global temperature time series has a large influence on the thickness of permafrost calculated. For the last glaciation, *Annan and Hargreaves* (2013) suggest temperatures for southern England and Wales to be 8°C to 12°C below present, and for northern England and Scotland to be 12°C to 20°C below present day temperatures. In contrast, *Westaway and Younger* (2013) reconstruct a temperature difference to present day temperatures for southern England of 20°C, and for northern England of 18°C. Scaling the minimum temperature of a Pliocene-Pleistocene stack of 57 globally distributed benthic $\delta^{18}\text{O}$ records to temperatures of 14°C, 18°C and 25 °C below the present day, the maximum modelled permafrost thickness for Case 1 reached 171 m, 248 m, and 475 m, and for Case 2 80 m, 138 m, and 238 m. The difference between the two Cases is due to the variation in subsurface properties.

The results from this report can be compared to previously modelled permafrost thickness at other GDF sites. Previously modelled permafrost thicknesses in the UK modelled in the Phase 1 report range between 30 m-180 m for the average estimate climate and 180 m -235 m for the cold estimate climate (*Busby et al.*, 2014). The large range in permafrost thickness is due to different geologies as well as different surface temperature time series used. At Forsmark, Sweden, maximum modelled permafrost depth for the repetition of the last cycle is between 160-290 m and for the severe permafrost case 310-460 m (*Hartikainen et al.*, 2010). For Mol, Belgium the maximum permafrost depth (defined as 50% frozen) is between 160-215 m (*Holmén et al.*, 2011).

6.1.1.2 SUBSURFACE THERMAL PROPERTIES AND HEAT FLOW

Thickest permafrost is to be expected where there is a low heat flow, a high thermal conductivity and a low porosity.

Thermal properties and heat flow were varied according to their range in the UK. The influence of thermal and geological properties on the permafrost thickness is non-linear and the relative importance of different parameters is related to the magnitude of the other parameters. For the temperature T-14 time series, the simulated permafrost thickness ranged between tens of metres and 400 m as the thermal conductivity and heat flow were varied. The sensitivity of permafrost thickness to changes in porosity was simulated to be in the range 0 to 300 m. Mass heat capacity and density were found to have a minor impact on the maximum permafrost thickness, with maximum permafrost thickness varying by 30-40 m.

It was found that the simulated permafrost thickness is most sensitive to variations in:

- porosity when heat flow is low and thermal conductivity is high;
- heat flow when thermal conductivity is high and porosity is low;
- thermal conductivity when porosity is low and heat flow is high.

Whereas here the thermal properties and heat flow were varied according to their range in the UK, they were varied for a specified site at Forsmark, Sweden. There, the combined

uncertainties of heat flow, heat capacity and thermal conductivity result a variation in permafrost depth between 230-290 m using a variation in geothermal heat flow of -14% to 12%, a variation in thermal conductivity of -6.1% and 8.6% and thermal diffusivity of -11.5% and 14.6% (*Hartikainen et al.*, 2010).

6.1.1.3 LATENT HEAT AND CHANGE IN THERMAL PROPERTIES OF FROZEN OR UNFROZEN GROUND

When pure water freezes the thermal conductivity increases by a factor of four, the mass heat capacity decreases by half, and it releases heat equivalent to that required to raise the temperature of an equal volume of rock by $\sim 150^{\circ}\text{C}$. The effect of this latent heat is that during freezing ground temperatures initially remain around 0°C . As the thermal conductivity of frozen soil is larger than that of unfrozen soil, heat penetrates frozen soil faster than unfrozen soil (*Williams and Smith*, 1989; *French*, 2007).

The water filled pore space or, for fully saturated media, porosity determines the amount the thermal properties change with freeze/thaw and the uptake of latent heat. With higher porosity permafrost thicknesses are lower, i.e. there is a negative relationship between porosity and permafrost thickness. When thermal conductivity is high and heat flow is low, the range of simulated permafrost thickness was 326 m (from 270 m to 596 m) for the T-14 temperature time series (see Figure 37). In contrast, when porosity is low, the effects are negligible.

6.1.1.4 HEAT ADVECTION

The effect of heat advection on the thickness of permafrost has been found to be strongly dependent on the permafrost permeability function. When the permeability of the permafrost decreases by six orders of magnitude ($\Omega=6$), the difference in permafrost thickness around topographic highs and lows, simulated by the conduction only and the conduction-advection models is small (~ 10 m). In contrast, when the permeability of the permafrost decreases by only one order of magnitude ($\Omega=1$), the effect of heat advection is larger and the influence of advective heat flow on permafrost thickness can be ~ 80 m. Again, the effect of advective heat flow is largest when permafrost is shallow and decreases with increasing permafrost thickness.

Permeability in permafrost is dependent on the liquid water and ice content and decreases with decreasing water content similarly to what is known for the vadose zone (Figure 18). In general, permafrost is regarded to be low permeability, so the scenario of $\Omega=6$ would be most likely. However, over a larger scale, the relative permeability might decrease less than on a smaller scale, as intra-permafrost taliks along fractures or higher permeable zones might persist and increase the overall permeability of the permafrost. Therefore, for a homogeneous system, a low permeable permafrost case (e.g. $\Omega=6$) is plausible, but in a fractured/heterogeneous system the overall relative permeability could be higher.

Where cold water flows vertically downwards beneath hills, heat advection causes thicker permafrost to develop. Where water upwells to topographic lows heat advection thins permafrost. Advective heat flow thaws permafrost beneath the topographic lows and develops permafrost beneath topographic highs.

The finding here that greater permafrost thaw occurs at topographic lows contradicts *McKenzie and Voss* (2013) who model permafrost thaw in a nested groundwater flow system under an atmospheric temperature rise scenario. Their model results suggest that thaw is largest on hilltops where warm water recharges and that thawing occurs more slowly at low-elevation discharge points where water temperatures have cooled to near zero as a result of latent heat loss during thaw. A difference to the model reported here is the inclusion of a seasonal temperature cycle, with temperature amplitudes ranging from 5 to 20°C . This seasonal amplitude will allow recharge of up to 20°C when the mean annual temperature is 0°C . In addition, the earlier study used a linear permafrost permeability function, which the authors state exaggerates the impact of advective heat flow on thaw.

A further contrasting observation has been made by *Bense et al.* (2012) using a similar approach to *McKenzie and Voss* (2013). The authors conclude that during permafrost thaw, hydraulic head increases and results in groundwater uptake into elastic storage. This increased groundwater recharge is suggested to result in modified recharge and discharge trends. Furthermore, *Bense et al.* (2012) point out that recharge in a thawing permafrost environment is not sufficient for advective heat flow to be significant and have an impact on permafrost degradation. However, they note that advective heat flow impacts transient taliks, where the recharge is not limited by effective rainfall, where flow is strongly focused, or where geothermal heat flow anomalies occur.

6.1.1.5 SURFACE WATER BODIES

Surface water bodies insulate the ground beneath them from the air and can prevent the subsurface below from freezing, or cause permafrost to thaw locally if they form when permafrost is present. The importance of advective heat flow is compared for the scenario including taliks (model T-14_Talik) and the base case model without taliks (model T_14_Max). When the base case model is fully frozen, heat advection does not significantly affect the temperature distribution. In contrast, when there are open taliks, heat advection is of greater importance in the weathered layer directly beneath the lakes and between the taliks in the sandstone. Considering Case 1, during thaw, advection concentrates heat at the foot of the steep slope. This discharge of heat means that heat advection becomes less important further downstream over the lowlands compared to the model without lakes (Figure 48).

More extensive modelling of the transient nature of taliks has previously been undertaken. *Rowland et al.* (2011) study the effects of advective heat flow beneath a lake in shallow permafrost and find that with the presence of sub-permafrost groundwater flow, permafrost thickness was up to five times less than without groundwater flow. In addition, they find that advective heat flow accelerates thawing beneath thermal disturbances, such as surface water bodies. The influence of groundwater flow from a river to the plain or from a plain to a river during a glaciation scenario has been modelled by *Grenier et al.* (2013). The authors find that the evolution of the talik is primarily controlled by the size of the river; however, advective heat flow is an important correction to this. Flow from the river to the plain results in delayed closure times of the talik, as warm water is introduced into the aquifer. In contrast, flow from the plain to the river can result in faster closure times than for a conduction only scenario, as cold water is advected from below the permafrost into the river. Similarly, the subsurface temperature and permafrost evolution beneath newly formed lakes have been found to behave differently depending on the hydrogeological scenario (*Wellman et al.*, 2013). The authors find that warm water entering the subsurface from surface water enhances permafrost degradation. In contrast, a lake gaining groundwater degrades permafrost more slowly compared with the lake losing water to groundwater. The presence of several lakes within a nested groundwater flow system in a thawing permafrost environment has been found to accelerate thaw compared to the scenario without lakes, as regional groundwater flow between the lakes enhances heat advection (*McKenzie and Voss*, 2013).

6.1.1.6 GLACIATION

Temperature distribution

Glaciations influence the thickness and distribution of permafrost by isolating the ground from the air. When ice is undergoing pressure melting at the glacier bed, temperatures at the base of the ice are close to 0°C. When the base of an ice sheet is cold-based, temperatures can be lower than 0°C and permafrost forms beneath the ice.

Three time series were constructed in which the temperatures were set to either 0°C, -1°C or -5°C, when ice was estimated to cover the land-surface. Adjusting the T-14 temperature scenario in this way had a profound impact on the maximum permafrost thickness for Case 1 over the past

one million years. For the maximum glaciation scenario with subglacial temperatures at 0°C, the maximum permafrost thickness is 100 m, compared to 171 m without glaciation. When the subglacial temperature is set to -5°C, the maximum permafrost thickness is 177 m. Whether the maximum or the medium glaciation scenario is selected does not have a large influence on the maximum permafrost thickness overall, as the medium glaciation scenario is glaciated when temperatures are coldest.

Groundwater flow

High hydraulic gradients beneath an ice sheet considerably alter the groundwater flow system compared to ambient conditions. When the ice flow is in the opposite direction to the groundwater flow direction under unglaciated conditions, groundwater flow reverses during the presence of ice.

When the ice is present, hydraulic heads beneath the ice and at depth increased to the ice overburden (1500-2000 m) for the one layer model representing basement and Case 1. Similar observations have been made for a continental groundwater model of the Canadian landscape during the Wisconsinian glaciation (*Lemieux et al.*, 2008b; c; a), where hydraulic head values up to 3000 m were simulated down to a depth of 1.5 km. However, for Case 2 the changes due to the propagation of high hydraulic heads are dampened and penetrate slowly in the low permeability units. The hydraulic gradient is greatest during ice advance and ice retreat, resulting in velocity magnitudes that are one to two orders of magnitude higher than under ambient conditions. During ice advance, flows are in a downward direction (recharging), and in upward direction (discharging) during ice retreat. For the model including glaciation, as presented in this report, the lateral flow directions are reversed during the glaciation and its magnitude is highest during advance and retreat.

In the model, the velocity magnitudes and direction at depth take tens of thousands of years to return to their pre-glaciation states after the Anglian glaciation. This only takes several thousand years after the Devensian glaciation. This difference is due to the length of time the region was glaciated, 20 ka for the Anglian and 2 ka for the Devensian. *Bense and Person* (2008) and *Lemieux et al.* (2008a) find that the present day fluid pattern is still responding to the last glaciation at 10 ka BP for an intercratonic sedimentary basin and the Canadian Shield, respectively, which might be due to the immense volume and correspondingly slow decay of the Laurentide Ice Sheet.

Ice sheet loading

The mechanical loading efficiency of the rock matrix determines how the ice load is apportioned between the rock and pore fluid and depends on the relative compressibility of the porous media to the pore fluid and the porosity (*Neuzil*, 1995; *Normani and Sykes*, 2012). For the one layer model and Case 1, the influence of ice sheet loading is minimal. *Vidstrand et al.* (2013) noted that in hard, high strength, fractured (permeable) crystalline rock, all pressure changes during a glacial cycle are often assumed instantaneous. Ice sheet loading has thus been excluded for modelling a crystalline basement (*Vidstrand et al.*, 2010; *Scheidegger and Bense*, 2014; *Vidstrand et al.*, 2014). However, for Case 2, the effect of ice sheet loading is large in the low permeability layers using the properties as listed in Table 4. The loading may result in an expulsion of water due to a consolidation of the bedrock matrix. For the model excluding loading, the high hydraulic heads propagate slowly in the low permeability layers, resulting in high gradients around the low permeability layer. In contrast, when loading is included, the high hydraulic heads propagate the low permeability layers at a slower rate than in the aquifer above, however at a faster rate than when loading is not considered.

6.1.1.7 SALINITY

Generally, as the surface freezes, recharge ceases, and the freezing front of the downward penetrating permafrost base drives a front of increasingly saline fluid. These more saline fluids at the permafrost base will act to decrease the freezing point.

The effects of salinity on the groundwater flow system and the freezing point have not been considered in the modelling presented in this report. However, in a parallel study, the geochemical aspects of permafrost development have been studied for a fluid parcel using the Frezchem database in PHREEQC (*Kilpatrick, 2016*). This model allows the simulation of the chemical composition, mineral precipitation, hydrate formation and freezing point depression of a fluid under given pressures and temperatures. The freezing point depression at a depth of 200 m for different UK groundwaters ranges from 6.9-9.7°C for Meteoric water, 8-14.3°C for seawater, -16.6°C for basinal brine, 7.8-13.9°C for crystalline basement fluid, 5.9-6.3°C for fresh sandstone groundwater, 8.9-9.8°C for fresh chalk groundwater, and 9.1-16.3°C for clay porewater (*Kilpatrick, 2016*). The magnitude of the freezing point depression suggested is for a stationary fluid parcel. If mixing of the higher concentrated brine with less saline water occurs, then the magnitude of the freezing point depression is likely to be lower.

6.1.1.8 COMPARISON TO PERMAFROST THICKNESS DERIVED IN PHASE 1 REPORT

The modelling for the Phase 1 report did not include the latent heat effects of water-ice phase changes or the effects of heat advection by groundwater flow. The latent heat affects the maximum permafrost thickness, but will also delay and reduce the permafrost thickness when permafrost is forming, and delay thawing. The magnitude of the latent heat effect depends on the porosity, but also thermal conductivity and heat flow. The effects of latent heat on the maximum permafrost thickness will be largest where thermal conductivity is larger and heat flow is small, as shown in more detail in Figure 36.

The influence of heat advection on the permafrost thickness strongly depends on the location of profile modelled, and the hydrogeological scenario. The modelling indicates that the effect of heat advection is likely to reduce permafrost thickness by a maximum of tens of metres.

6.1.2 Relevant factors and processes influencing the hydrogeology in a permafrost environment

6.1.2.1 PERMAFROST DISTRIBUTION

In the model used here, when the model domain is unfrozen, recharge and discharge are topography-driven. When ice starts to form at the surface, recharge and discharge decrease by several orders of magnitude, as specified by the permafrost permeability function. For Case 1, decreased recharge and discharge result in a drop in hydraulic heads beneath the permafrost, as water drains out the side of the model, resulting in reduced flows at depth. A decrease in velocity magnitudes at depth can also be observed for Case 2, but hydraulic heads do not decrease to the same extent as for Case 1, as the lateral boundary is closed and the hydraulic gradient is less. During permafrost thaw, hydraulic heads rise, resulting in an uptake of groundwater into elastic storage, which has been discussed in more detail by *Bense et al. (2012)*.

For the scenario in which permafrost is set to be more permeable ($\Omega = 1$), recharge and discharge both decrease when permafrost starts to form, but discharge focusses on topographic lows resulting in taliks. Flow into the taliks is focused, resulting in higher velocity magnitudes than under unfrozen conditions.

Simulations of the plume of a tracer released at depth have shown that under ambient conditions the plume spreads towards the surface in the two Cases used in this report and affects a small area. The existence of permafrost can fundamentally alter the size and distribution of the plume.

During a permafrost event, discharge to the surface ceases, the flow direction changes, and the tracer spreads laterally. The tracer concentrates below the permafrost and is then released after the permafrost has thawed, resulting in a pulse of the tracer being released to the surface.

6.1.2.2 SURFACE WATER BODIES

In the talik model (T_14_Talik) the taliks remain open during the entire simulation. For scenarios when there is thick permafrost, the surface fluxes remain high in the taliks. The flux at the location of the lake at ~11 km focuses groundwater from the area of steeper slope in Case 1 and is higher than under unfrozen conditions.

During thaw the discharge at the valley bottom interfluvium is larger for the model without surface water bodies. For the T-14_Max model, discharge is focused at only one location at the foot of the steeper slope, whereas for the talik model discharge is distributed at the locations of the three surface water bodies.

6.1.2.3 BUOYANCY DRIVEN FLOW

The contrast in density of cold and potentially saline water at the permafrost base and warmer, potentially less saline water at greater depths can result in the downward movement of plumes of saline fluid and upwelling of warmer, less saline water, which will then act to reduce the freezing point depression.

In the study by *Kilpatrick (2016)* it was found that meteoric water is unlikely to produce brines in quantities that will affect the local groundwater flow. In contrast, freezing of seawater and crystalline basement fluid can produce brines in significant volumes (10-30% of initial fluid volume), which can be >10% denser than their parent fluid, and which could lead to gravity driven flow, depending on the nature of the underlying fluids. Furthermore, *Kilpatrick (2016)* showed that freezing of fresh chalk, fresh sandstone and clay pore waters produces brines in relatively small volumes. However, should significant migration of these fluids occur during the freezing process (i.e. before the vast majority of fluid is frozen), then they may also have the potential to migrate to depth and affect the regional groundwater flow.

As noted by *McEvoy et al. (2016)* even if permafrost does not reach the depth of the repository, unfrozen ground below permafrost and sub-glacial environments may encompass the stability fields of several gas hydrates, of which methane hydrate is the most common. These ice-like phases require cool temperatures, elevated pressures, and a source of methane to form, but importantly, are stable at temperatures above 0°C. It is possible that, even though ice may not be stable at potential repository depths, methane hydrate could form if methane or carbon dioxide is present. If hydrates do form, then they may grow and destabilise several times over the next million years in response to glacial cycles. It is however unlikely that significant volumes of CH₄ or CO₂ will be generated from the wastes at a time this far into the future.

6.2 CONCLUSIONS

Objective 1: Identify the parameters affecting permafrost thickness.

This report investigates the sensitivity of simulated permafrost thickness and dynamics to a variety of climatic, geological and hydrogeological conditions for two geological environments (Case 1 and Case 2). A combination of one dimensional heat conduction modelling, including the effects of freeze-thaw, and two dimensional heat conduction-advection modelling including freeze thaw has been undertaken to simulate permafrost development in two contrasting geological environments, (Case 1 and Case 2) and to assess sensitivities to a range of possible geological parameters, and advective heat flow. The assessment of the individual parameters are described below:

1a: Understand the influence of different scaling of the surface temperature time series on the maximum permafrost thickness.

The maximum permafrost thickness is strongly dependent on the scaling of the surface temperature time series. Scaling the minimum temperature of a Pliocene-Pleistocene stack of 57 globally distributed benthic $\delta^{18}\text{O}$ records to temperatures of 14°C, 18°C and 25 °C below the present day, the maximum modelled permafrost thickness for Case 1 reached 171 m, 248 m, and 475 m, and for Case 2, 80 m, 138 m, and 238 m. The difference between the two Cases is due to the variation in subsurface properties.

1b: Identify the influence of different geological properties found in the UK on the maximum permafrost thickness.

The sensitivity study of geological parameters has shown that there is a strong non-linear relationship between thermal conductivity, latent heat and heat flow for a temperature time series representative of the glacial cycles of the past one million years. This is in contrast to a steady state temperature profile, where permafrost thickness relates linearly to thermal conductivity, heat flow and ground surface temperature. Thickest permafrost is to be expected where there is a low heat flow, a high thermal conductivity and a low porosity, as for example in the North of Scotland.

1c: Understand the influence of advective heat transport by groundwater flow for a periglacial scenario.

Results have shown that when the temperature regime is dominated by heat conduction, such as for the low permeability Case 2, a heat conduction only model is sufficient to estimate the thickness and distribution of permafrost.

However, when heat advection is likely to be important, such as for Case 1, the coupling of permafrost and groundwater is necessary to simulate the permafrost distribution during freeze and thaw, or during shallow permafrost events. This is especially important when permafrost is assumed to be relatively permeable. Here it is found that heat advection of cold water at recharge points (interfluvies) results in cooling and thicker permafrost compared to discharge points where discharge of warmer water results in thinner permafrost. This stands in contrast with a model including a seasonal temperature amplitude, where during summer warm water recharges at the hill tops, resulting in permafrost thaw there (*McKenzie and Voss, 2013*). However, these variabilities in local permafrost thickness are of minor importance considering the time scales of 123 ka to one million years.

1d: Understand the influence of glacial conditions on the permafrost thickness and dynamics at the selected localities.

Glaciation influences the thermal regime by insulating the ground surface from the colder air during these periods. The timing of the onset or retreat of glaciation compared to the ground surface temperature is crucial for the permafrost thickness. If the ice sheet bed is at the pressure melting temperature, a reduction in permafrost depth compared to an unglaciated scenario can be expected. If the glacier bed is cold based the maximum permafrost thickness can be expected to be similar to the scenario without glaciation or increase if the temperatures at the glacier bed are colder than the ground surface temperatures. However, in reality the temperature regime underneath a glacier is much more complex and would require a transient thermo-mechanical model of ice flow coupled to a thermal model of bedrock.

Objective 2: Understand the influence of periglacial and glacial conditions on the groundwater flow direction and magnitude at the selected localities.

Recharge and discharge decrease considerably during periods of permafrost coverage. For Case 1, decreased recharge and discharge result in a drop in hydraulic heads beneath the permafrost, as water drains out the side of the model. This results in lower groundwater flows at depth. An open boundary at the side was chosen because the modelled domain finishes near

present day sea-level and not at the boundary of a catchment. A decrease in flow at depth can also be observed for Case 2, but hydraulic heads do not decrease to the same extent as for Case 1, as the boundary to the side is closed and the hydraulic gradient is smaller. During permafrost thaw, hydraulic heads rise, resulting in an uptake of groundwater into elastic storage from recharge over the top boundary of the model domain. As discussed in *Bense et al. (2012)*, it is unclear whether the strong increases in hydraulic head in sub-permafrost aquifer during permafrost thaw occurs in natural systems, however GRACE data have suggested an increase in groundwater storage in thawing permafrost regions (*Velicogna et al., 2012*).

When taliks underneath surface water bodies develop, the groundwater flow system remains more active than during continuous permafrost. Recharge and discharge are focused to lakes, and a regional groundwater flow system connecting the lakes can develop. Heat advection remains more important during thick permafrost when through taliks remain open.

In the model, during periods of glaciation hydraulic heads increase by ~1500 m at depth for Case 1 and Case 2 including loading. This signal is dampened in low permeability layers when no ice sheet loading is considered for Case 2. During glacial advance, groundwater recharge increases by up to two orders of magnitude, and during glacial retreat discharge increases. Depending on the flow direction of the glacier, groundwater flow directions can be reversed as a result of glaciation. After the Anglian glaciation, which is set to last for 20 ka, the signal of the glaciation remains in the groundwater system for tens of thousands of years, whereas after the Devensian glaciation, which is set to last for 2 ka, the signal remains for thousands of years.

For Case 1 the maximum permafrost thicknesses over the past 123 ka, based on the temperature time series of 14°C, 18°C and 25°C below the present day, were simulated to be 171 m, 248 m, and 475 m, respectively. For Case 2 these simulated thicknesses were 80 m, 138 m, and 238 m, respectively. In geological environments where the thermal conductivity is higher than for Case 1 and 2, the maximum permafrost thickness is likely to be greater (Profile 1 in Figure 39).

High hydraulic heads because of glaciation are likely to modify the groundwater flow around the GDF.

6.3 RECOMMENDATIONS AND POTENTIAL FOR FURTHER WORK

- Assess the influence of surface properties on the permafrost development

As already pointed out by *Busby et al. (2014)* and *Hartikainen et al. (2010)*, the surface temperature history is the main driver of permafrost development and uncertainties in the mean annual temperatures profoundly impact the maximum permafrost thickness. The sensitivity of the scaling of the temperature time series has been assessed for both environments. In addition, the effects at the ground-atmosphere boundary could be considered in the future. The surface cover (e.g. vegetation, snow cover, soil cover) is one of the most important factors determining the permafrost depth after air temperature (*Hartikainen et al., 2010*).

- Assess the most favourable case for permafrost development for a site/case

For future assessment of permafrost on a GDF, a combination of different parameters (e.g. scaling of temperature, surface conditions, glaciation, geological uncertainty, hydrogeology) favouring permafrost growth would give the maximum permafrost depth expected at a specific location. This approach has been undertaken by (*Hartikainen et al., 2010*).

- Assess the impact of geological variability

Geological variability and geometrical uncertainties will have a big impact on the hydrogeology and thus on advective heat transport. For example, the inclusion of fault zones

in the model will have a large effect on the groundwater flow system, and these should be explored further, in particular at a site-specific scale.

- Consider the impacts of erosion and sedimentation on permafrost development

For the models used for this study, the land-surface has been kept at a constant elevation. However, especially when assuming a warm-based ice sheet, glacial and fluvio-glacial erosion will be active and their magnitude will vary locally. The location of erosion depends on where active ice streams, major glacial meltwater drainage routes and major fluvio-glacial outflow incisions occur, and the magnitude of glacial erosion depth will probably be in the 200 m rather than the 1 km range for the UK (*McEvoy et al., 2016*). Therefore, the model assumption of constant topography might at certain localities not be realistic. Glacial erosion would influence permafrost formation at a GDF location by reaching deeper depths during subsequent cold phases, than at a non-eroded location. For future modelling, erosion scenarios could be taken into account when considering permafrost development at a GDF location.

- Consider the life-time of a lake for talik simulations

In addition, the life-cycle of lakes is likely transient over space and time, and their location and timing and lake bed temperature from a lake model could be used as model input.

- Apply a full THC model to take into account the effects of salinity on permafrost development

In the modelling reported here, heat conduction-advection, including phase change has been used to estimate the permafrost development in two different environments, which we have referred to as Cases 1 and 2. We have assumed fully saturated fluid flow, and no variations of density or viscosity because of temperature or salinity have been included. The interactions between heat flow, fluid flow and hydrogeochemistry are however strongly coupled. Permafrost formation acts to decrease the permeability and increase salinity, resulting in a decrease of the freezing point, and increased density, which then can result in gravity driven groundwater flow. Groundwater flow and associated heat transport then will influence the distribution of permafrost, potentially reducing its predicted depth. In order to combine the study by *Kilpatrick (2016)* and the study in this report, a fully coupled model of groundwater flow, heat transport and hydrogeochemistry could be used.

- Use relative permeability curves that are characteristic for each geological unit

For the models presented here, a uniform relative permeability curve for all layers has been used. However, as seen in Figure 18, the decrease in relative permeability differs for different geologies, and thus this should be added for a more site-specific model.

- Expanding the models from 2D to 3D

The impacts of glaciation or lakes are not very well represented within a 2D model as they influence groundwater flow and hence advective heat flow laterally and vertically. Therefore, the model would benefit from expansion from 2D to 3D, as especially glaciation and talik development are a 3D processes.

- Include variably saturated groundwater flow

Further model development to a variable saturated groundwater model would allow simulation of a more realistic groundwater flow regime. This would require a model that solves the Richards equation and is highly parallelized. However, given all the uncertainties, unsaturated flow may not have a first order effect on permafrost development, thickness and evolution.

- Use an output from an ice sheet model as the boundary condition for the model including glaciation, and undertake more sensitivity scenarios for models including glaciation regarding boundary conditions and glacial loading

The length, timing and temperature regime during glaciations significantly impact the simulated thickness and duration of permafrost, but these are all uncertain. Therefore, the model could be greatly improved by using the model output from an ice sheet model as the temperature boundary conditions for the permafrost-groundwater model. However, the uncertainties of the glacial scenario remain, and more sensitivity runs could be undertaken. Examples could include glacial advance and retreat over permafrost or over unfrozen ground, different thicknesses and profiles of the covering ice sheet (e.g. variation of the factor A for calculating the ice sheet profile) and periods of warm and cold based ice. Additionally, a tracer could be assigned to glacial meltwater and its residence time and flow-paths could be analysed. Furthermore, using a virtual tracer at a point source in models using different loading efficiencies would more clearly show the influence of glacial loading on the groundwater flow system.

- Include the effects of pressure on the melting temperature underneath glaciers

For future models, the pressure-melting temperature underneath an ice sheet should be adjusted, as this will differ from the previously assigned 0°C .

- Assess the stability field of gas hydrates if a source of methane is present

As mentioned above, gas hydrates are stable at cool temperatures and elevated pressures. Therefore, further work to estimate the stability field underneath the permafrost at the depth of the repository could be considered. As a first step, pressures and temperatures obtained from this model can be used to estimate the hydrate stability field. A multiphase model including fluid and gas flow patterns, temperature and salinity fields as used in Frederick and Buffett (2014), could be applied to investigate these processes.

- Requirements for a site specific model

For a site specific model, the following data will be required to perform similar modelling: thermal conductivity, heat capacity, density, porosity, hydraulic conductivity, heat flow, compressibility, and dispersivity on a regional scale. In addition, ice saturation with temperature and hydraulic conductivity with temperature should be measured for the different geologies of the chosen site. Moreover, soil types, soil saturation, lake distribution, lake and landscape development over time, snow cover and vegetation cover will also impact permafrost distribution and thickness. For a well-studied site, palaeo-groundwater flow modelling, including the effects of permafrost and glaciation, is likely to improve our understanding of the system and supports the evaluation of a GDF. Comparing modelled pressures and temperature distributions with present day observations would show whether all relevant processes are considered in the model and for how long the influence of the initial conditions might be expected to persist.

Appendix 1 Theoretical background to numerical modelling of groundwater in permafrost

HEAT TRANSPORT

The subsurface temperature distributions (T [K]) are calculated using the advection-diffusion equation, including the transient effects of latent heat of fusion (L_f [J/m³]) to simulate freezing and thawing as follows:

$$\nabla \cdot [\kappa_a \nabla T] - C_w \vec{q} \cdot \nabla T = C_p \frac{\partial T}{\partial t} + L_f \frac{\partial \theta_w}{\partial t} \quad \text{Equation 1}$$

where κ_a [W/(m K)] is the effective thermal conductivity the rock/water/ice mixture, C_w [J/(m³K)] is the heat capacity of water, C_p [J/(m³K)] is the effective heat capacity of the rock/water/ice composite, \vec{q} [m/s] is the Darcy flux and is coupled with the fluid flow equation. The first term on the left-hand side of the equation describes the diffusive heat transport and the second term heat advection by groundwater flow. For a heat conduction only permafrost model, the second term on the left hand side is ignored and the heat equation can be written as follows:

$$\nabla \cdot [\kappa_a \nabla T] = C_p \frac{\partial T}{\partial t} + L_f \frac{\partial \theta_w}{\partial t} \quad \text{Equation 2}$$

The thermal effects of pore water phase change can be conceptualised in apparent heat capacity C_a of the soil over the temperature range in which freezing occurs. The source/sink term of the latent heat can be expressed as followed:

$$L_f \frac{\partial \theta_w}{\partial t} = L_f \frac{\partial \theta_w}{\partial T} \frac{\partial T}{\partial t} \quad \text{Equation 3}$$

Combined with the thermal storage of the composite material, the apparent heat capacity is defined as:

$$C_a = C_p + L_f \frac{\partial \theta_w}{\partial T} \quad \text{Equation 4}$$

Soil freezing curve

Water freezes over a range of temperatures in the subsurface. Pure water freezes at 0°C, but the occurrence of salt lowers the free energy and there is a depression of the freezing point. An additional effect is that of capillarity and adsorption; the migration of water to the freezing front and the forces emanating from the mineral particle surfaces reduces the free energy in the absorbed layer on the particles (*Williams and Smith*, 1989). The unfrozen water content for subzero temperatures is measured for silt, illite and clay by *Burt and Williams* (1976) and presented in Figure 18.

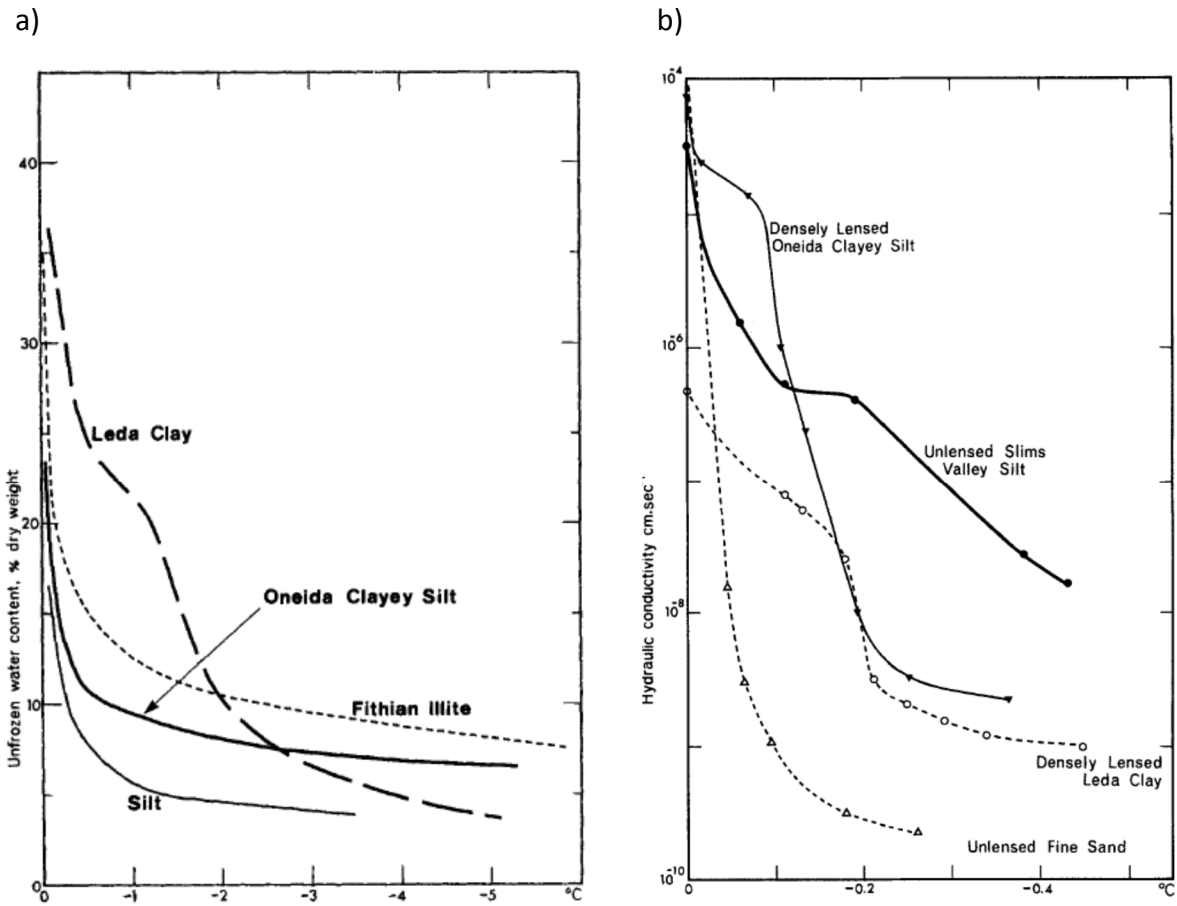


Figure 18. a) Unfrozen water content and b) hydraulic conductivity for subzero temperatures for clay, silt and illite, after Burt and Williams (1976).

McKenzie *et al.* (2007) were the first to review the freezing function (S_w [-]) in the context of coupled permafrost and groundwater models, and suggest two empirical freezing functions, a linear function, or an exponential function.

The exponential function suggested by McKenzie *et al.* (2007) is also used in the Interfrost model comparison project (Rühaak *et al.*, 2015; Grenier *et al.*, 2016) and given below:

$$S_w = S_{wres} + (1 - S_{wres})e^{-((T-273.15)/W)} \tag{Equation 5}$$

where S_{wres} [-] is the residual saturation and W [-] is a fitting parameter.

Bense *et al.* (2009); Bense *et al.* (2012); Scheidegger *et al.* (2012); Scheidegger and Bense (2014) use a smooth stepping function described with an error function:

$$S_w = \left(\operatorname{erf} \left(2.1 + \frac{T - 273.15}{0.25} \right) + 1 \right) \tag{Equation 6}$$

Similarly, here a smoothed Heaviside function is used, which is a built in step-function in COMSOL. The function is dependent on T [°C], the freezing interval d and S_{wres} :

$$S_w = \begin{cases} S_{wres}, & \text{if } T \leq -d \\ 1, & \text{if } T \geq 0 \end{cases} \tag{Equation 7}$$

$$0.5 + \frac{S_{wres}}{2} + (1 - S_{wres}) \left(0.9375 \left(\frac{T+d}{d} \right) - 0.625 \left(\frac{T+d}{d} \right)^3 + 0.1875 \left(\frac{T+d}{d} \right)^5 \right), \text{ if } 0 < T < S_{wres}$$

The different freezing functions are compared in Figure 19. All of these functions are from a S_{wres} of 0.05 and over a transition interval of 1°C. The error, exponential and Heaviside functions are similar, however, especially near 0°C the rate of change differs, with the error function showing the slowest decline in water saturation and the linear function the fastest decline.

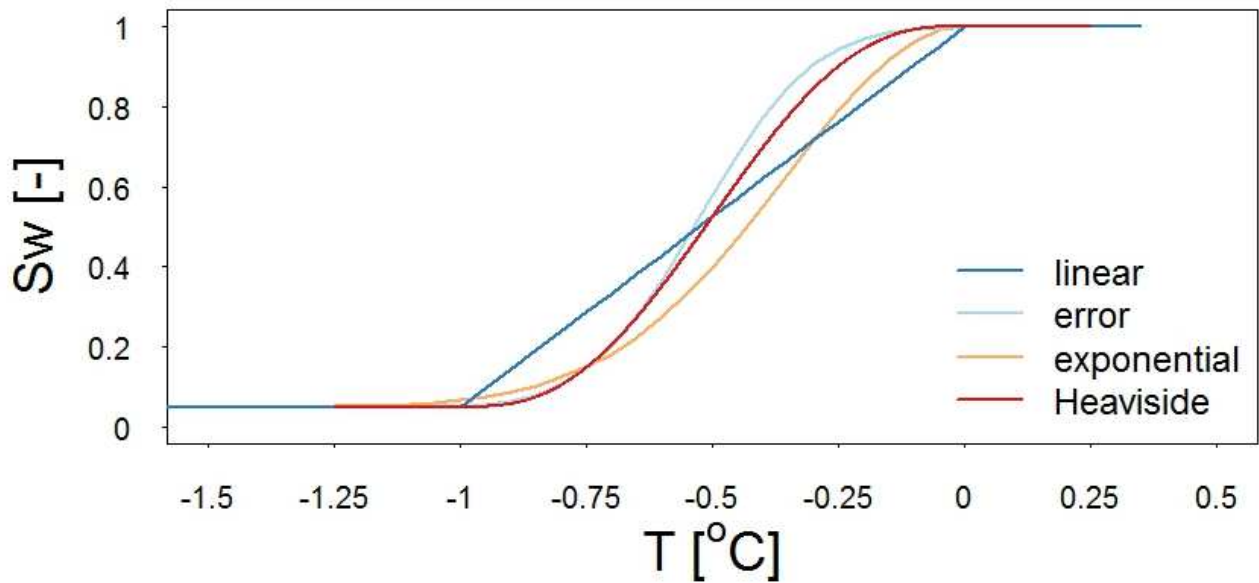


Figure 19. Comparison of freezing curves.

Porosity, thermal conductivity and heat capacity over the freezing range

For a fully saturated media, all free pore space is filled with water / ice so that:

$$\theta_s + \theta_w + \theta_i = 1 \quad \text{Equation 8}$$

where $\theta_w = \varepsilon S_w$ and $\theta_i = \varepsilon - \theta_w$. The porosity is ε [-], and the volume fractions of solid, water and ice are $\theta_s, \theta_w, \theta_i$ respectively.

The presence of ice and water near their freezing/thawing temperature has a dominant effect on the thermal and hydraulic properties of the subsurface. When water freezes, the thermal conductivity increases four-fold, its mass heat capacity decreases by half, it releases heat equivalent to that required to raise the temperature of an equal volume of rock by about 150°C, and its hydraulic conductivity decreases several orders of magnitude (*Williams and Smith, 1989; Woo, 2012*).

The thermal conductivity of ice is more than four times higher than that of water, and thus frozen ground has a higher thermal conductivity than unfrozen ground. The effective thermal conductivity of rock λ_e [W/m K] is calculated as a weighted geometric mean from the thermal conductivities of rock (λ_s), water (λ_w) and ice (λ_i):

$$\lambda_e = \lambda_s^{\theta_s} \lambda_w^{\theta_w} \lambda_i^{\theta_i} \quad \text{Equation 9}$$

The volumetric heat capacity C_a [J/(m³K)] is the amount of heat required to change the temperature of 1 m³ by 1°C. For a composite material, a weighted average for the heat capacities of solid (C_s), water (C_w) and ice (C_i) is used.

$$C_a = C_s \theta_s + C_w \theta_w + C_i \theta_i \quad \text{Equation 10}$$

FLUID TRANSPORT

Assuming that ice is immobile, the mass balance for water can be expressed as follows:

$$\frac{\partial}{\partial t} (\varepsilon(S_w \rho_w + S_i \rho_i)) = -\nabla \cdot [\rho_w \vec{q}] \quad \text{Equation 11}$$

where ε [-] is the porosity, ρ [kg/m³] density, \vec{q} [m/s] fluid velocity, S_w is the liquid water saturation, and S_i is the ice saturation.

For fully saturated media, $S_w=1-S_i$. Subscripts of w and i refer to liquid water and ice.

The mass balance for the solid matrix, assuming the solid matrix is immobile is given below:

$$\frac{\partial}{\partial t} (1 - \varepsilon) \rho_s = 0 \quad \text{Equation 12}$$

Fluid flow is simulated using fully saturated fluid flow described by Darcy's Law. The transient hydraulic head (h [m]) field is calculated as follows:

$$-\nabla \cdot [k_{rw} K \nabla h] = S_w S_s \frac{\partial h}{\partial t} + \varepsilon \frac{(\rho_i - \rho_w)}{\rho_w} \frac{\partial S_w}{\partial t} \quad \text{Equation 13}$$

where K [m/s] is the hydraulic conductivity, k_{rw} [-], is the relative permeability as a function of temperature, S_w [-] is the water saturation, ρ_w [kg/m³] and ρ_i [kg/m³] the density of water and ice, S_s [1/m] the aquifer specific storage, and ε the porosity.

The term $\varepsilon \frac{(\rho_i - \rho_w)}{\rho_w} \frac{\partial S_w}{\partial t}$ describes a source/sink term that is related to the volume change between water and ice. When ice forms, the volume of the water fraction expands and the hydraulic head increases. When ice melts, the volume of water drops and generates a drop in hydraulic head.

Relative permeability

In perennally frozen ground, where all pore fluids are frozen, water is immobile and the hydraulic conductivity is effectively zero. However, over the freezing process, porewater freezes progressively from larger pores through to smaller pores and there will be a steep decrease in hydraulic conductivity (*Ireson et al.*, 2013). How groundwater flow decreases over the freezing interval has a profound control on how permafrost and changes in permafrost distribution impacts groundwater flow.

Several experimental or theoretical relations describing the change of hydraulic conductivity as a function of ice content or temperature over the freezing interval can be found in the literature for sand, silt, and clay. The decrease in hydraulic conductivity with temperature has been measured for sand, silt and clay (*Burt and Williams*, 1976; *Kleinberg and Griffin*, 2005; *Watanabe and Flury*, 2008; *Azmatch et al.*, 2012). Model descriptions of how the permeability decreases over the freezing interval commonly assume an analogue to unsaturated fluid flow, in which the increase in ice content resembles the relationship between moisture content and suction described by a soil water retention curve (*McKenzie et al.*, 2007; *Kurylyk and Watanabe*, 2013).

The simplest function for relative permeability is a linear decrease in k_r for temperatures between freezing and the temperature at which the residual saturation is reached (T_{res}). At this point, an arbitrary small minimum value of k_r is used, for example 10^{-6} , as the flow equation cannot be solved for a value of zero (*McKenzie et al.*, 2007):

$$k_{rw} = \left(\frac{10^{-6} - 1}{T_{res}} \right) (T - 273.15) + 1 \quad \text{Equation 14}$$

Alternatively, *McKenzie et al.* (2007) propose an impedance factor law for which the minimum k_r is limited to 10^{-6} :

$$k_r = 10^{-Q\Omega} \quad \text{Equation 15}$$

where $Q=S_i\varepsilon$ and S_i is the ice saturation, ε the porosity and Ω an empirical derived impedance factor. For the Interfrost project, this relative permeability curve was used, using $\Omega=50$ and a porosity of 0.37.

Alternatively, it has been suggested that Q is the ratio of the ice content to the total minus the residual water content (*Hansson et al.*, 2004). Q thus increases with ice saturation and Q accounts for the fact that blocking becomes more effective as the ice content part of the total water content increases.

Here, a similar approach to *Hansson et al.*, 2004 is taken with Q equal to the ice saturation.

$$k_{rw} = 10^{-S_i\Omega} \quad \text{Equation 16}$$

where $\Omega=6$. This means that the relative permeability decreases by six orders of magnitude.

Bense and Person (2008) use a model described by *Kleinberg and Griffin* (2005), who compared theoretical models of hydraulic conductivity decreases with measured data. The models used represented ice coating the walls of capillary tubes, ice occupying the centre of capillary tubes, ice coating the surface of a grain pack, and ice occupying the centres of grain pack pore space. The model where ice occupies the grain pack pore space represented the measured data best. From this theoretical model, the permeability reduction could be described as a function of water-saturation state ($p_w=S_w/\varepsilon$), applying a minimum value of 10^{-8} .

$$k_{rw} = \frac{p_w^4}{(1 + (1 - p_w)^{0.5})^2} \quad \text{Equation 17}$$

Figure 20 compares the relative permeability curves that decrease over six orders of magnitude over one degree for a linear model (Equation 14), an impedance model (Equation 15), an exponential model (Equation 16) and the experimental model (Equation 17). The linear function has the slowest decrease in permeability with decreasing temperature. The impedance and exponential model decrease faster compared to the experimental curve after Kleinberg, but overall have a similar shape.

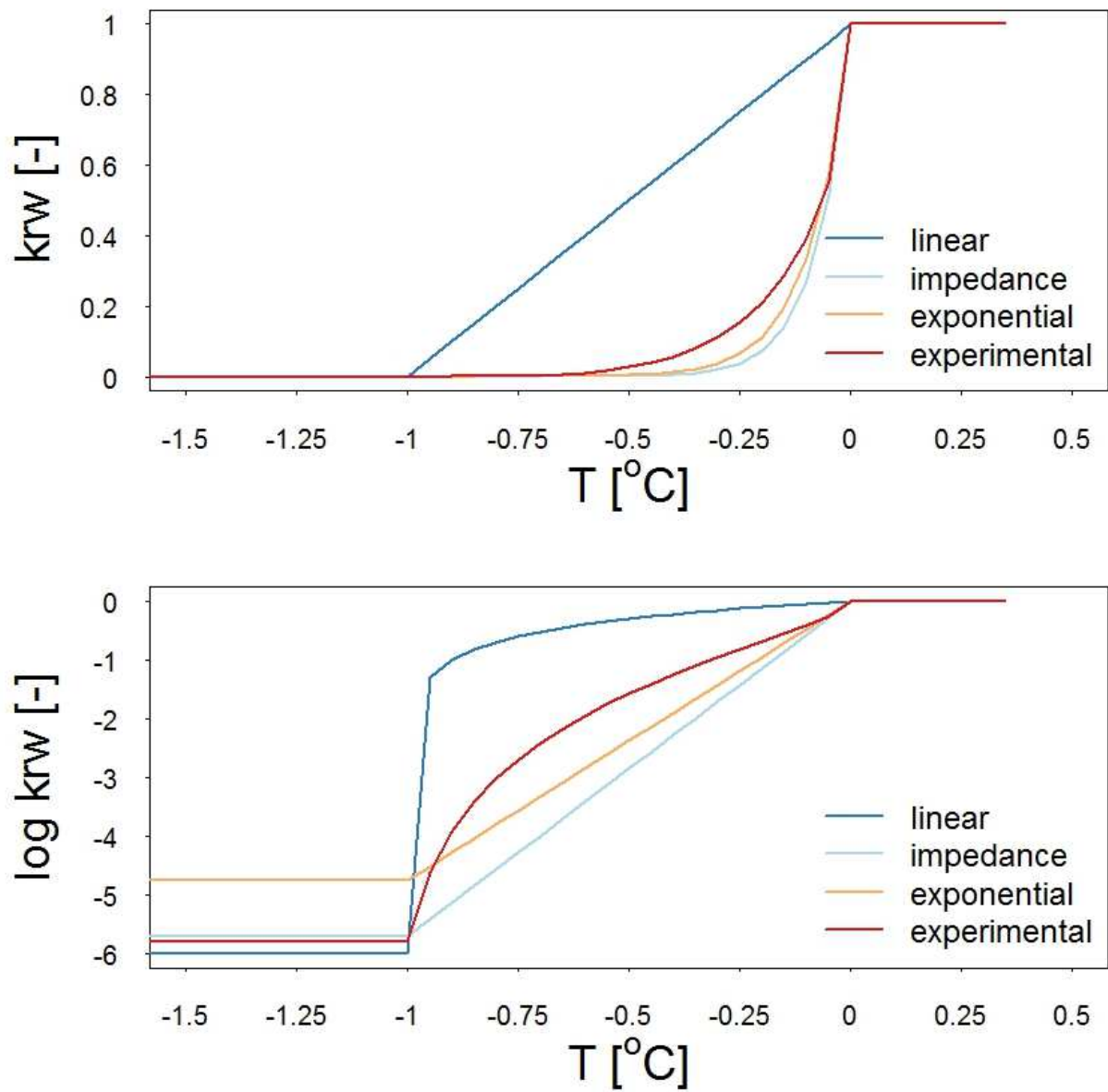


Figure 20. Comparison of relative permeability curves over 1°C decreasing by six orders of magnitude. Shown with a linear and a log scale.

GROUNDWATER FLOW INCLUDING THE EFFECTS OF GLACIAL LOADING

The loading efficiency of the rock matrix determines how the ice load is apportioned between the rock and pore fluid *Neuzil* (1995). The amount of stress transferred depends on the relative compressibility of the porous media to the pore fluid and the porosity (*Normani and Sykes*, 2012). Following the approach by *Lemieux et al.* (2008c) and *Normani and Sykes* (2012), a one-dimensional vertical loading and unloading is used for hydromechanical coupling, whereas a source/sink term is added to the flow equation to effectively increase or decrease the fluid pore pressure or hydraulic head. It has been shown that the assumption of purely vertical strain can be used to describe flow in 2D and 3D with small resulting errors provided that only homogeneous and laterally extensive overburden changes occur (*Wang*, 2000; *Neuzil*, 2003; *Lemieux et al.*, 2008c).

Adding the source term, the flow equation for hydraulic head becomes:

$$-\nabla \cdot [k_{rw}K\nabla h] = S_w S_s \frac{\partial h}{\partial t} - S_s \zeta \frac{\rho_i}{\rho_w} \frac{\partial h_{ice}}{\partial t} \quad \text{Equation 18}$$

where ζ is the one-dimensional loading efficiency given by:

$$\zeta = \frac{\alpha}{\alpha + \varepsilon\beta} \quad \text{Equation 19}$$

where α [1/Pa] is the compressibility of the porous media, β [1/Pa] is the compressibility of the pore fluid, and ε [-] is the porosity.

The loading efficiency varies between 0 and 1 and specifies how much of the surface loading is transferred to the subsurface fluid.

Appendix 2 Boundary conditions and model conceptualisation

Modelled localities

The localities used in this study are conceptual and hypothetical geological environments relevant to the UK, however their parameterisation is based on Environment 2 and Environment 5 described in *Towler et al.* (2008b). It should be noted though that the environments have been modified slightly from *Towler et al.* (2008b); the model domains for both environments have been extended to include an upstream water divide, any faults have been removed, and the hydrogeology characterised as topographically-driven systems that do not take into account variations in density or viscosity due to temperature or salinity.

Environment 2 in *Towler et al.* (2008b) is referred to here as Case 1, and describes a basement under sedimentary cover (BUSC) located on the margin of a Permo-Triassic sedimentary basin. The hydrogeology is characterised by a very shallow groundwater system within the drift deposits, a shallow fresh system in the uppermost 50-100 m, and a deeper, relatively stagnant system in the basement rocks. The groundwater flow in the basement rocks is influenced by dense brines that are derived from evaporite deposits offshore. In the host rock, fracture flow is dominant and in the sedimentary cover rocks matrix flow is dominant (*Towler et al.*, 2008b). During the last ice age, the Case 1 environment was ice-covered (*Chiverrell and Thomas*, 2010).

Environment 5, referred to here as Case 2, is based on a type of geological setting found in the east of England and consists of Lower Jurassic shales and mudstones and Triassic mudstones and siltstones, dipping uniformly to the east. The environment has a very low topographic relief and is hundreds of kilometres from the nearest areas of significant topography. During the last glacial maximum, this locality was at the margin of the ice sheet. There are two aquifers within the sequence, the Mid-Jurassic limestone aquifer and Triassic sandstones. The other formations consist of mudstones, siltstones, and Cretaceous Chalk. The upper part of the sequence has been modelled by *Towler et al.* (2008a), however, in this study the model thickness has been extended to a greater depth and captures the full lateral extent of the outcrop of the Permian basin. Because of the low hydraulic gradient, the flow rates in the higher permeable zones are suggested to be low (*Towler et al.*, 2008b).

MODEL SET-UP

Case 1

For the initial 1D permafrost sensitivity analysis, the profile from Figure 21 is used and the thermal properties as described in Table 2.

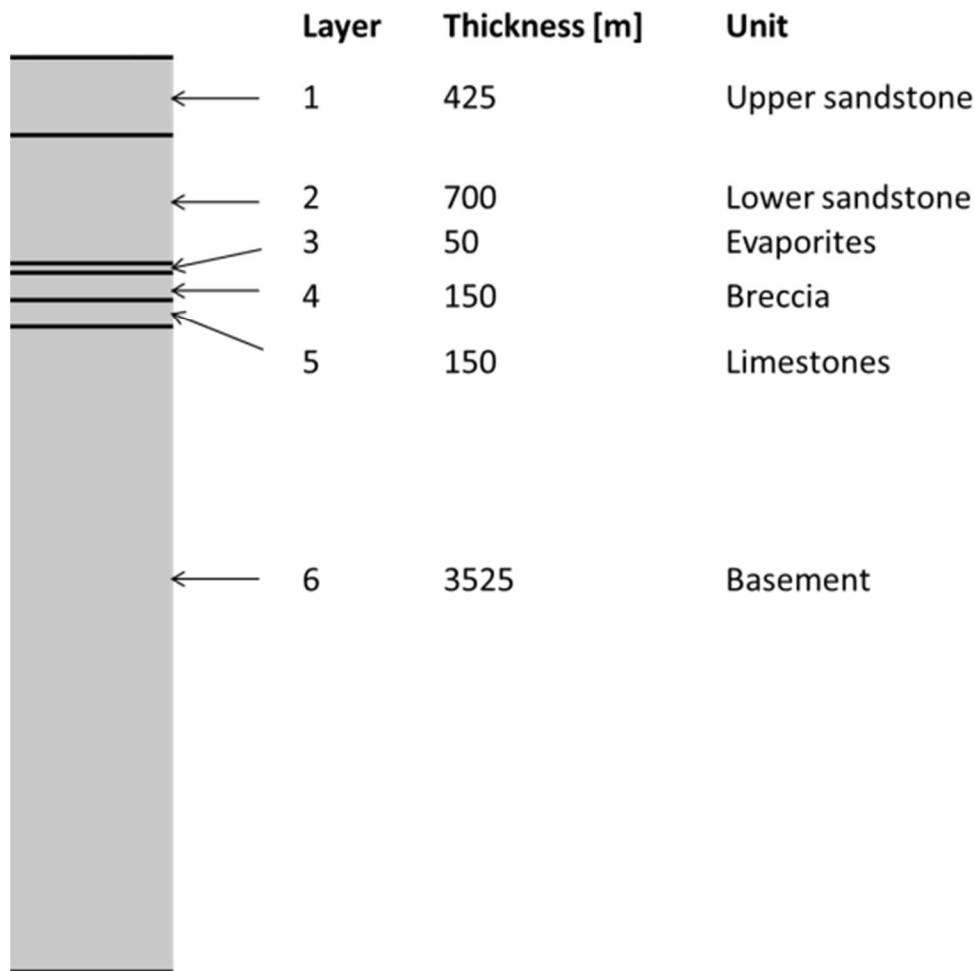


Figure 21. Layers for 1D model for Case 1.

Table 2. Thermal properties for 1D model for Case 1.

| Layer | λ [W/mK] | Cs [J/kgK] | ε [-] | ρ [kg/m ³] |
|-------|------------------|------------|-------------------|-----------------------------|
| 1 | 3.1 | 850 | 0.2 | 2650 |
| 2 | 3.1 | 850 | 0.1 | 2650 |
| 3 | 4 | 850 | 0.01 | 2650 |
| 4 | 3.1 | 850 | 0.1 | 2650 |
| 5 | 3.1 | 850 | 0.01 | 2650 |
| 6 | 4 | 850 | 0.01 | 2650 |

The model set up for the 2D coupled groundwater-permafrost model, excluding glaciation, is shown in Figure 4. The model domain is 20 km long and 2 km deep. The right hand boundary is closed to heat flow (red) and to fluid flow (blue), as this represents a topographic high. The left hand boundary is a specified head and a flux boundary for heat flow. At the top boundary, the hydraulic head is set to the elevation of the land-surface, and the temperature is specified in time. The base of the model is closed to fluid flow and a constant heat flow is specified, allowing heat to enter the model domain by heat conduction. The layers used for Case 1 are a basement, overlain by a lower and upper sandstone, and a weathered layer and the thermal and hydraulic properties used for the different layers are taken from *Towler et al. (2008b)* and listed in Table 3. The model domain is characterised by a higher ground near the right hand boundary, followed by

a steeper slope (10-20 km of the model domain). The left hand side of the model domain (0-10 km) is characterised by lowlands and the topography is characterised by three hills (at 1 km, 5 km and 9 km and of 2 m, 10 m and 18 m height) and topographic depressions (at 3 km, 7 km, 11 km of 6 m, 14 m and 18 m depth).

Case 1 including glaciation

For the model runs of Case 1, including glaciation, the model domain is expanded and the same topography as in Case 2 is used (Figure 22). The glacial model for Case 1 uses the same boundary conditions as for Case 2, which allows the differences between the model runs to be associated to geological factors only and exclude any differences in topography or ice sheet history or geometry.

Case 2

The model set up is presented in Figure 5. The model domain is 300 km long and 1500 m deep. For fluid flow, hydraulic head is assigned at the top boundary and is set to the elevation of the topography. The sides and the base of the model are no-flow for fluid flow. For temperature, the ground surface temperature is assigned at the top boundary, and a constant heat flow is specified at the base. The sides of the model are closed boundaries. The thermal and hydraulic properties used for the different geological layers are from *Towler et al.* (2008b) and listed Table 4.

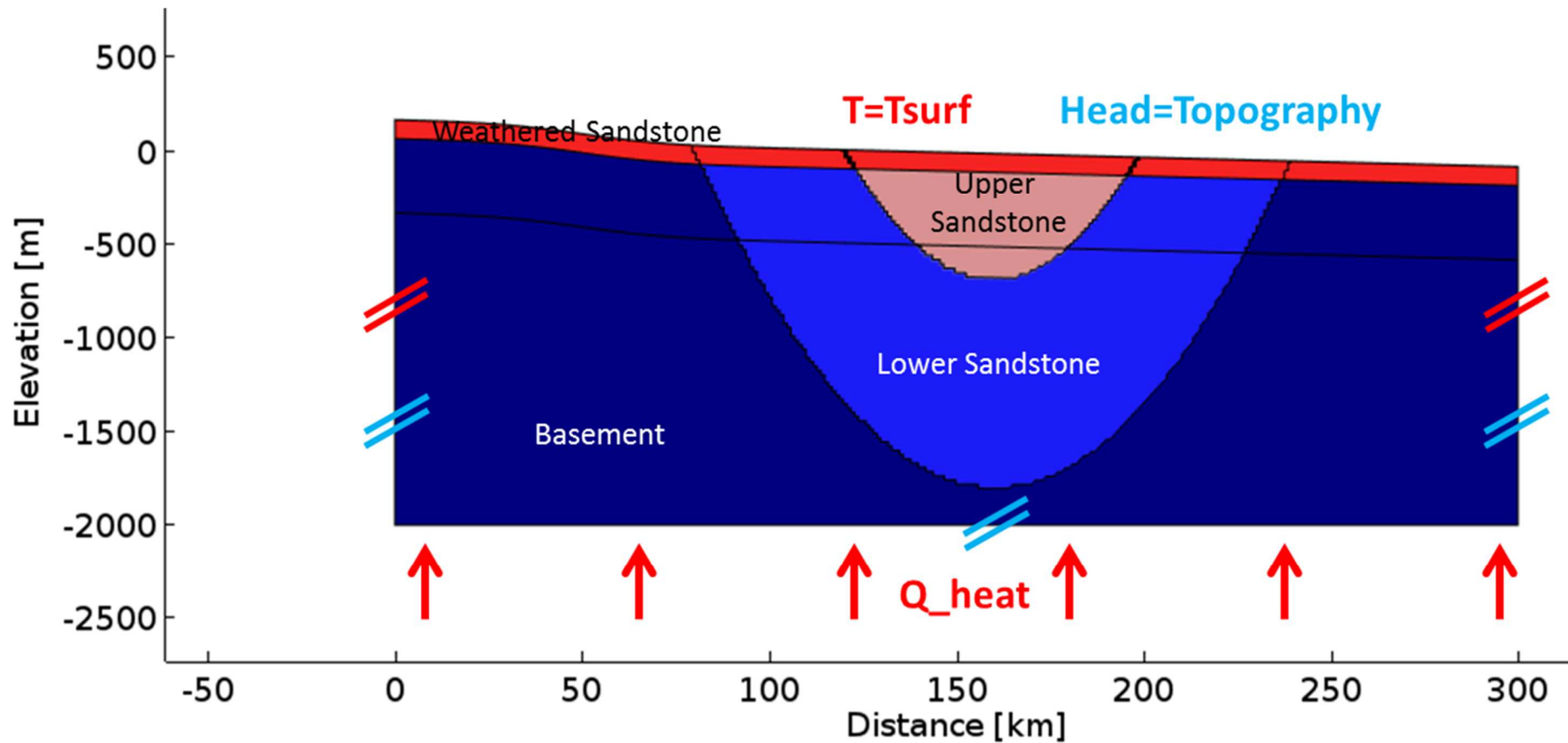


Figure 22. Model set-up and boundary conditions for Case 1 including glaciation. The boundary conditions in blue correspond to hydraulic head and those in red to temperature. The scale of the vertical axis is exaggerated 50 times

Table 3. Thermal and hydraulic properties for Case 1. The different Kx values refer to the minimum, medium and maximum permeability scenario.

| Layer | λ [W/m K] | Cs [J/kg K] | ϵ [-] | ρ [kg/m ³] | Kx [m/s] | Ky [m/s] | Ss [1/m] |
|---------------------|-------------------|-------------|----------------|-----------------------------|------------------------|----------|----------|
| Weathered Sandstone | 3.1 | 850 | 0.12 | 2650 | 3.16e-6, 1e-6, 3.16e-7 | Kx | 1E-4 |
| Upper Sandstone | 3.1 | 850 | 0.15 | 2650 | 1e-6, 1e-7, 1e-8 | Kx/10 | 1E-4 |
| Lower Sandstone | 3.1 | 850 | 0.075 | 2650 | 1e-7, 1e-8, 1e-9 | Kx/10 | 1E-4 |
| Weathered Basement | 3.1 | 850 | 0.05 | 2650 | 3.16e-6, 1e-6, 3.16e-7 | Kx | 1E-6 |
| Basement | 4 | 850 | 0.001 | 2650 | 1e-9, 5e-11, 1e-12 | Kx | 1E-6 |

Table 4. Thermal and hydraulic properties for Case 2.

| Layer | λ [W/mK] | Cs [J/kgK] | ϵ [-] | ρ [kg/m ³] | Kx [m/s] | Ky [m/s] | Ss [1/m] |
|-------------------------------------|------------------|------------|----------------|-----------------------------|----------|----------|----------|
| Cretaceous chalk | 1.88 | 1958 | 0.1 | 2000 | 1e-10 | kx | 1e-4 |
| Upper Jurassic LMS | 2.3 | 1034 | 0.25 | 2500 | 1e-9 | kx | 1e-4 |
| Middle Jurassic Clay | 1.45 | 901 | 0.2 | 2300 | 1e-9 | kx | 1e-4 |
| Middle Jurassic aquifers | 2.75 | 850 | 0.1 | 2490 | 1e-5 | kx | 1e-4 |
| Lower Jurassic shales and mudstones | 1.55 | 895 | 0.15 | 2340 | 1e-12 | kx/10 | 1e-4 |
| Triassic mudstones/siltstones | 2.07 | 897 | 0.15 | 2430 | 1e-10 | kx/10 | 1e-4 |
| Triassic sandstones | 2.75 | 850 | 0.1 | 2490 | 1e-6 | kx | 1e-4 |
| Permian | 2.38 | 850 | 0.15 | 2500 | 1e-8 | kx | 1e-4 |
| Variscan basement | 3.3 | 859 | 0.05 | 2630 | 1e-9 | kx | 1e-6 |

BOUNDARY CONDITIONS AND MODEL CONCEPTUALISATION

Temperature time series

The climate has oscillated between glacial and interglacial conditions in the past, as seen by palaeo-climatic proxies such as deep ocean sediment records, lake sediments, or ice cores. In this current work, a Pliocene-Pleistocene stack of 57 globally distributed benthic $\delta^{18}\text{O}$ records is used and scaled for different climate scenarios (*Lisiecki and Raymo, 2005*). Foraminiferal $\delta^{18}\text{O}$ is a function of the temperature and $\delta^{18}\text{O}$ of the water in which the sediment forms, and the $\delta^{18}\text{O}$ of the water is a function of the global ice volume and the water salinity (*Lisiecki and Raymo, 2005*). This global $\delta^{18}\text{O}$ record (Figure 23) serves to estimate the shape and the general trend of the temperature curve, which is characterised by a decrease in temperature over ~100 ka followed by a fast increase in temperature over ~10 ka, rather than very detailed temperature variations over short time periods.

The global $\delta^{18}\text{O}$ time series needs to be scaled in order to serve as a proxy for a Great Britain temperature time series. The present day mean annual air temperature is 8.6 °C for north-west England, and is set to 8.5°C in the model. Different scenarios for temperature differences over the last one million years are used; the minimum temperature is set to 10, 12, 14, 18, 20, and 25 °C below the present day temperatures. The present day temperature and the minimum temperature are used to scale the proxy record linearly, and the resulting temperature time series is presented in Figure 24. The use of this scaled proxy record serves as an estimate of the pattern of the temperature time series; the overall pattern is characterised by a slow decrease followed by an abrupt rise in temperature over a glacial cycle of ~100 ka for the past 500 ka.

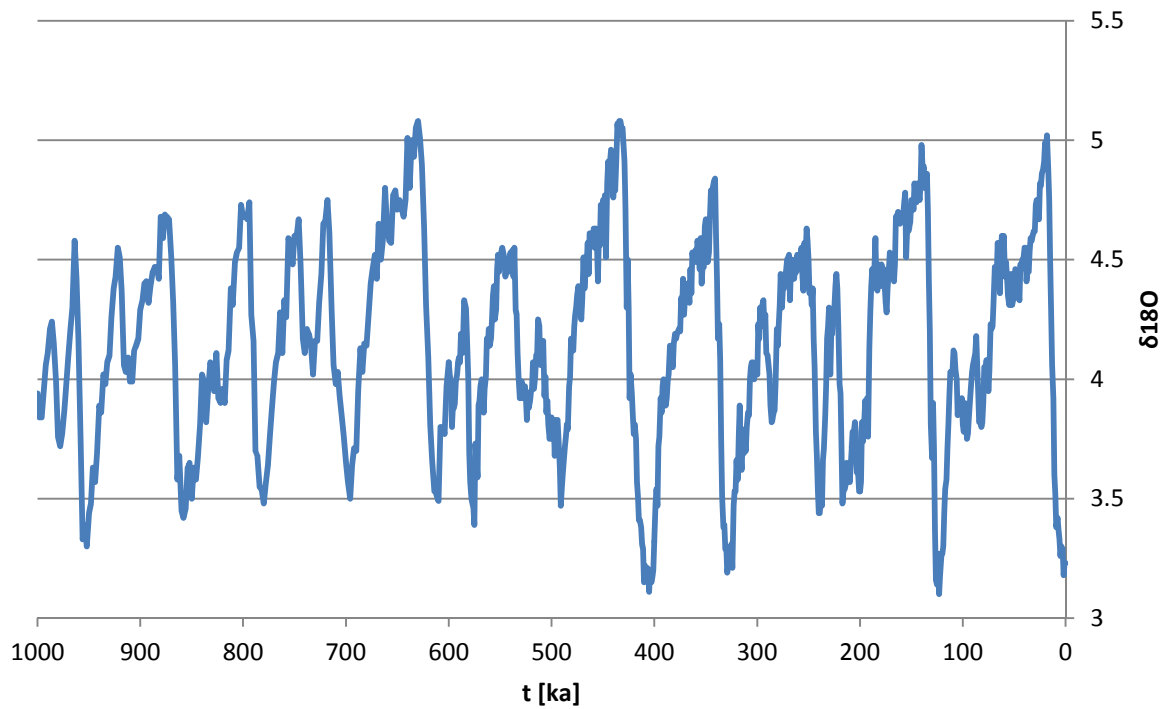


Figure 23. Global $\delta^{18}\text{O}$ time series after *Lisiecki and Raymo (2005)*.

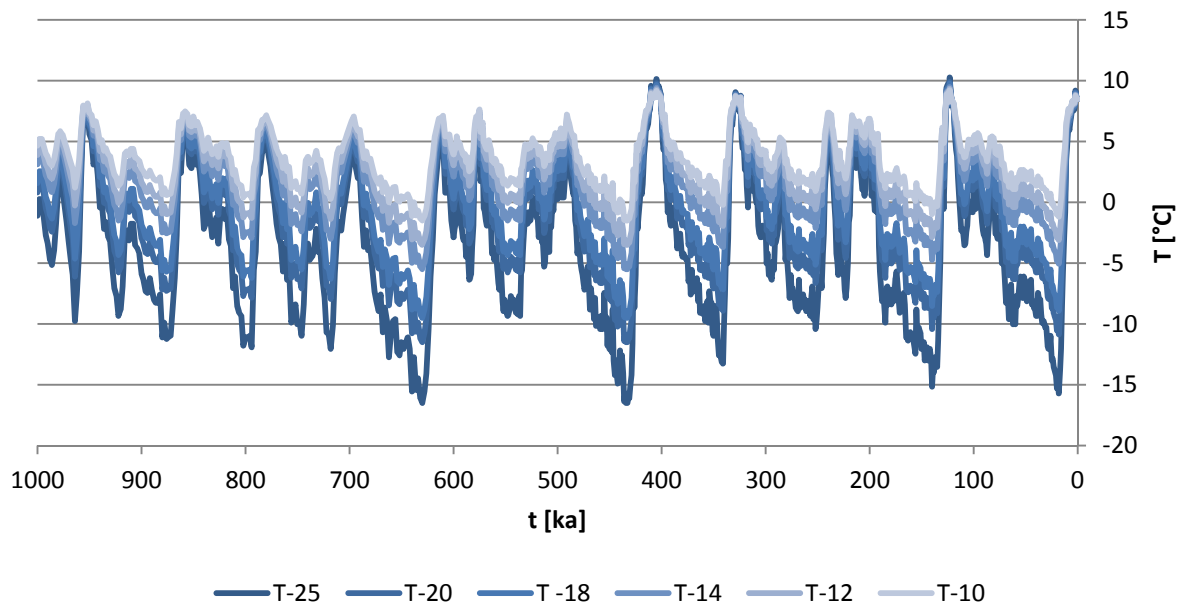


Figure 24. Scaled temperature time series after *Lisiecki and Raymo (2005)* using ΔT ranging from 10°C to 25°C .

Figure 25 compares the scaled temperature time series by *Busby et al. (2014)* with the $\delta^{18}\text{O}$ proxy derived temperature time series. In comparison to the previous project, the full temperature record is used as model input and is not a step change model. The maximum and minimum temperatures are comparable, but the duration of the extreme events differ.

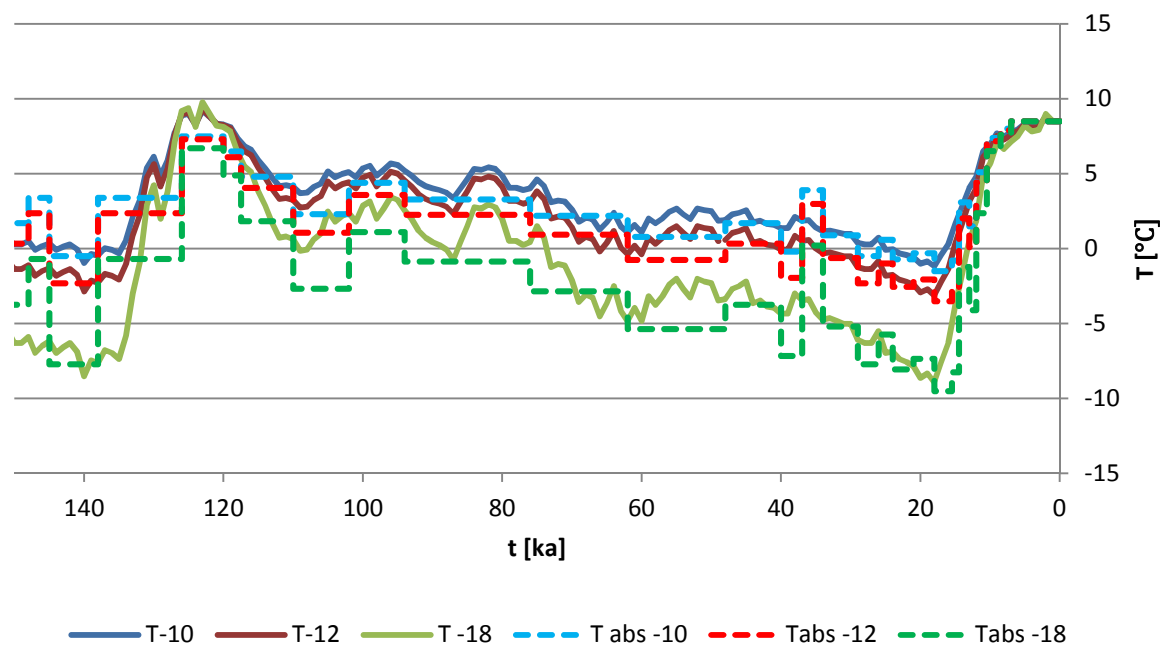


Figure 25. Comparison of scaled temperature time series with temperature time series used in the Phase I study (*Busby et al., 2014*). Tabs -10, Tabs-12 and Tabs-18, are the temperature time series used in *Busby et al. (2014)* and refers to the temperature difference between the present day and minimum temperature during the last 123 ka of 10°C, 12°C and 18°C.

The initial conditions for the first series of simulations using a one-dimensional model were derived as follows: an initial steady state simulation is run with the temperature set at the top boundary to the average temperature over the last 200 ka. This provides the initial conditions for a subsequent transient simulation in which the surface temperature boundary condition is specified as the temperature history of the last 123 ka. For the 2D coupled model, the computational run-time increases significantly and this approach was unsuitable. Therefore, the temperature at the top boundary was set to the surface temperature of the first time step. An initial temperature profile, for subsequent transient runs, was then calculated by running a steady state simulation that incorporated heat conduction and advection.

Hydraulic head boundary conditions

Hydraulic head is set to be topography driven, where the hydraulic head along the top surface is set to the elevation of the land-surface. This is a simplification of the real hydrogeological regime. However the focus lies on the influence of a permafrost layer, the presence of an ice sheet or sea level fluctuations on the flow regime.

The hydraulic head boundary is modified when there is an ice sheet present or when it is submerged by the sea. When the land-surface is covered by an ice sheet, the ice overburden is added to the local elevation, and when the sea is present, the depth of the sea is added to the local elevation.

Glacial history over the last one million years

The timing, duration and the temperature of a glacier influence the ground surface temperature. Warm-based, or temperate, ice insulates the ground from the subzero air temperatures, whereas cold-based ice that has been advected from up-glacier can be colder than temperatures without ice coverage.

Whereas the maximum ice extent and the deglaciation history of the last British Ice Sheet is relatively well constrained from glacial geomorphological evidence (*Clark et al.*, 2012), and numerical modelling (*Boulton and Hagdorn*, 2006; *Hubbard et al.*, 2009), the timing of ice coverage during the Quaternary is more uncertain.

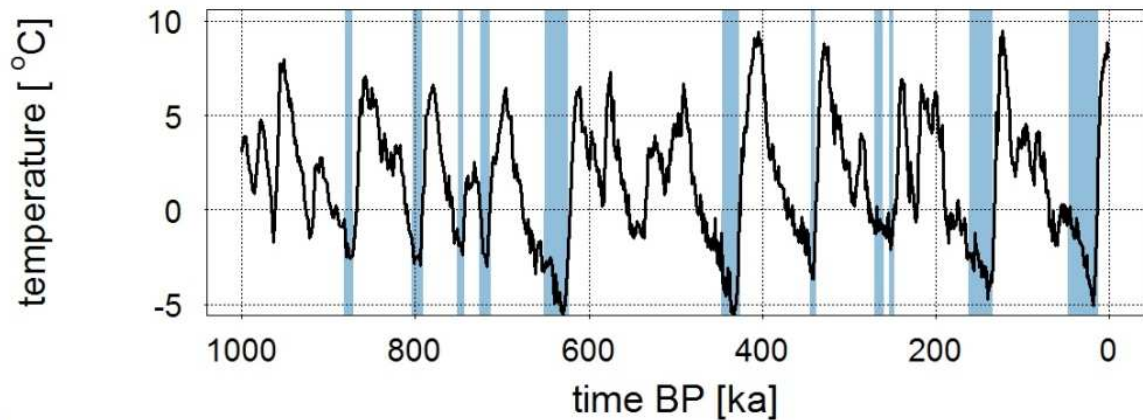
Lee et al. (2012) review pre-Weichselian Quaternary glaciations of the British Isles and present evidence of glacial stratigraphy in Britain for MIS 2, 6, 12, 18, 22 and potentially the stages 8, 10, 16, and 20.

For Case 1, a model of the British Ice Sheet over the last 500 ka is taken from *Boulton and Broadgate* (1993). Ice extent with time along a transect as well as subglacial discharge are presented in *Boulton and Broadgate* (1993). The authors present three glaciation scenarios, a minimum, medium and a maximum scenario. The minimum scenario assumes that the locations were never covered by a glacier. The medium and the maximum scenarios are presented in Figure 26 a-b.

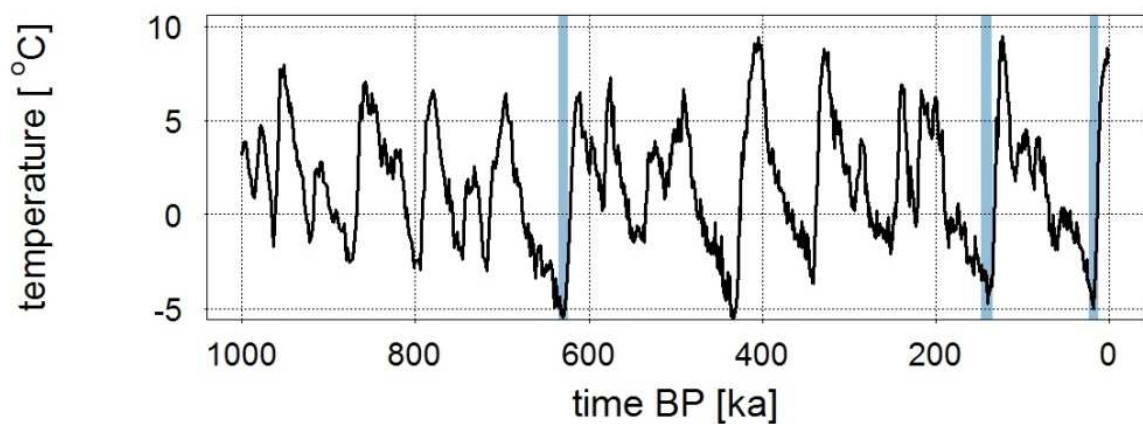
It is assumed in this study that the Anglian Glaciation (480-430 ka) and the Late Devensian (19-17 ka) glaciation affected Case 2 (Figure 26 c). The precise timing of ice during the Anglian is not known and only generic ages can be given which correspond to the timing of the Anglian (480-430 ka). The Late Devensian glaciation was around 19-17 ka based on *Bateman et al.* (2015) and *Clark et al.* (2012). Using the times of the glaciated times at Case 2 during the Devensian as an analogy for the glaciated times during the Anglian glaciation, it is likely that the glaciated times during the Anglian glaciation occurred during 20-30% of the duration of the glaciation.

In this modelling study it is assumed that the Anglian glaciation occurred from 465-445 ka BP, 10 ka for build-up, 5 ka at its maximum stage, and 5 ka for retreat. The location of the ice margin during build-up and retreat are calculated as a linear function of distance and time.

a)



b)



c)

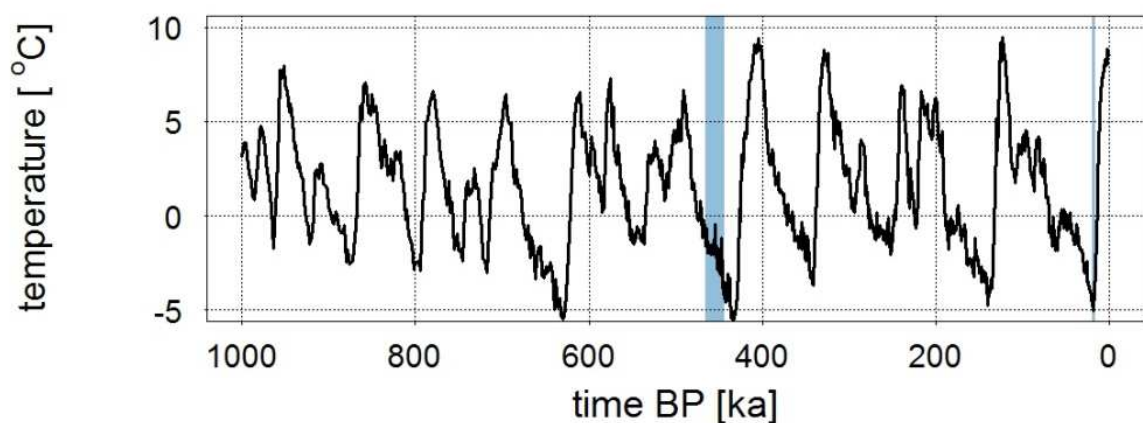


Figure 26. Temperature time series with modelled (a) maximum and (b) median ice coverages after *Boulton and Broadgate (1993)* for Case 1, and (c) ice coverage for Case 2. The blue lines indicate glaciated times.

TEMPERATURE BOUNDARY CONDITIONS UNDER GLACIATIONS

The temperature distribution of an ice sheet or glacier is controlled at the surface by the climate. If the ice is sliding, geothermal heat and friction warm or melt the base, while ice deformation and refreezing of meltwater warm the interior. In addition, heat conduction and advection

through ice movement, and in some cases water flow, transfer heat within a glacier. The temperature distribution is thus a combination between ice flow and heat flow (*Paterson, 1994*).

Generally speaking, the temperature distribution within a glacier can have four forms:

- All the ice is below pressure melting
- Melting point is only reached at the bed
- A basal layer of finite thickness is at the melting point
- All the ice is at the melting point

It is of note that more than one temperature distribution can be present at once for different locations of the glacier, e.g. at parts of the glacier all the ice is below pressure melting and other parts the glacier bed is at pressure melting. Furthermore, the thermal distribution can change seasonally or interannually.

Boulton and Hagdorn (2006) model the British Ice Sheet during the last glacial cycle. The simulation which satisfies the extent, elevation and relative sea-level best is one in which major ice streams are fixed. The simulations show that the basal temperature of these ice streams would have been at pressure melting, whereas the core upland areas of the ice sheet were cold based during the last glacial maximum.

The ground surface temperature time series is corrected for ice coverage by setting the temperature to 0°C when ice is present. During the Devensian, the ice was likely to be warm based *Boulton and Hagdorn (2006)*. During the Anglian, the temperatures at the ice bed are less well known and are likely warm based and cold based for some time. There is evidence of chalk rafts, which would imply a cold glacier bed. *Eyles et al. (1989)* suggest that ice movement may have detached frozen slabs of chalk from unfrozen chalk at depth. Evidence for a warm glacier bed is provided by tunnel valleys that were formed during the Anglian glaciation (*Phillips and Lee, 2013*). Seasonal variation in the temperature regime of the glacier bed could have occurred, with a cold-based glacier bed during winter and a warm-based glacier bed during summer glaciation (*Phillips and Lee, 2013*).

As a seasonal temperature variation goes beyond the scope of this study, a uniform, warm based glacier bed is assumed through the simulation time for Case 2.

As the subglacial temperature estimate is uncertain, a range of different temperature scenarios is used for the sensitivity study in 1D with ice bed temperatures of 0°C, -1°C and -5°C. For the coupled 2-D model, one temperature scenario assuming wet-based basal conditions with a temperature of 0°C was used.

HYDRAULIC BOUNDARY CONDITIONS UNDER GLACIATIONS

To model the exchange of groundwater between the glacier bed and underlying aquifers, a flux boundary or a head boundary can be applied. A flux boundary condition based on estimated rates of basal melting may have an error of several orders of magnitude, whereas setting the hydraulic head to the flotation value provides probably only a mild overestimate of actual heads at the bed surface (*Iverson and Person, 2012*). Potentiometric heads from palaeo-pore water pressures have been estimated to be equivalent to 72% of the ice thickness based on the stress characteristics of the fine-grained sediments (*Piotrowski, 2006*). The maximum head that can be reached by the ice overburden is 92% of the local ice thickness, however in the transition from warm-based to cold-based ice near ice margins of polythermal glaciers, artesian water pressures can exist. *Lemieux et al. (2008c)* argue that all meltwater reaching the glacier bed in excess of the flotation level of the ice sheet thickness should be treated as overland flow and leave the glacier through channelized flow because, otherwise, the ice sheet would become unstable.

The ice height is calculated after *Paterson* (1994) considering a steady-state ice sheet on a horizontal bed:

$$H_{ice} = A\sqrt{x - x_M}$$

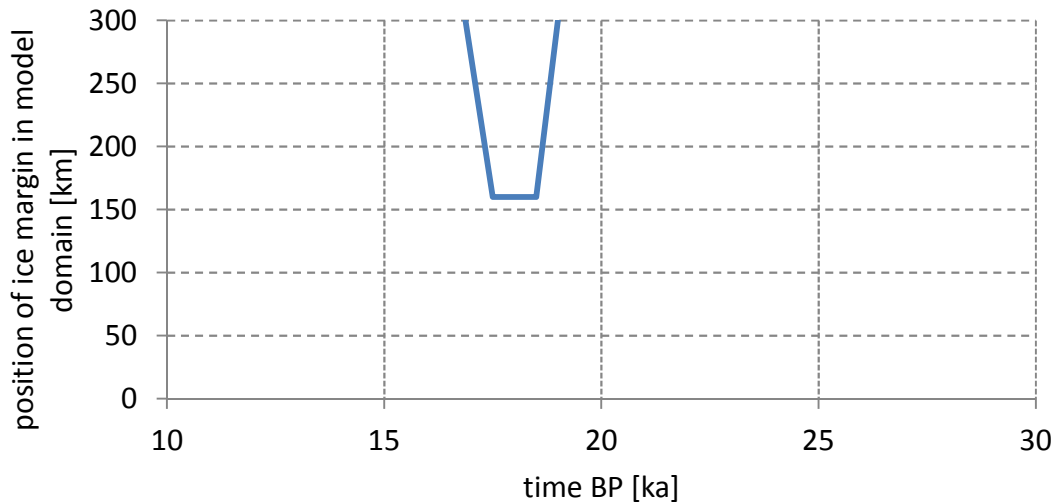
where $H_{ice}(x[m], t[a])$ is the height of the glacier as a function of space and time, $x[m]$ is distance along an ice flow line and $x_M(t[a])$ is the location of the ice margin as a function of time. This equation is derived from the calculation of shear stress (τ) at the glacier bed as follows:

$$\tau = -\rho g H \frac{dH}{dx}$$

Assuming the base is horizontal and the ice is in steady state, and the ice is treated as perfectly-plastic material, then this equation can be integrated to give the equation of the surface profile. $\sqrt{2\tau/\rho g}$ is equal to the factor A . Assuming a basal shear stress of 50 kPa, $A=3.4$. After *Paterson* (1994) the shear stress for alpine valley glaciers lies usually between 50 and 150 kPa, and for ice sheets between 0 to 100 kPa, with a mean value of ~ 50 kPa. A similar approach has been used in *Bense and Person* (2008) and *Scheidegger and Bense* (2014), and is suitable for conceptual models.

The position of the ice margin for the Devensian and Anglian glaciation are presented in Figure 27. To set the hydraulic head value at the top boundary, the local ice sheet elevation multiplied by 0.9 is added to the local land-surface elevation.

a)



b)

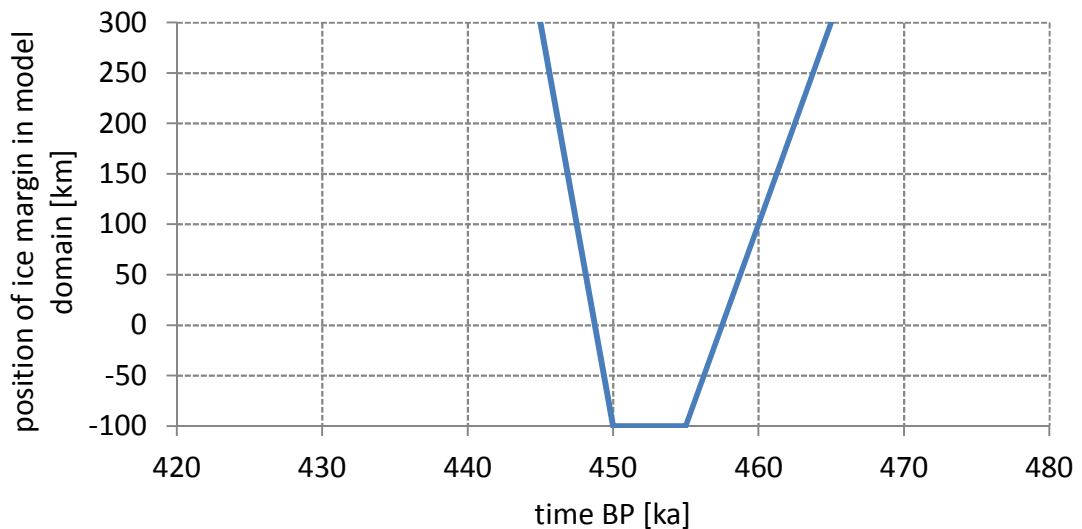


Figure 27. Position of the ice margin in the model domain for the Devensian (a) and Anglian glaciation (b). The distance is relative to the left hand boundary of the model domain.

Sea-level change

Local relative sea-level curves for use in Case 2 are only available for the past ~20ka (e.g. *Peltier et al.*, 2002; *Shennan and Horton*, 2002). Over the past one million years, the global relative sea-level curve is used (Figure 28). Before the Anglian glaciation, in regard to Case 2 the coast is assumed to be distant to the cross section.

For modelling sea-level changes in relation to Case 2, it is assumed that when the land-surface is covered by the sea, the temperature at the boundary for the submerged locations is set to be 7°C in order to prevent freezing, and the hydraulic head at the boundary is set to be the elevation of the shore position. Therefore, the base level of hydraulic head varies over time.

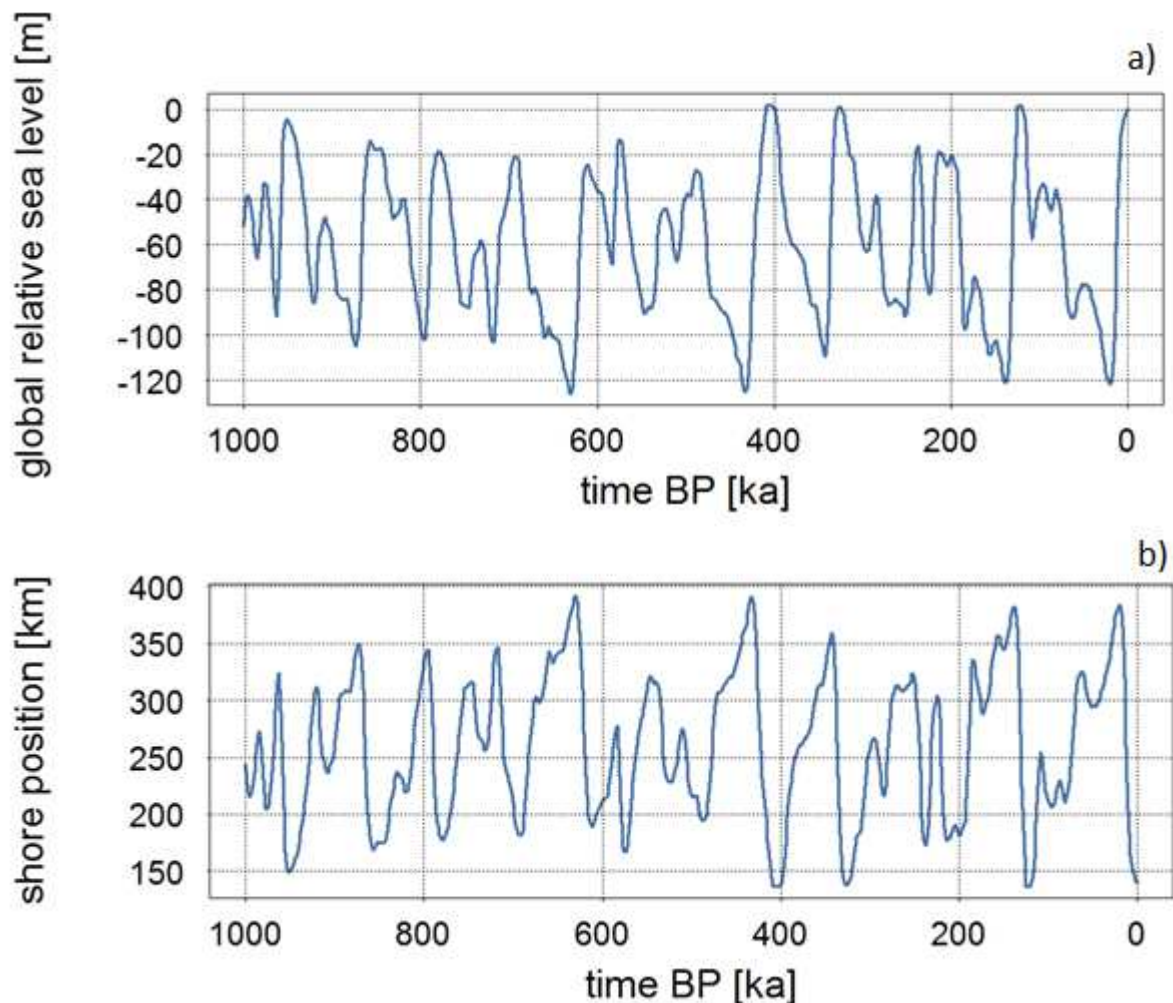


Figure 28. (a) Global relative sea-level curve after *Bintanja et al.* (2005), and (b) global relative sea-level curve translated to shore position.

Temperature boundary condition for lakes

The temperature at the lake location is imposed and set to 4°C for the T-14_MaxTalík model and to 2°C for the T-14_MaxTalík2 model. We note that assigning a temperature that is fixed in time and space is a large simplification. In reality, the lifecycle of a lake is transient, and gets often filled with sediment or peat. In addition, the depth of a lake together with climatic factors will drive the temperature at the bottom of the lake. Therefore, setting a fixed temperature in time and

space is a first attempt to investigate the maximum influence of a talik, however future modelling should take into account the lifecycle of lakes.

MODELLING METHODOLOGY

Modelling assumptions and limitations

The modelling presented in this study uses the generic Cases 1 and 2, and boundary conditions as described above with the following assumptions and limitations.

- Hydrogeology
 - Fully saturated flow was assumed.
 - Topographically driven flow was assumed i.e. the hydraulic head at the top boundary was set to the land-surface elevation.
 - Buoyancy driven flow was not considered. The influence of temperature or salinity on density and viscosity were not considered.
- Temperature
 - The scaled temperature time series were used for the upper temperature boundary. Thermal effects at the ground-atmosphere boundary were not considered e.g. effects of soil, vegetation, and snow cover.
 - One freezing curve and relative permeability curve are used for all layers.
- Model domain and subsurface properties
 - The domains were simplified to 2D cross sections.
 - The model domain and topography did not change over one million years. No erosion or deposition was included in the model.
 - Thermal, hydraulic and geological properties did not change over one million years. For example, permeability and porosity remain unchanged after a glaciation.
- Ice sheet
 - The pressure underneath the ice sheet is set to the ice overburden.
 - The basal temperatures are assumed to be constant over time.
 - For the 2D coupled models, the basal temperature is assumed to be at pressure melting.
 - Deformation of the model domain due to isostatic depression and forebulge is not considered.

Modelling approach

The first set of simulations was performed using a 1D heat conduction only model including phase change; a sensitivity study of different model input parameter was undertaken. For the 1D models, two different sets of parameters were used. The first set uses the geology for Case 1 and tests the influence of different temperature time series, glaciation scenarios and geothermal heat fluxes on the permafrost depth. The second set of 1D model consists of a column with the same properties (referred to as: one layer model) and is used to test the influence of different model input parameters (thermal conductivity, heat capacity, geothermal heat flow, and porosity) on the maximum permafrost depth.

For the one layer runs, several hundred combinations of different geological input parameters are run, which are not listed here. The model runs for Case 1 are listed in Table 5.

Table 5. 1D model runs for Case 1.

| Run | Description |
|----------------|---|
| T-10 | Using the T-10 temperature time series for a 1D conduction only case. |
| T-12 | Using the T-12 temperature time series for a 1D conduction only case. |
| T-14 | Using the T-14 temperature time series for a 1D conduction only case. |
| T-16 | Using the T-16 temperature time series for a 1D conduction only case. |
| T-18 | Using the T-18 temperature time series for a 1D conduction only case. |
| T-20 | Using the T-20 temperature time series for a 1D conduction only case. |
| T-25 | Using the T-25 temperature time series for a 1D conduction only case. |
| T-14, IceMax_0 | Using the T-14 temperature time series corrected for the maximum ice sheet scenario and a subglacial temperature of 0°C. |
| T-14, IceMax_1 | Using the T-14 temperature time series corrected for the maximum ice sheet scenario and a subglacial temperature of -1°C. |
| T-14, IceMax_5 | Using the T-14 temperature time series corrected for the maximum ice sheet scenario and a subglacial temperature of -5°C. |
| T-14, IceMed_0 | Using the T-14 temperature time series corrected for the medium ice sheet scenario and a subglacial temperature of 0°C. |
| T-14, IceMed_1 | Using the T-14 temperature time series corrected for the medium ice sheet scenario and a subglacial temperature of -1°C. |
| T-14, IceMed_5 | Using the T-14 temperature time series corrected for the medium ice sheet scenario and a subglacial temperature of -5°C. |

The second set of simulations were performed using the 2D coupled models based on the approach described in Appendix 1, and the set-ups for Case 1 and Case 2 described in Section 3.2.2. Simulations for Case 1 are listed in Table 6, for Case 2 in Table 7, and for the runs including glaciation in Table 8.

Table 6. Coupled model runs for Case 1.

| Run | Description |
|-----------------|---|
| T-14_Cond | Using the T-14 temperature time series for a conduction only case. |
| T-14_Min | Using the T-14 temperature time series for a minimum permeability case. |
| T-14_Med | Using the T-14 temperature time series for a medium permeability case. |
| T-14_Max | Using the T-14 temperature time series for a maximum permeability case. |
| T-25_Cond | Using the T-25 temperature time series for a conduction only case. |
| T-25_Min | Using the T-25 temperature time series for a minimum permeability case. |
| T-25_Med | Using the T-25 temperature time series for a medium permeability case. |
| T-25_Max | Using the T-25 temperature time series for a maximum permeability case. |
| T-25_Max_Omega3 | Using the T-25 temperature time series for a maximum permeability case, using $\Omega=3$ for Equation 16. |
| T-25_Max_Omega1 | Using the T-25 temperature time series for a maximum permeability case, using $\Omega=1$ for Equation 16. |
| T-14_Talik | Using the T-14 temperature time series for a maximum permeability case, and imposing three lakes of a width of 200 m with a temperature of 4°C. |
| T_14_tracer | Using the T-14 temperature time series for a maximum permeability case and releasing a tracer of 1 kg m ⁻³ a ⁻¹ at 500 m depth and 7 km from the left hand boundary with dimensions of 200 m by 20 m. |

Table 7. Model runs for Case 2.

| Run | Description |
|-----------|--|
| T-14 | Using the T-14 temperature time series for the past one million years. |
| T-25 | Using the T-25 temperature time series for the past one million years. |
| T-25_Cond | Using the T-25 temperature time series for a conduction only case |

Table 8. Model runs including glaciation.

| Run | Description |
|-----------------------|--|
| T-14_OneLayer | One layer model, representing basement, using the T-14 temperature time series and ice sheet scenario for Case 2. |
| T-14_OneLayer_Loading | One layer model, representing basement, using the T-14 temperature time series and ice sheet scenario for Case 2, including ice sheet loading. |
| T-14_Case1_Loading | Geology representing Case 1, using the T-14 temperature time series and ice sheet scenario for Case 2, including ice sheet loading. |
| T-14_Case2 | Geology representing Case 2, using the T-14 temperature time series and ice sheet scenario for Case 2. |
| T-14_Case2_Loading | Geology representing Case 2, using the T-14 temperature time series and ice sheet scenario for Case 2, including ice sheet loading. |

Appendix 3 Factors and processes influencing the thickness and extent of permafrost in a geological environment

TEMPERATURE

Steady state vs transient model

Under unchanging climatic conditions when mean annual ground surface temperatures are below freezing, the permafrost thickness will reach a steady state. This means that the permafrost thickness is in equilibrium with the climate, and the maximum permafrost thickness is generated for the climate scenario.

Assuming a uniform ground condition, the temperature, $T(z)$, at a depth, z , is given by:

$$T(z) = T_s + z * q_{heat}/K \quad \text{Equation 20}$$

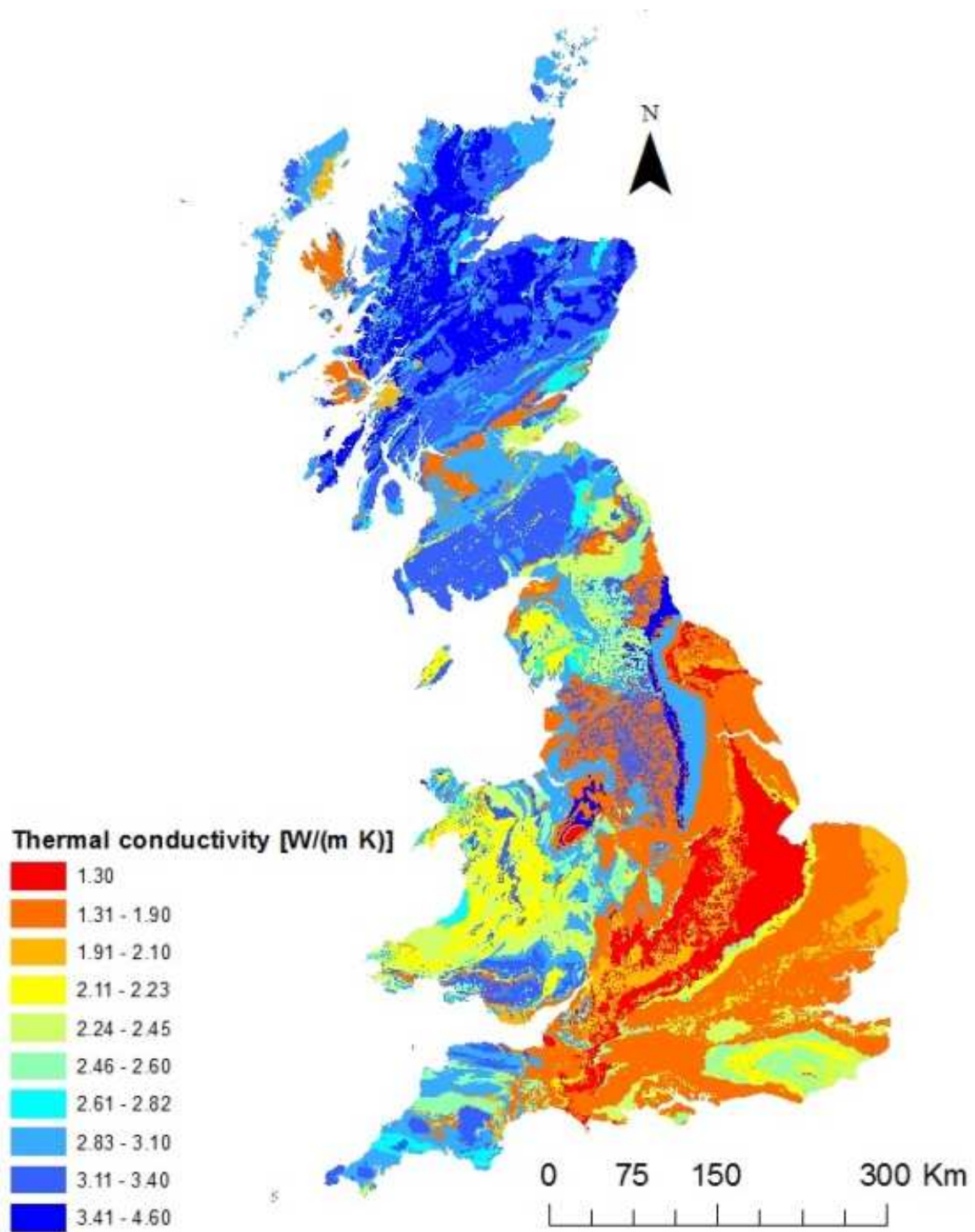
where (T_s) is the ground surface temperature, q_{heat} is the heat flow density, and K is the thermal conductivity.

Where the long-term mean surface temperature is below 0°C, permafrost is present at a depth z_p . Setting 0°C for $T(z)$ and rearranging gives the permafrost thickness for a steady state profile:

$$z_p = T_s K / q_{heat} \quad \text{Equation 21}$$

It is evident that permafrost thickness under steady state conditions is a function of the surface temperature, the thermal conductivity and the heat flow, and that the permafrost thickness is equally sensitive to all three parameters (*Williams and Smith, 1989*).

Using the UK thermal conductivity of the surface bedrock and a heat flow map (Figure 29), and a ground surface temperature of -5°C, the steady state permafrost thickness based on these parameters can be calculated. The steady state permafrost thickness for a surface temperature of $T_s = -5^\circ$ is presented in Figure 30. The permafrost thickness ranges between 78 m and 560 m. Generally, permafrost is thicker where the thermal conductivity is larger and where the heat flow density is smaller.



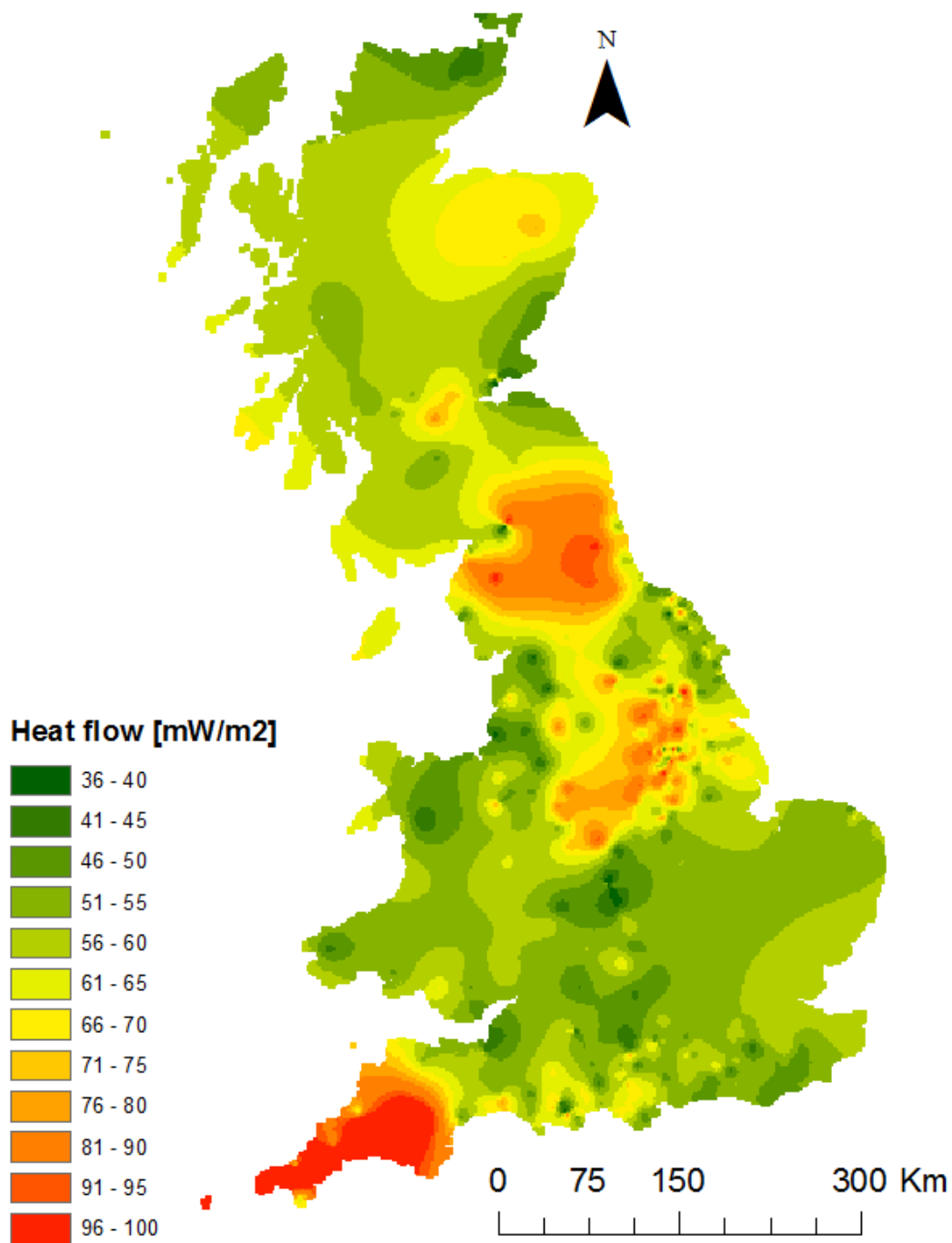


Figure 29. Thermal conductivity and heat flow density of Great Britain (Rollin, 2002; Busby et al., 2011). Heat flow density estimation combines bottom hole temperature observation with a mean thermal resistance at each depth, derived from the borehole geology and a databank of mean thermal conductivity (Rollin, 2002; Busby et al., 2011)

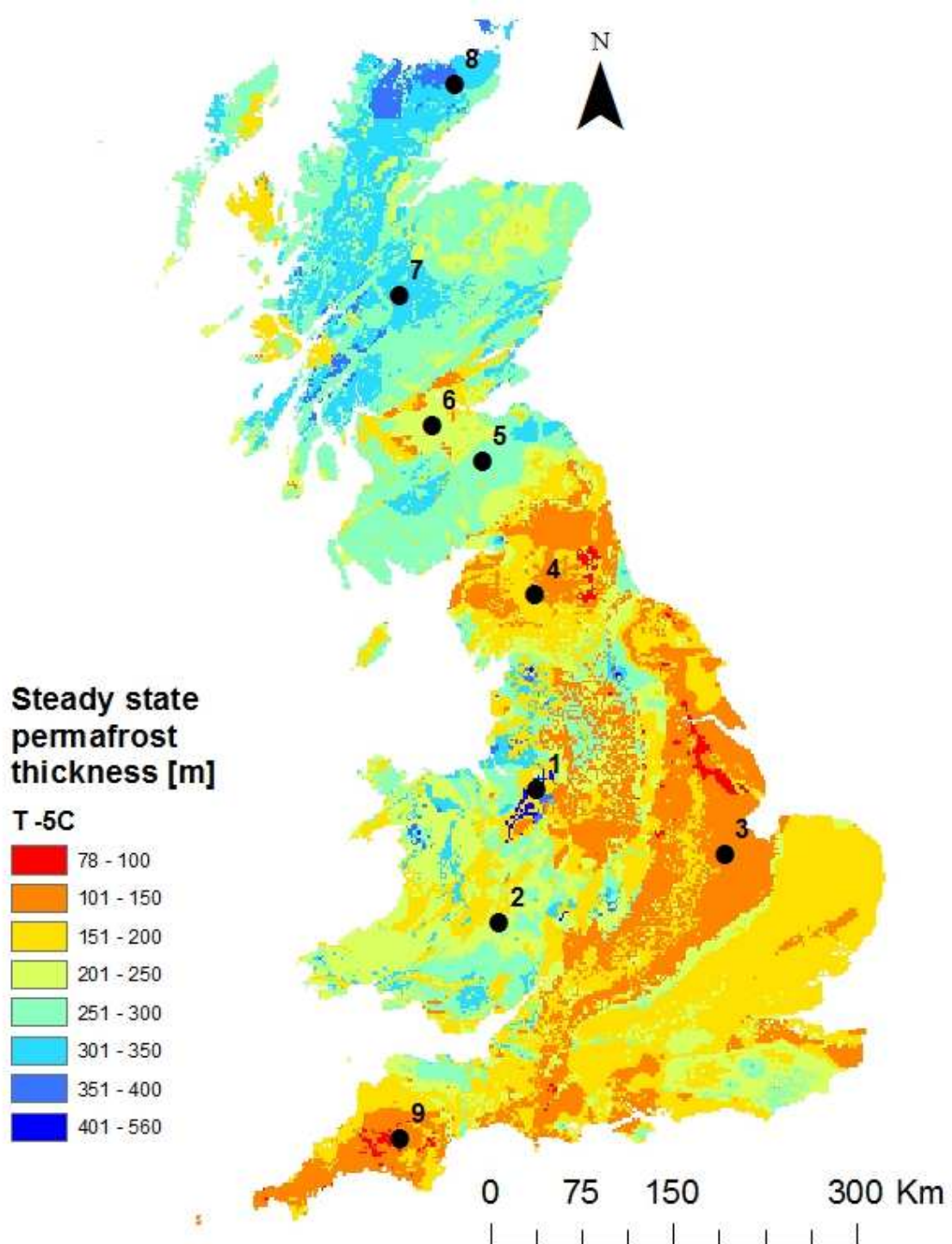


Figure 30. Steady state permafrost simulation for $T_s = -5^\circ\text{C}$, using the thermal properties from Figure 29.

In order to test whether steady state permafrost thickness is realistic in Great Britain, transient 1D permafrost models were run for the past one million years at the nine locations shown in Figure 30 and compared to the steady state permafrost estimates (Table 9) using a homogeneous 1D model of the surface bedrock geology. The range of permafrost depths for the steady state simulation at the nine locations is from 87 to 487 m and for the transient simulation the range is

between 77 and 320 m. The temperature time series for the nine locations is presented in Figure 31. The comparison between the steady state and the transient permafrost thicknesses leads to the conclusion that assuming the temperature oscillations from the past one million years, a pseudo steady state permafrost thickness did not have time to occur in Great Britain.

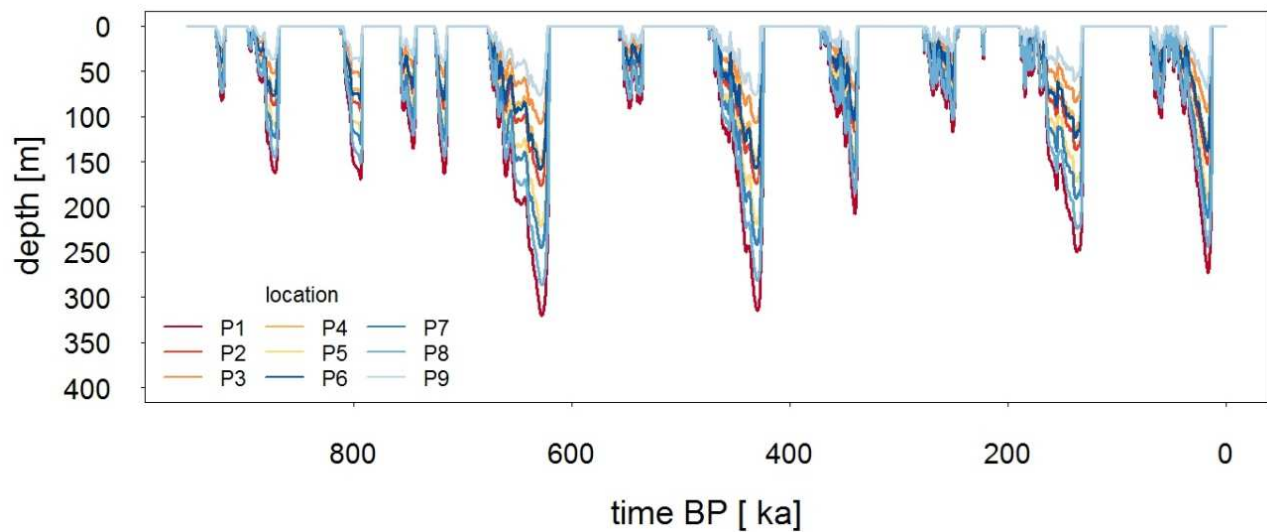


Figure 31. Permafrost thickness over time at the nine locations from Figure 30.

Table 9. Thermal properties, steady state permafrost thickness and maximum permafrost thickness for a transient simulation using a T_{min} of -5.5°C (T-14 scenario).

| Location | Thermal conductivity [W/(m K)] | Heat flow density [mW/ m ²] | Density [kg/m ³] | Heat capacity [J/(kg K)] | Thermal diffusivity [m ² /s] | SS permafrost thickness for $T_{-5.5^{\circ}\text{C}}$ [m] | Transient max. permafrost depth [m] | Relative PF thickness difference [%] |
|----------|--------------------------------|---|------------------------------|--------------------------|---|--|-------------------------------------|--------------------------------------|
| 1 | 4.6 | 52 | 2420 | 900 | 2.1E-06 | 487 | 320 | 34 |
| 2 | 2.4 | 56 | 2680 | 890 | 1.0E-06 | 236 | 177 | 25 |
| 3 | 1.3 | 56 | 2400 | 920 | 5.9E-07 | 128 | 108 | 15 |
| 4 | 2.9 | 85 | 2500 | 840 | 1.4E-06 | 188 | 149 | 21 |
| 5 | 3.4 | 61 | 2680 | 840 | 1.5E-06 | 307 | 221 | 28 |
| 6 | 2.9 | 79 | 2590 | 840 | 1.3E-06 | 202 | 158 | 22 |
| 7 | 3.8 | 60 | 2700 | 860 | 1.6E-06 | 348 | 245 | 30 |
| 8 | 3.4 | 43 | 2720 | 800 | 1.6E-06 | 435 | 286 | 34 |
| 9 | 1.79 | 113 | 2600 | 920 | 7.5E-07 | 87 | 77 | 12 |

Sensitivity of the scaling of the temperature time series

The scaling of the temperature time series is one of the main uncertainties for estimating the permafrost thickness over the last glaciation or over the past one million years. For the last glaciation, *Annan and Hargreaves* (2013) compile a dataset based on a combination of numerical models and pollen temperature proxies. For southern England and Wales, temperatures are estimated to be $8\text{-}12^{\circ}\text{C}$ below present, and for northern England and Scotland $12\text{-}20^{\circ}\text{C}$ below the present day temperature. In contrast, *Westaway and Younger* (2013) reconstruct a temperature difference to the present day temperature for southern England of 20°C , and for northern England of 18°C .

In order to address this uncertainty, a range of temperature scenarios is used, ranging from a ΔT of 10°C to ΔT of 25°C. (Figure 32a)

The maximum permafrost thickness for Case 1 ranges between 49 m for a ΔT of 10°C and 475 for a ΔT of 25°C (Figure 32b;

Table 10).

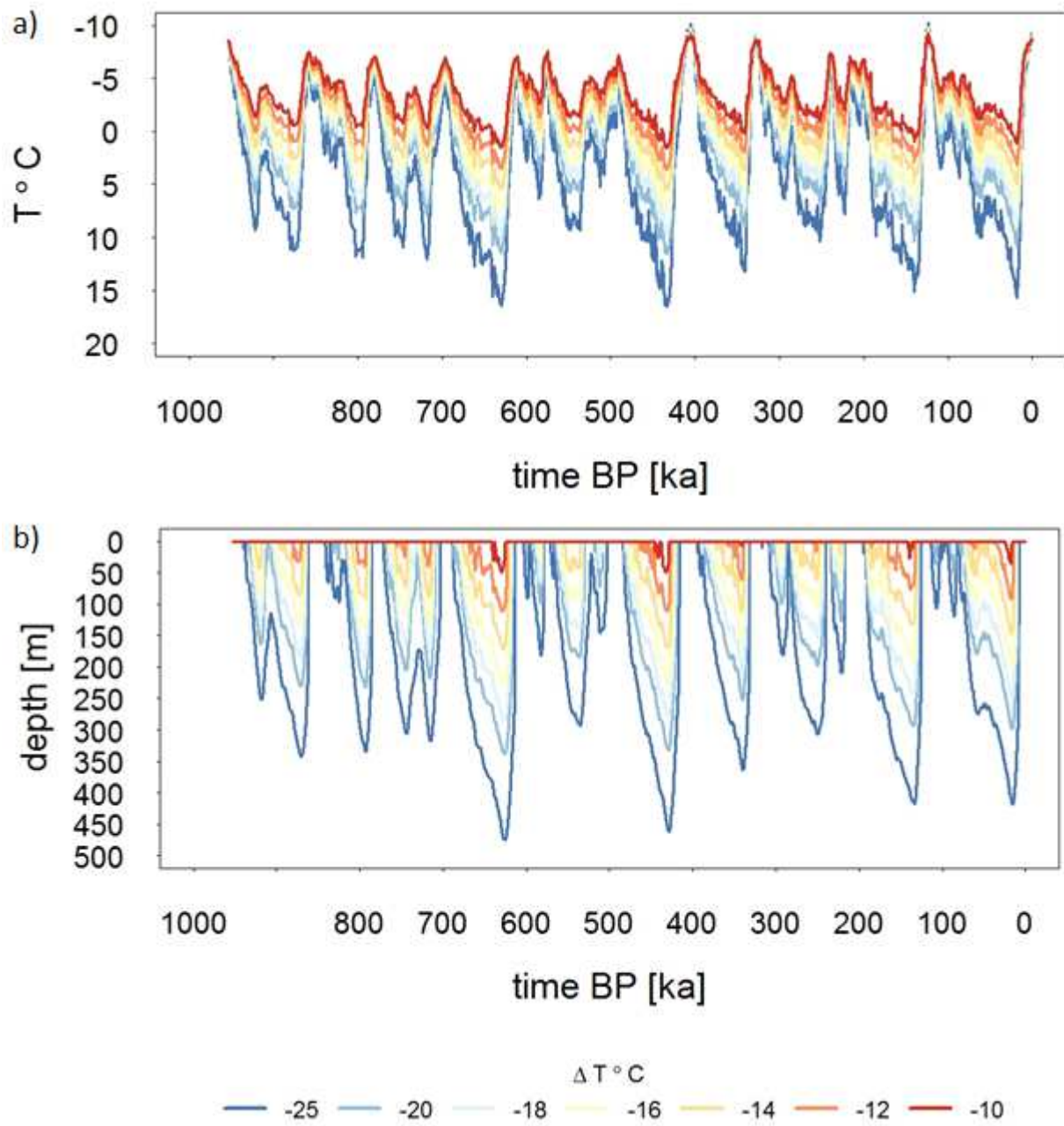


Figure 32. Permafrost thickness for Case 1 using temperature time series that are scaled between 10 and 25 °C below the present day temperature.

Table 10. Maximum permafrost thickness for Case 1 using temperature time series that are scaled between 10 and 25 °C below the present day temperature.

| Model Run ΔT | Max permafrost thickness (m) |
|----------------------|------------------------------|
| -25 | 475 |
| -20 | 338 |
| -18 | 248 |
| -14 | 171 |
| -12 | 111 |
| -10 | 49 |

Correction of the temperature time series for ice cover and its influence on permafrost thickness

Subglacial temperatures of 0°C, -1°C and -5°C were run for both the maximum ice coverage and medium ice coverage conditions for the temperature scenario of T -14°C for Case 1. This temperature correction is a simplified approach, and full coupling of ice sheet models with permafrost may change the permafrost thickness due to a temporal variation of ice sheet bed temperatures.

The permafrost time series for all scenarios are presented in Figure 33 and the maximum permafrost thickness in Table 11. The difference in permafrost thickness caused by the insulating effects of an ice sheet for Case 1, with a temperature scenario of T-14, ranges between -71 m and + 6 m. If a warm-based ice sheet is assumed, the ground surface temperatures are insulated from the air temperatures and there is a reduction in permafrost thickness. However, if cold based ice is assumed, ice coverage might lead to an increase in permafrost thickness compared to the base case scenario.

Table 11. Maximum permafrost thickness for temperature time series corrected for the insulating effect of an ice coverage. Max, and Med denote the glaciation scenario from Figure 26 a and b and the value the subglacial temperature is set to.

| Model Run | Max PF thickness (m) |
|------------------|----------------------|
| T -14, no Ice | 171 |
| T-14, Ice Max 0 | 100 |
| T-14, Ice Max -1 | 101 |
| T-14, Ice Max -5 | 177 |
| T-14, Ice Med 0 | 169 |
| T-14, Ice Med -1 | 169 |
| T-14, Ice Med -5 | 177 |

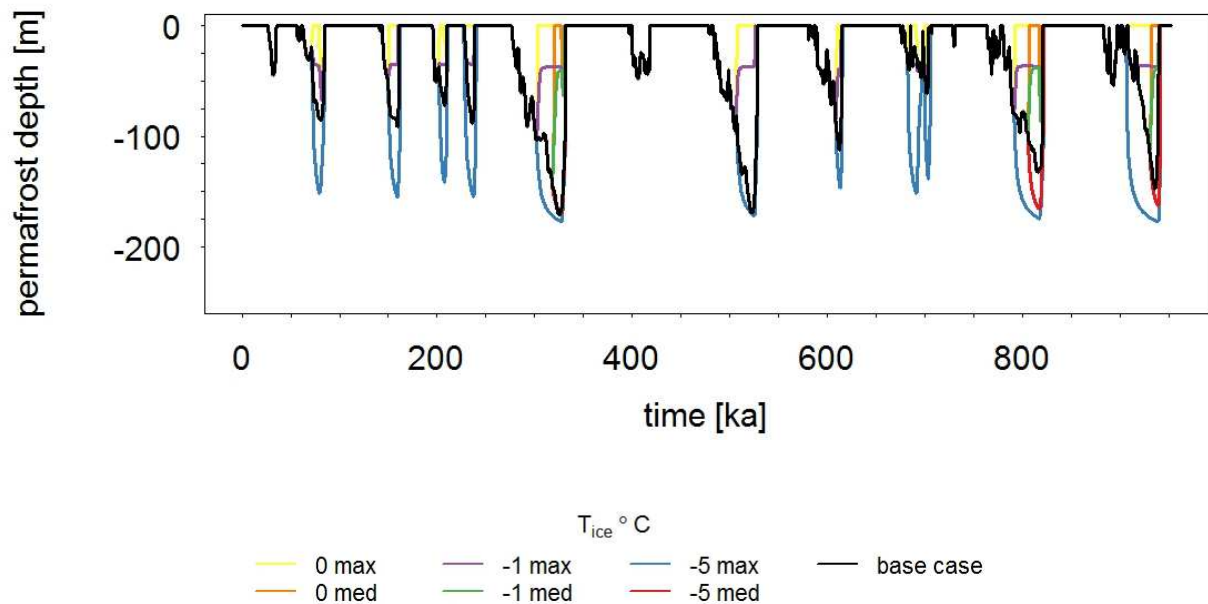


Figure 33. Permafrost thickness for different glaciation scenarios. “max” refers to a maximum glaciation scenario and “med” refers to the medium glaciation scenario after *Boulton and Broadgate (1993)* presented Figure 26 a and b.

GEOLOGICAL VARIABILITY

Subsurface thermal properties

As seen above, the permafrost thickness for a temperature scenario of T-14 for the nine different locations across Britain varies between 77 m and 286 m. Variables controlling the permafrost thickness are the surface temperature time series, which is kept constant for this exercise, and the following parameters: thermal conductivity, heat capacity, density, porosity and heat flow density. Porosity alters the thermal conductivity and heat capacity of the rock, whereas density is used for the calculation of volumetric heat capacity.

For thermal conductivity, porosity, heat capacity, heat flow density and density, one parameter is changed whilst all the others are left at combinations of three different values, a minimum, maximum and a median value. Some of the parameters are not independent, nevertheless, treating the parameters as independent enables us to rank their relative importance and show whether their relative importance deviates from that of a steady state, where temperature, thermal conductivity and heat flow contribute equally.

To examine the sensitivity to heat flow, thermal conductivity and porosity, heat capacity and density are set to their medium value, whilst all other parameters are altered. For the sensitivity to heat capacity and density, all values are altered between the minimum, medium and maximum value (Table 12).

Table 12. Parameters for sensitivity study: thermal conductivity, λ , porosity, ϵ , heat capacity, C_s , heat flow density, q_{heat} , and density, ρ .

| | λ [W/m K] | ϵ [-] | C_s [J/kg K] | q_{heat} [mW/m ²] | ρ [kg/m ³] |
|-----|-------------------|----------------|----------------|---------------------------------|-----------------------------|
| min | 1.2 | 0.01 | 780 | 36 | 1900 |
| med | 2.95 | 0.2 | 880 | 86 | 2680 |
| max | 4.6 | 0.4 | 1100 | 136 | 2900 |

HEAT FLOW

Heat flow and permafrost thickness are inversely related; when heat flow is low permafrost is thicker than when heat flow is high (Figure 34). For the steady state permafrost model the relationship between permafrost thickness and heat flow is linear, but it is non-linear for the transient model. The relative importance of heat flow on permafrost thickness is also dependent on the thermal conductivity and porosity. For a high thermal conductivity and low porosity, the range of permafrost thickness is 406 m, from 576 m for a low heat flow to 170 m for a high heat flow. In contrast, for a low thermal conductivity and a high porosity, the range of permafrost thickness is 91 m, ranging from 52 m to 143 m.

The variation in heat flow is particularly important to consider when estimating the permafrost thickness of an area larger than several tens of kilometres. For Case 1, approximating a location in north-west England, the local variation in heat flow density is between 50 and 100 mW/m² over a distance of 50 km (Figure 35). For the base case model, a heat flow of 70 mW/m² is assigned. The maximum permafrost thickness for 50 mW/m² is 218 m, for 70 mW/m² 171 m, and for 100 mW/m² 129 m.

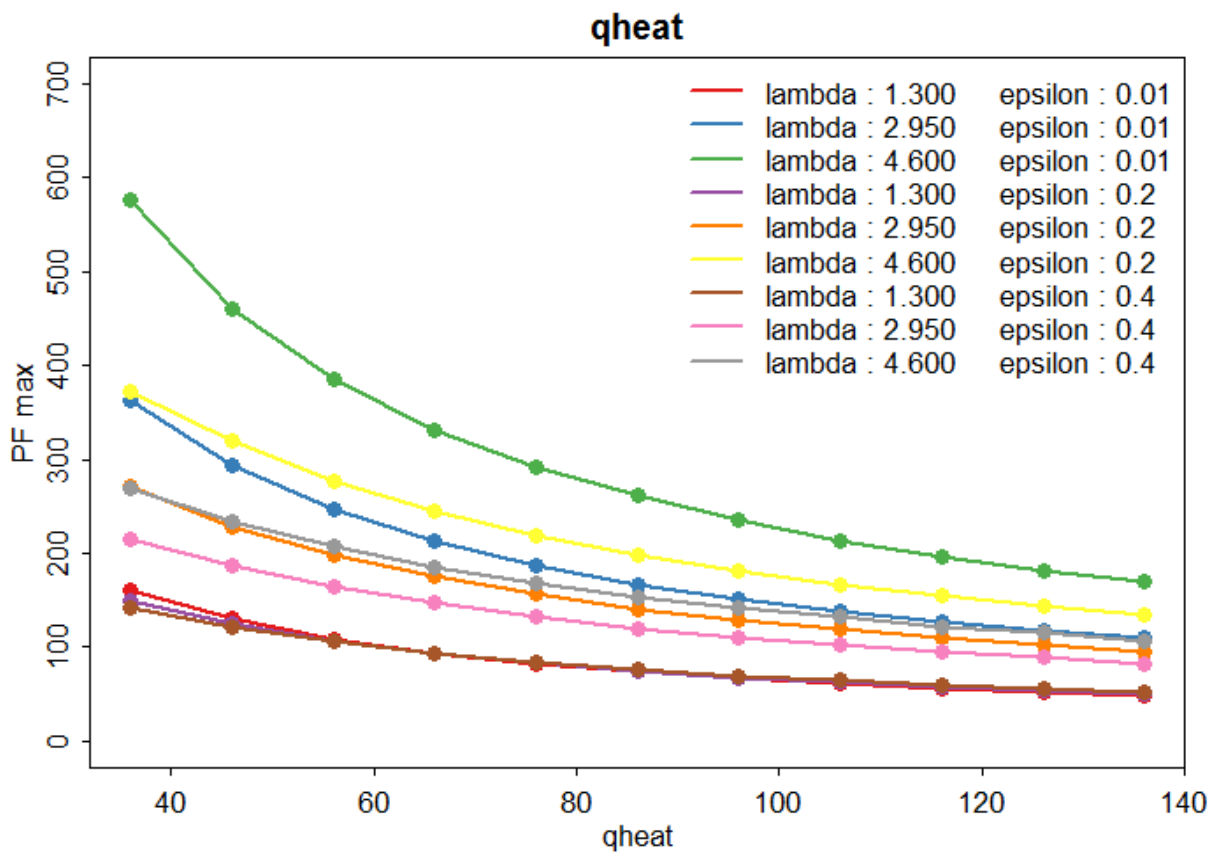


Figure 34. Sensitivity of heat flow using a combination of three different thermal conductivities (lambda) and porosity (epsilon).

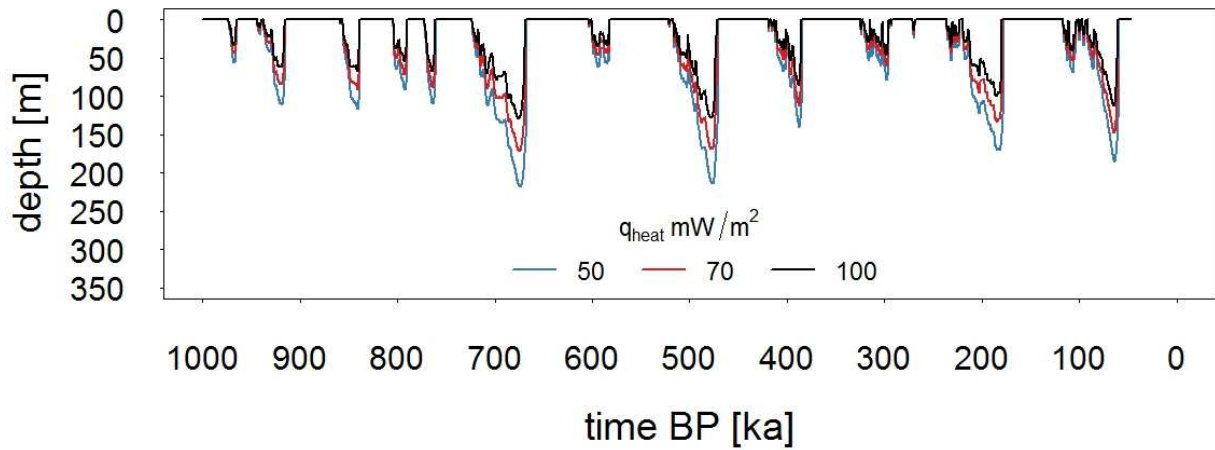


Figure 35. Permafrost thickness for Case 1 using a heat flow density of 50, 70, and 100 mW/m².

THERMAL CONDUCTIVITY

There is a positive relationship between thermal conductivity and permafrost thickness (Figure 36). The maximum influence of thermal conductivity occurs when heat flow and porosity are both low, with a range of permafrost thickness of 416 m, ranging from 160 m to 576 m. The smallest influence of thermal conductivity occurs when porosity is large and heat flow is low, with a range of 56 m, from 52 m to 108 m.

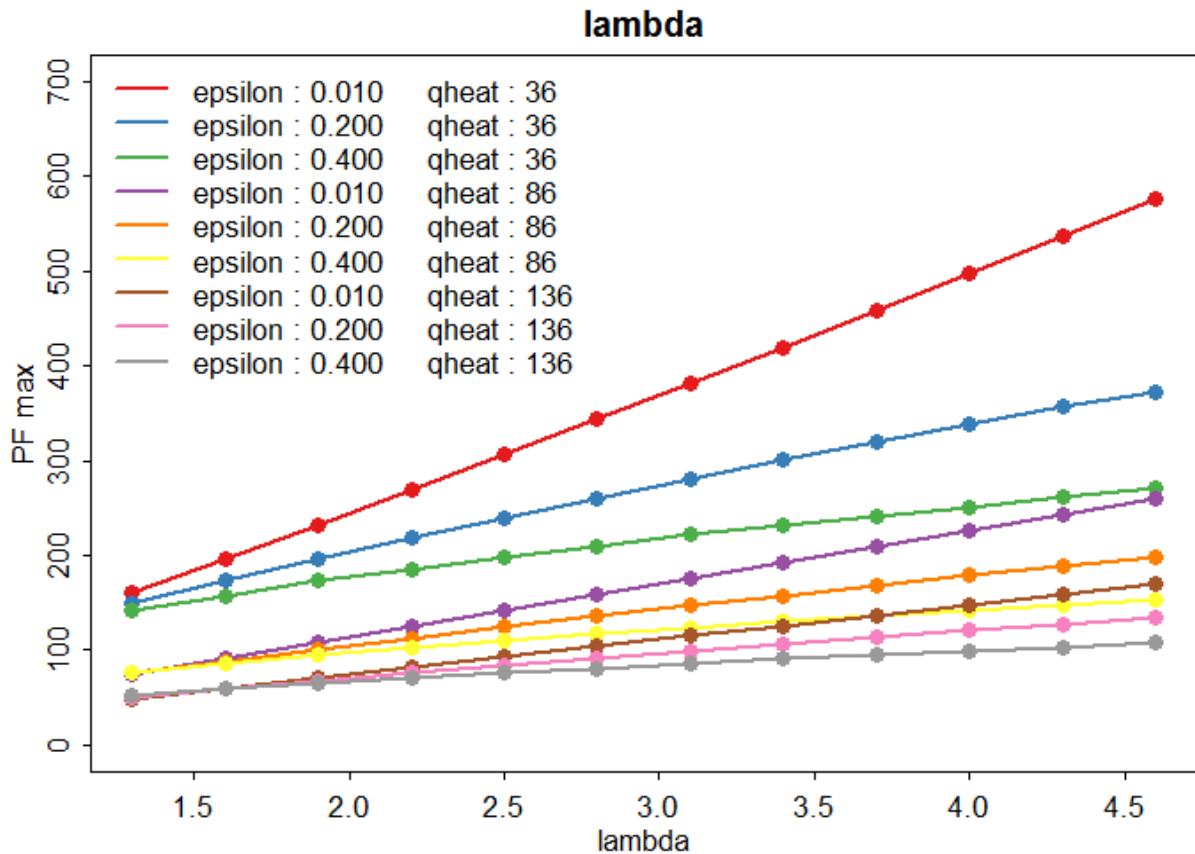


Figure 36. Sensitivity of thermal conductivity (lambda) using a combination of three different heat flows (qheat) and porosity (epsilon).

POROSITY AND LATENT HEAT

Porosity determines the amount the thermal properties change with freeze/thaw and release/uptake of latent heat. Porosity is inversely related to permafrost thickness (Figure 37). There is a negative relationship between porosity and permafrost thickness when thermal conductivity is high and heat flow is low, with a range of permafrost thickness of 489 m, from 107 m and 596 m. In contrast, there is a small positive relationship between permafrost thickness and porosity for low thermal conductivity and a high heat flow, with a range of permafrost thickness of 3 m from 49 m to 52 m, which is of minor importance and might be due to model error.

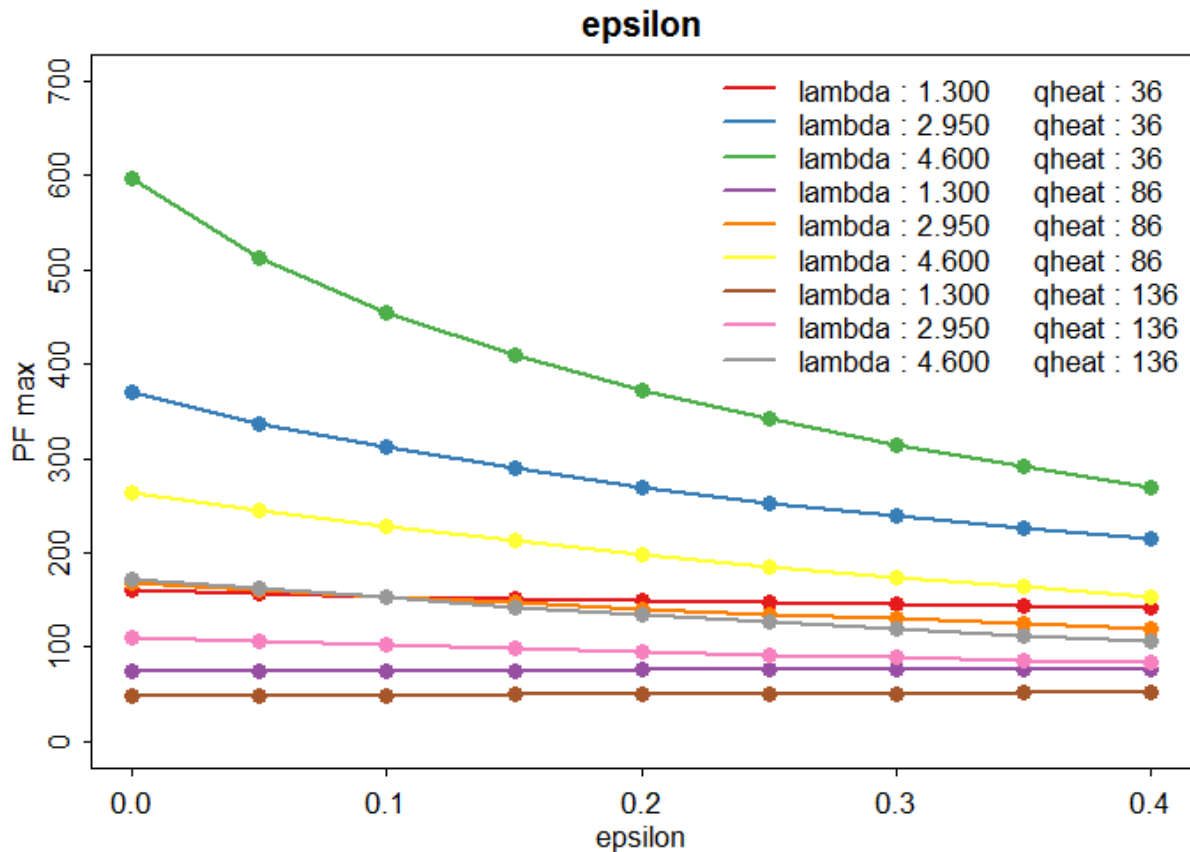


Figure 37. Sensitivity of porosity (epsilon) using a combination of three different heat flows (qheat) and thermal conductivity (lambda).

The main causes for this non-linearity are the transient effects of freeze-thaw. First, the thermal diffusivity, which is specified by the ratio of thermal conductivity and heat capacity, determines how fast a temperature change propagates in the subsurface, and affects whether a medium is frozen or unfrozen. When water freezes, the thermal conductivity increases by a factor of 4 and the mass heat capacity decreases by half. Secondly, the energy required for water to freeze, or released when ice thaws, is equal to that required to raise the temperature of an equal volume of rock by ~150°C.

HEAT CAPACITY AND DENSITY

The choice of heat capacity and density has been found to be of lesser importance for estimating maximum permafrost thickness (Figure 38). The maximum range of permafrost thickness by altering the heat capacity is 29 m and the minimum range is 0 m. Similarly for density, the

maximum range in permafrost thickness by altering density is 36 m and the minimum range is 1 m.

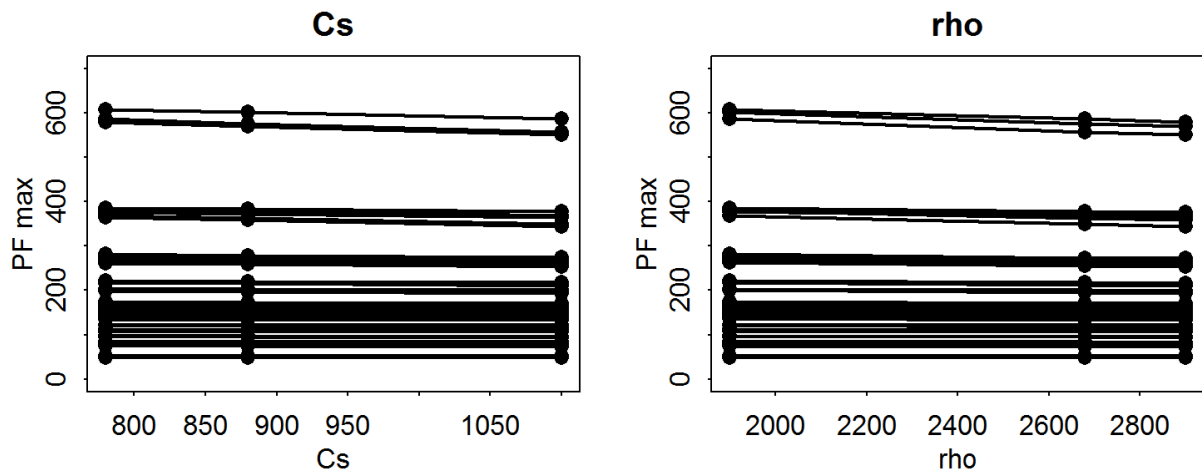


Figure 38. Sensitivity of heat capacity (C_s) and density (ρ) using a combination of three different heat flows, thermal conductivity, and porosity.

SUMMARY GEOLOGICAL VARIABILITY

The maximum and the minimum range of permafrost thickness for different geological parameter values, leaving all other parameters unchanged, are presented in Table 13. The largest ranges in permafrost thickness were simulated when thermal conductivity and heat flow were modified, followed by porosity. Mass heat capacity and density result in sensitivity ranges about one order of magnitude less than the first three parameters. The minimum ranges are close to zero for density, mass heat capacity and porosity. As there are non-linearities between the parameters, the variation of one parameter from a reference case might not show the true sensitivity of a parameter. Furthermore, porosity influences more than one parameter: the amount of latent heat required to freeze the ground, change in thermal conductivity and heat capacity.

Table 13. Influence of geological parameters on the range of permafrost thickness.

| Parameter | maximum range [m] | minimum range [m] |
|------------------------------------|-------------------|-------------------|
| Thermal conductivity (λ) | 437 | 54 |
| Heat flow (q _{heat}) | 433 | 89 |
| Porosity (ϵ) | 331 | 1 |
| Mass heat capacity (C_s) | 29 | 0 |
| Density (ρ) | 36 | 1 |

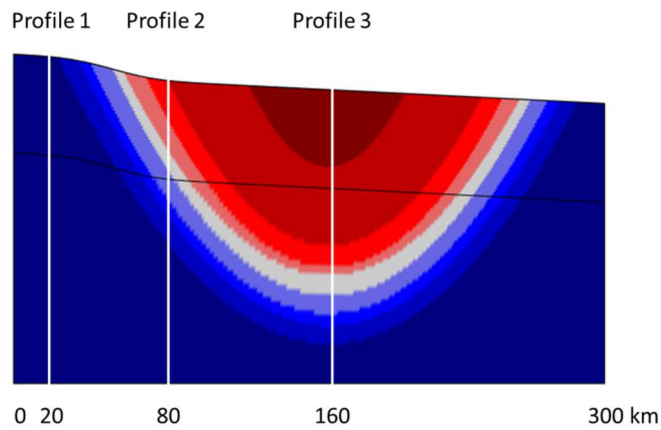
EXAMPLE: PERMAFROST TIME SERIES FOR CASE 2 AT DIFFERENT PROFILES

The influence of geological variability, namely thermal conductivity and porosity, can be illustrated with the example of Case 2 (Figure 39 b and c). At three different locations, at 20 km, 80 km, and 160 km from the left hand side of the model domain, a permafrost depth time series is compared. The first profile is through the basement, the second profile through the Jurassic sequence, and the third profile is through the Cretaceous Chalk overlying the Jurassic sequence.

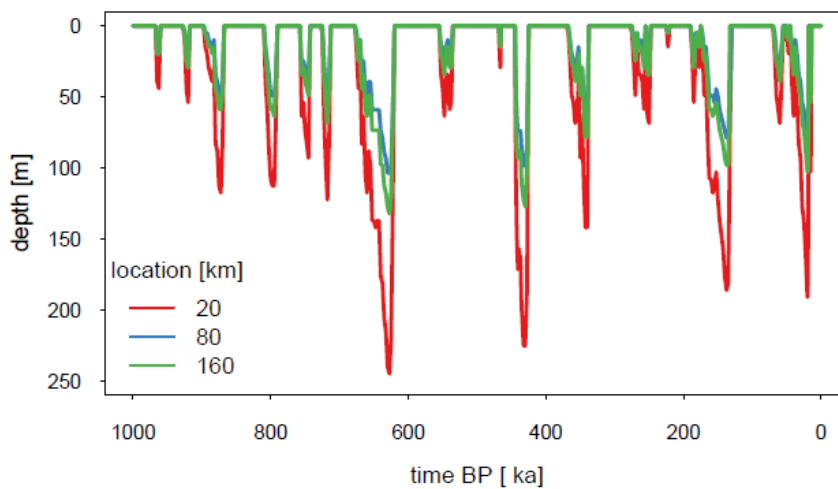
For both, the T-14 and T-25 temperature time series, permafrost is thickest in the basement, followed by the profile through the Cretaceous sequence and then the profile through the Jurassic

strata. The maximum permafrost thicknesses for T-14 temperature time series are 245 m, 103 m and 132 m for profiles 1-3, and for the T-25 temperature time series the maximum permafrost thicknesses are 688 m, 363 m and 323 m.

a)



b) T-14



c) T-25

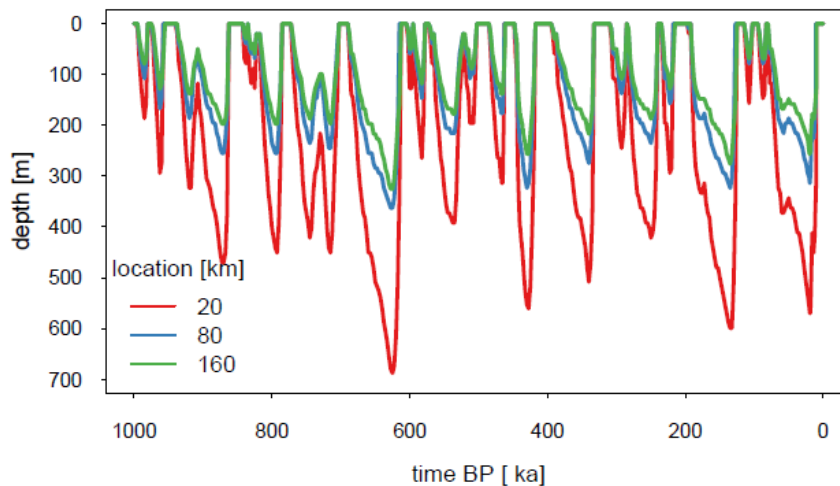


Figure 39. a) Three different location of the depth profiles: Profile 1 at 20 km, Profile 2 at 80 km and Profile 3 at 160 km with respect to left hand edge of the modelled domain. Profile 1 is through the basement, profile 2 through the Jurassic sequence, and profile 3 through the Cretaceous Chalk overlying the Jurassic sequence. The filled contours in a) represent the location of the different geological layers. These profiles refer to the locations 20 km, 80 km and 160 km of b) and c). Permafrost depth time series for one Million years is presented for the three profiles of Case 2 for the T-14 run (b) and (c) T-25 run.

INFLUENCE OF ADVECTIVE HEAT FLOW ON THE THICKNESS AND DISTRIBUTION OF PERMAFROST

Permafrost thickness

Case 2

Models discussed in this section for Case 2, as described in Table 7:

- T-25
- T-25_Cond

For Case 2, the permafrost thicknesses for the models including heat conduction only, and heat conduction and advection, are similar (Figure 40). This is an expected outcome, given the low permeability of the geological layers. As the cell size in the vertical is 10 m for Case 2, the difference between the two scenarios lies within the cell size. The temperature distribution for Case 2 is conduction dominated, except for the two aquifers where heat advection is also important.

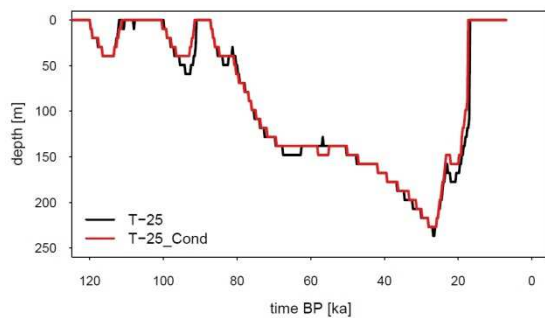


Figure 40. Permafrost thickness for the T-25 temperature scenario for Case 2 using a heat conduction model and a conduction-advection model.

Case 1

Models discussed in this section for Case 1, as described in Table 6:

- T_14_Cond
- T_14_Min
- T_14_Med
- T_14_Max
- T_25_Cond
- T_25_Min
- T_25_Med
- T_25_Max

For Case 1, in which the geology is more permeable than for Case 2, four different permafrost time series are compared: one heat conduction only simulation, and three conduction-advection simulations based on a minimum, medium and maximum permeability scenario. Figure 41 and Figure 42 are for a temperature scenario of T-14 and T-25, respectively, and in each the model results are compared at three locations: at the foot of a hill at 7 km, at a hill top at 9 km and at the point of significant slope at 13 km of the model domain Figure 4.

First considering the T-14 temperature scenario, at the valley bottom. At times when the permafrost is shallow, permafrost is simulated to be thinner when heat advection is included. However, when permafrost is thicker, e.g. during the last cold period between 35-15 ka BP, there is little difference between the conduction-only and conduction-advection models. In contrast, at the hill top, during shallow permafrost events permafrost is deeper for the advection scenarios than for the conduction-only scenario. Therefore, in this model, advective warming can be observed at the hill foot, where warmer water is discharging, and advective cooling at the hill top where cooler water is recharging.

Similarly, for the T-25 temperature scenario, the effect of advective cooling at the hill top and advective warming at the valley bottom can be observed when permafrost thickness is shallow. In contrast, at the point of higher slope, there is a larger effect of heat advection than for the T-14 scenario.

Generally, the maximum permafrost thicknesses for the conduction-advection scenarios are similar to the conduction-only scenarios, with differences 1- 5 m for the hill top and foot and difference up to 10 m on the larger slope. Considering a maximum permafrost thickness of over 500 m on the larger slope, a difference of 10 m is very small.

Temporally, the permafrost thickness for a conduction-advection scenario can differ considerably from a conduction-only scenario. For example for Figure 42, there are spikes in the permafrost thickness differences, which are due to earlier or later thaw of permafrost. For the locations at 7 km and 9 km, there are spikes in the differences just before 80 ka, where permafrost thaws earlier than for the conduction-only scenario. At the valley bottom (7 km) where advective warming is expected, there is a spike for the maximum scenario that would suggest advective cooling. This could be due to discharge of cooler water, decelerating permafrost thaw locally.

When permafrost forms, permeability decreases by several orders of magnitude, and thus advective heat flow decreases within the permafrost. During a permafrost event, the temperature distribution within the permafrost is dominated by heat conduction. However, as it is uncertain how much the permeability will decrease when the ground is frozen, the influence of advective heat flow in a permafrost environment is strongly dependent on the relative permeability function.

However, the temperature distribution changes locally before the cold event and advective cooling can be observed at recharge points or advective warming at discharge points. If there is recharge of warmer water and discharge of colder water than the ambient temperature, advective warming could be expected at recharge points and advective cooling at discharge points.

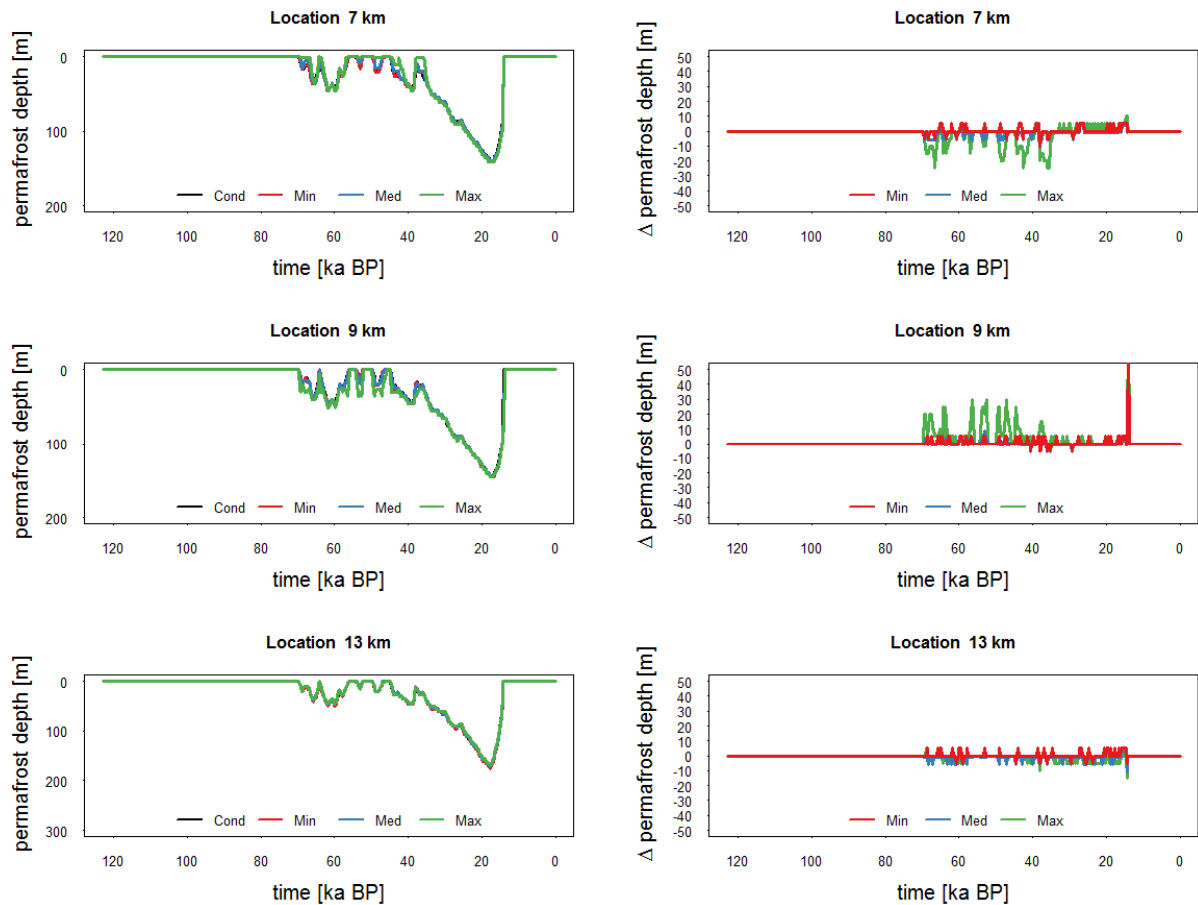


Figure 41. Permafrost thickness for the T-14 temperature scenario for Case 1 using a heat conduction-only (C) model, and a conduction-advection (CA) model using a minimum, medium and maximum permeability scenario. The left-hand plots show permafrost depth and those on the right the difference between the two types of model (C minus CA). The permeability scenarios used here refer to the minimum, medium, and maximum permeability as listed in Table 3, using $\Omega=6$.

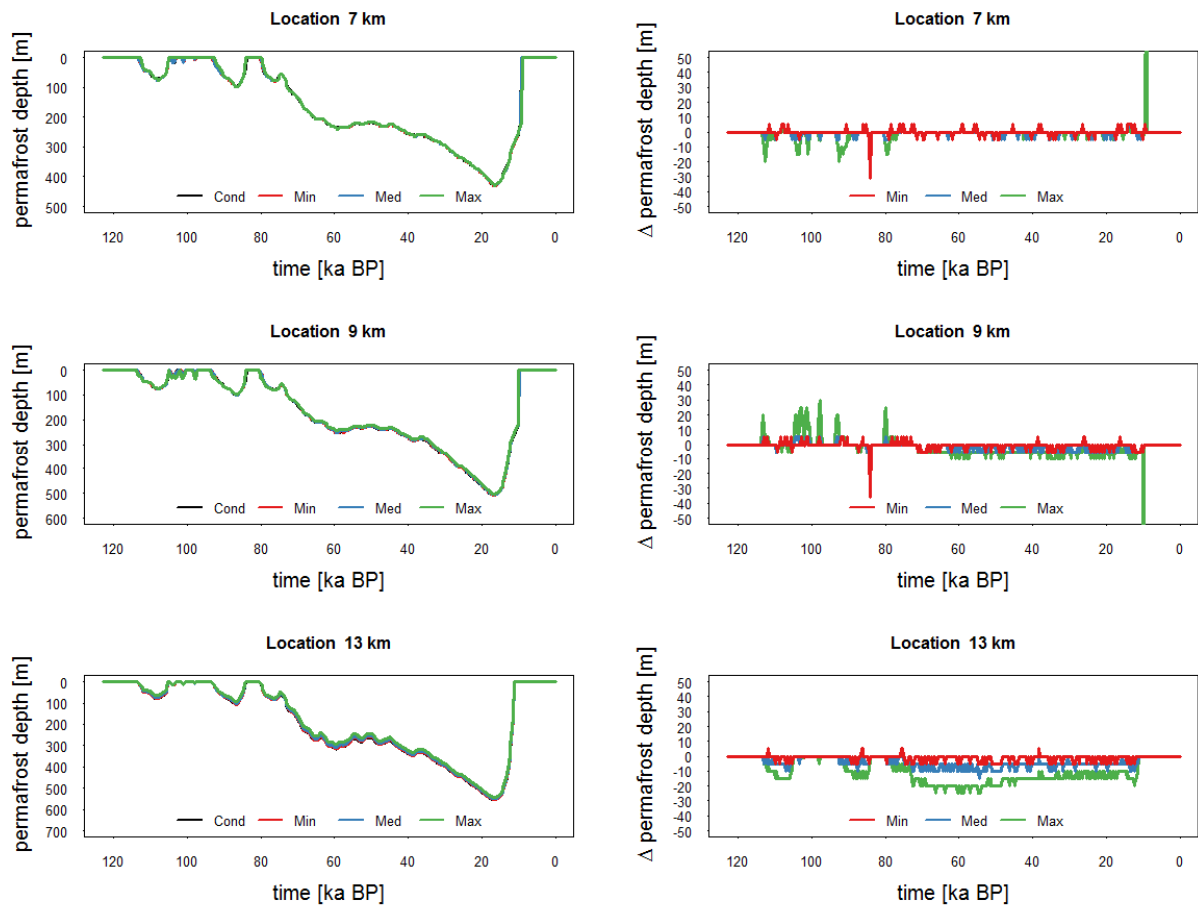


Figure 42. Permafrost thickness for the T-25 temperature scenario for Case 1 using a heat conduction-only (C) model, and a conduction-advection (CA) model using a minimum, medium and maximum permeability scenario. The left-hand plots show permafrost depth and those on the right the difference between the two types of model (C minus CA). The permeability scenarios used here refer to the minimum, medium, and maximum permeability as listed in Table 3, using $\Omega=6$.

PERMAFROST THICKNESS AND PERMEABILITY REDUCTION FUNCTION

Models discussed in this section for Case 1, as described in Table 6:

- T_25_Cond
- T_25_Max (Omega6)
- T_25_Max_Omega3
- T_25_Max_Omega1

In the model, the permeability of permafrost is defined by Equation 16. The factor Ω determines how many orders of magnitude the permeability decreases when frozen. For the default models, $\Omega=6$, but to test the importance of heat advection on the permafrost thickness, Ω is also set to 1 and 3.

For the locations at 7 km and 9 km, there is a large difference in permafrost thickness depending on the choice of Ω . More permeable permafrost enhances the effects of advective heat flow and results in a considerable difference in permafrost depth (Figure 43).

Figure 44 compares the temperature and the ice saturation for the simulations in which Ω varies, at 7 km (foot of the hill), 9 km (hill top) and 13 km (slope) for Case 1. The largest difference between the conduction and the advection scenarios can be found at the base of the foot of the

hill. When there is no permafrost, the temperatures of the advection scenarios are warmer compared to the conduction scenario, however when it is frozen, the temperature difference between the conduction and advection scenario are close to zero. For the cold events around 110 ka BP and 90 ka BP, the runs with an $\Omega=6$ are fully frozen, whereas for the $\Omega=3$ is partially frozen for the first cold event and for the $\Omega=1$ is unfrozen.

At the hill top, the models including heat advection are cooler than the models for conduction only, with the difference being largest under unfrozen conditions.

In conclusion, the relative importance of advective heat flow is strongly dependent upon the relative permeability function used in the model.

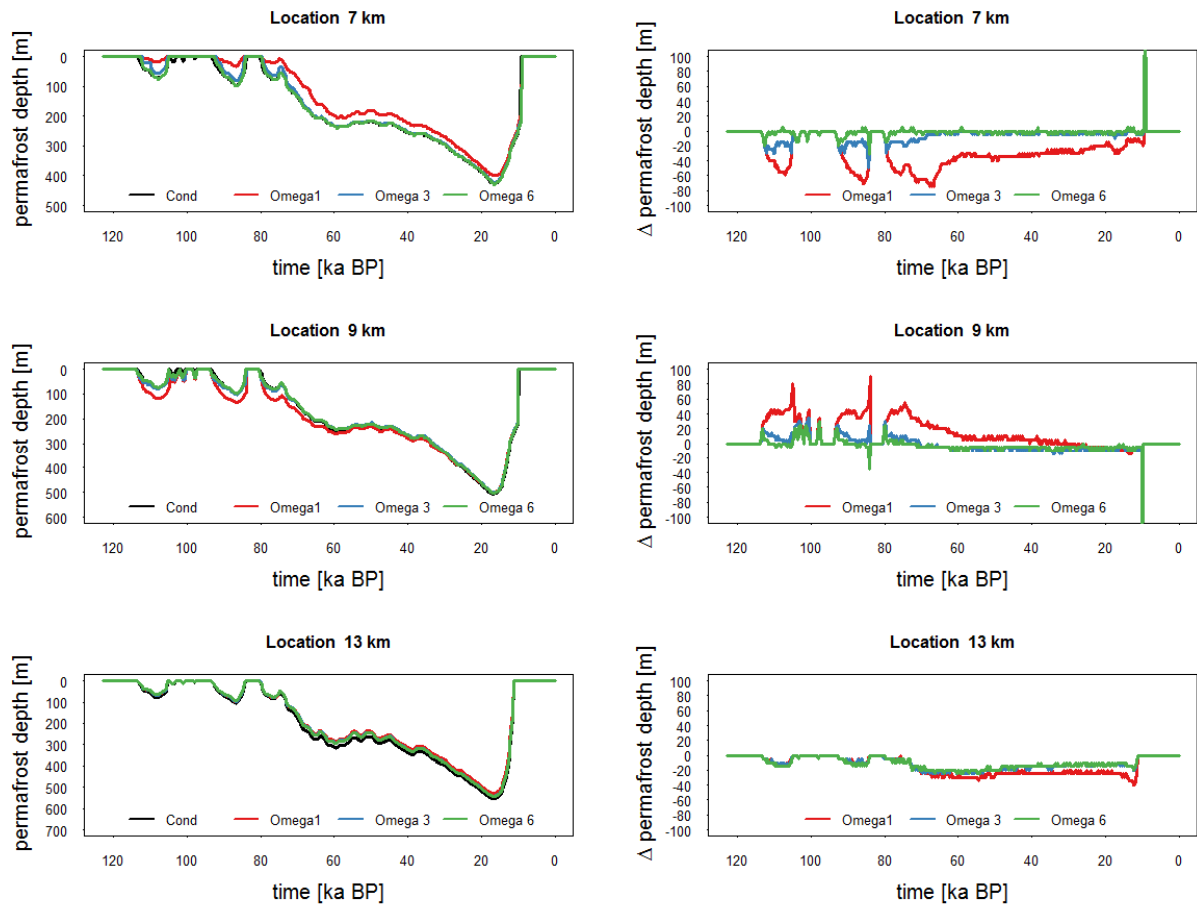


Figure 43. Permafrost time series for the T-25 scenario using different Ω from Equation 16.

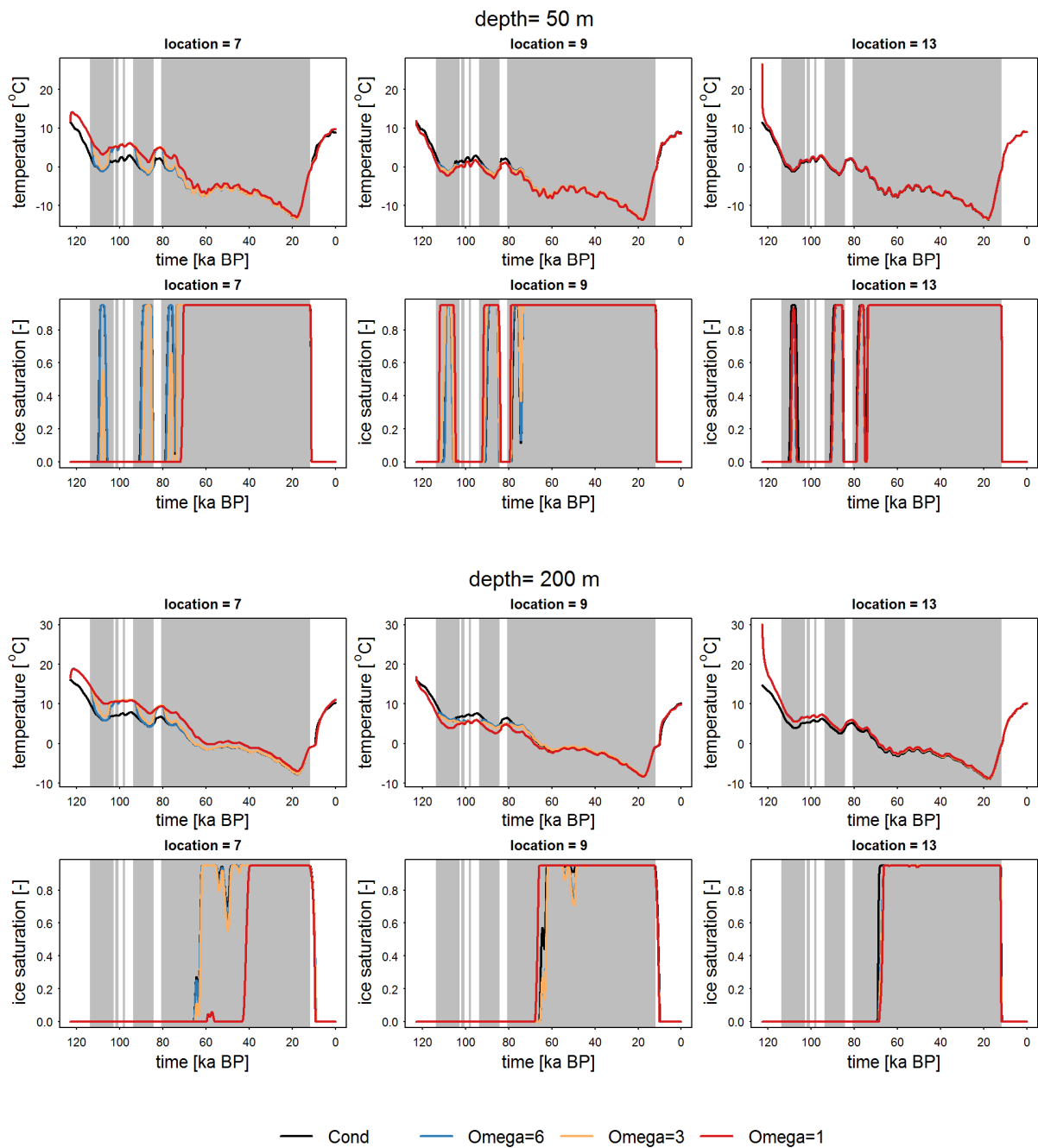


Figure 44. Temperature and ice saturation for model T-25 using a conduction scenario and a max permeability scenario using $\Omega = 6, 3,$ and 1 .

Permafrost distribution

T-25_MAX CASE 1

Models discussed in this section for Case 1 as described in Table 6:

- T-25_Max
- T_25_Max_Omega1

The distribution of permafrost depends on the geometry of the model domain, the thermal properties of the subsurface, the driving surface temperature time series, and the advective heat flow.

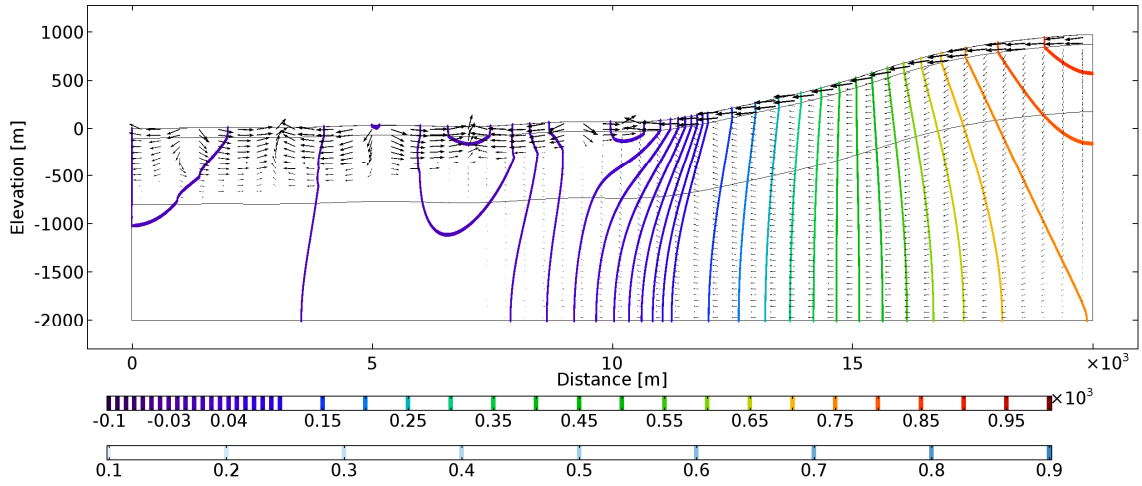
Figure 45 presents the hydraulic head distribution, flow vectors and ice saturation for different time steps, representing fully unfrozen (a), frozen at the top few metres (b), frozen within the weathered layer (c), deep permafrost (d) and during thaw (e & f) of permafrost.

When unfrozen, the hydraulic head follows the topography and flow is topography driven. Flow velocities are largest within the weathered layer on the steeper slope, and in the sandstone driven by topographic undulations.

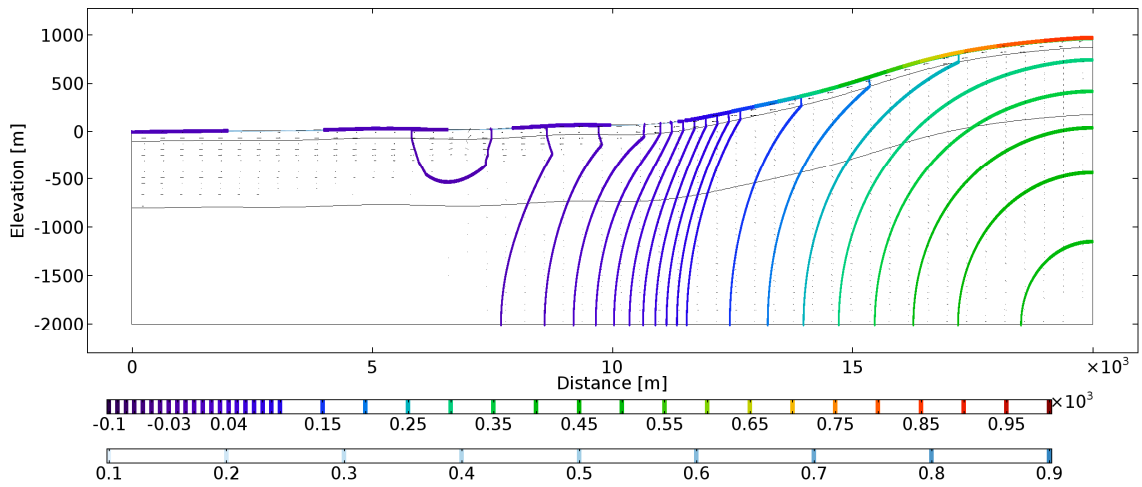
When permafrost forms at the surface (Figure 45b-d), flow is greatly reduced in, and below, the permafrost. The hydraulic head below the permafrost drops and the gradient of hydraulic head in the domain becomes very small. This is because recharge ceases, and water continues to drain at the side of the model. The hydraulic head gradient in the permafrost however remains high, but as the permeability is reduced there by six orders of magnitude, this does not affect flow.

Permafrost thaw is driven by a combination of processes; surface temperatures above 0°C result in a temperature gradient and heat flow from the top, heat flow from the base of the model, and advective heat flow. Whereas permafrost from the top thaws relatively slowly for both the sandstone and the basement, permafrost thaw from below in the basement is faster than in the sandstone, due to the higher thermal conductivity of the basement. Permafrost disappears first in the weathered layer, followed by the basement, leaving a relic permafrost layer within the sandstone disconnected from the surface.

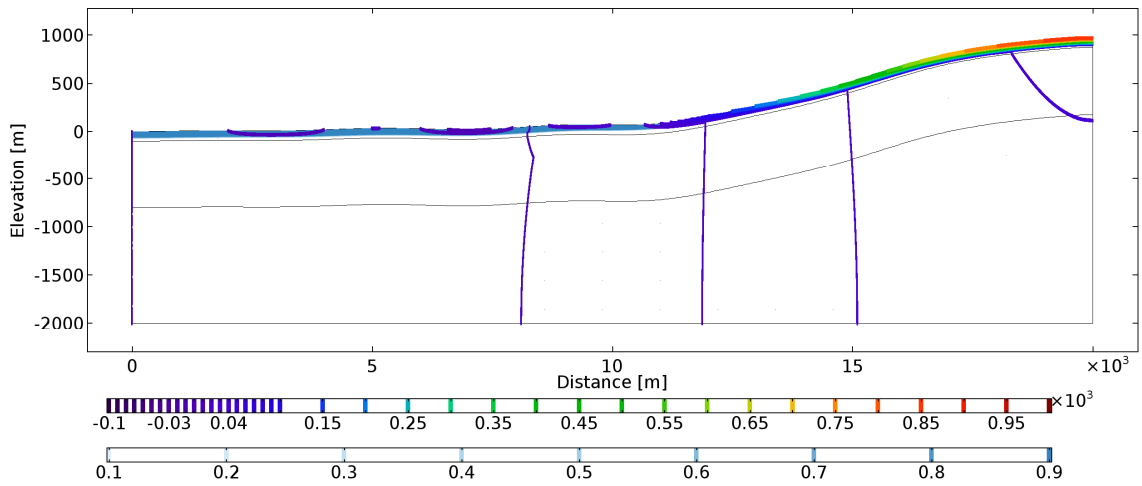
a)
113.5
ka BP



b)
112.75
ka BP



c)
108 ka
BP



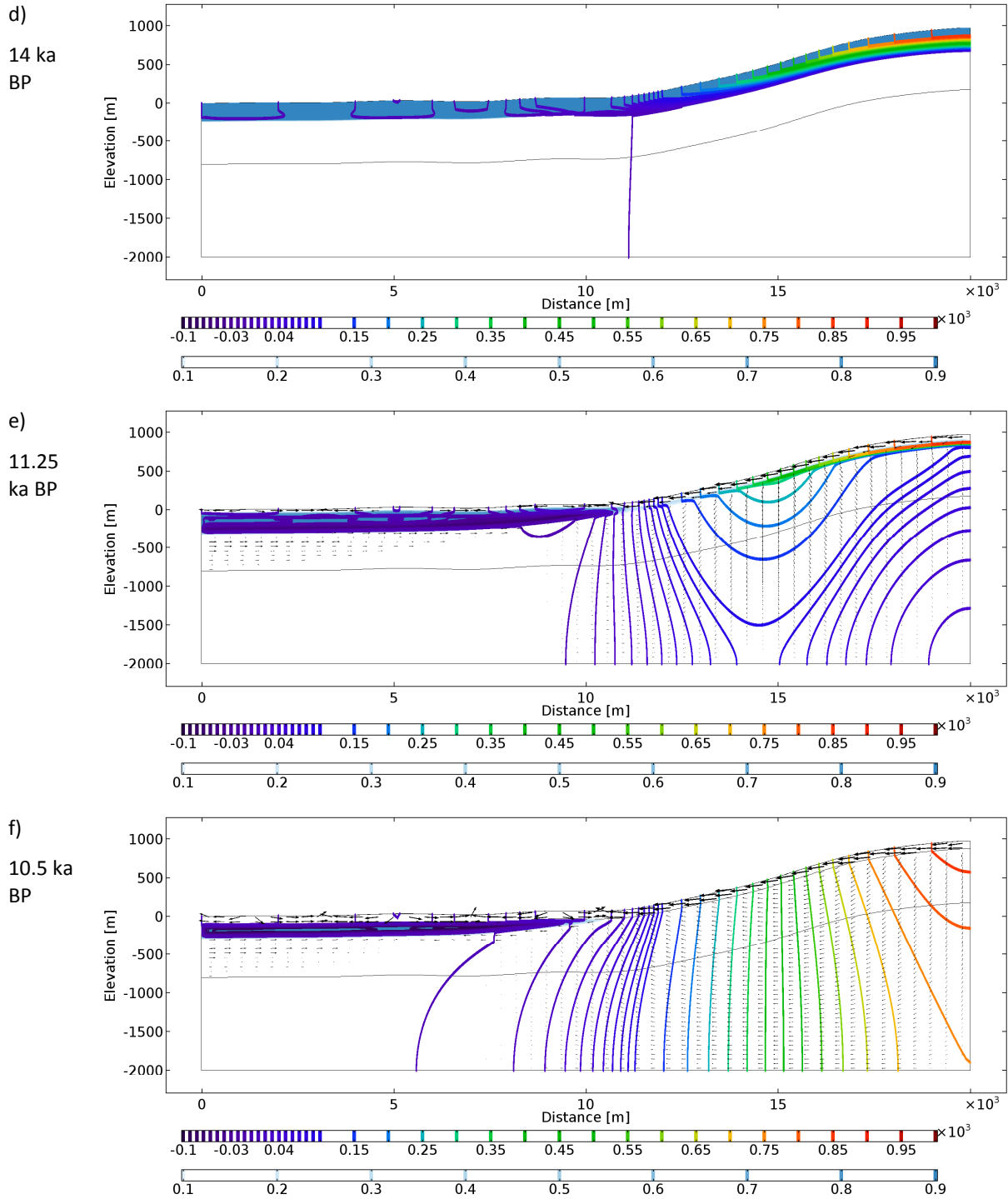
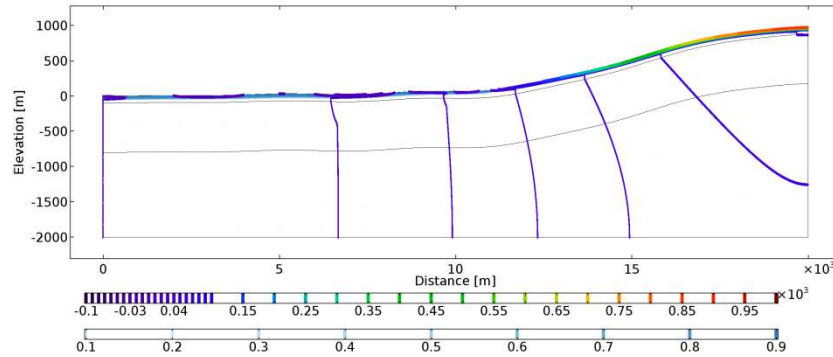


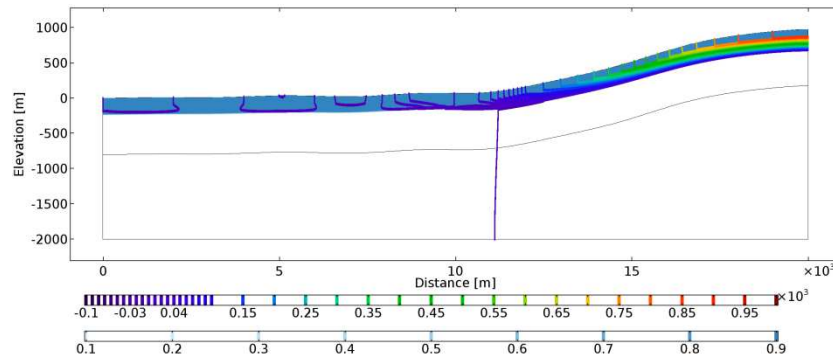
Figure 45. Hydraulic head (spectrum contours), ice saturation (blue fill) and flow vectors for model T-25_Max for different time steps.

Time $\Omega = 6$
(ka BP)

a) 74.75

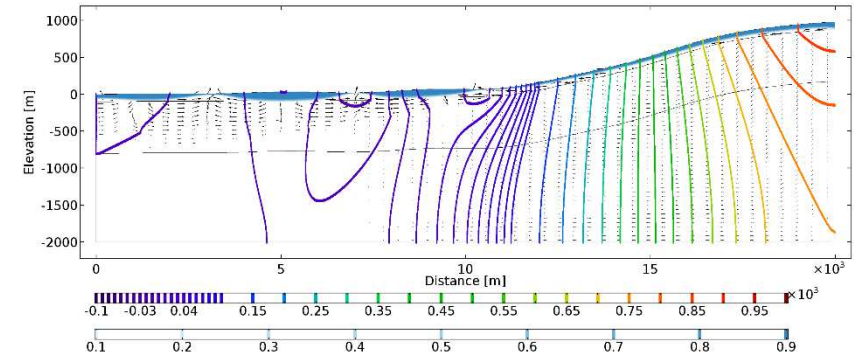


c) 58.25



$\Omega = 1$

b)



d)

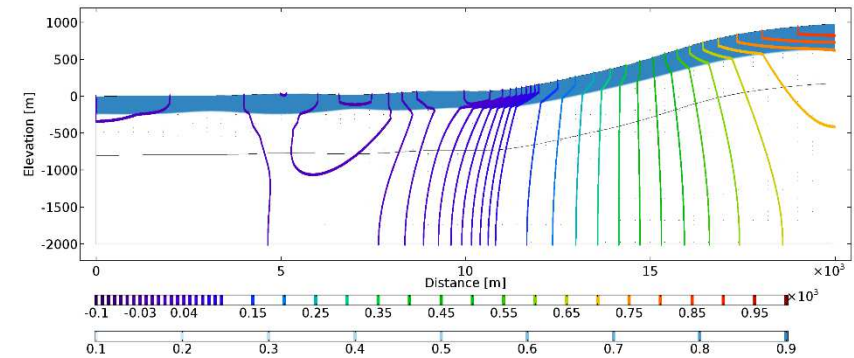


Figure 46. Comparison of permafrost distribution for two different time steps for the T-25_Max models using $\Omega = 6$ (a, c) and 1 (b, d). Hydraulic head (spectrum contours), ice saturation (blue fill) and flow vectors are presented.

As discussed in above, the choice of the permafrost permeability function greatly influences the role of advective heat flow. Comparing a model using $\Omega = 6$ and $\Omega = 1$ (Figure 46), the permafrost distribution for a shallow permafrost event is fundamentally different. For the $\Omega = 6$ scenario, permafrost is continuous across the entire model domain, inhibiting recharge and discharge. As a result, the hydraulic head below the permafrost is reduced, resulting in little flow below the permafrost. In contrast, for the $\Omega = 1$ scenario, permafrost coverage across the model domain is discontinuous, with local areas of discharge at topographic lows. Advective cooling underneath the hills results in locally thicker permafrost than for the $\Omega = 6$ scenario.

For a more severe permafrost event, both scenarios have a similar permafrost thickness, however for the $\Omega = 1$ scenario, permafrost is deeper underneath hills than underneath topographic lows. In addition, as permafrost is more permeable for the $\Omega = 1$ scenario than for the $\Omega = 6$ scenario; recharge is still possible at a reduced rate, resulting in a hydraulic head field underneath the permafrost that is not as greatly reduced as for the $\Omega = 6$ scenario.

INFLUENCE OF TALIKS ON THE THICKNESS AND DISTRIBUTION OF PERMAFROST

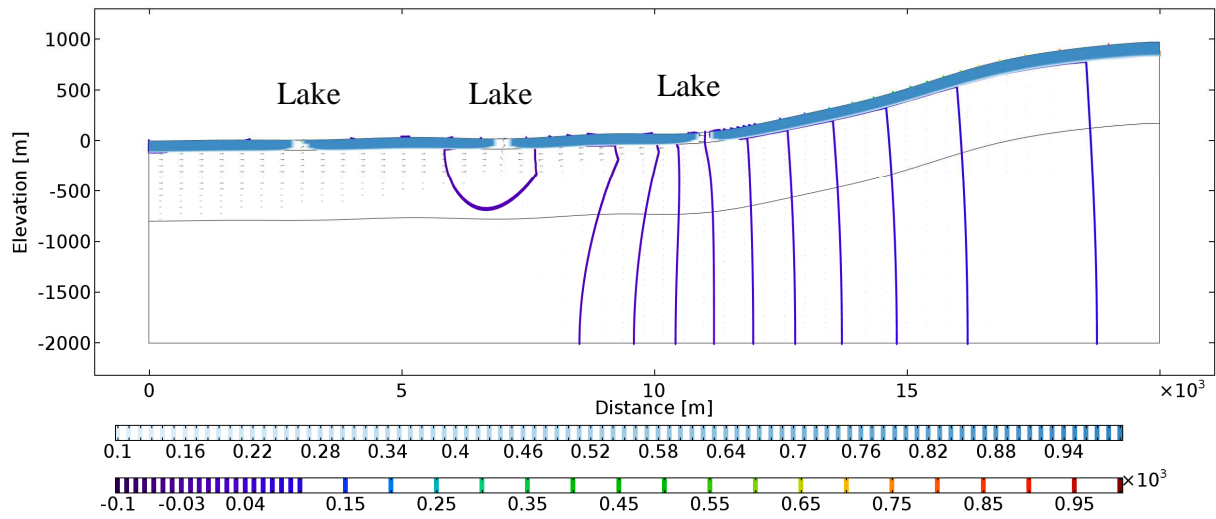
Model discussed in this section for Case 1, as described in Table 6:

- T_14_Talik

Currently, lakes are widespread in the Arctic, as surface water cannot infiltrate into the subsurface and water ponds in topographic lows. These lakes insulate the ground from the air temperatures, and if the mean annual lake bottom temperature is above zero, a talik forms below it.

A model was constructed that incorporates taliks based on the set-up for Case 1. Within this model the temperature is set to 4°C in three zones of 200 m width. For the T-14 temperature scenario, permafrost does not form underneath the lakes, and through taliks persist during the last glacial cycle. The flow for 21.75 ka BP (Figure 47 a) is reduced compared to periods when permafrost is absent, especially across the region of steeper slope in the bedrock. In the sandstone, the flow is larger and water is discharging into the lakes. During thaw (Figure 47 b), flow from the larger slope intensifies, as well as discharge into the lakes.

a) 21.75 ka BP



b) 14.5 ka BP

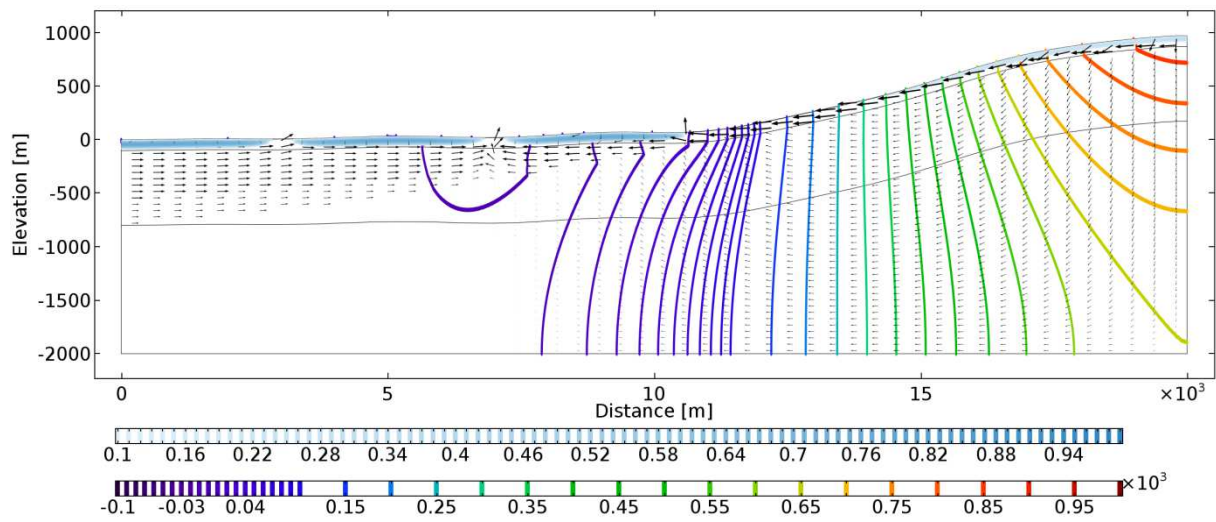


Figure 47. Permafrost and hydraulic head distribution for a scenario with lakes at topographic low places.

THERMAL PECKET NUMBER

Models discussed in this section:

Case 1:

- T_14_Max
- T_14_Talik

Case 2:

- T_14

The thermal Peclet number defines the ratio of heat conduction to heat advection; when the Peclet number is less than 1, heat conduction is the dominant mechanism, and when the Peclet number is greater than 1, heat advection is the dominant process.

When unfrozen, heat advection is dominant in the weathered layer and in most of the upper sandstone for Case 1, as the permeability there is higher than the lower formations.

When frozen, for the base case scenario T-14_Max, heat conduction is the dominant process (Figure 48). However, when there are taliks (T-14_Max_Talik), heat advection is dominant beneath surface water bodies in the weathered layer. Heat advection also drives the temperature distribution between the lakes and towards the open boundary at the side in the upper sandstone.

For the T-25 temperature scenario, the distributions of the thermal Peclet number are compared for times corresponding to a shallow thaw, a shallow permafrost event and thawing of deep permafrost (Figure 49). For thawing of a short, shallow permafrost event, heat advection becomes dominant over the region of the steeper slope, and beneath the high ground at approximately 10 km from the left hand boundary for the T-25_Max model. In contrast, for the T-25_Max_Omega1 model, heat advection is larger beneath the topographic depressions where the permafrost thaws and taliks form.

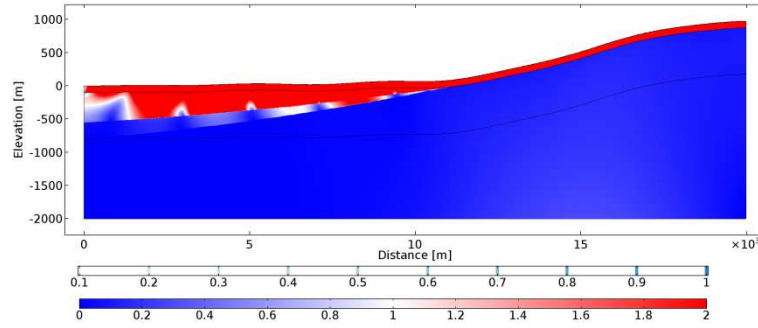
For the shallow permafrost event that does not exceed the thickness of the weathered layer, heat advection is equally important at the base of the upper sandstone for the T-25_Max model. For the T-25_Max_Omega1 model, heat advection is dominant for large parts of the upper sandstone, thawing the permafrost from upwelling groundwater.

For the thaw event of deep permafrost, the relative importance of heat advection for the T-25_Max and T-25_Max_Omega1 model are similar.

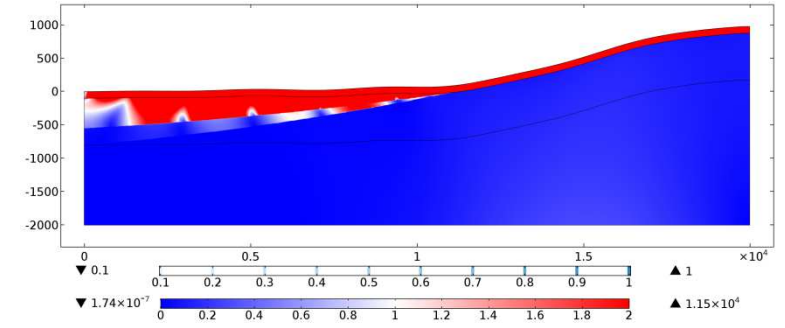
For Case 2, heat advection is only dominant in the two aquifers, and remains dominant in lower parts of the aquifer during permafrost events for T-14 (and T-25, not shown). Otherwise, Case 2 is dominated by heat conduction. The variation of permafrost thickness in Case 2 is mainly due to geological variability, ranging from basement to the Jurassic sequence, and the sea-level rise, thawing the permafrost from the right boundary.

present day

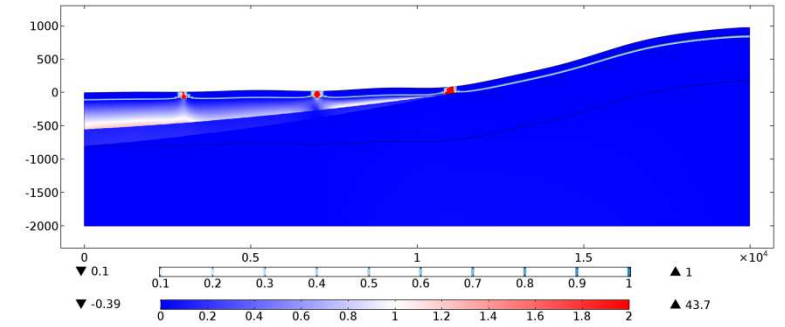
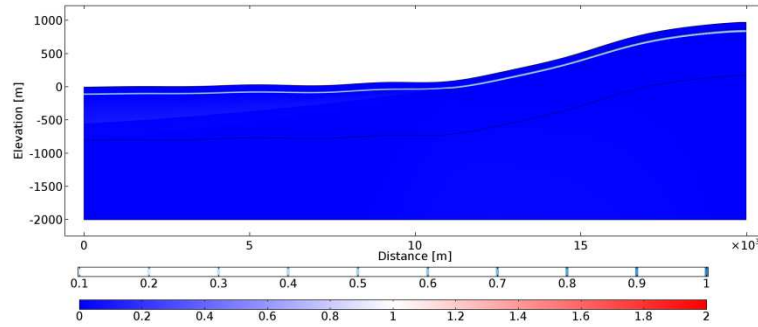
Case 1 T-14 Max



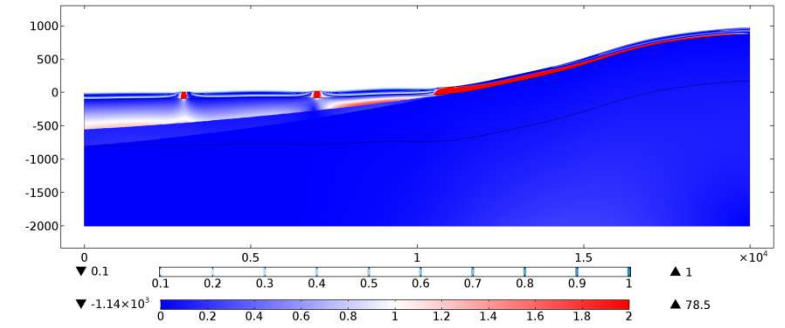
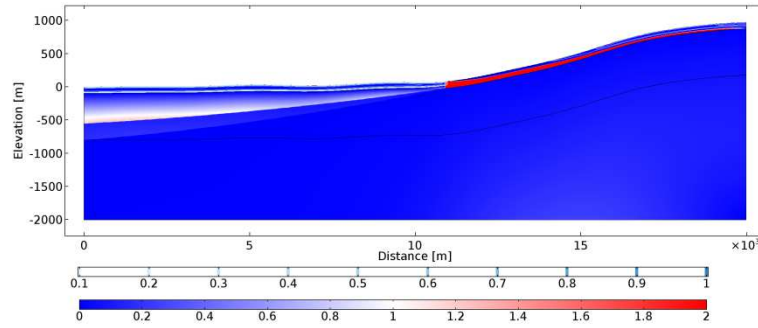
Case 1 T-14 Max Talik



Frozen (21.75 ka BP)

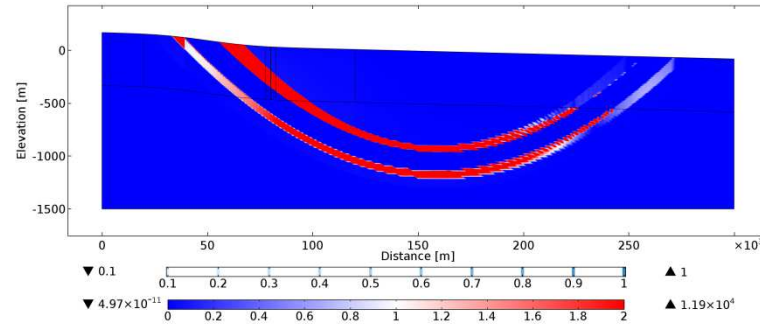


Thawing (14.5 ka BP)

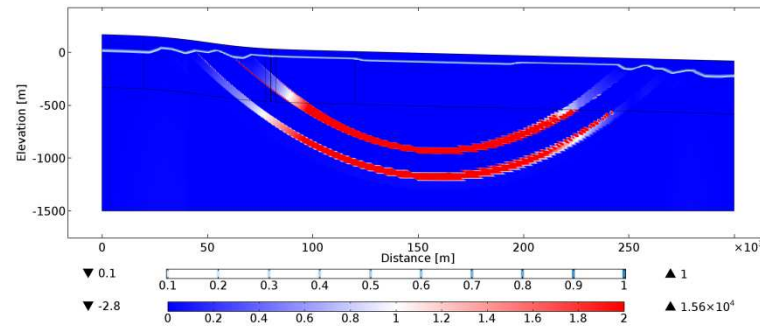


Case 2T-14

present day



Frozen (21.75 ka BP)



Thawing (14.5 ka BP)

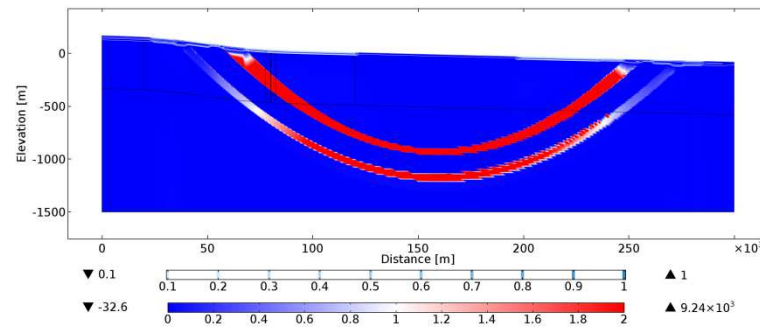


Figure 48. Thermal Peclet number for different model runs; Case 1: T-14_Max, T-14_Talik, and T-14 Case 2 T-14, for unfrozen, fully frozen and thawing conditions.

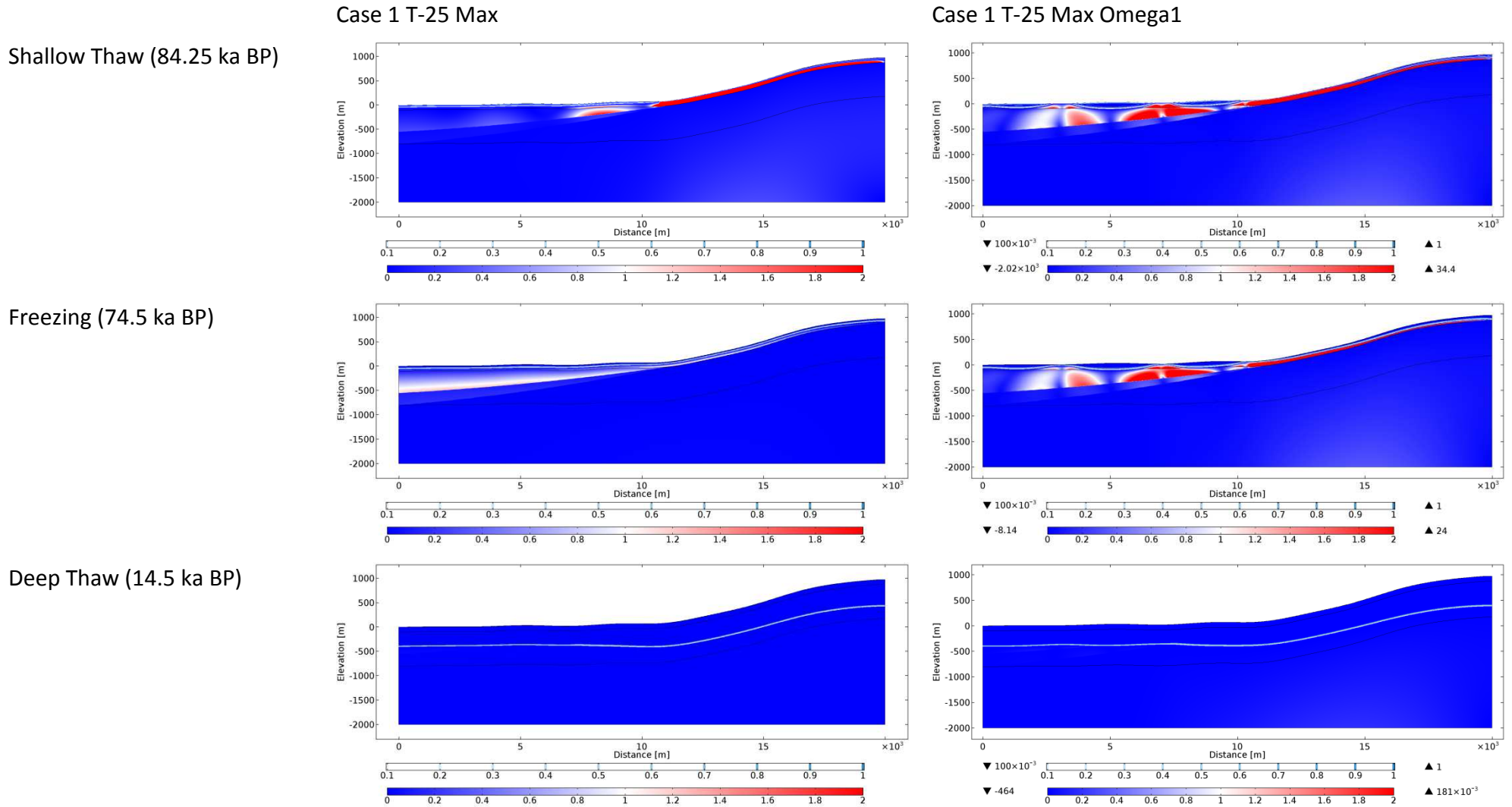


Figure 49. Thermal Peclet number for different T-25_max and T-25_Max_Omega_1 runs, for shallow thawing, freezing and deep thawing.

Appendix 4 Influences of periglacial and glacial conditions on the groundwater flow system

PERIGLACIAL INFLUENCE ON THE GROUNDWATER FLOW SYSTEM

Surface fluxes

Models discussed in this section for Case 1, as described in Table 6:

- T_25_Max
- T_25_Max_Omega1
- T_14_Max
- T_14_Talik
- T_14_Max_rep

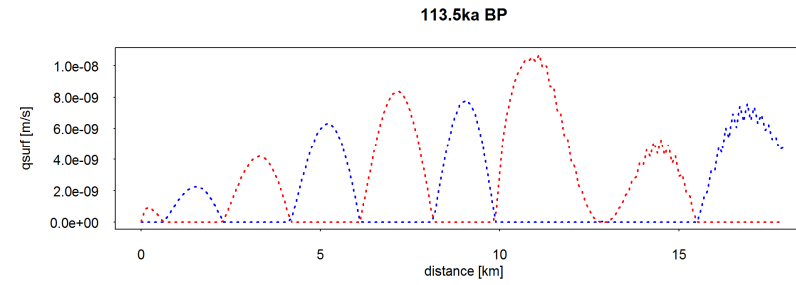
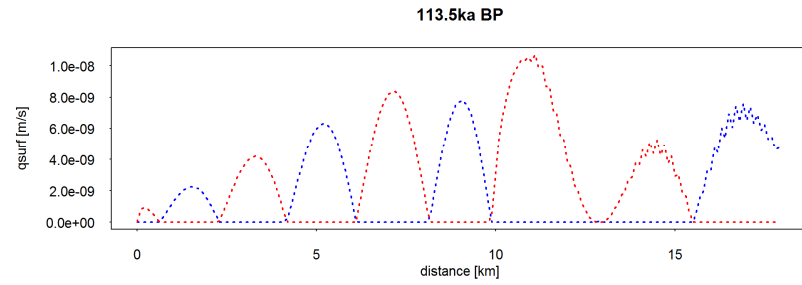
When the model domain is unfrozen (Figure 50a), recharge and discharge are driven by the topographic gradient and the permeability of the weathered layer. Water is recharged at the higher topography and in the lowlands on the smaller hills, and discharges in valleys and other topographic lows. For the model with $\Omega = 6$, when ice starts to form at the surface, recharge and discharge decrease by up to six orders of magnitude. The decrease is most pronounced in the lowlands, and recharge across the steeper slope remains higher (Figure 50b and c). When permafrost thickness exceeds the thickness of the weathered layer, recharge and discharge decrease further (Figure 50e). During thaw, discharge first peaks at the base of the larger hill (Figure 50f). When there is only relict permafrost in the lowlands below the weathered layer, recharge and discharge are similar to unfrozen conditions.

When permafrost is more permeable with $\Omega = 1$, recharge and discharge both decrease when permafrost starts to form, but discharge focusses on topographic low places, preventing permafrost to form there, and taliks form in these locations (Figures 50b-d). For Figure 50d, discharge at the topographic depressions is higher than when permafrost is absent (Figure 50a). When there is thick permafrost, the surface flux pattern is similar to the model in which $\Omega = 6$, but the decrease is only one order of magnitude compared to six orders of magnitude (Figure 50e). The pattern for thaw (Figures 50f-g) is again similar to the $\Omega = 6$ case, however recharge and discharge are slightly higher.

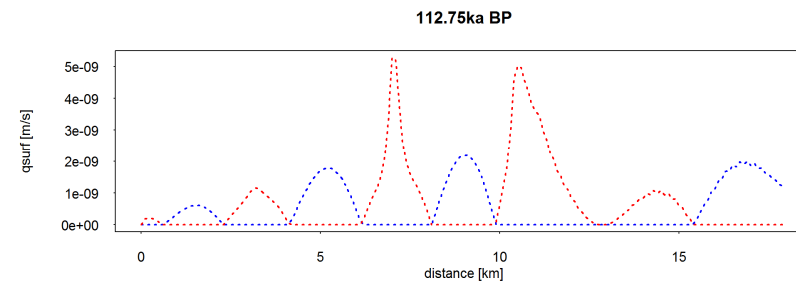
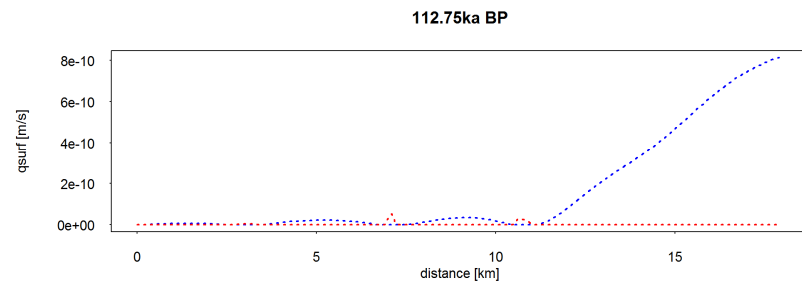
$\Omega 6$

$\Omega 1$

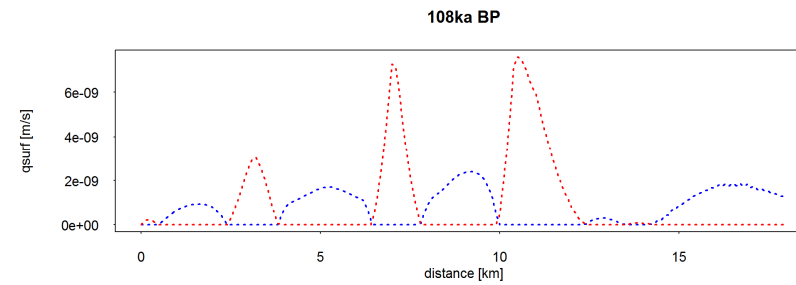
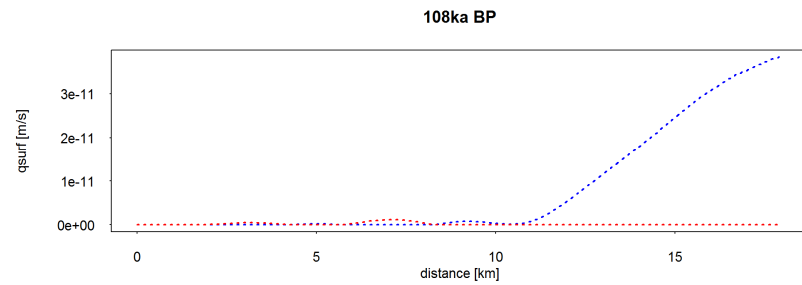
a

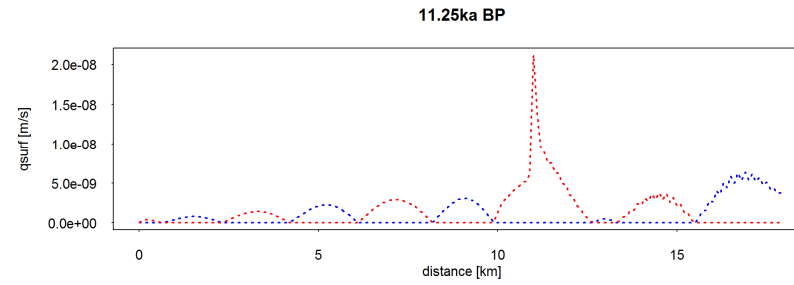
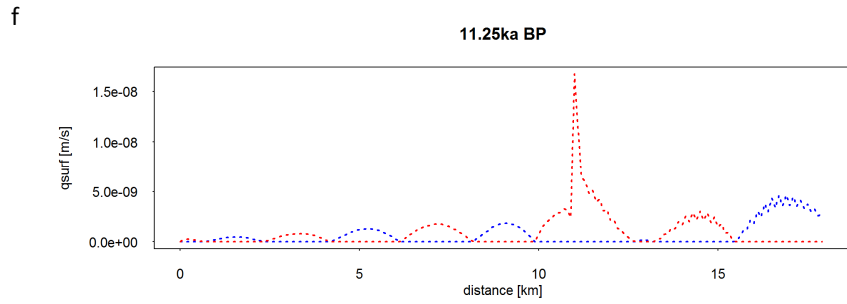
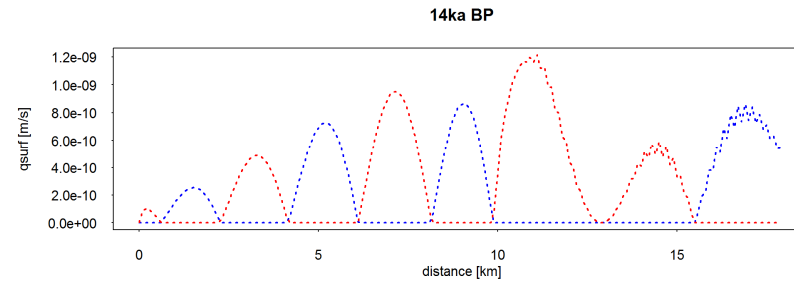
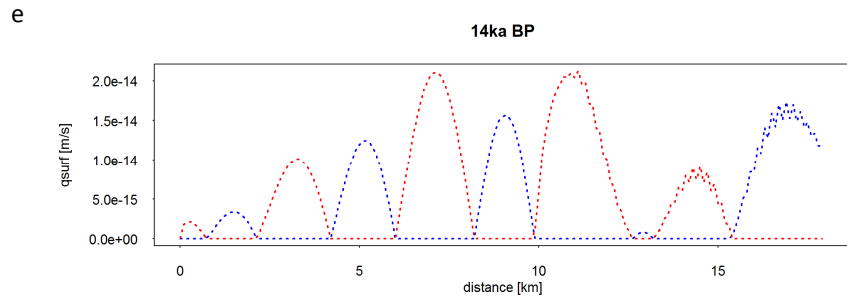
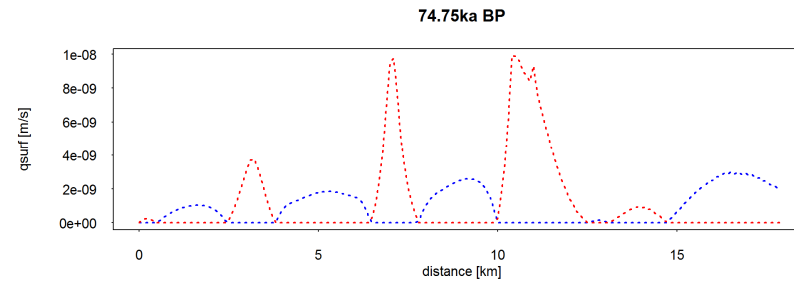
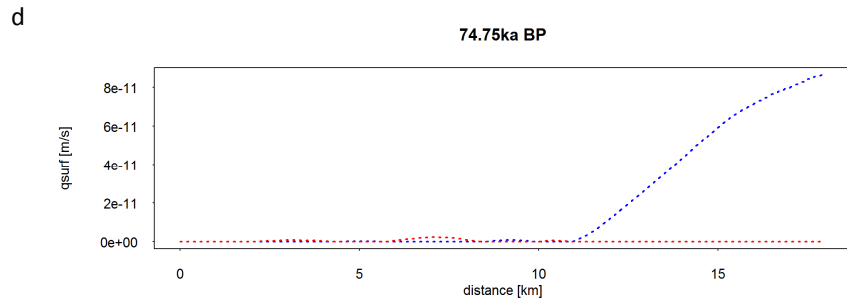


b



c





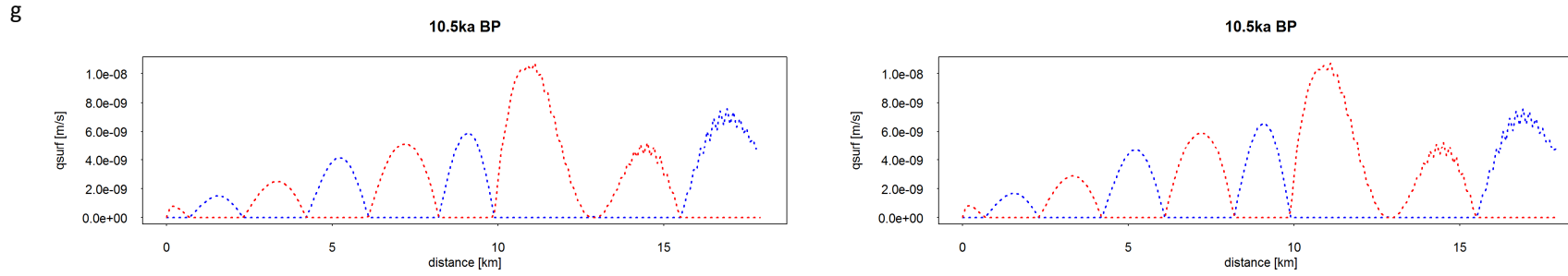


Figure 50. Recharge (blue) and discharge (red) for the time steps as Figure 45 and Figure 46 for run T-25_Max.

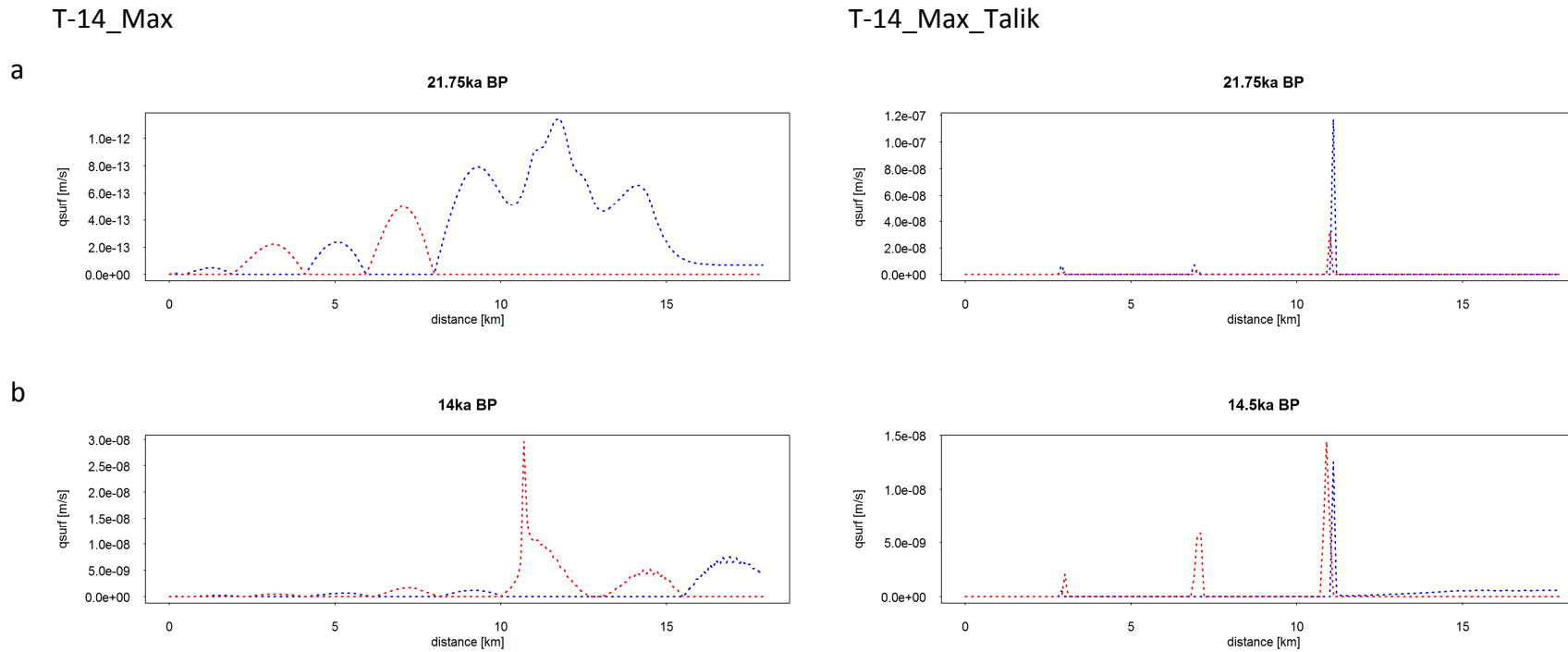


Figure 51. Surface fluxes for the T-14_Max model and the T-14_Max_Talik model for the time steps as in Figure 47.

In the talik model (T_14_Max_Talik), the taliks remain open during the entire simulation, and surface fluxes remain high when these are through thick permafrost (Figure 51a). The flux at the location of the lake at ~11 km is higher than under unfrozen conditions.

During thaw (Figure 51b) the discharge at the valleys is larger for the model without surface water bodies. For the T-14_Max model, discharge is focused at only one location at the foot of the larger hill, whereas for the talik model discharge is distributed at the locations of the three surface water bodies.

Velocity magnitudes within the permafrost and below the permafrost

Case 1

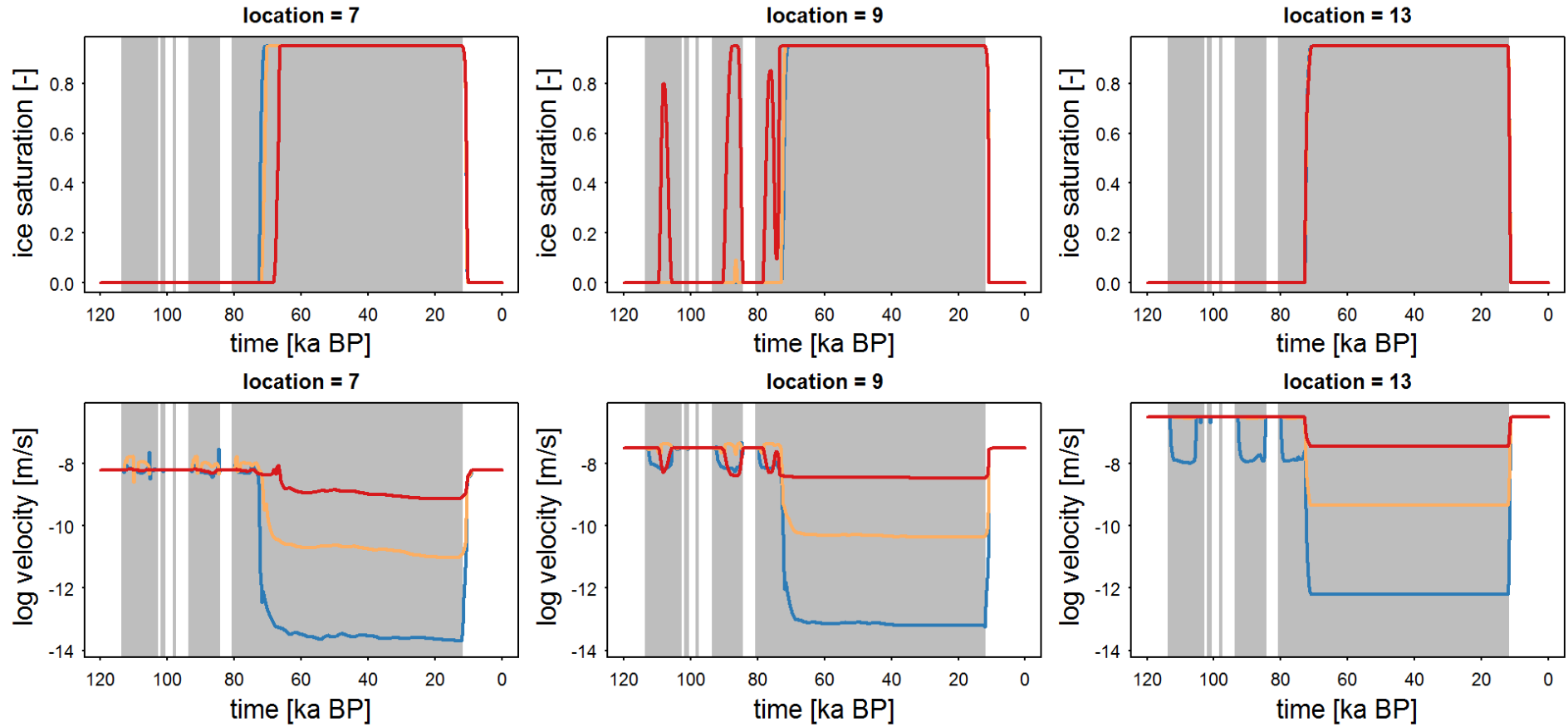
Models discussed in this section for Case 1 as described in Table 6:

- T_25_Max (Omega 6)
- T_25_Max_Omega3
- T_25_Max_Omega1

When the ground is frozen, the velocity magnitudes decrease by as many orders of magnitude as specified with the Ω parameter. This can be observed at the depth of 100 m between 70-15 ka BP (Figure 52).

At 400 m, permafrost is only present between 25-15 ka BP, however, the velocity magnitude also decreases below the permafrost before 25 ka BP to a lesser extent than when the ground is fully frozen. This is because recharge and discharge at the surface decreases and water drains the domain at the left hand boundary, resulting in a lower hydraulic head beneath the permafrost than under unfrozen conditions. This low hydraulic head gradient underneath the permafrost is responsible for the lower velocity magnitudes than under ambient conditions.

depth= 100 m



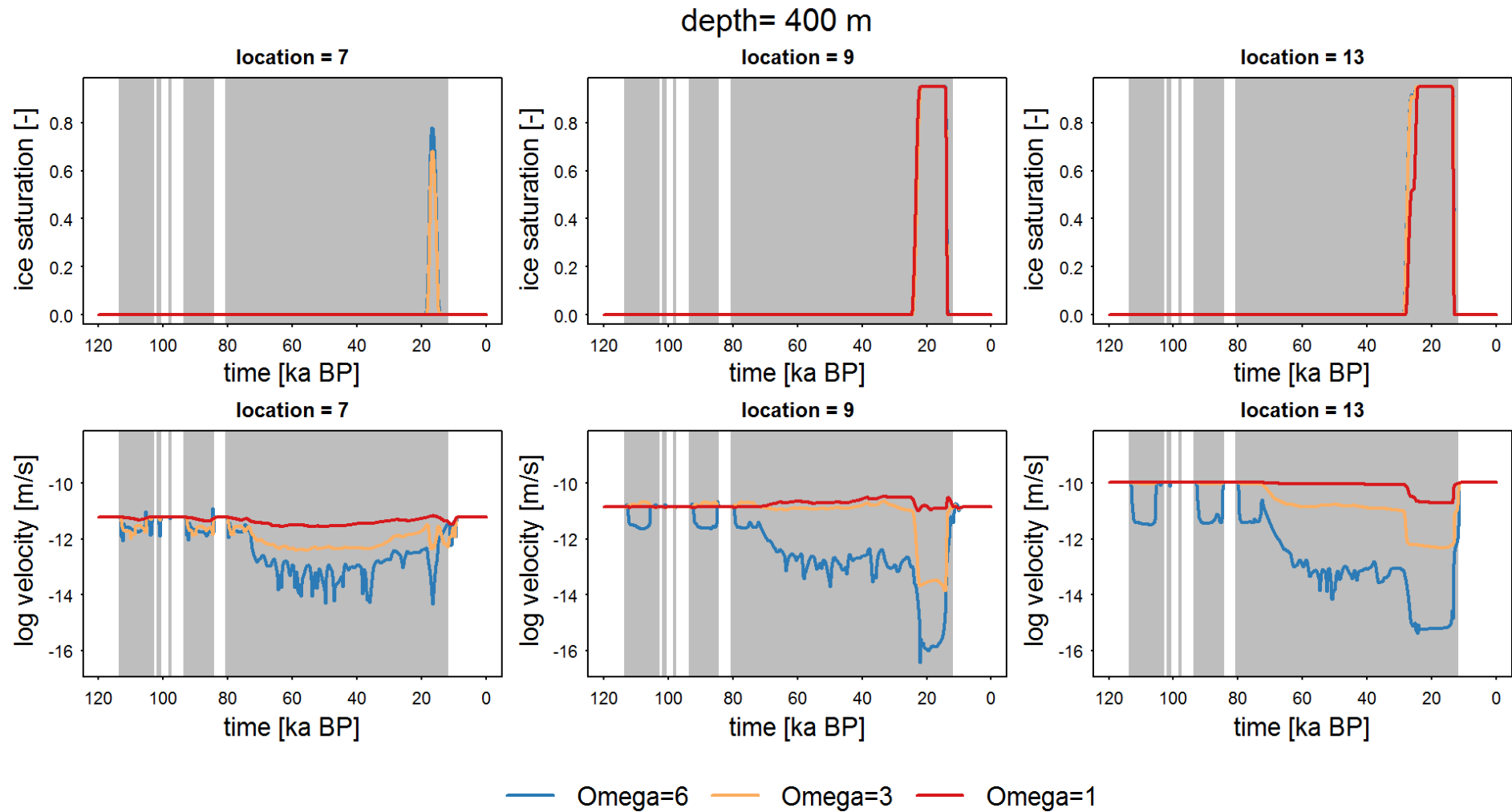


Figure 52. Ice saturation and velocity at 100 m and 400 m depth for locations of 7 km, 9 km and 13 km for Case 1 for model runs T-25_Max (Omega 6), T-25_Max_Omega3 and T-25_Max_Omega1. The grey shaded times are for when the surface is frozen.

Case 2

Model discussed in this section for Case 2, as described in Table 7:

- T_25

For Case 2, the velocity magnitudes are lower than for Case 1 in most of the domain, except for the aquifer at 300 m depth for profile 2 located at 80 km from the left hand model boundary (see Figure 39a). Nevertheless, the pattern of flow velocities is similar to Case 1; the velocities decrease ~six orders of magnitude when it is frozen (100 m depth), and respond at depth when the surface is frozen (Figure 53). In the aquifer at a depth of 300 m, this decrease in flow velocities is most pronounced when the surface is frozen. For one instance, before 600 ka BP, the permafrost penetrates to a depth of 300 m and the velocity magnitude decreases further. In the lower Jurassic, (450 m depth) velocity magnitudes are generally very low and of the order of 10^{-13} m/s. After the instance before 600 ka BP, when permafrost forms in the aquifer, flow velocities in the lower Jurassic decrease by ~50%. The signal of decreasing velocities in the lower Jurassic is delayed compared to the permafrost event at shallower depths.

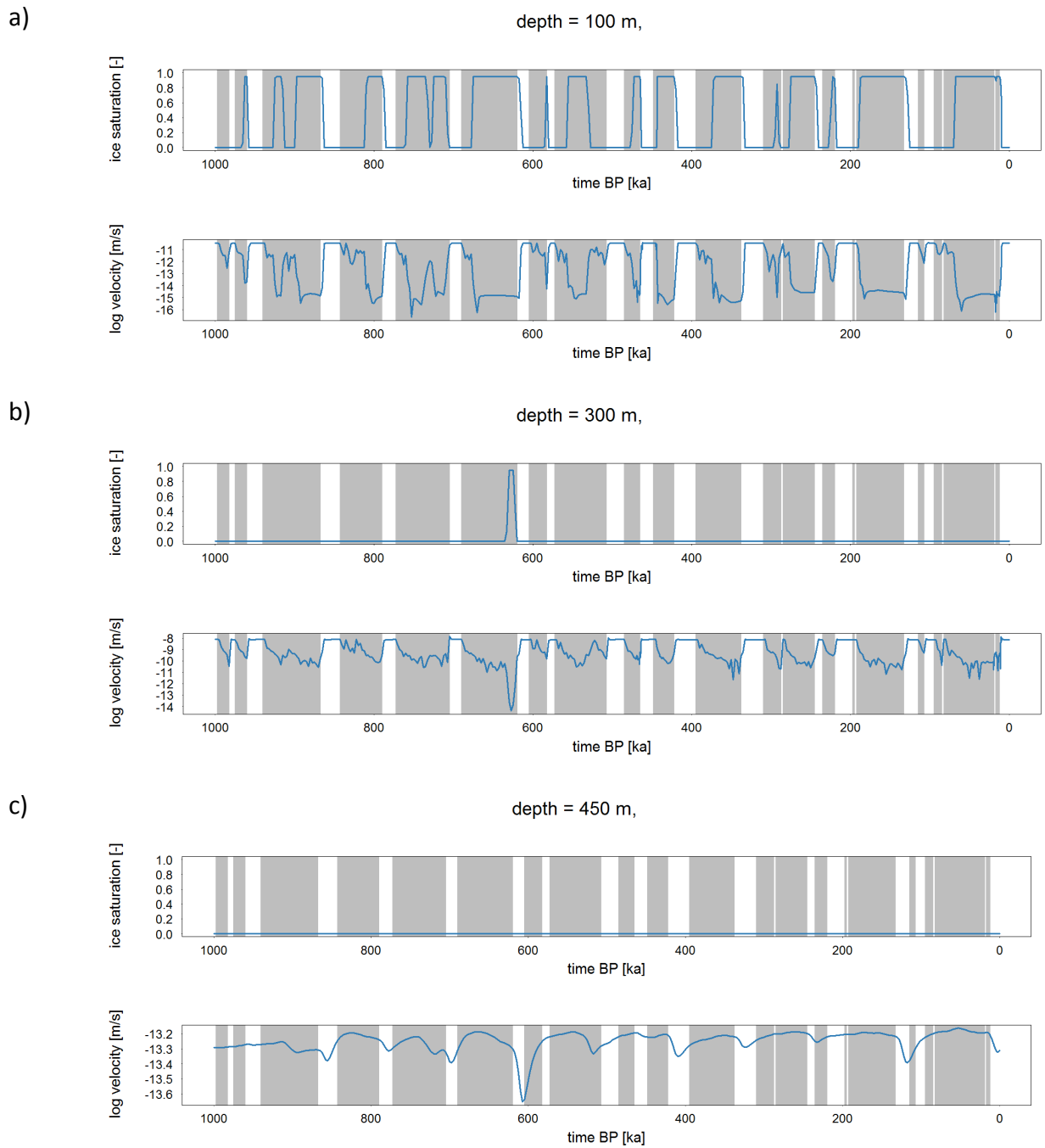


Figure 53. Ice saturation and groundwater flow velocities at a) 100m, b) 300m and c) 450 m depth at the location of the repository for Case 2 for model run T-25. The grey shading indicates the times when the surface is frozen.

Tracing of groundwater during a permafrost event

In order to assess the potential travel time from a point source release to the surface or the side of the system, a mass source of $1 \text{ kg m}^{-3}\text{a}^{-1}$ was released at 500 m depth and 7 km from the left hand boundary in a simulation based on Case 1 T-14_Max (T_14_tracer). For the entire model, the lateral dispersivity is 50m, the transverse dispersivity is 5m and the solute diffusivity $10^{-10} \text{ m}^2\text{s}^{-1}$.

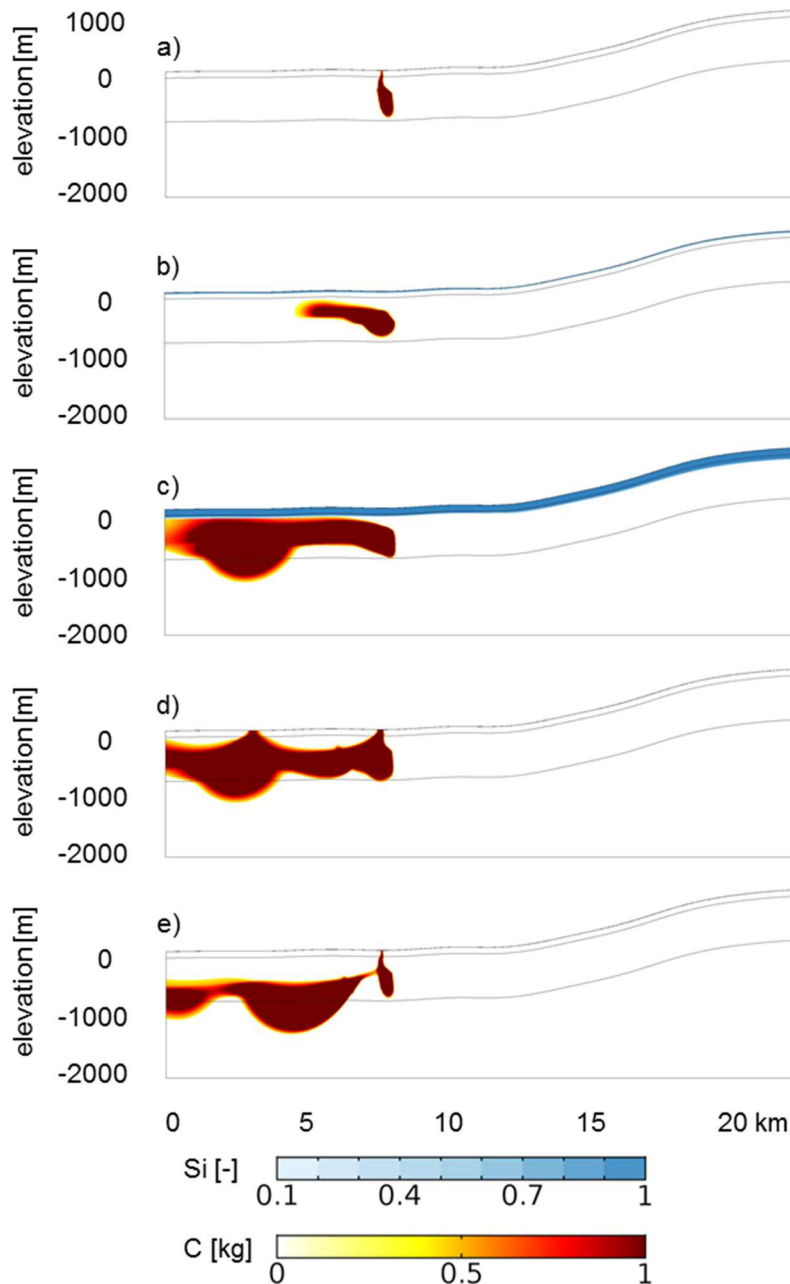


Figure 54. Tracer from a point source release at 500 m depth and 7 km from the left hand boundary to the surface under a) ambient conditions (100 ka BP), b) forming permafrost (65 ka BP), permafrost (18 ka BP), thawing permafrost (14 ka BP) and post permafrost conditions (0 ka BP) for Case 1 run T_14_tracer.

During ambient conditions, the tracer plume is driven towards the surface (Figure 54a). Under unchanged hydrogeological conditions, the plume remains like this. When permafrost starts to form, advection to the surface ceases and the plume spreads laterally towards the left hand boundary (Figure 54b). During a prolonged permafrost event (e.g. Devensian glaciation) the tracer plume spreads laterally, and the area affected by the tracer is more extensive than under

ambient conditions (Figure 54c). When permafrost thaws, the plume spreads towards the surface again and the plume leaves the system at the same location as before the permafrost event, but also to a discharge point further downstream (Figure 54e-f).

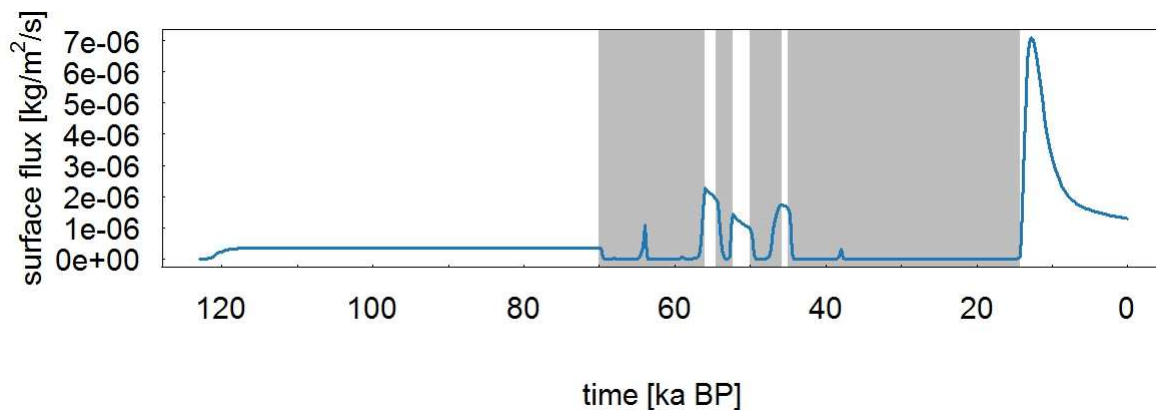


Figure 55. Integrated surface flux of the tracer over time for the point source release placed at 500 m depth and 7 km from the left hand boundary for Case 1 run T_14_tracer.

The integrated flux to the surface across the entire model domain decreases to zero when permafrost forms (Figure 55), however after a permafrost event the flux increases again. During the permafrost event, the tracer gets concentrated underneath the permafrost, and after the longest permafrost event lasting ~35,000a, the flux to the surface increases by 20 times compared to the flux without the occurrence of permafrost.

This simulation run, releasing a tracer at a point source, demonstrates that the existence of permafrost can fundamentally alter the area which is affected by a tracer and the flux of the tracer to the surface. During a permafrost event, discharge to the surface stops and the tracer spreads laterally, affecting a larger area than under unfrozen conditions. The tracer concentrates below the permafrost and is then released after the permafrost has disappeared, resulting in higher surface flux after a permafrost event than under constantly unfrozen conditions.

GLACIAL INFLUENCE ON THE GROUNDWATER FLOW SYSTEM

The following models are used to evaluate the glacial influence on the groundwater flow system. The geometry/topography of the model domain is based on Case 2 and the boundary conditions are the same for each run. The following model variations are considered:

- T-14_OneLayer: Conceptual one layer model, representing basement
- T-14_OneLayer>Loading: Conceptual one layer model, representing basement, and consideration of mechanical loading
- T-14_Case1>Loading: Geology representing Case 1 mechanical loading as shown in Figure 22.
- T-14_Case2: Geology representing Case 2
- T-14_Casse2>Loading: Geology representing Case 2 mechanical loading

Two glaciations are assumed to impact the model domain: the Anglian glaciation and the Devensian. During the Anglian glaciation, the entire model domain is covered by the ice sheet, whereas for the Devensian, only the right hand side of the model is covered by the glacier.

The hydraulic head distribution underneath an advancing or retreating ice sheet during the Anglian glaciation is shown for different model runs (Figure 56). As the ice sheet is advancing

against the general groundwater flow direction, groundwater flow directions are reversed during the presence of the ice sheet. Generally, hydraulic head is high beneath the ice and propagates to the base of the model domain. An exception is for Case 2 in which no loading is considered. The change in hydraulic head induced by the ice sheet only propagates very slowly through the clay and mudstone layers, resulting in a very large hydraulic gradient at the boundary between the aquifers and the low permeability layers. This is also why the groundwater flow velocities are highest compared to the other runs in the aquifer for Case 2. For Case 2, when loading is considered, then the hydraulic head distribution is much more similar to the other runs.

For Case 1, groundwater flows underneath the ice sheet are largest in the weathered layer and the sandstones; the hydraulic conductivity is higher than in the basement.

Uniform properties

For this model, all layers have been removed and the uniform thermal and hydraulic properties correspond to those of the basement.

The time series for hydraulic head, temperature, velocity magnitude and Darcy flows in x and y directions at 400 m depth for profile 3 at 160 km into the model domain (Figure 39a) are presented in Figure 56. The two spikes in hydraulic head correspond to the Anglian and Devensian glaciation.

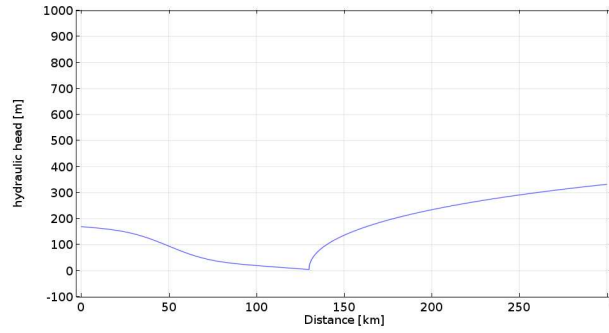
During the Anglian glaciation, hydraulic head increases even at depth to ~2 km, and the groundwater velocity magnitudes increase during the glaciation. The groundwater velocity magnitudes are highest at the start and the end of the glaciation when ice is advancing or retreating and high hydraulic gradients are imposed on the boundary. During ice advance groundwater flows are in a downward direction, whereas they are upward during ice retreat. The lateral groundwater flow direction is reversed during the glaciation and its magnitude is highest during ice advance and retreat.

The signal of the Devensian glaciation is smaller compared to that of the Anglian glaciation, as the ice only covers the right half of the model domain. It is notable that the signal of the Devensian glaciation at a depth of 400 m is delayed compared to the signal at the surface; the peak in hydraulic head reaches this depth at the end of the Devensian glaciation.

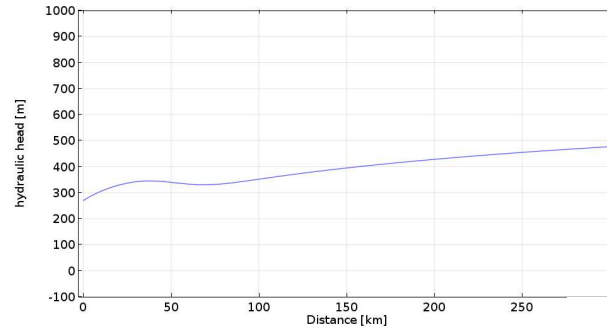
After both glaciations permafrost forms as soon as the ice has retreated, as temperatures are still subzero. The permafrost layer inhibits the higher hydraulic heads at depth in propagating to the surface, and therefore the hydraulic heads are higher at depth as long as the surface is frozen. The velocity magnitude at depth during the permafrost event after the glaciation event decreases over time and is lower than under unfrozen conditions. The lateral groundwater flow direction reverses during the permafrost event and when permafrost thaws the flow direction reverses to its original direction.

460.75 ka

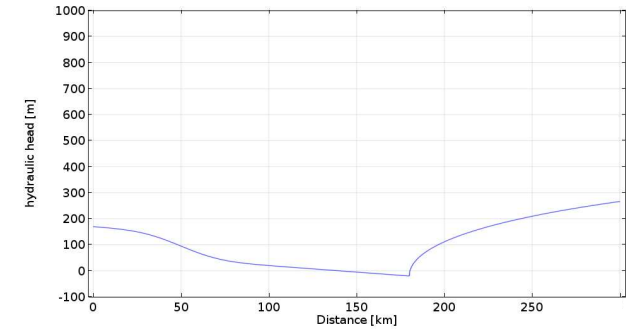
hydraulic head boundary



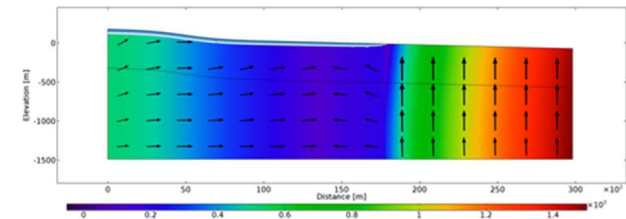
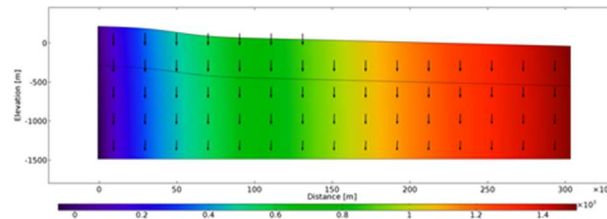
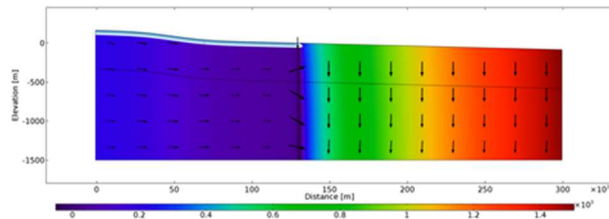
542.75 ka



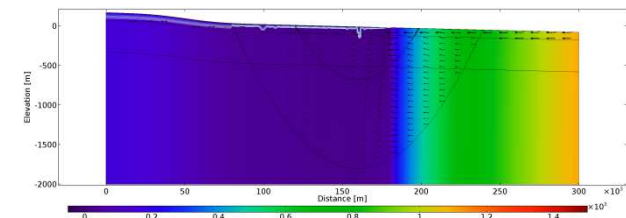
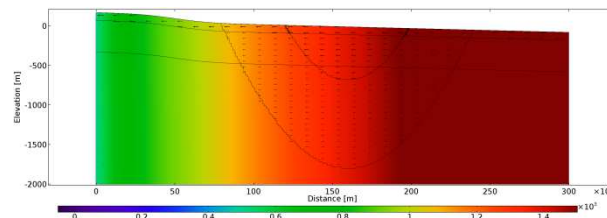
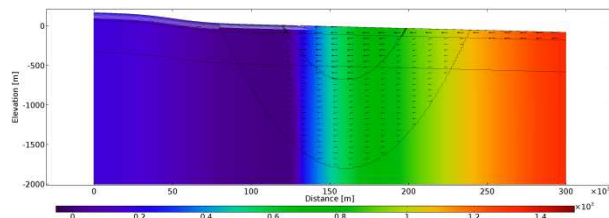
446.5 ka



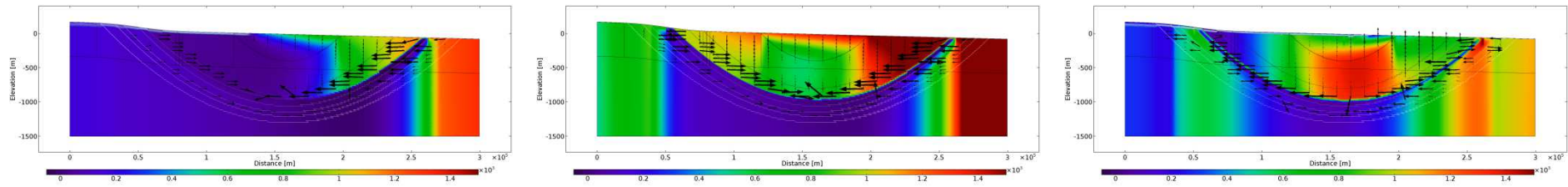
Case 2 with one layer with mechanical loading



Case 1 with mechanical loading



Case 2 without mechanical loading



Case 2 with mechanical loading

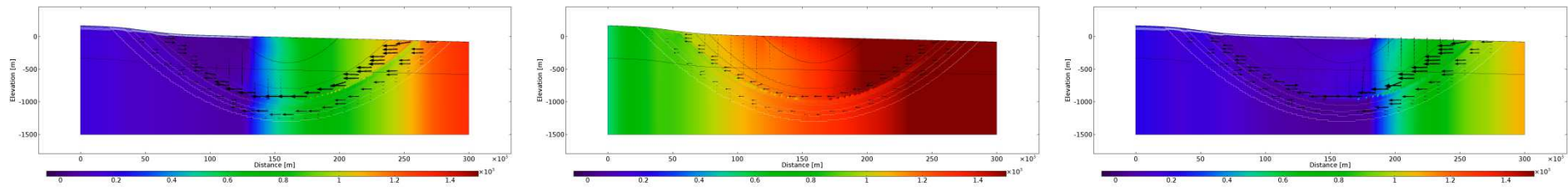


Figure 56. Hydraulic head, permafrost distribution and flow vectors for different glaciation scenarios during ice advance (left) at 539.25 ka, fully glaciated at 542.75 ka (middle), and ice retreat (right) at 553.5 ka

Global relative sea level fluctuated during the Quaternary and is represented here with the global relative sea level curve by *Bintanja et al.* (2005) in Figure 28. During sea level rise and sea level drop, hydraulic head increases and decreases by tens of metres. The velocity magnitude overall decreases as lateral flow drops to zero, as there is no lateral hydraulic gradient where submerged. During sea level rise, there is downward flow or recharge of groundwater and during sea level drop there is upward flow or discharge of groundwater.

Comparison of one layer model, Case 1 and Case 2

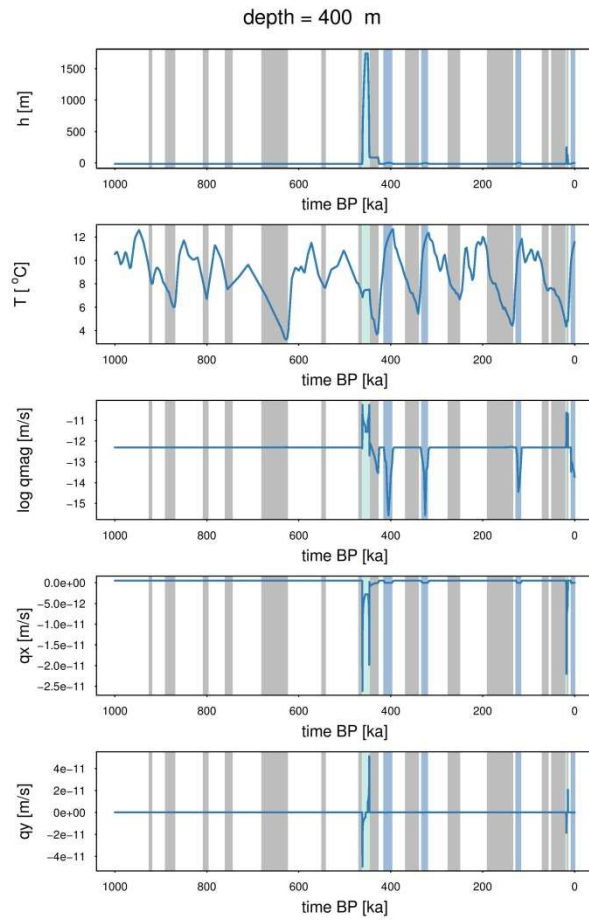
Figure 57 compares the time series of hydraulic head, temperature, velocity magnitude, and Darcy flow in x and y directions at Profile 2, 80 km of the model domain (Figure 39a) for the different model runs.

For the model with uniform properties (one layer model) the time series with and without loading are very similar. Hydraulic heads reach ~1500 m for both model runs, but the flows are higher for the model including loading. Overall, however, the effect of loading is small for a one layer model representing basement geology.

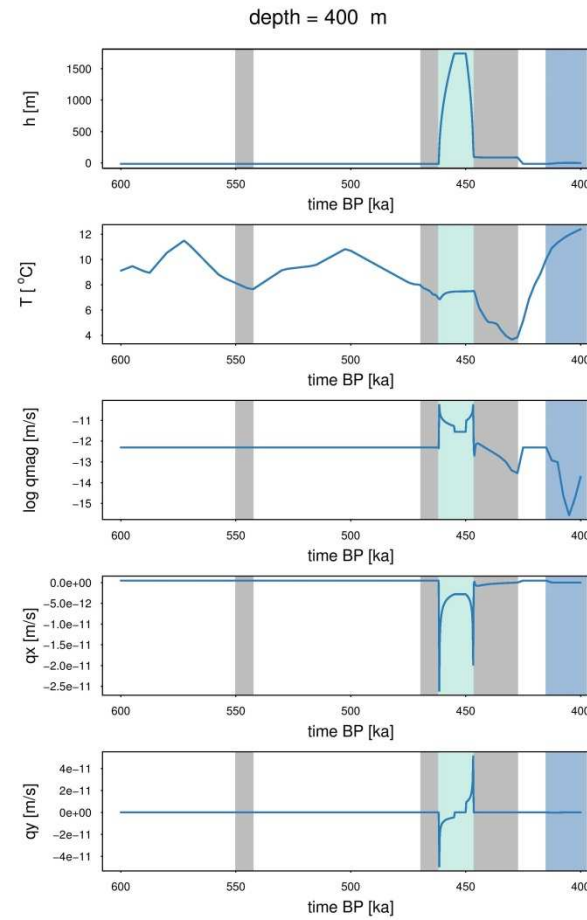
Case 1 behaves similarly to the one layer model. Hydraulic heads reach ~1500 m at the depth of the repository with loading. However, whereas the heads remain high after the glaciation during the period of permafrost coverage for the one layer model, they return to pre-glaciation levels in the Case 1 simulation. This higher drop in hydraulic head at the end of the glaciation compared to the one layer model results in a higher velocity magnitudes and lateral flows.

The influence of loading is larger for Case 2, as shown by the magnitude of hydraulic head at 400 m depth in Figure 57. Hydraulic heads reach ~600 m for the model excluding loading at a depth of 400 m, whereas for the model including loading they reach ~1400 m. The increase in hydraulic heads due to glaciation for the model including loading is dampened by ~100 m compared to the one layer model at depth. In the model excluding loading, the propagation of the high hydraulic heads due to glaciation is dampened and delayed in the low permeability layers even stronger (600 m vs 1500 m of hydraulic head). As the high hydraulic heads only propagate slowly and are dampened in the low permeability layer in the model without loading, strong gradients persist and result in higher velocity magnitudes compared to the model with loading. Flows increase due to glaciation by two orders of magnitude at the repository depth for the model excluding loading and one order of magnitude for the model including loading.

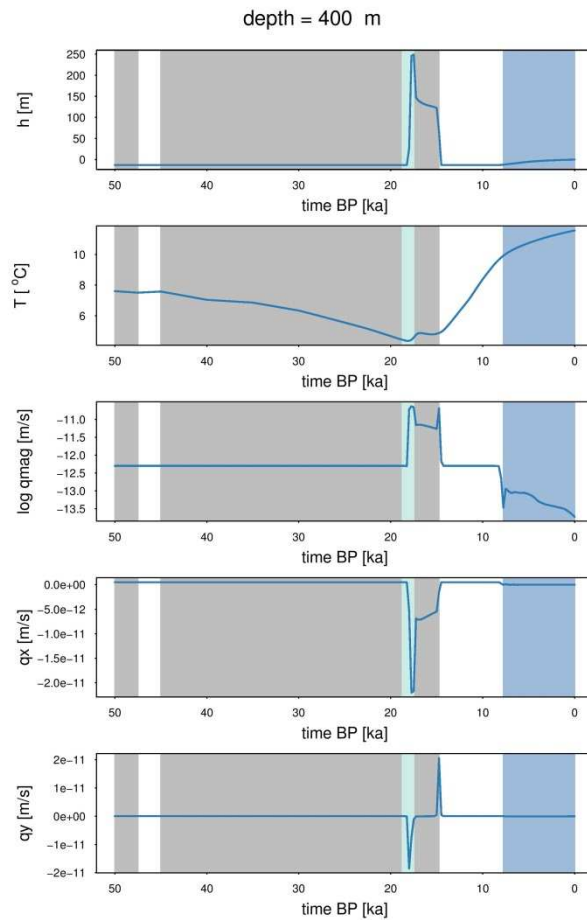
a) Entire simulation



b) Anglian glaciation



c) Devensian glaciation



d) Sea level fluctuations

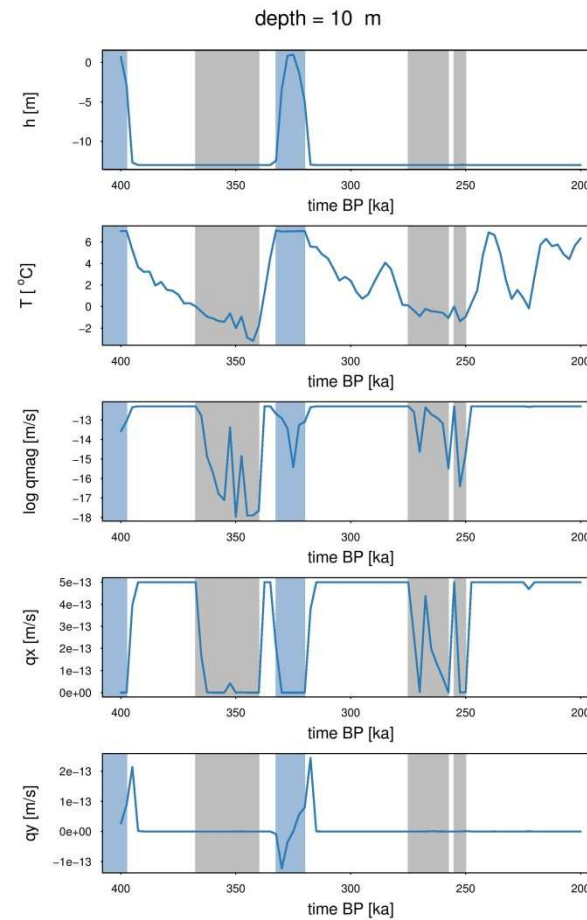
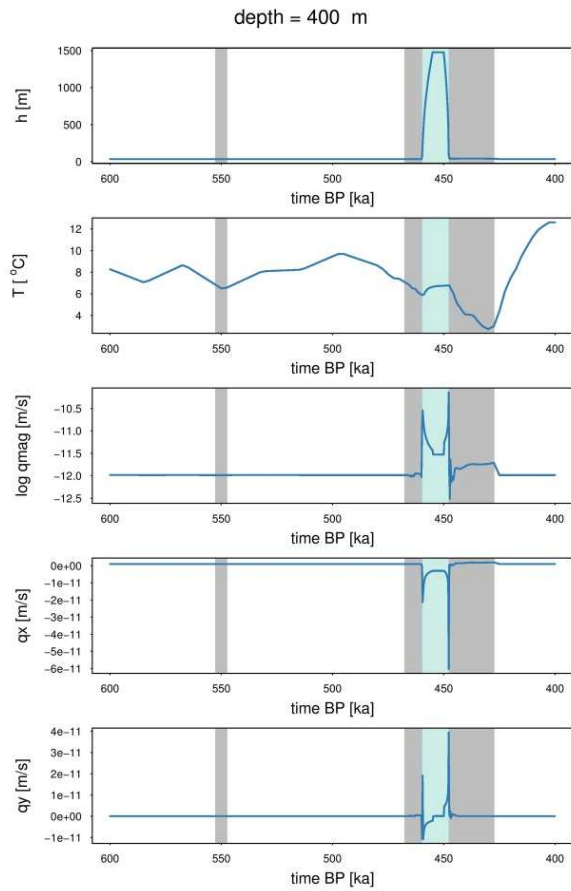
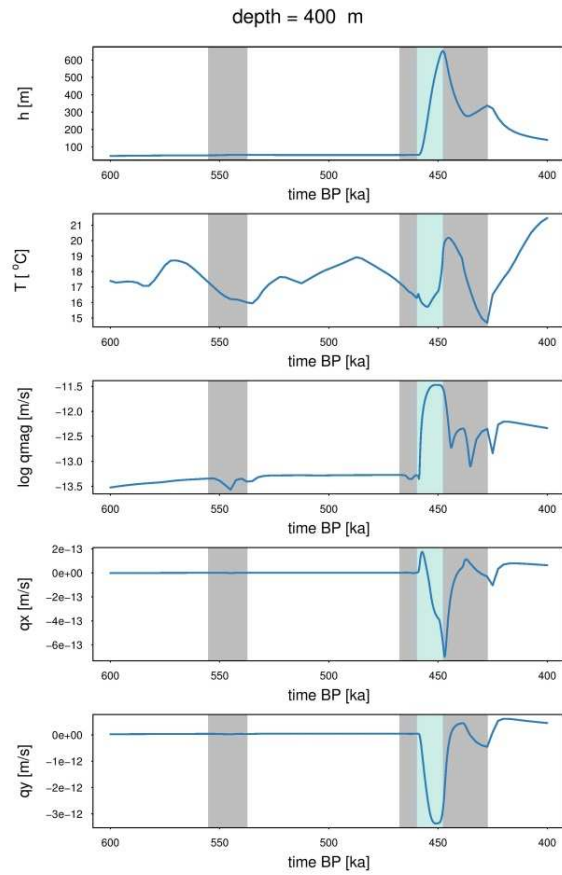


Figure 57. Time series for hydraulic head, temperature, velocity magnitude, and Darcy velocity in x and y for the one layer model for Profile 3 at 160 km. Times presented are a) the entire simulation time, b) the Anglian glaciation c) the Devensian glaciation and d) during submerged conditions. The grey shaded times are when the surface is frozen, dark blue submerged and light blue covered by an ice sheet.

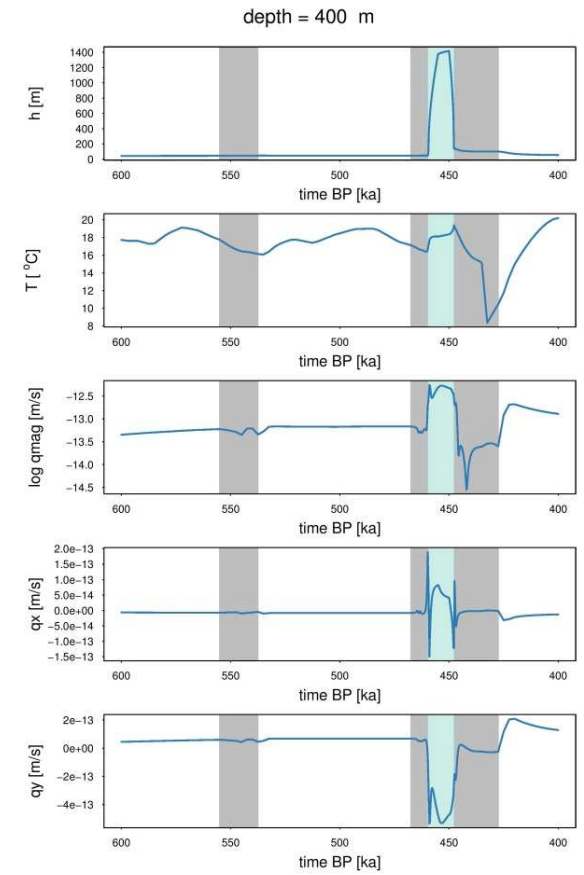
Case 1 with mechanical loading



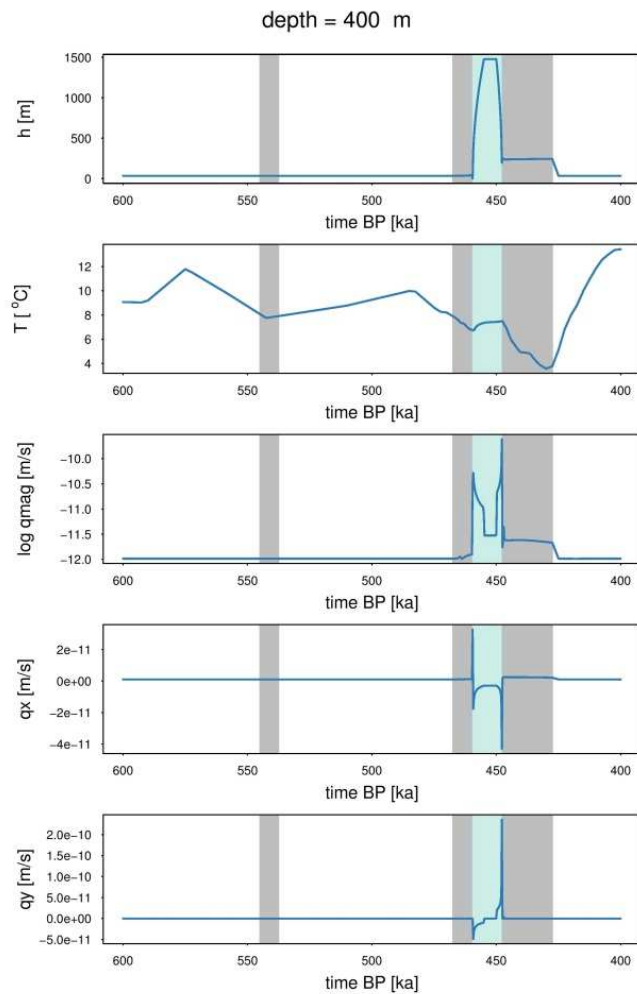
Case 2 without mechanical loading



Case 2 with mechanical loading



1 Layer model Loading



1 Layer model

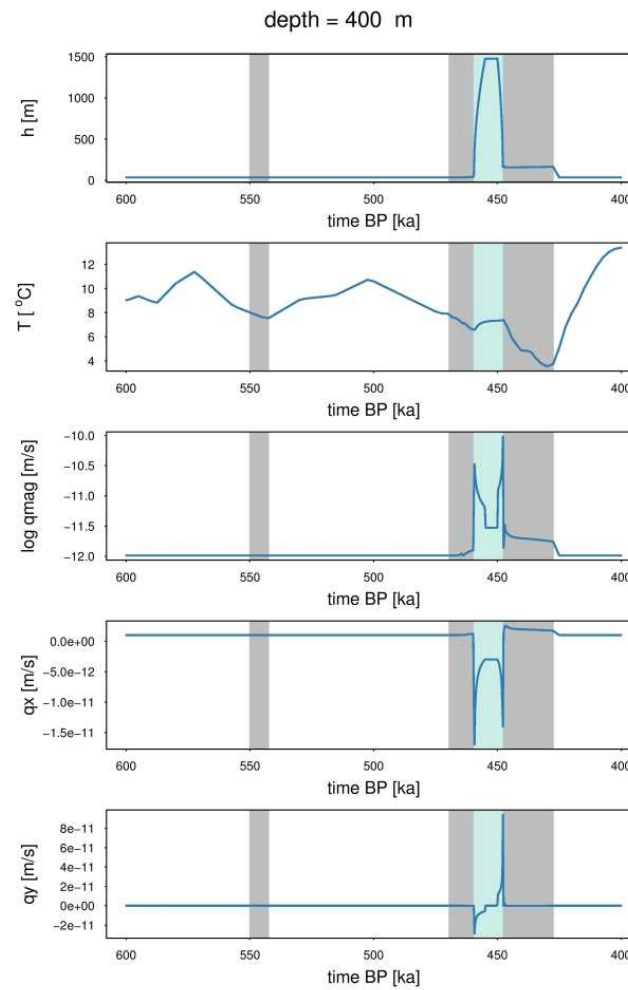
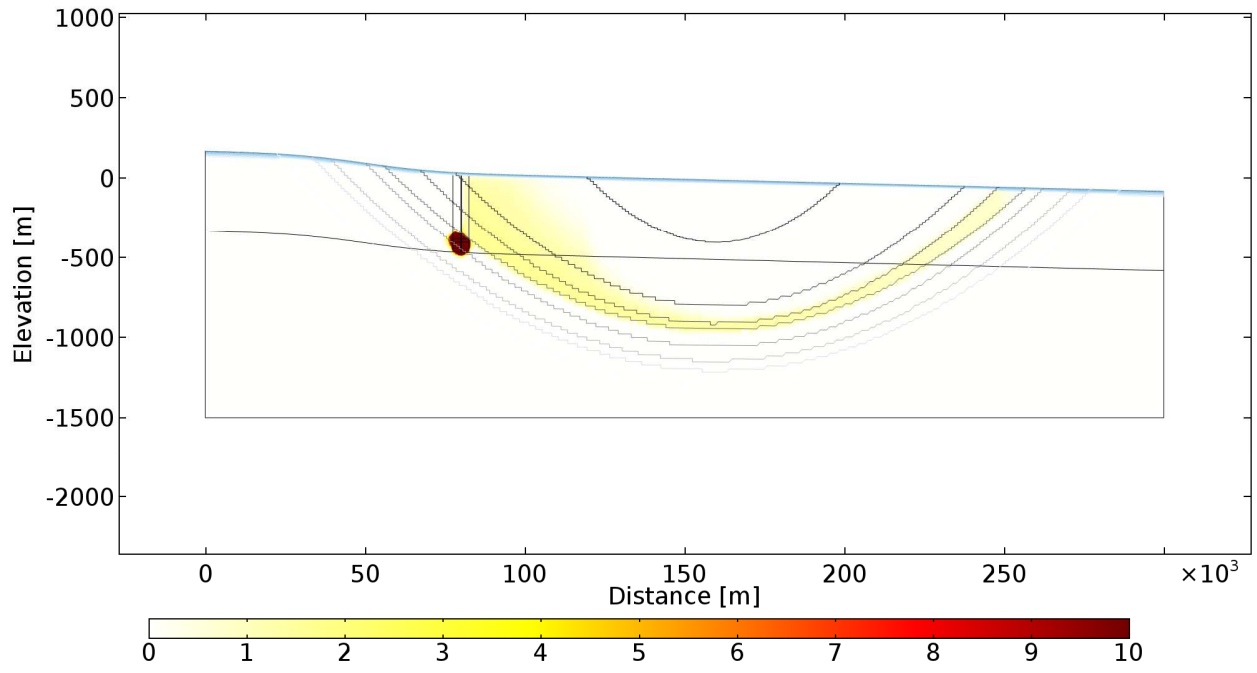
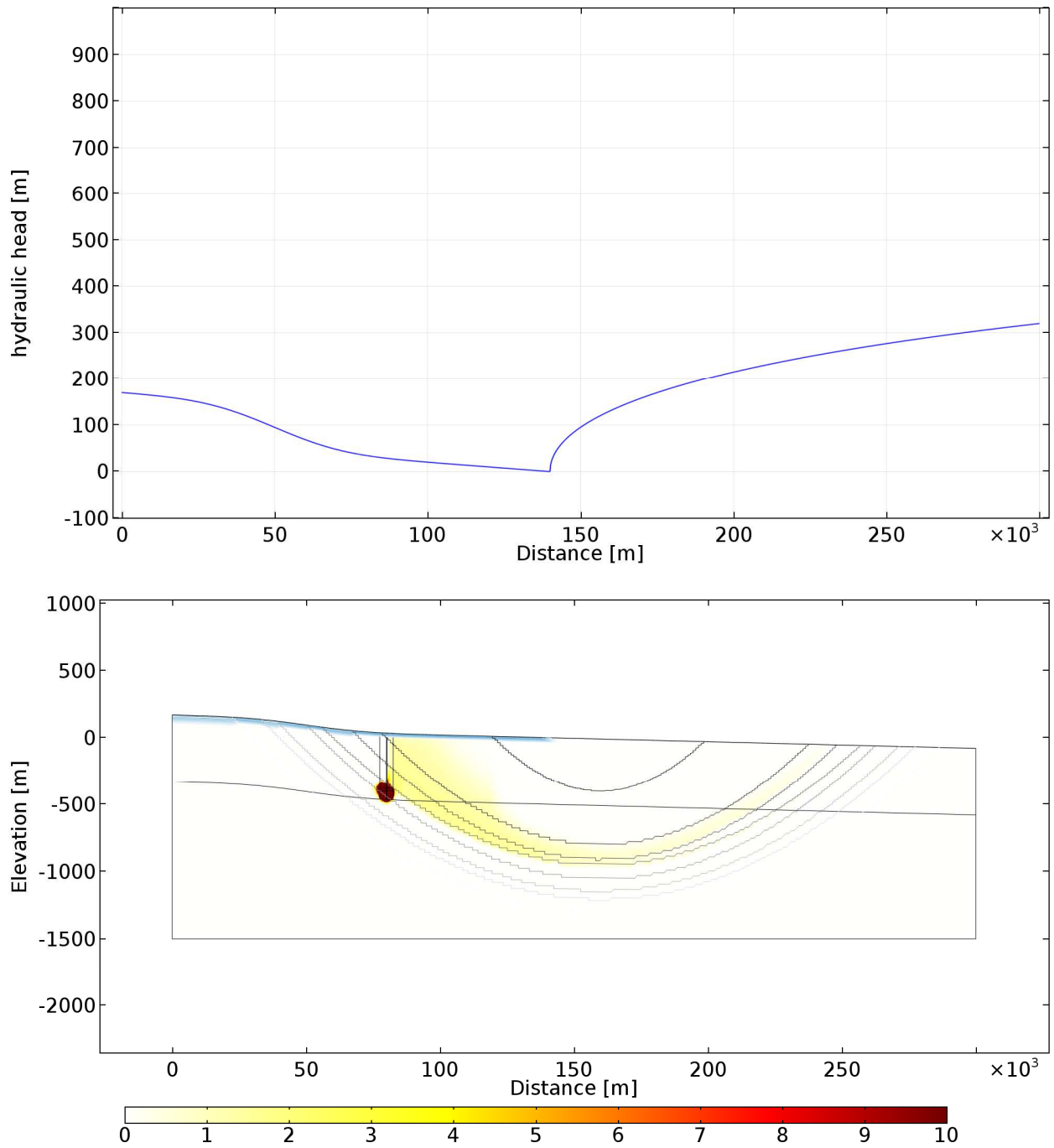


Figure 58. Time series of hydraulic head, temperature, velocity magnitude and Darcy flow in x and y at the location of the repository over the duration of the Anglian glaciation.

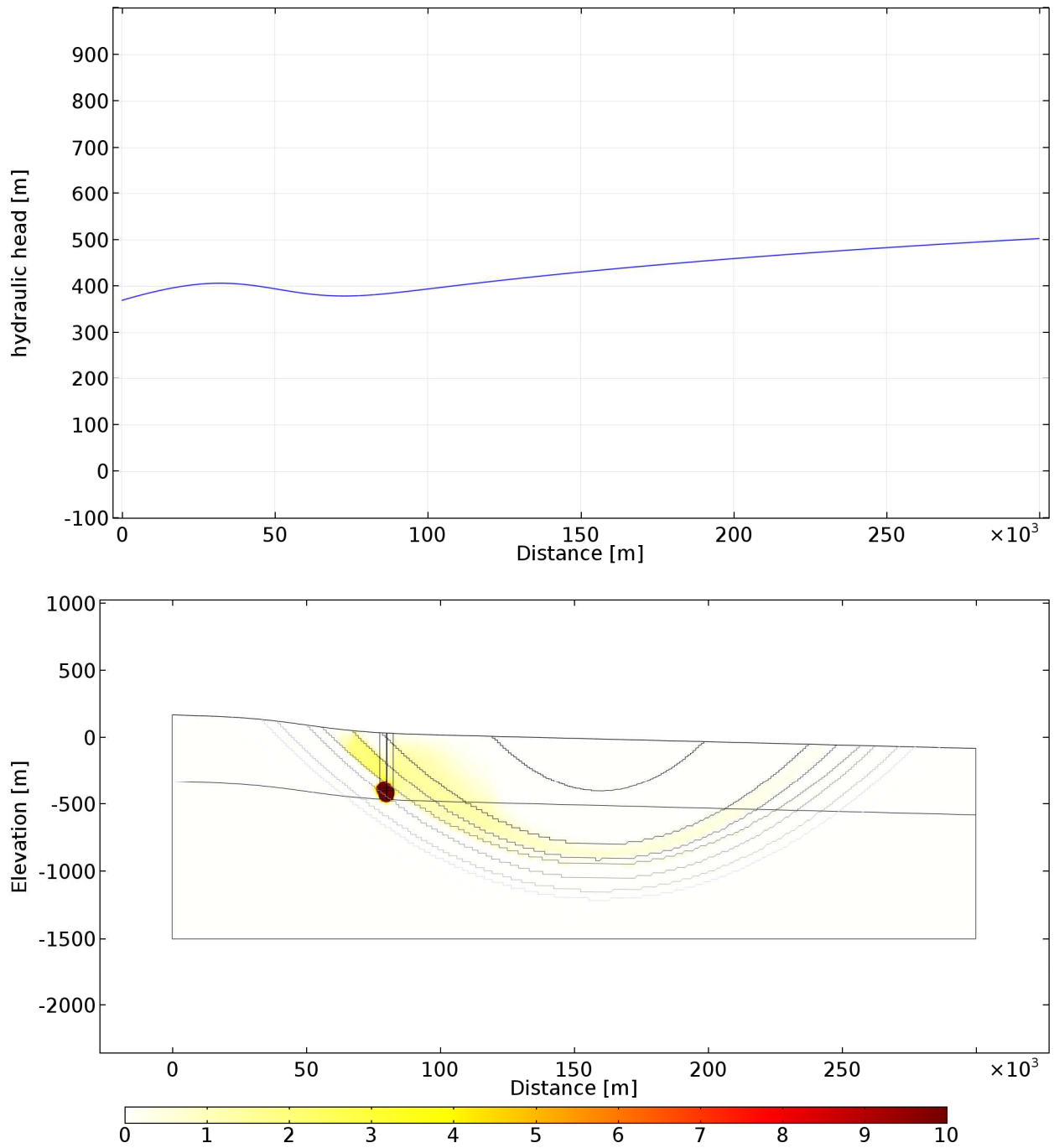
Pre glaciation at 465 ka BP



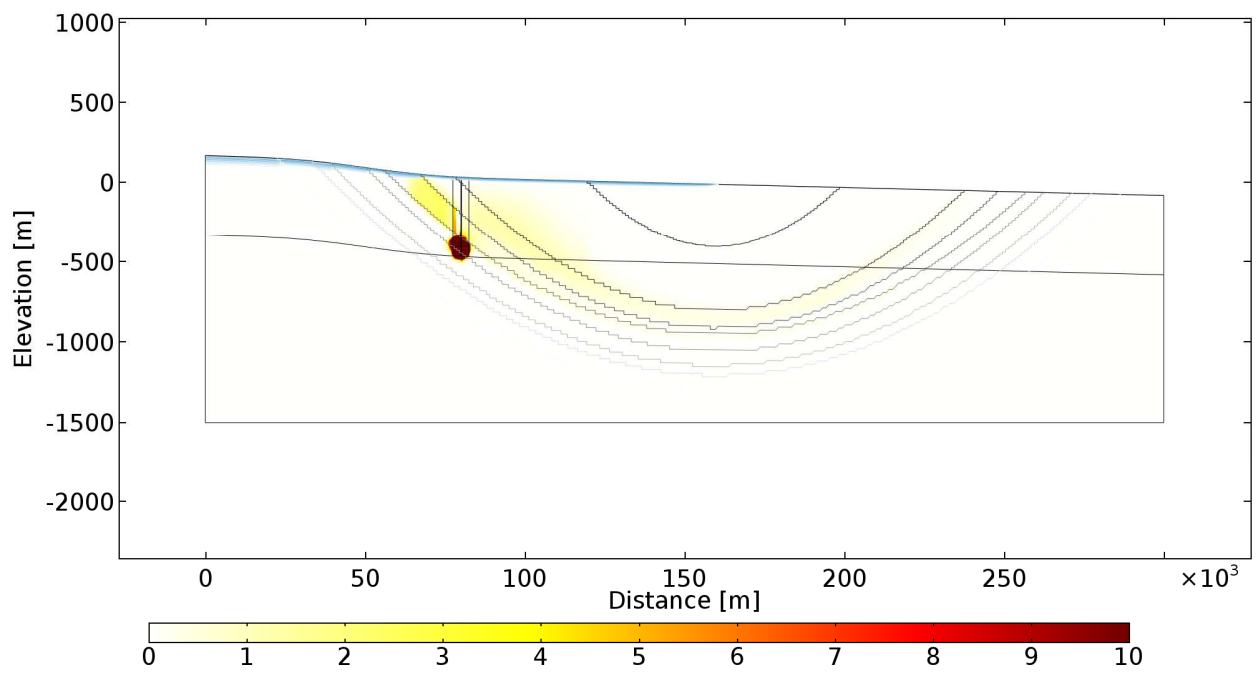
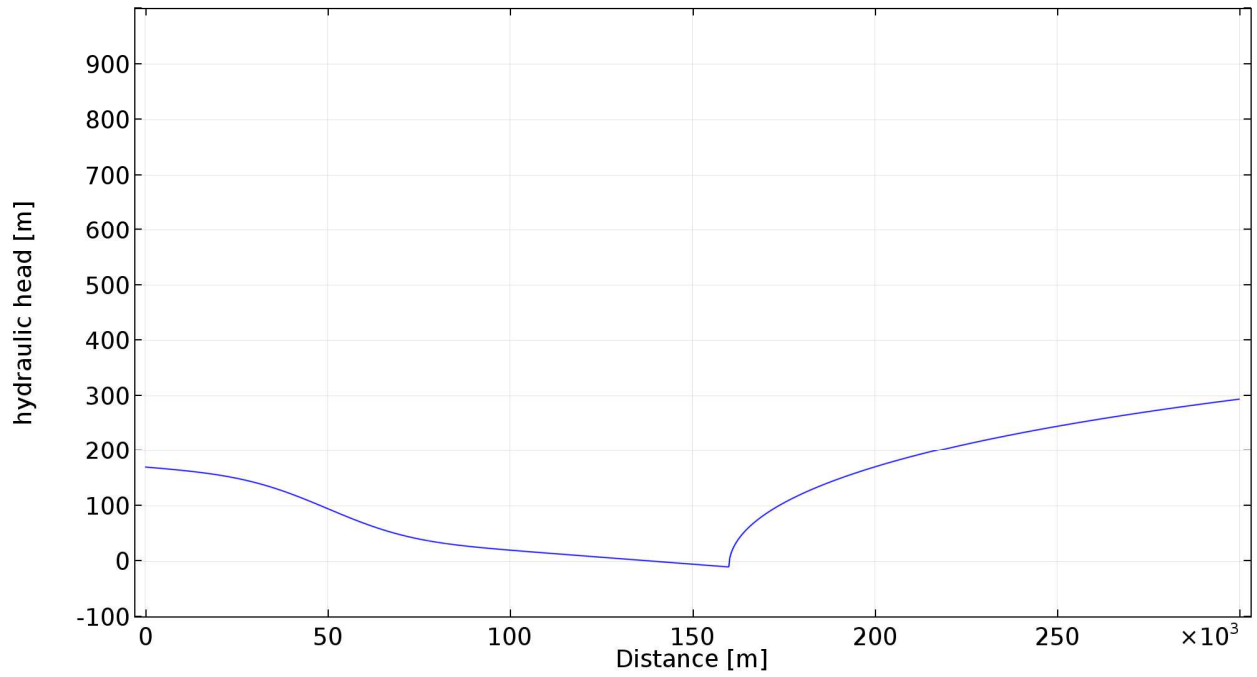
Ice advance at 460.75 ka BP



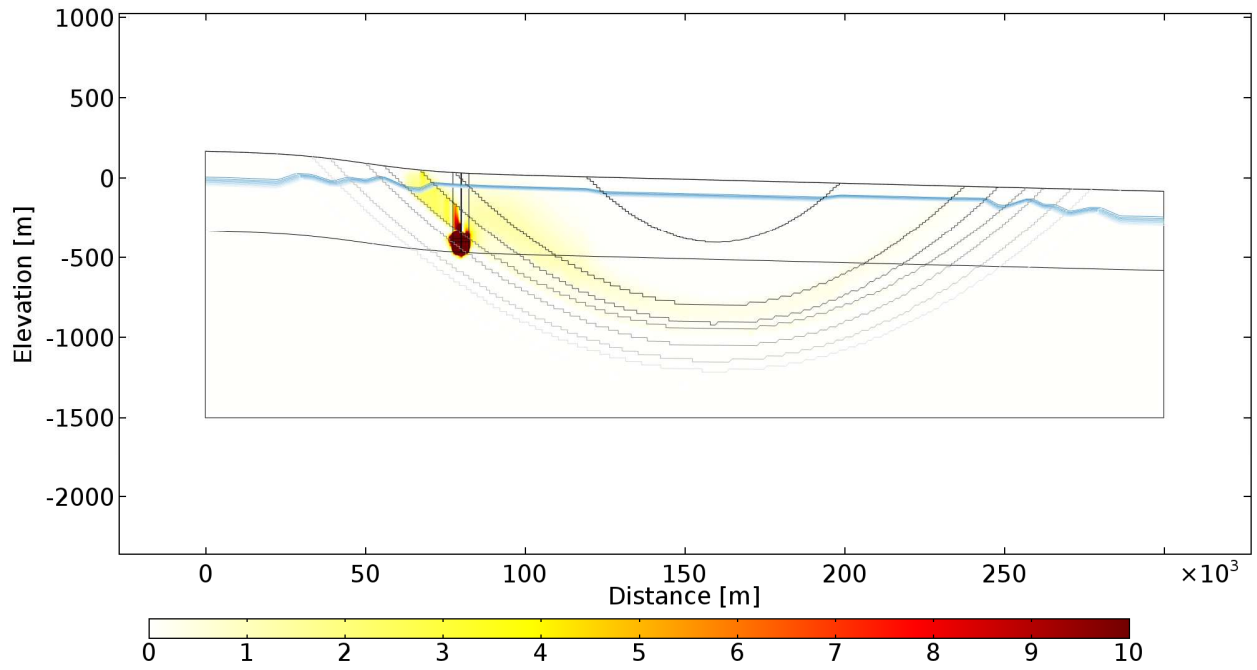
Ice max 457.25at ka BP



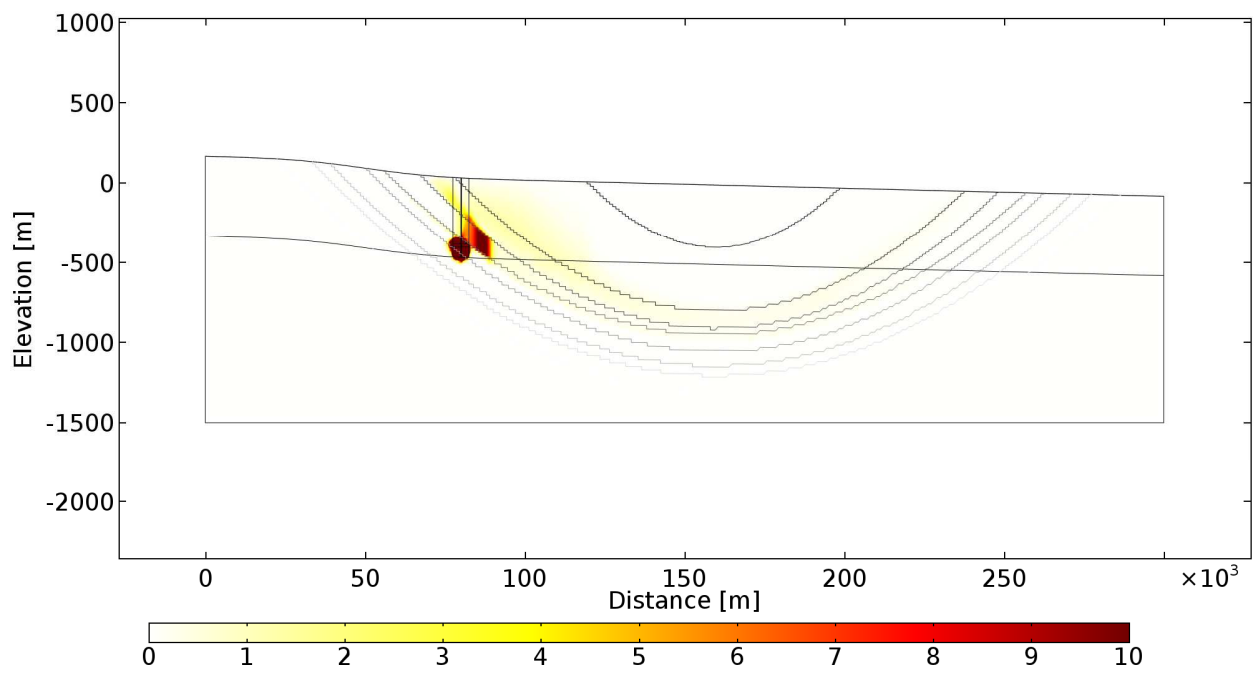
Ice retreat



Post ice with permafrost 430 ka BP



Post ice no permafrost at 420 ka BP



Present day

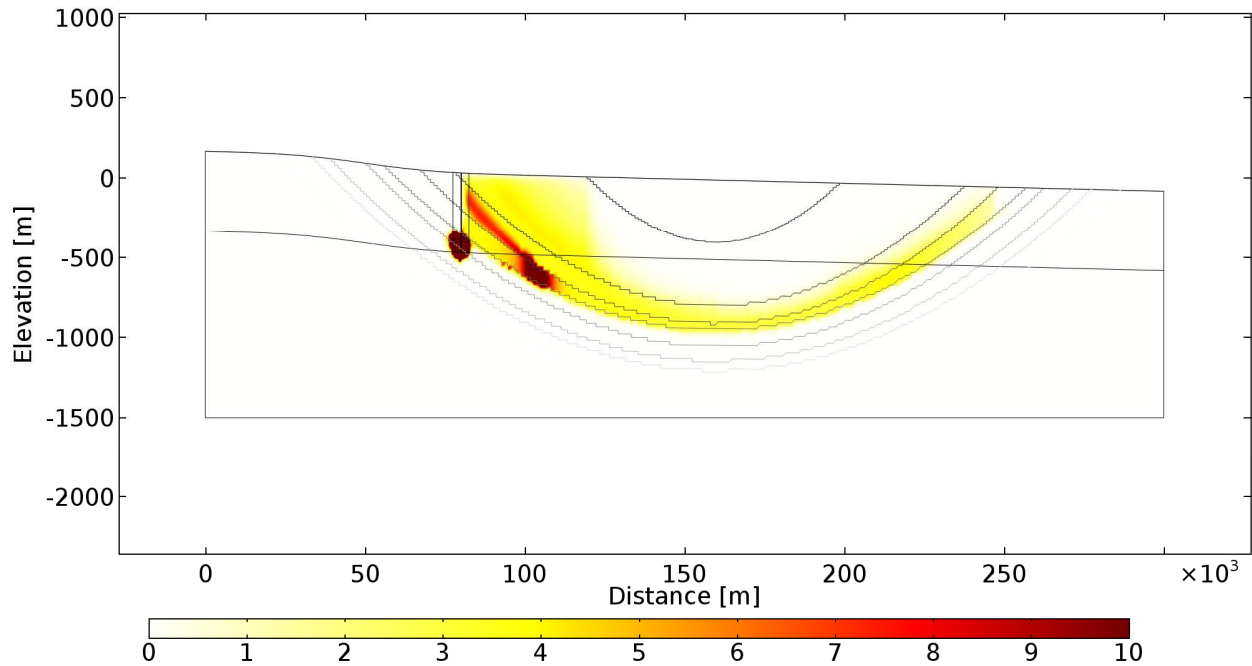


Figure 59. Model results including a tracer for Case 2 including ice sheet loading for pre-glaciation, during ice advance, during ice retreat, post glaciation and present day.

The tracer disperses in the lower Jurassic until it reaches the boundary of the aquifer approximately 130 ka after its release (Figure 59). Once the tracer reaches the aquifer, it is transported by advection until it discharges to the surface, approximately 250 km from the boundary. The tracer also spreads horizontally as it moves upwards, mainly through dispersion, and reaches the surface above the repository. During permafrost coverage, the tracer cannot leave the system and concentrates in the aquifer above the source. After the permafrost event, this pulse travels through the aquifer towards the surface at around 250 km of the model domain. During glacial advance, the lateral flow direction is reversed and the tracer spreads upwards from the repository. After the glaciation, the flow direction reverses to its original direction, and the tracer spreads along the aquifer.

In the model, the tracer only leaves the model through advection, as suggested by *Goode* (1996). This might be a limitation to this approach, as in low permeable layers transport is dominated by hydrodynamic dispersion. This means, that the boundary might be representative for the aquifers, but less so for the low permeable layers and that the tracer might accumulate in the model as a result of it not being able to leave the system. Further modelling would be necessary to address this limitation.

Appendix 5 COMSOL Multiphysics benchmarking with InterFrost test cases

To date, numerical codes can only be compared against analytic solutions for thermic equations including phase change such as the Lunardini analytical solution.

However for coupled Thermo-Hydraulic systems, the only means for validation is the comparison of different codes with each other or the comparison of a code with a controlled laboratory test case. InterFrost is a model inter-comparison project for Thermo Hydro (TH) coupled heat and water transfers in permafrost regions and is in the process of comparing 14 codes from laboratories across Europe and America. The British Geological Survey are contributing to this benchmarking exercise using COMSOL Multiphysics.

Comparison of analytical test cases and InterFrost benchmarks are presented below. More information about the InterFrost project can be found here: https://wiki.lscce.ipsl.fr/interfrost/doku.php?id=test_cases:all.

COMPARISON TO ANALYTICAL SOLUTIONS

Heat conduction – Comparison to Lunardini analytical solution

The comparison of a numerical model, including phase change, with the Lunardini analytical solution has first been proposed by *McKenzie et al.* (2007) and is part of the InterFrost model comparison as case T1.

The domain is divided into a fully frozen zone ($T1$), a mushy zone ($T2$), and a thawed zone ($T3$) (Figure 60).

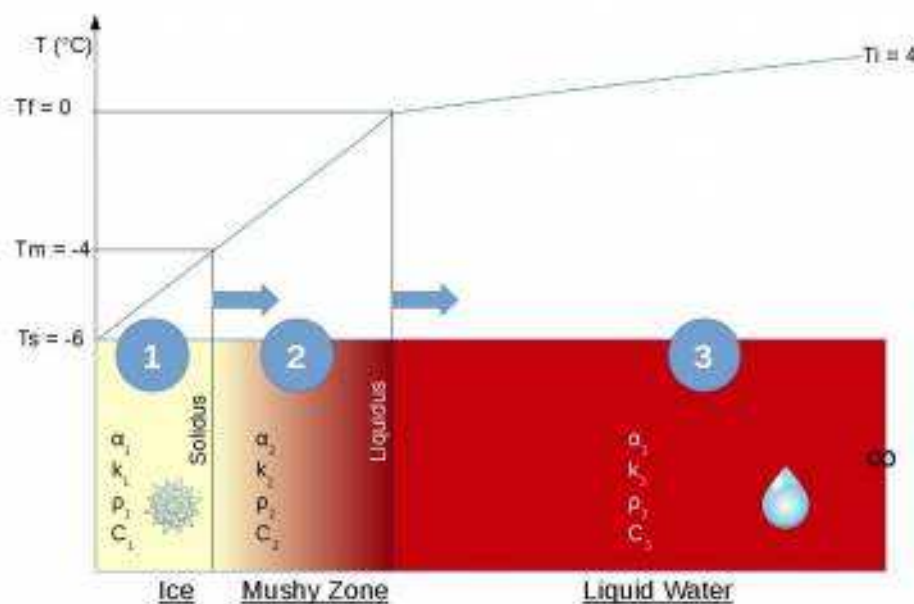


Figure 60. Three-zone model with an ice, mushy zone and liquid water zone.

The analytical solution models the movement of a freezing zone from an initially unfrozen medium that undergoes a step change in temperature from T_0 to T_s at the left boundary over time. Initially, the temperature of the entire model domain is set to $T_0 = 4^\circ\text{C}$ and the temperature at the left boundary at $x=0$ is cooled to $T_s=-6^\circ\text{C}$.

The Lunardini solution for the temperatures $T1-T3$ in the three zones over x is given by:

$$T1 = (T_m - T_s) \frac{\text{erf}(x/2\sqrt{\alpha_1 t})}{\text{erf}(\psi)} + T_s \quad (22)$$

$$T2 = (T_f - T_m) \frac{\text{erf}(x/2\sqrt{\alpha_4 t - \text{erf}(\gamma)})}{\text{erf}(\gamma) - \text{erf}(\psi \sqrt{\frac{\alpha_1}{\alpha_2}})} + T_f \quad (23)$$

$$T3 = (T_0 - T_f) \frac{-\text{erfc}(x/2\sqrt{\alpha_3 t})}{\text{erfc}(\gamma \sqrt{\frac{\alpha_4}{\alpha_3}})} + T_0 \quad (24)$$

Where T_0 is the temperature of the initial conditions, T_m the temperature of the solidus, T_f , the temperature of the liquidus, and T_s is the temperature at the boundary. α [m^2/s] is the thermal diffusivity and defined as κ/C for zone 1 and 3 respectively, where κ [J/s m K] is the bulk thermal conductivity and C [$\text{J/m}^3\text{K}$] the volumetric bulk heat capacity for the frozen and unfrozen zone. For the mushy zone, the thermal diffusivity α_2 is regarded as constant and defined as:

$$\alpha_2 = \frac{\kappa_2}{C_2 + \frac{\gamma_d L_f \Delta\xi}{F_f - T_m}} \quad (25)$$

Where $\gamma_d = (1-\varepsilon)\rho_s$ [kg/m^3] is the dry unit density of soil solids, and $\Delta\xi = \xi_0 - \xi_f$, where ξ_0 and ξ_f are the ratio of unfrozen water to solid mass for the fully thawed and frozen conditions.

$T1$ is valid for a time t in the region from $0 \leq x \leq X1(t)$ where

$$X1(t) = 2\psi\sqrt{t\alpha_1} \quad (26)$$

$T2$ is valid from $X1(t) \leq x \leq X(t)$ where

$$x(T) = 2\gamma\sqrt{t\alpha_2} \quad (27)$$

And $T3$ is valid for $x \geq X(t)$.

The parameters γ and ψ are found iteratively, but for this comparison they are taken from the INTERFROST project (https://wiki.lsce.ipsl.fr/interfrost/doku.php?id=test_cases:one).

The Lunardini analytical solution uses a uniform heat capacity for zones $T1-T3$, and thus the model in COMSOL is adjusted to that. In addition, the thermal conductivity in the mushy zone is constant in the analytical model and this has been adjusted in COMSOL.

Parameter values used for the analytic and numeric solution are represented in Table 14. The freezing interval for the numeric solution lies between T_f and T_m , in which the water content decreases from 1 to S_{res} .

Table 14: Parameter values used for the Lunardini analytical solution, after McKenzie et al. 2007 and INTERFROST.

| Parameter | Symbol | Value | Units |
|---|------------|---------------------|-------------------|
| Initial temperature | T_0 | 4 | °C |
| Temperature at surface | T_s | -6 | °C |
| Temperature of liquidus | T_f | 0 | °C |
| Temperature of solidus | T_m | -1 | °C |
| Thermal conductivity of frozen zone | κ_1 | 3.462696 | $W m^{-1} K^{-1}$ |
| Thermal conductivity of mushy zone | κ_2 | 2.939946 | $W m^{-1} K^{-1}$ |
| Thermal conductivity of unfrozen zone | κ_3 | 2.417196 | $W m^{-1} K^{-1}$ |
| Volumetric heat capacity of frozen zone | C_1 | 690030 | $J m^{-3} K$ |
| Volumetric heat capacity of mushy zone | C_2 | 690030 | $J m^{-3} K$ |
| Volumetric heat capacity of unfrozen zone | C_3 | 690030 | $J m^{-3} K$ |
| kg water / kg solid frozen condition | ξ_f | 0.0782 | - |
| kg water /kg solid unfrozen condition | ξ_0 | 0.2 | - |
| Volumetric latent heat of fusion | L_f | $3.3472 \cdot 10^8$ | $J m^{-3}$ |
| Dry unit density of solid | γ_d | 1680 | $kg m^{-3}$ |
| parameter | γ | 2.062 | - |
| parameter | ψ | 0.1375 | - |
| Average matrix porosity | n | 0.336 | - |
| Residual saturation | S_{res} | 0.391 | - |

The temperatures are driven at the sides of the model, T_s at the left side and T_0 at the right side. The top and bottom boundary of the model are no-flow boundaries. The temperature distribution at $t=0$ and $t=168$ h are shown in Figure 61. Figure 62 presents the numeric and the analytic solution for 1, 2, and 3 days of simulation time. The temperature difference between both solutions is presented in Figure 63. The maximum difference of the two solutions lies between 0.0066685 °C and -0.0021883 °C. The mean error is $3.5 e-6$ °C.

The error of the numeric solution is strongly dependent on the selection of the mesh and the absolute tolerance. A mapped mesh with a maximum element size of 0.01m has been used here. As there is a steep temperature gradient in the forcing temperature the finer meshing results in a more accurate solution. In addition, the relative tolerance is set to $1e-7$ and the absolute tolerance to $1e-6$. Using an absolute tolerance of 1 order of magnitude higher increases the temperature difference in this case by nearly an order of magnitude, but also increases simulation time.

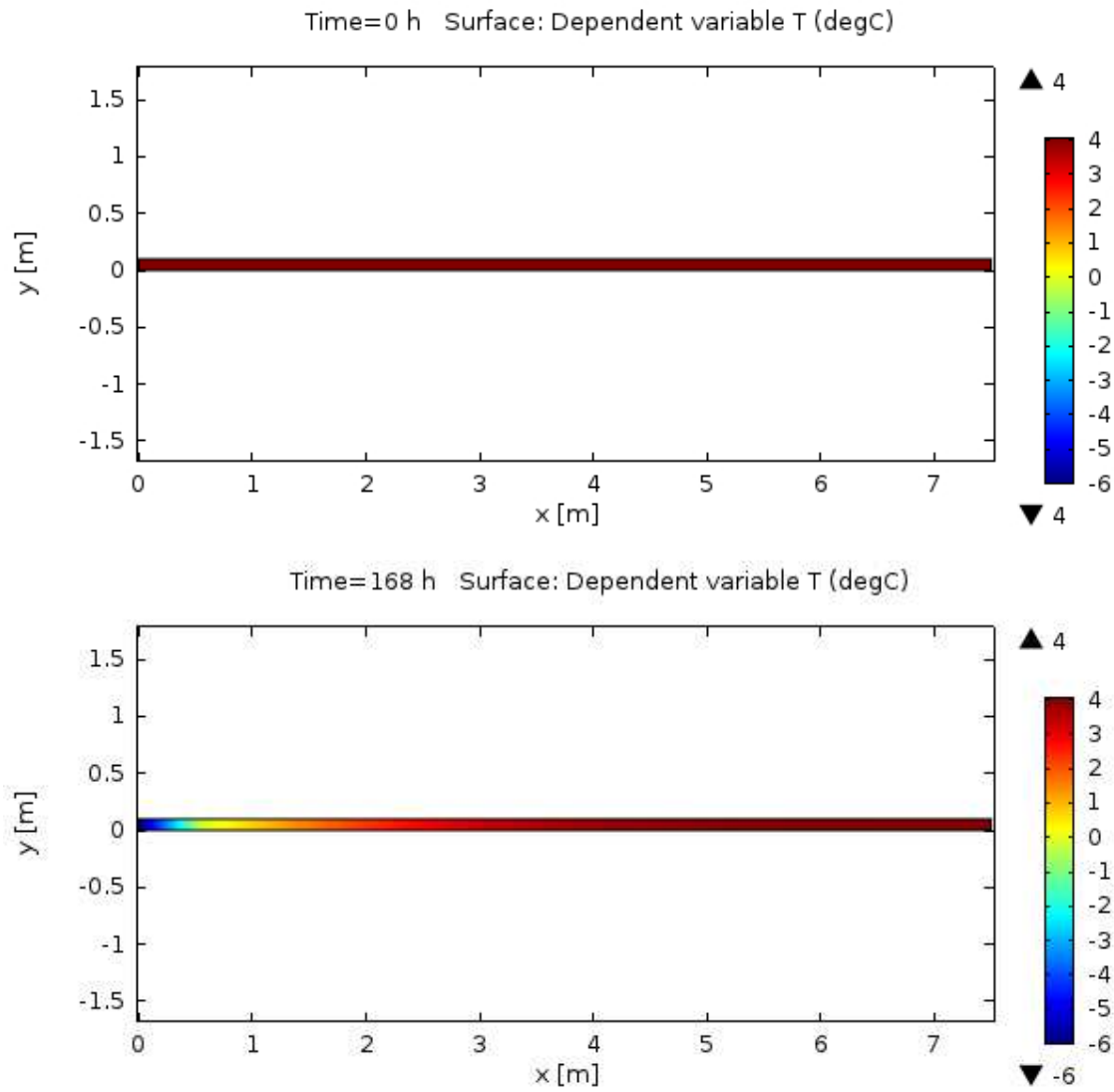


Figure 61. Temperatures at t=0 and t=168 h for the one dimensional three phase heat flow model after Lunardini.

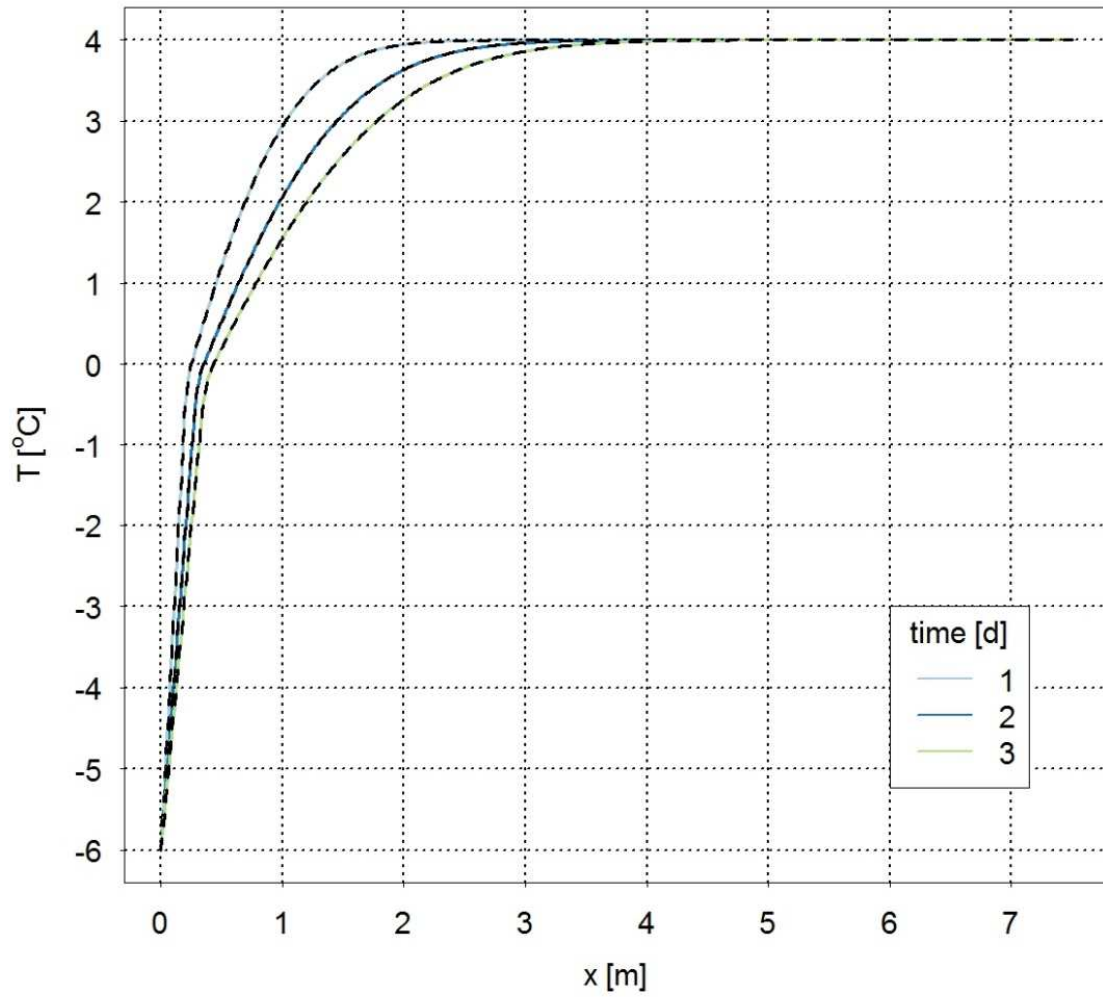


Figure 62. Comparison of the modelled temperatures of the analytical Lunardini solution and the numerical solution from Comsol for different time steps. The coloured lines are the numeric solution and the black dotted line the analytical solution.

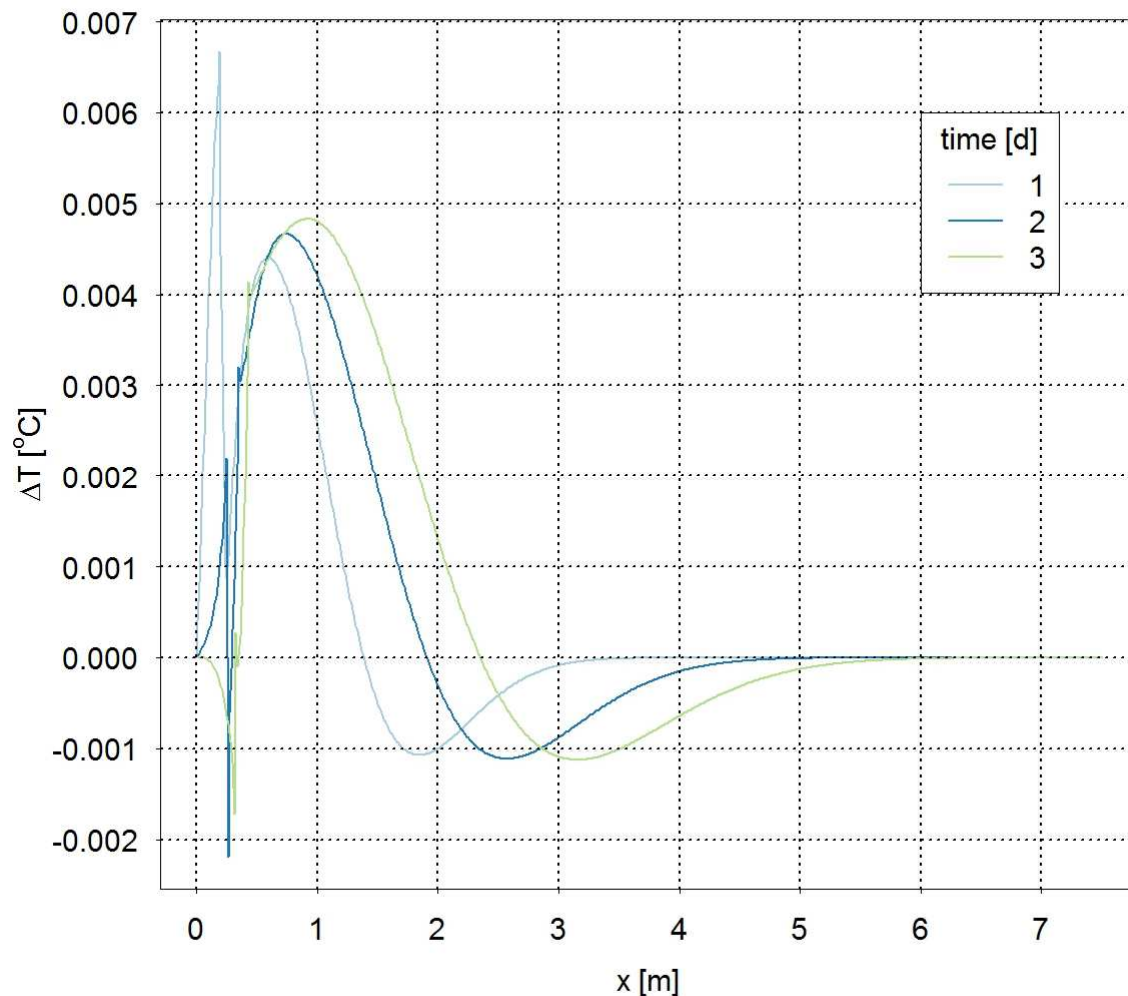


Figure 63. Temperature difference between numerical and analytical Lunardini solution.

1D soil thaw with conduction and advection by Kurylyk and InterFrost case TH1

Here, in addition to heat conduction with phase change, heat advection via constant pore water velocity is considered. The analytical solution is obtained from *Kurylyk et al. (2014)* based on a reassessment of solutions by *Lunardini (1998)*. This analytical solution assumes that there is constant velocity independent of ice saturation, which is not physically realistic, but can be used for benchmarking purposes. As *Kurylyk et al. (2014)* states, “lack of fidelity to physical processes does not limit ability to serve as a benchmark”.

The setup uses an initially frozen 1 D column with temperature set to very close to freezing ($T = -0.001^\circ\text{C}$) and the surface temperature increases to 1°C at $t = 0$ s (Figure 64). The system thaws from the top. The initially uniform temperatures of near 0°C simplify the energy balance at the thawing front as there is no thermal gradient in the frozen medium. The water is advected through the entire medium, but the divergence of the advective flux is zero below the thawing front due to the uniform thermal conditions.

The benchmark suggests using two different velocities; $v_1 = 10$ m/a, and $v_2 = 100$ m/a.

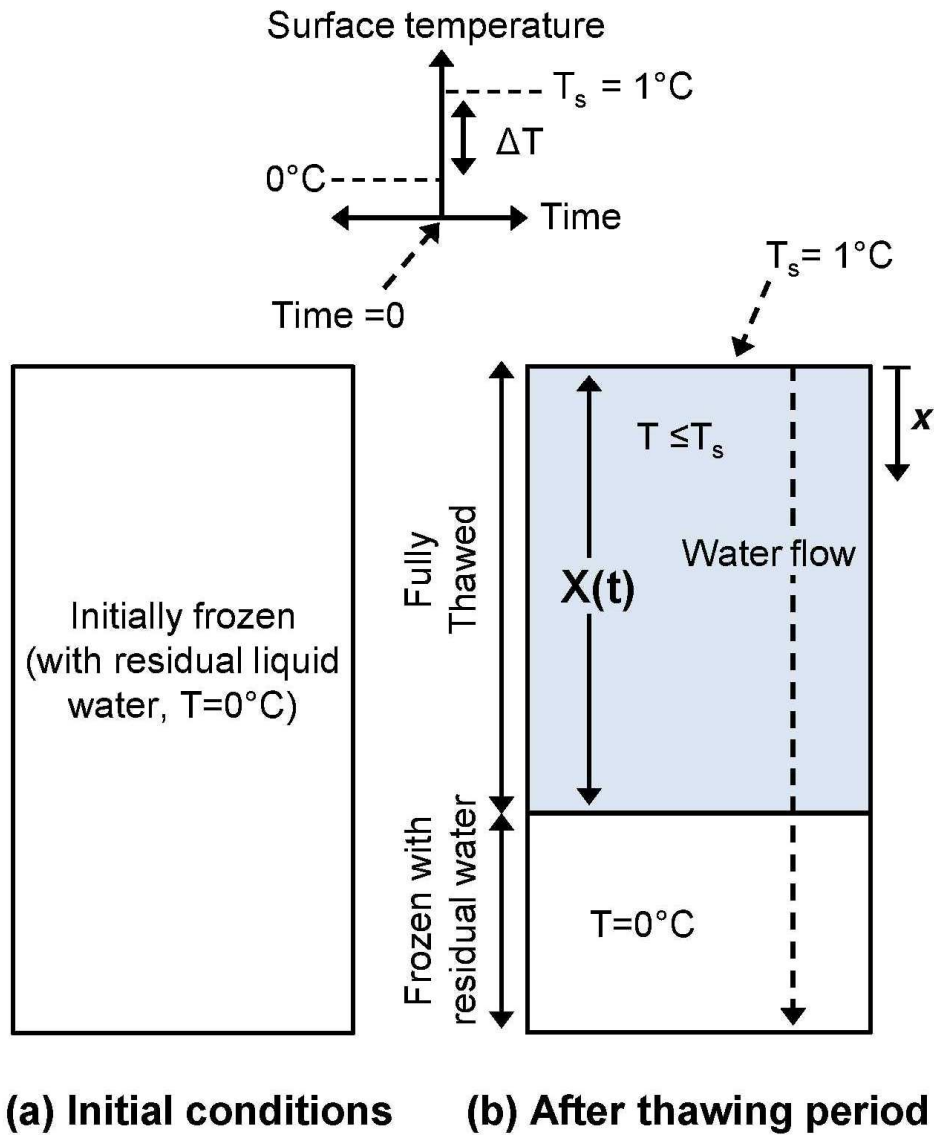


Figure 64. Model set up. After Kurylik et al. (2014).

These benchmarks are based on the following analytical solution:

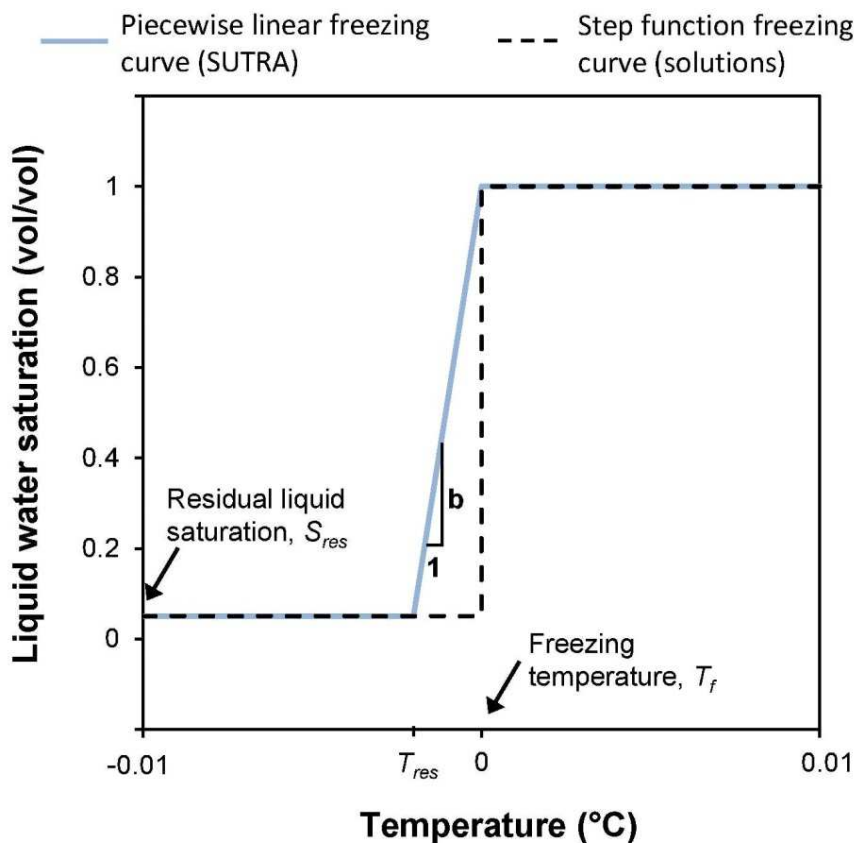
$$X + \frac{\alpha}{v_t} \left\{ \exp\left(-\frac{v_t X}{\alpha}\right) - 1 \right\} = v_t S_T t$$

where X is the depth to the thawing front, α is the thermal diffusivity, v_t is the thermal plume velocity due to advection, t is time, and S_T is the dimensionless Stefan number.

The parameter values from Kurylik et al. (2014) are used and listed in Table 15.

Table 15. Parameters for TH1

| Parameter | Symbol | Value | Units |
|---|--------------|------------------------|--|
| Porosity | ϵ | 0.50 | - |
| Relative permeability | k_{rel} | off | - |
| Darcy velocity (downwards) | v | 10, and 100 | m yr^{-1} |
| Gravity | g | 0 | m s^{-2} |
| Water saturation (total) | S_w | 1 | - |
| Sat. available for freezing ($S_w - S_{res}$) | S_{wf} | 1 (for solutions) | - |
| Thermal conductivity of thawed zone | λ | 1.839 | $\text{W m}^{-1} \text{ }^\circ\text{C}^{-1}$ |
| Heat capacity of thawed zone | $c\rho$ | 3.201×10^6 | $\text{J m}^{-3} \text{ }^\circ\text{C}^{-1}$ |
| Thermal diffusivity of thawed zone | α | 5.743×10^{-7} | $\text{m}^2 \text{ s}^{-1}$ |
| Thermal diffusivity of frozen zone | α_f | 1.205×10^{-6} | $\text{m}^2 \text{ s}^{-1}$ |
| Thermal dispersivity | - | 0^b | m |
| Density of water | ρ_w | 1000 | kg m^{-3} |
| Specific heat of water | c_w | 4182 | $\text{J kg}^{-1} \text{ }^\circ\text{C}^{-1}$ |
| Heat capacity of water | $c_w \rho_w$ | 4.182×10^6 | $\text{J m}^{-3} \text{ }^\circ\text{C}^{-1}$ |
| Latent heat of fusion for water | L_f | 334,000 | J kg^{-1} |
| Specified temperature | T_s | 1 | $^\circ\text{C}$ |
| Initial temperature | T_i | 0 | $^\circ\text{C}$ |
| Freezing temperature (solutions) | T_f | 0 | $^\circ\text{C}$ |
| Residual freezing temp. (SUTRA) | T_{res} | -0.0005 | $^\circ\text{C}$ |
| Residual liquid saturation | S_{res} | 0.0001 | - |
| Slope of freezing function | b | 1999.8 | $^\circ\text{C}^{-1}$ |

**Figure 65. Freezing function for TH1. From Kurylik et al. (2014).**

A piecewise linear freezing curve (Figure 65) is used in the benchmark, and is characterised by the residual liquid saturation S_{res} , the freezing temperature T_f , and the residual freezing temperature T_{res} .

The comparison between COMSOL and the analytical solution is shown in Figure 66 and Figure 67. The maximum difference between the two solutions is within 0.004°C and -0.002°C .

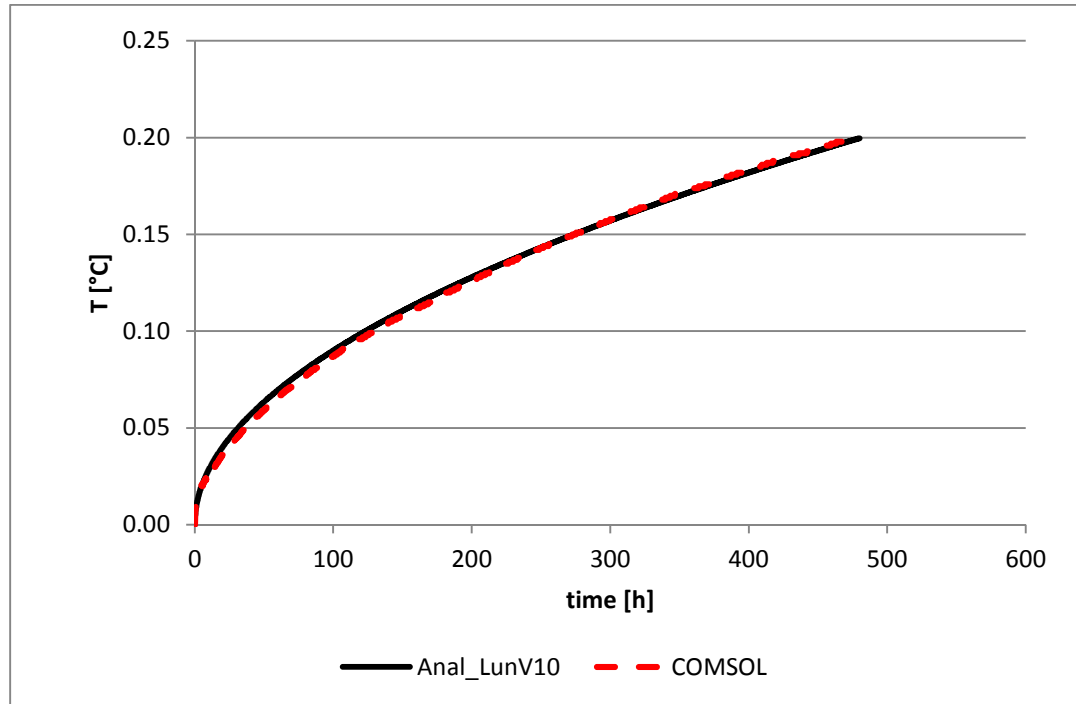


Figure 66. Comparison of numerical and analytical solutions for $v = 10$ m/a.

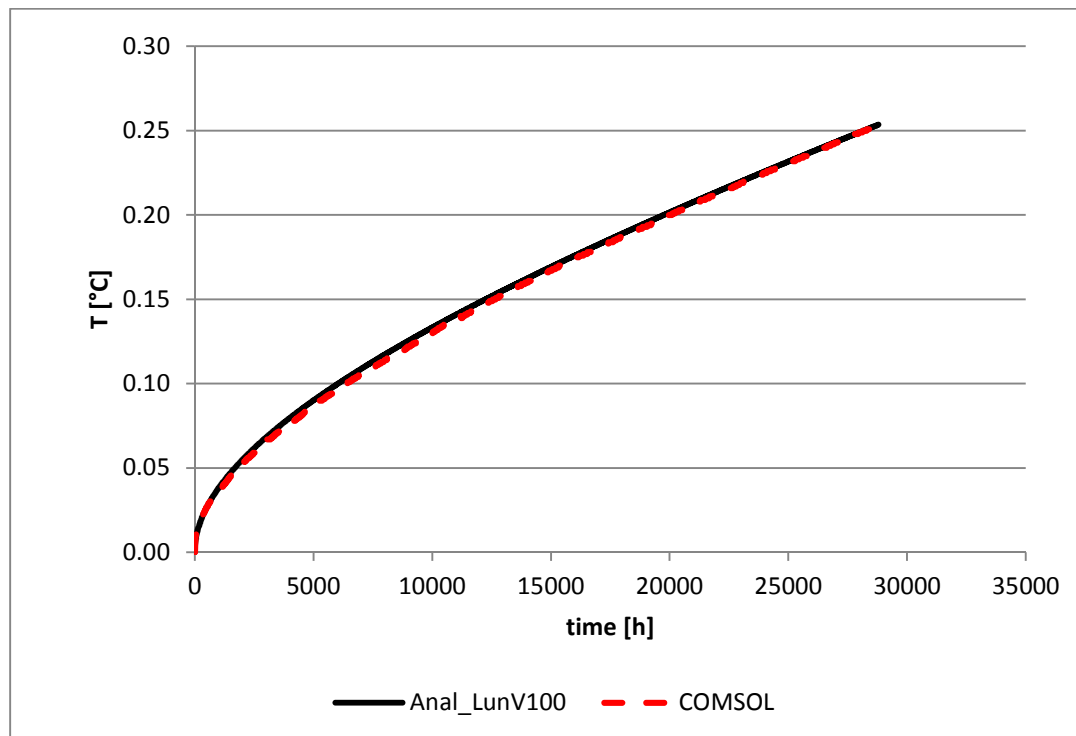


Figure 67. Comparison of numerical and analytical solutions for $v = 100$ m/a.

TH2 Frozen Inclusion in a coupled system

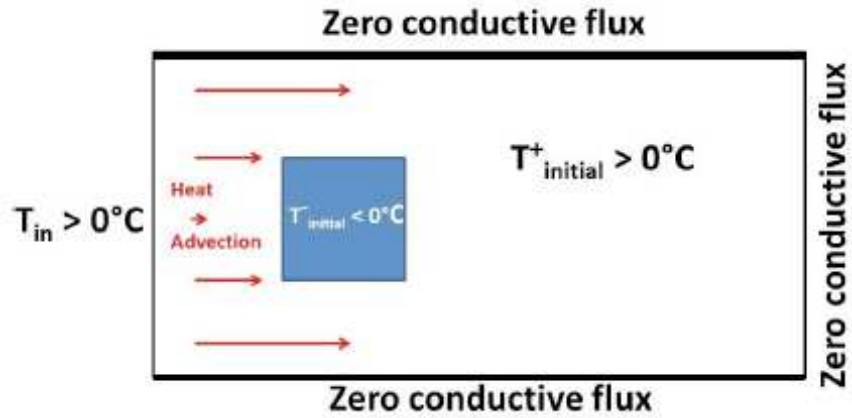


Figure 68. Geometrical setup for TH2 Test Case.

TH2 uses a fully coupled model of heat and fluid flow to model the temperature distribution of the domain over time, the evolution of the total heat flux exiting the system and the evolution of the total liquid water volume over time. The parameters used in this model are listed in Table 16.

Table 16. Model parameters for TH2.

| Parameter | Symbol | Value | Units |
|---|----------------|---|----------------------------------|
| Porosity | ϵ | 0.37 | - |
| Compressibility | β | 10^{-8} | Pa^{-1} |
| Acceleration of gravity | g | 9.81 | m s^{-2} |
| Thermal conductivity of water | λ_w | 0.6 | $\text{W m}^{-1} \text{K}^{-1}$ |
| Thermal conductivity of ice | λ_i | 2.14 | $\text{W m}^{-1} \text{K}^{-1}$ |
| Thermal conductivity of solid matrix | λ_s | 9 | $\text{W m}^{-1} \text{K}^{-1}$ |
| Equivalent thermal conductivity | λ_{eq} | $\epsilon(S_w \lambda_w + (I - S_w) \lambda_i) + (I - \epsilon) \lambda_s$ | $\text{W m}^{-1} \text{K}^{-1}$ |
| Specific heat of water | C_w | 4182 | $\text{J kg}^{-1} \text{K}^{-1}$ |
| Specific heat of ice | C_i | 2060 | $\text{J kg}^{-1} \text{K}^{-1}$ |
| Specific heat of solid matrix | C_s | 835 | $\text{J kg}^{-1} \text{K}^{-1}$ |
| Density of water | ρ_w | 1000 | kg m^{-3} |
| Density of ice | ρ_i | 920 | kg m^{-3} |
| Density of solid matrix | ρ_s | 2650 | kg m^{-3} |
| Volumetric heat capacity of water | $C_w \rho_w$ | 4.182×10^6 | $\text{J m}^{-3} \text{K}^{-1}$ |
| Equivalent volumetric heat capacity | $C\rho$ | $\epsilon(S_w \rho_w C_w + (I - S_w) \rho_i C_i) + (I - \epsilon) \rho_s C_s$ | $\text{J m}^{-3} \text{K}^{-1}$ |
| Latent heat of fusion for water | L_f | 334,000 | J kg^{-1} |
| Water dynamic viscosity | μ | 1.793×10^{-3} | $\text{kg m}^{-1} \text{s}^{-1}$ |
| Water saturation for $T \geq 273.15$ | $S_w(T)$ | 1 | - |
| Water saturation for $T < 273.15$ | $S_w(T)$ | $(1 - S_{wres})e^{-((T - 273.150)/W)^2} + S_{wres}$ | - |
| Residual liquid saturation | S_{wres} | 0.05 | - |
| Parameter in $S_w(T)$ | W | 0.5 | K |
| Hydraulic conductivity | K_w | $k_r k_{int} \rho_w g / \mu$ | m s^{-1} |
| Intrinsic permeability | k_{int} | 1.3×10^{-10} | m^2 |
| Relative permeability for $k_r(S_w) > 10^{-6}$ | $k_r(S_w)$ | $10^{-\Omega e(1 - S_w)}$ | - |
| Relative permeability for $k_r(S_w) \leq 10^{-6}$ | $k_r(S_w)$ | 10^{-6} | - |
| Impedance factor | Ω | 50 | - |

The initial temperature distribution of the model domain is characterised by a uniform temperature of 5 °C and of -5 °C in the frozen inclusion (Figure 68). The flow field is characterised with a hydraulic head gradient from the left to the right side of the model domain. For heat flow, the temperature is specified at the left boundary to 5 °C and a zero conductive flux (heat advection only) on the right side.

Figure 69 presents a comparison of the temperature field for the conduction only scenario (left) and conduction and advection using a gradient $dh/dx=0.15$ for different time steps. Heat advection for this test case results in faster thaw of the frozen inclusion and in advection of the cold temperature towards the right hand boundary.

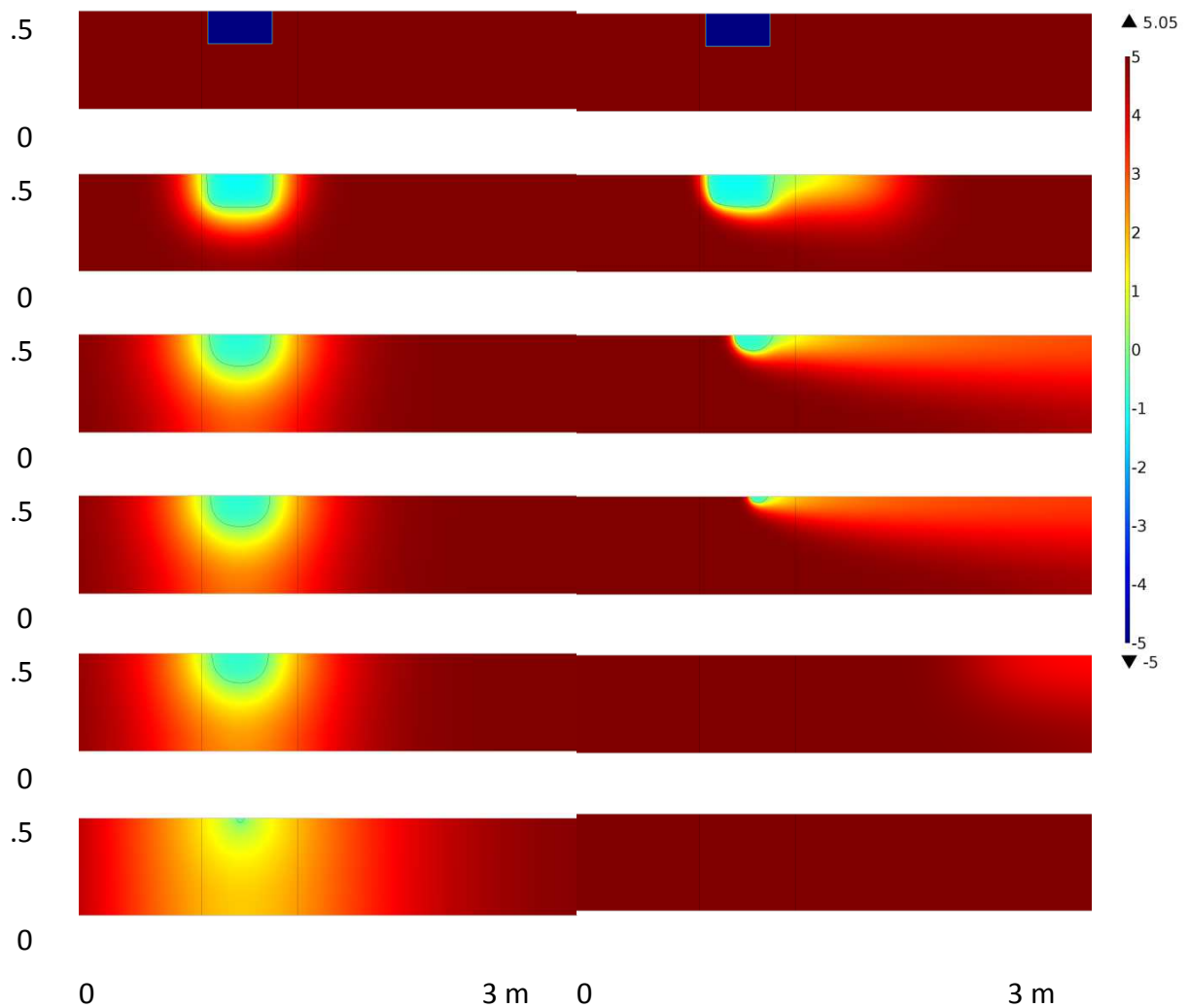


Figure 69. Comparison of conduction only (left) and advection scenario (right) with $dh/dx=0.15$ for test case TH2. Time steps presented are 0, 90, 420, 525, 675, 2040 min.

Figure 70 presents the minimum temperature over time for different hydraulic gradients. The gradient of dh/dx 0.03 is then compared to other codes as part of the InterFrost project (Figure 71) (Grenier *et al.*, 2016). The temperature curve from COMSOL lays within the spread of the other benchmarked curves, and is thus a suitable code to model coupled heat and fluid flow.

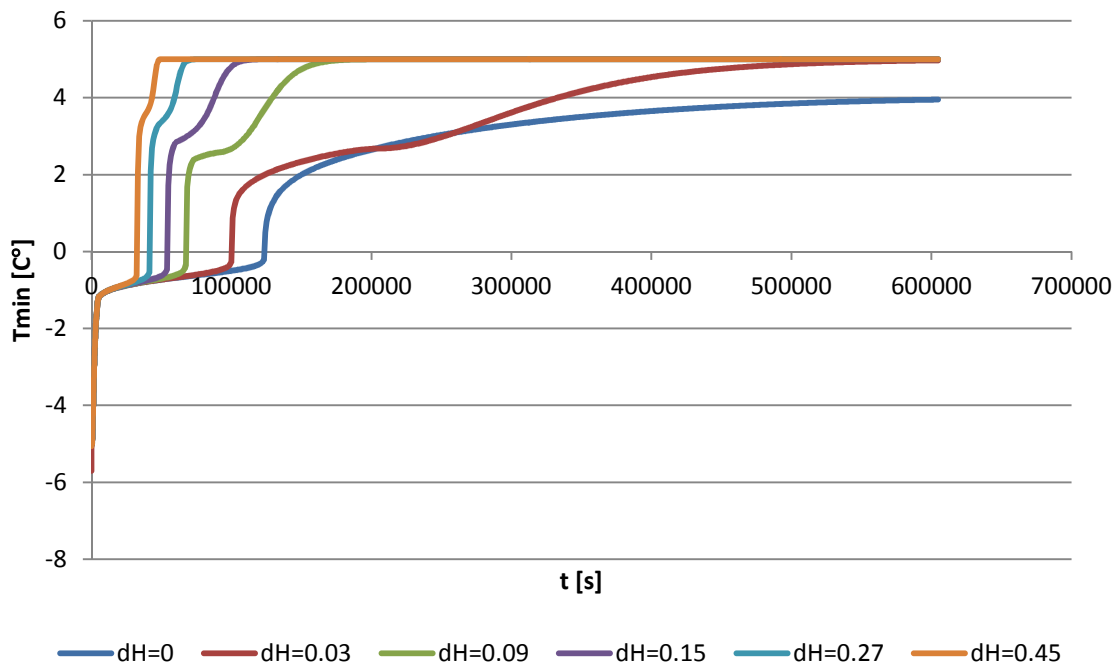


Figure 70. Minimum temperature over time for different dH scenarios.

TH2: Temperature minimum, Gradient 3 %

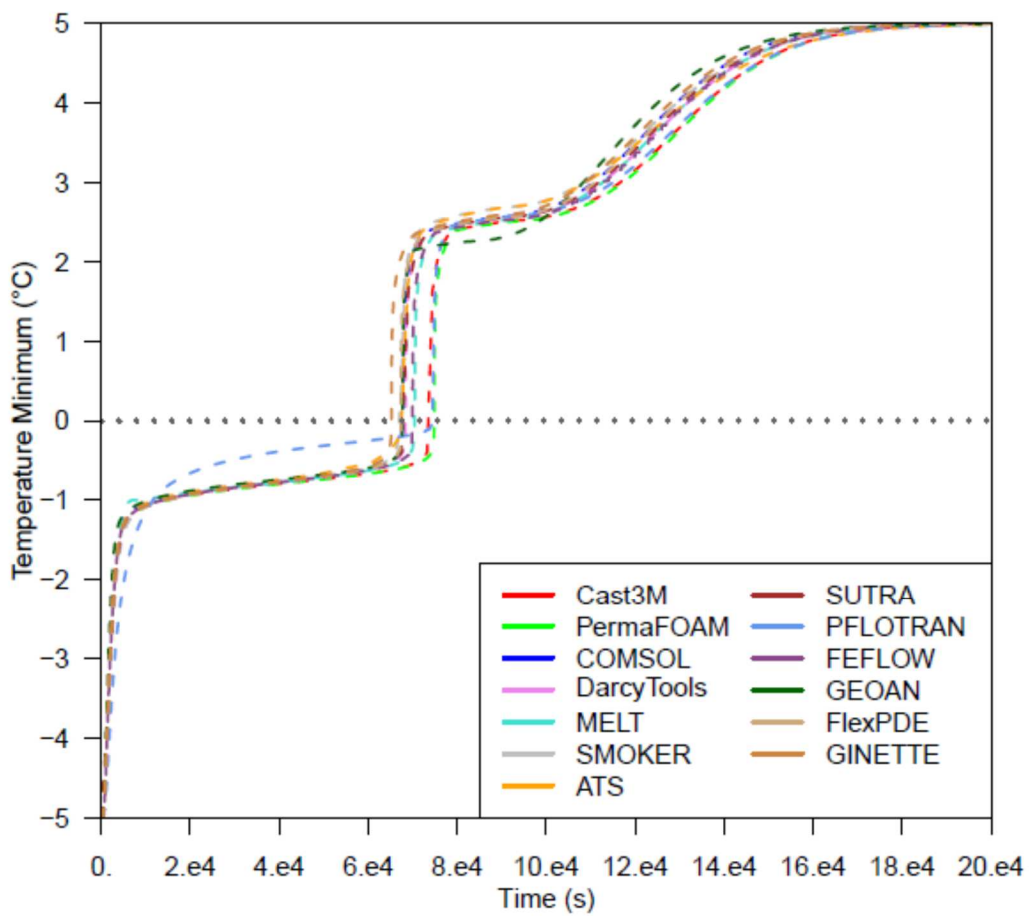


Figure 71. Comparison of COMSOL to other TH codes (Grenier et al., 2016).

References

- ANNAN, J. D., and J. C. HARGREAVES (2013), A new global reconstruction of temperature changes at the Last Glacial Maximum, *Climate of the Past*, 9(1), 367-376, doi:10.5194/cp-9-367-2013.
- AZMATCH, T. F., D. C. SEGO, L. U. ARENSON, and K. W. BIGGAR (2012), Using soil freezing characteristic curve to estimate the hydraulic conductivity function of partially frozen soils, *Cold Regions Science and Technology*, 83-84, 103-109, doi:10.1016/j.coldregions.2012.07.002.
- BATEMAN, M. D., D. J. A. EVANS, P. C. BUCKLAND, E. R. CONNELL, R. J. FRIEND, D. HARTMANN, H. MOXON, W. A. FAIRBURN, E. PANAGIOTAKOPULU, and R. A. ASHURST (2015), Last glacial dynamics of the Vale of York and North Sea lobes of the British and Irish Ice Sheet, *Proceedings of the Geologists' Association*, 126(6), 712-730, doi:<http://dx.doi.org/10.1016/j.pgeola.2015.09.005>.
- BENSE, V. F., and M. A. PERSON (2008), Transient hydrodynamics within intercratonic sedimentary basins during glacial cycles, *Journal of Geophysical Research-Earth Surface*, 113(F4), doi:10.1029/2007jf000969.
- BENSE, V. F., G. FERGUSON, and H. KOOI (2009), Evolution of shallow groundwater flow systems in areas of degrading permafrost, *Geophysical Research Letters*, 36, doi:10.1029/2009gl013925.
- BENSE, V. F., H. KOOI, G. FERGUSON, and T. READ (2012), Permafrost degradation as a control on hydrogeological regime shifts in a warming climate, *Journal of Geophysical Research-Earth Surface*, 117, doi:10.1029/2011jf002143.
- BINTANJA, R., R.S.W. VAN DE WAL, and J. OERLEMANS (2005), Modelled atmospheric temperatures and global sea levels over the past million years, *Nature Climate Change*, 437, 125-128, doi:10.1038/nature03975
- BOULTON, G. S., and M. BROADGATE (1993), A glacial model for TIME4 applicable to the Sellafeld and Dounreay areas. TIME4: Time-dependent effects on deep disposal sites, 12677-017-401.
- BOULTON, G. S., T. SLOT, K. BLESSING, P. GLASBERGEN, T. LEIJNSE, and K. VANGIJSEL (1993), Deep Circulation of Groundwater in Overpressured Subglacial Aquifers and Its Geological Consequences, *Quaternary Science Reviews*, 12(9), 739-745, doi:10.1016/0277-3791(93)90014-D.
- BOULTON, G. S., and M. HAGDORN (2006), Glaciology of the British Isles Ice Sheet during the last glacial cycle: form, flow, streams and lobes, *Quaternary Science Reviews*, 25(23-24), 3359-3390, doi:DOI 10.1016/j.quascirev.2006.10.013.
- BURT, T. P., and P. J. WILLIAMS (1976), Hydraulic conductivity in frozen soils, *Earth Surface Processes and Landforms*, 1(4), 349-360.
- BUSBY, J. P., A. KINGDON, and J. WILLIAMS (2011), The measured shallow temperature field in Britain, *Quarterly Journal of Engineering Geology and Hydrogeology*, 44, 373-387, doi:10.1144/1470-9236/10-049.
- BUSBY, J. P., S. KENDER, J. P. WILLIAMSON, and J. R. LEE (2014), Regional modelling of the potential for permafrost development in Great Britain, *British Geological Survey, CR/14/023*, 62 pp, Keyworth.
- BUSBY, J. P., J. R. LEE, S. KENDER, J. P. WILLIAMSON, and S. NORRIS (2015a), Modelling the potential for permafrost development on a radioactive waste geological disposal facility in Great Britain, *Proceedings of the Geologists' Association*, 126(6), 664-674.
- BUSBY, J. P., J. R. LEE, S. KENDER, P. WILLIAMSON, and S. NORRIS (2015b), Regional modelling of permafrost thickness over the past 130 ka: implications for permafrost development in Great Britain, *Boreas*, 45, 46-60, doi:10.1111/bor.12136.
- CHAPOY, A., B. TOHIDI, J. SMELLIE, and I. PUIGDOMENECH (2011), The potential for methane hydrate formation in deep repositories of spent nuclear fuel in Granitic rocks, paper presented at Proceedings of the 7th International Conference on Gas Hydrates, Edinburgh, Scotland, United Kingdom.
- CHIVERRELL, R. C., and G. S. P. THOMAS (2010), Extent and timing of the Last Glacial Maximum (LGM) in Britain and Ireland: a review, *Journal of Quaternary Science*, 25(4), 535-549, doi:10.1002/Jqs.1404.
- CLARK, C. D., A. L. C. HUGHES, S. L. GREENWOOD, C. JORDAN, and H. P. SEJRUP (2012), Pattern and timing of retreat of the last British-Ice Sheet, *Quaternary Science Reviews*, 44, 112-146.
- COMSOL (2016), COMSOL Multiphysics.
- EYLES, N., C. H. EYLES, and A. M. MCCABE (1989), Sedimentation in an ice-contact subaqueous setting: The mid-Pleistocene 'North Sea Drifts' of Norfolk, U.K., *Quaternary Science Reviews*, 8(1), 57-74, doi:10.1016/0277-3791(89)90021-8.
- FREDERICK, J. M., and B. A. BUFFETT (2014), Taliks in relict submarine permafrost and methane hydrate deposits: Pathways for gas escape under present and future conditions, *Journal of Geophysical Research: Earth Surface*, 119(2), 106-122, doi:10.1002/2013jf002987.
- FRENCH, H. M. (2007), *The Periglacial Environment*, Wiley-Blackwell.
- GOODE, D. J. (1996), Direct simulation of groundwater age, *Water Resources Research*, 32(2), 289-296, doi:Doi 10.1029/95wr03401.
- GRENIER, C., D. RÉGNIER, E. MOUCHE, H. BENABDERRAHMANE, F. COSTARD, and P. DAVY (2013), Impact of permafrost development on groundwater flow patterns: A numerical study considering freezing cycles on a two-dimensional vertical cut through a generic river-plain system, *Hydrogeology Journal*, 21(1), 257-270, doi:10.1007/s10040-012-0909-4.
- 2016GRENIER, C., N. ROUX, H. ANBERGEN, V. BENSE, E. COON, N. COLLIER, F. COSTARD, M. FERRY, A. FRAMPTON, J. FREDERICK, H. HOLMEN, A. JOST, S. KOKH, B. KURYLYK, J. MCKENZIE, J. MOLSON, L. ORGOGOZO, R. PANNETIER, A. RIVIÈRE, W. RÜHAAK, J. SCHEIDEGGER, J.-O. SELROOS, R. THERRIEN, P. VIDSTRAND, and C. VOSS (2016), The InterFrost benchmark of Thermo-Hydraulic codes for cold regions hydrology – first inter-comparison phase results, in *ICOP*, edited, Potsdam.
- HANSSON, K., J. SIMUNEK, M. MIZOGUCHI, L. C. LUNDIN, and M. T. VAN GENUCHTEN (2004), Water flow and heat transport in frozen soil: Numerical solution and freeze-thaw applications, *Vadose Zone Journal*, 3(2), 693-704.
- HARTIKAINEN, J., R. KOUHIA, and T. WALLROTH (2010), Permafrost simulations at Forsmark using a numerical 2D thermo-hydro-chemical model, *SKB, TR-09-17*, 142 pp.
- HOLMÉN, J., H. BENABDERRAHMANE, A. BUORO, and J. BRULHET (2011), Modelling of permafrost freezing and melting and the impact of a climatic cycle on groundwater flow at the Meuse/Haute-Marne site, *Physics and Chemistry of the Earth, Parts A/B/C*, 36(17-18), 1531-1538, doi:10.1016/j.pce.2011.10.021.

- HUBBARD, A., T. BRADWELL, N. GOLLEDGE, A. HALL, H. PATTON, D. SUGDEN, R. COOPER, and M. STOKER (2009), Dynamic cycles, ice streams and their impact on the extent, chronology and deglaciation of the British–Irish ice sheet, *Quaternary Science Reviews*, 28(7-8), 758-776, doi:10.1016/j.quascirev.2008.12.026.
- IRESON, A., G. VAN DER KAMP, G. FERGUSON, and H. WHEATER (2013), Hydrogeological processes in seasonally frozen northern latitudes: understanding gaps and challenges, *Hydrogeology Journal*, 21, 53-66, doi:10.007/s10040-012-0916-5.
- IVERSON, N., and M. PERSON (2012), Glacier-bed geomorphic processes and hydrologic conditions relevant to nuclear waste disposal, *Geofluids*, 12(1), 38-57, doi:10.1111/j.1468-8123.2011.00355.x.
- KARRA, S., S. L. PAINTER, and P. C. LICHTNER (2014), Three-phase numerical model for subsurface hydrology in permafrost-affected regions, *The Cryosphere Discussions*, 8(1), 149-185, doi:10.5194/tcd-8-149-2014.
- KILPATRICK, A. (2016), Geochemical Aspects of Permafrost Development - Preliminary Modelling.
- KLEINBERG, R. L., and D. D. GRIFFIN (2005), NMR measurements of permafrost: unfrozen water assay, pore-scale distribution of ice, and hydraulic permeability of sediments, *Cold Regions Science and Technology*, 42(1), 63-77, doi:10.1016/j.coldregions.2004.12.002.
- KURYLIK, B. L., J. M. MCKENZIE, K. T. B. MACQUARRIE, and C. I. VOSS (2014), Analytical solutions for benchmarking cold regions subsurface water flow and energy transport models: One-dimensional soil thaw with conduction and advection, *Advances In Water Resources*, 70, 172-184.
- KURYLYK, B. L., and K. WATANABE (2013), The mathematical representation of freezing and thawing processes in variably-saturated, non-deformable soils, *Advances In Water Resources*, 60, 160-177, doi:10.1016/j.advwatres.2013.07.016.
- LEE, J. R., F. S. BUSSCHERS, and H. P. SEJRUP (2012), Pre-Weichselian Quaternary glaciations of the British Isles, The Netherlands, Norway and adjacent marine areas south of 68°N: implications for a long-term ice sheet development in northern Europe, *Quaternary Science Reviews*, 44, 213-228.
- LEMIEUX, J. M., E. A. SUDICKY, W. R. PELTIER, and L. TARASOV (2008a), Dynamics of groundwater recharge and seepage over the Canadian landscape during the Wisconsinian glaciation, *Journal of Geophysical Research-Earth Surface*, 113(F1), doi:10.1029/2007jf000838.
- LEMIEUX, J. M., E. A. SUDICKY, W. R. PELTIER, and L. TARASOV (2008b), Simulating the impact of glaciations on continental groundwater flow systems: 2. Model application to the Wisconsinian glaciation over the Canadian landscape, *Journal of Geophysical Research-Earth Surface*, 113(F3), doi:10.1029/2007jf000929.
- LEMIEUX, J. M., E. A. SUDICKY, W. R. PELTIER, and L. TARASOV (2008c), Simulating the impact of glaciations on continental groundwater flow systems: 1. Relevant processes and model formulation, *Journal of Geophysical Research-Earth Surface*, 113(F3), doi:10.1029/2007jf000928.
- LISIECKI, L. E., and M. E. RAYMO (2005), A Pliocene-Pleistocene stack of 57 globally distributed benthic $\delta^{18}\text{O}$ records, *Paleoceanography*, 20(1), doi:10.1029/2004pa001071.
- LUNARDINI, V. J. (1998), Effect of convective heat transfer on thawing of frozen soil, in *Proceeding of the seventh international conference on permafrost*, edited by V. J. Lewkowicz and M. Allard, pp. 689-695, Canada: Yellowknife.
- MCEVOY, F.M., SCHOFIELD, D.I, SHAW, R.P. and S. NORRIS. 2016. Tectonic and climatic considerations for deep geological disposal of radioactive waste: A UK perspective, *Science of the Total Environment*, 571, 507-521),
- MARSHALL, S. J. (2012), *The cryosphere*, edited, p. 228, Princeton University Press.
- MCEWEN, T., and G. DE MARSILY (1991), The Potential Significance of Permafrost to the Behaviour of a Deep Radiactive Waste Repository, *SKI Report TR 91:8*.
- MCKENZIE, J. M., C. I. VOSS, and D. I. SIEGEL (2007), Groundwater flow with energy transport and water-ice phase change: Numerical simulations, benchmarks, and application to freezing in peat bogs, *Advances In Water Resources*, 30(4), 966-983, doi:10.1016/j.advwatres.2006.08.008.
- MCKENZIE, J. M., and C. I. VOSS (2013), Permafrost thaw in a nested groundwater-flow system, *Hydrogeology Journal*, 21(1), 299-316, doi:10.1007/s10040-012-0942-3.
- NEUZIL, C. E. (1995), Abnormal Pressures as Hydrodynamic Phenomena, *American Journal of Science*, 295(6), 742-786.
- NEUZIL, C. E. (2003), Hydromechanical coupling in geological processes, *Hydrogeology Journal*, 11(1), 41-83.
- NORMANI, S. D., and J. F. SYKES (2012), Paleohydrogeologic simulations of Laurentide ice-sheet history on groundwater at the eastern flank of the Michigan Basin, *Geofluids*, 12(1), 97-122, doi:10.1111/j.1468-8123.2012.00362.x.
- ORGOGOZO, L., N. RENON, C. SOULAIN, F. HÉNON, S. K. TOMER, D. LABAT, O. S. POKROVSKY, M. SEKHAR, R. ABABOU, and M. QUINTARD (2014), An open source massively parallel solver for Richards equation: Mechanistic modelling of water fluxes at the watershed scale, *Computer Physics Communications*, 185(12), 3358-3371, doi:<http://dx.doi.org/10.1016/j.cpc.2014.08.004>.
- PATERSON, W. S. B. (1994), *The Physics of Glaciers. Third edition*.
- PELTIER, W. R., I. SHENNAN, R. DRUMMOND, and B. HORTON (2002), On the postglacial isostatic adjustment of the British Isles and the shallow viscoelastic structure of the Earth, *Geophys. J. Int.*, 148, 44.
- PERSON, M., J. MCINTOSH, N. IVERSON, C. E. NEUZIL, and V. BENSE (2012a), Geologic isolation of nuclear waste at high latitudes: the role of ice sheets, *Geofluids*, 12(1), 1-6, doi:10.1111/j.1468-8123.2011.00358.x.
- PERSON, M., V. BENSE, D. COHEN, and A. BANERJEE (2012b), Models of ice-sheet hydrogeologic interactions: A review, *Geofluids*, 12(1), 58-78, doi:10.1111/j.1468-8123.2011.00360.x.
- PHILLIPS, E., and J. R. LEE (2013), Development of a subglacial drainage system and its effect on glacial tectonism within the polydeformed middle pleistocene (anglian) glacial sequence of north norfolk, eastern England, *Proceedings of the Geologists' Association*, 124(5), 855-875, doi:10.1016/j.pgeola.2012.07.005.
- PIOTROWSKI, J. A. (2006), Groundwater Under Ice Sheets and Glaciers, in *Glacier Science and Environmental Change*, edited by P. G. Knight, pp. 50-59, Blackwell Publishing, Oxford.
- PROVOST, A. M., C. I. VOSS, and C. E. NEUZIL (2012), Glaciation and regional groundwater flow in the Fennoscandian shield, *Geofluids*, 12(1), 79-96, doi:10.1111/j.1468-8123.2012.00361.x.
- ROLLIN, K. E. (2002), Assessment of BGS data for ground source heat pump installations in the UK, *British Geological Survey, IR/02/196*, 50 pp, Keyworth.
- ROWLAND, J. C., B. J. TRAVIS, and C. J. WILSON (2011), The role of advective heat transport in talik development beneath lakes and ponds in discontinuous permafrost, *Geophysical Research Letters*, 38, L17,504, doi:10.1029/2011GL048497.

- RÜHAAK, W., HAUKE ANBERGEN, CHRISTOPHE GRENIER, JEFFREY MCKENZIE, BARRET L. KURYLYK, JOHN MOLSON, NICOLAS ROUX, and I. SASS (2015), Benchmarking Numerical Freeze/Thaw Models, paper presented at European Geosciences Union General Assembly 2015, EGU, Energy Procedia, Vienna.
- RUSKEEMIEMI, T., M. PAANANEN, L. AHONEN, J. KAIJA, A. KUIVAMÄKI, S. FRAPE, L. MOREN, and P. DEGNAN (2002), Permafrost at Lupin. Report of Phase I, *Permafrost Project GTK-SKB-POSIVA-NIREX-OPG*, Geological Survey of Finland, Nuclear Waste Disposal Research.
- SCHEIDEGGER, J. M., V. F. BENSE, and S. E. GRASBY (2012), Transient nature of Arctic spring systems driven by subglacial meltwater, *Geophysical Research Letters*, 39(12), doi:10.1029/2012gl051445.
- SCHEIDEGGER, J. M. (2013), Impact of permafrost dynamics on Arctic groundwater flow systems with application to the evolution of spring and lake taliks. Type thesis, 163 pp, University of East Anglia, Norwich.
- SCHEIDEGGER, J. M., and V. F. BENSE (2014), Impacts of glacially recharged groundwater flow systems on talik evolution, *Journal of Geophysical Research-Earth Surface*, 119(4), 758-778, doi:10.1002/2013jf002894.
- SHAW, R. P., A. C.A., B. BAPTIE, S. BROCKLEHURST, M. DUTTON, D. J. EVANS, L. P. FIELD, S. P. GREGORY, E. HENDERSON, A. J. HUGHES, A. E. MILODOWSKI, D. PARKES, J. G. REES, J. SMALL, N. SMITH, A. TYE, and J. M. WEST (2013), Potential Natural Changes and Implication for a UK GDF, *British Geological Survey, CR/12/127*, 198 pp, Keyworth.
- SHENNAN, I., and B. HORTON (2002), Holocene land- and sea-level changes in Great Britain, *Journal of Quaternary Science*, 17(5-6), 511-526.
- SLOAN, C., and R. VAN EVERDINGEN (1988), Region 28, Permafrost region, in *Hydrogeology*, edited, pp. 263-270, Geological Society of America.
- TOHIDI, B., A. CHAPOY, J. SMELLIE, and I. PUIGDOMENECH (2010), The potential for methane hydrate formation in deep repositories of spent nuclear fuel in granitic rocks, *SKB R-10-58*.
- TOWLER, G. H., J. A. BARKER, R. G. MCGARRY, S. P. WATSON, T. MCEWEN, U. MICHIE, and A. HOLSTEIN (2008a), Post-Closure Performance Assessment: Example Approaches for Groundwater Modelling of Generic Environments, *Quintessa, QRS-1378G-1*.
- TOWLER, G. H., J. A. BARKER, R. G. MCGARRY, S. P. WATSON, T. MCEWEN, U. M. MICHIE, and A. HOSSTEIN (2008b), Post-Closure Performance Assessment: Example Approaches for Groundwater Modelling of Generic Environmnets, *Quintessa, QRS-1378G-1*, 181 pp.
- VELICOGNA, I., J. TONG, T. ZHANG, and J. S. KIMBALL (2012), Increasing subsurface water storage in discontinuous permafrost areas of the Lena River basin, Eurasia, detected from GRACE, *Geophysical Research Letters*, 39, doi:10.1029/2012gl051623.
- VIDSTRAND, P., S. FOLLIN, and N. ZUGEC (2010), Groundwater modelling of periods with periglacial and glacial climate conditions - Forsmark, *SKB, R-09-21*.
- VIDSTRAND, P., S. FOLLIN, J. O. SELROOS, J. O. NASLUND, and I. RHEN (2013), Modeling of groundwater flow at depth in crystalline rock beneath a moving ice-sheet margin, exemplified by the Fennoscandian Shield, Sweden, *Hydrogeology Journal*, 21(1), 239-255, doi:10.1007/s10040-012-0921-8.
- VIDSTRAND, P., S. FOLLIN, J. O. SELROOS, and J. O. NASLUND (2014), Groundwater flow modeling of periods with periglacial and glacial climate conditions for the safety assessment of the proposed high-level nuclear waste repository site at Forsmark, Sweden, *Hydrogeology Journal*, 22(6), 1251-1267, doi:10.1007/s10040-014-1164-7.
- WANG, H. F. (2000), *Theory of Linear Proelasticity With Applications to Geomechanis and Hydrogeology*, Princeton Univeristy Press, Princeton, N.J.
- WATANABE, K., and M. FLURY (2008), Capillary bundle model of hydraulic conductivity for frozen soil, *Water Resources Research*, 44(12), doi:10.1029/2008WR007012.
- WELLMAN, T. P., C. I. VOSS, and M. A. WALVOORD (2013), Impacts of climate, lake size, and supra- and sub-permafrost groundwater flow on lake-talik evolution, Yukon Flats, Alaska (USA), *Hydrogeology Journal*, 21(1), 281-298, doi:10.1007/s10040-012-0941-4.
- WESTAWAY, R., and P. L. YOUNGER (2013), Accounting for palaeoclimate and topography: A rigorous approach to correction of the British geothermal dataset, *Geothermics*, 48, 31-51, doi:DOI 10.1016/j.geothermics.2013.03.009.
- WILLIAMS, J. (1970), Ground water in the permafrost regions of Alaska, *Geological Survey Professional Paper 696*.
- WILLIAMS, P., and M. SMITH (1989), *The Frozen Earth, Fundamental of Geocryology*, Cambridge University Press.
- WOO, M.-K. (2012), *Permafrost Hydrogeology*, Springer, Heidelberg.
- ZWALLY, H. J., W. ABDALATI, T. HERRING, K. LARSON, J. SABA, and K. STEFFEN (2002), Surface melt-induced acceleration of Greenland ice-sheet flow, *Science*, 297(5579), 218-222, doi:10.1126/science.1072708.